Developing 3D microstructures for tissue engineering

Mohanty, Soumyaranjan

Publication date:
2016

Document Version
Publisher's PDF, also known as Version of record

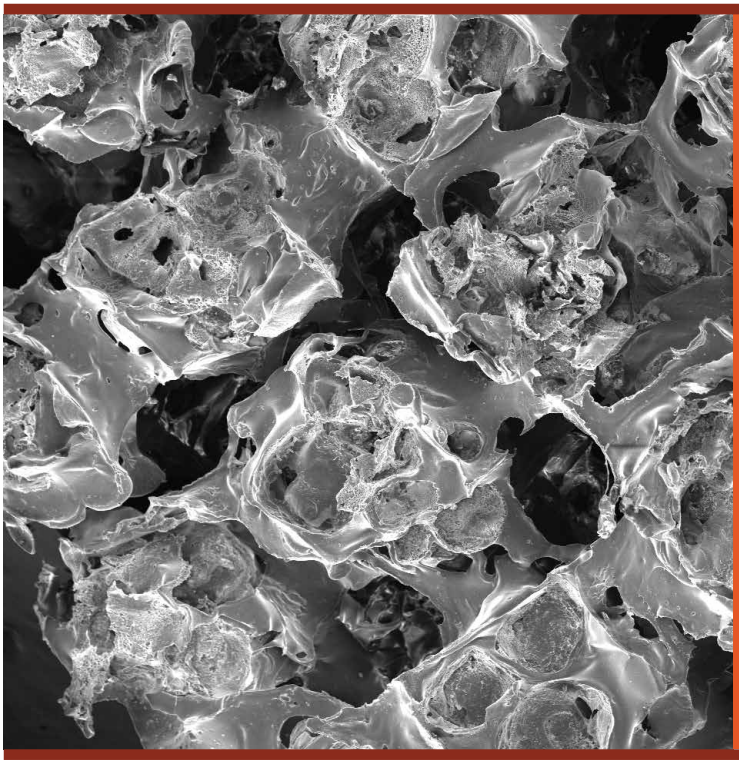

Developing 3D microstructures for tissue engineering

Soumyaranjan Mohanty
PhD Thesis March 2016

DTU Nanotech
Department of Micro- and Nanotechnology

Developing 3D microstructures for tissue engineering

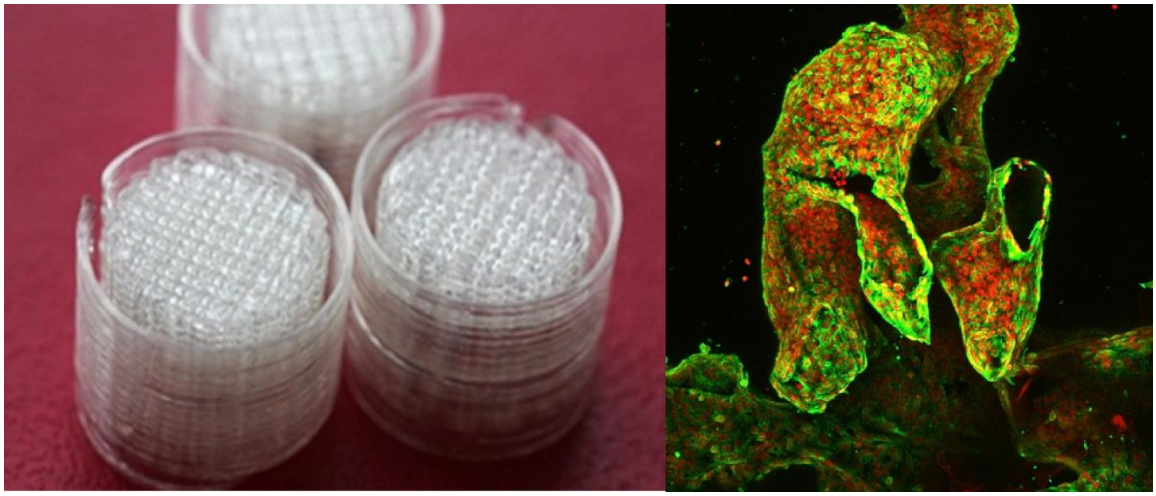

Soumyaranjan Mohanty

PhD Thesis January 2016

DTU Nanotech
Department of Micro- and Nanotechnology

Developing 3D microstructures for tissue engineering

By

Soumyaranjan Mohanty

DISSERTATION

Submitted in partial fulfillment of the requirements for the degree of Doctor of Philosophy in Electronics, Communication and Space Science in the department of Micro-and Nanotechnology of Technological University of Denmark

January 2016

Supervised by:

Associate Professor Anders Wolff

Professor Jenny Emnéus

Associate Professor Martin Dufva

Contents

Summary

Liver transplantation has been a major scientific and clinical breakthrough in the 20th century for many patients with nonmalignant and malignant liver diseases. However, there is a worldwide shortage of available organs; and many patients therefore deteriorate or die while on the waiting list. One path-breaking solution to these problems is the development of extracorporeal bioartificial livers (EBALs) and BALs, which essentially are bioreactors with embedded hepatocytes (liver cells) that perform the functions of a normal liver. The purpose of EBAL devices is not to permanently replace liver functions, but to serve as a supportive device, either allowing the liver to regenerate properly upon acute liver failure, or to bridge the individual's liver functions until a transplant is possible. Several types of BALs are being developed, including hollow fiber systems and flat membrane sheet systems with primary porcine hepatocytes, primary human hepatocytes, human hepatoblastoma (C3A), immortalized human cell lines and stem cells. However special attention needs to be paid to identifying a readily available and functional source of cells and to improving hepatocyte functionalities. Furthermore, bioreactor configurations that are not hollow-fiber based should be considered to improve both large-scale cell culture prior to therapy and mass transfers during treatment.

This thesis was a part of a EU project 'NanoBio4Trans', with the overall goal to combine induced pluripotent stem cells (iPSC), polymer hybrid bioactive scaffolds and biosensor technologies to develop BAL as an extracorporeal device and to perform biomedical research beyond the present state-of-the-art. One of the major challenges in producing large scale engineered tissue is the inability to create large, highly perfused scaffolds, in which cells can grow at high cell density and viability. In this project we explored several routes to create such large scaffolds with blood vessel-like networks. Such porous scaffold network helps the cells to adhere, proliferate and perform its biochemical functions for long periods. In fact we need to build two independent networks where one network will be "blood" while the other will take care of removing the waste. In nature, waste is collected and secreted into the intestine as bile, which essential means that the cells should be sandwiched between two fluidic networks.

With the aim of developing a process which is scalable, compatible with cell culture, rapid, and inexpensive, we explored the capability of a commercial 3D filament printer for printing of polyvinyl alcohol (PVA) as a sacrificial mould and a polymer

casting process to generate various large scale tissue engineering constructs with single pore geometry with the desired mechanical stiffness and porosity. In addition, a new technique was developed to fabricate dual-pore scaffolds for various tissue-engineering applications where 3D printing of the PVA mould was combined with a salt leaching process. In this case, the sacrificial PVA mould, defining a structured network- architecture of micro-channels, was filled with salt crystals to define random porous regions between the structured regions of the scaffold. The compatibility of fabrication methods were tested with various biocompatible synthetic polymers such as polydimethylsiloxane (silicone), poly(ϵ-caprolactone) and poly(2-hydroxyethyl methacrylate), but other natural and synthetic materials can also be adopted to this process. The *in-vitro* biocompatibility of the fabricated scaffolds was successfully tested with HepG2 cells. To demonstrate the potential of scaffolds to release drugs and hereby control the behavior of cells growing on its surface, the silicone elastomer based perfusable capillary network scaffolds, generated from previous steps, was exposed to supercritical CO_2 in the presence of a hydrogel to create an additional interpenetrating network (IPN) of hydrogel nanodeposits. Biocompatible IPNs of silicone elastomer with poly(2-hydroxyethyl methacrylate) (pHEMA) and Poly(ethylene glycol) methylether acrylate (PEGMEA) hydrogel 3D scaffolds were produced in this way. The model drug doxycycline was loaded into the hydrogel of the IPN materials, and the biological activity of released doxycycline was tested using a doxycycline regulated green fluorescent reporter gene expression assay in HeLa cells. Additionally, decellularized liver extracellular matrix (ECM) and natural silk protein materials have been developed and tested for enhancing the differentiation of hiPSC-derived hepatocytes and fabricating biodegradable scaffolds for *in-vivo* tissue engineering applications.

Along with various scaffolds fabrication methods we finally presented an optimized study of hepatic differentiation of hiPSC-derived DE cells cultured for 25 days in a 3D perfusion bioreactor system with an array of 16 small-scale tissue-bioreactors with integrated dual-pore pore scaffolds and flow rates. Hepatic differentiation and functionality of hiPSC-derived hepatocytes were successfully assessed and compared against freshly obtained human precision-cut liver slices (hPCLS) as an *ex vivo* liver representative model as gold standard, developed by other project partners.

Resumé

Udviklingen af levertransplantationer er et kæmpe videnskabeligt gennembrud, der har haft stor indflydelse på livskvaliteten og overlevelseschancerne for mange leverpatienter. Donorlevere er desværre en mangelvare, og mange leverpatienter dør derfor inden en lever er tilgængelig. Én banebrydende løsning på dette problem er at udvikle og benytte en kunstig lever (bioartificial liver, BAL), der, forsimplet, er en bioreaktor bestående af hepatocytes (leverceller), der biologisk set fungerer som en rigtig lever. I tilfældet af en extracorporeal bioartificial liver (EBAL) er det ikke målet at erstatte en rigtig lever, men at stabilisere patienten indtil at patientens lever har kommet sig (akut leversvigt) eller til at en donorlever bliver tilgængelig.

Dette projekt var en del af et EU-projekt, NanoBio4Trans, hvis overordnede mål var at kombinere stamceller med inducerede pluripotente stamceller (induced pluripotent stem cells, iPSC), bioaktive ”scaffold” af polymer, og teknologier fra biosensorer til at udvikle en ”extracorporeal” kunstig lever. En stor begrænsning for udviklingen af kunstige organer er at skabe store porøse ”scaffold” hvor celler kan trives i høj tæthed uden at opbygge affaldsstoffer eller løbe tør for næring. I projektet er kommercielle 3D filamentprintere blevet benyttet, da disse er hurtige, billige og fleksible. Specifikt er der i projektet blevet udviklet en 3-trins produktionsmetode, der involvere (1) 3D-print af vandopløselig polyvinyl alkohol (PVA) i den ønskede kanalgeometri, som derefter (2) fungerer som form for den færdige platform, der fx støbes i polydimethylsiloxane (PDMS). Herefter (3) opløses offermaterialet (PVA) og ”scaffolden” er færdig. For at opnå variationer i porøsitet blev der benyttet kombinationer af 3D-printet PVA og saltkrystaller som offermaterialer, hvor PVA-geometrien definerede ”scaffoldens” overordnede udformning, mens saltkrystallerne definerede områder med høj porøsitet og stokastisk natur. Ud over PDMS blev materialerne poly(ϵ-caprolactone) og poly(2-hydroxyethyl methacrylate) testet som platforms-materiale, men andre naturlige og syntetiske materialer kan også anvendes. Specifikt er også blevet eksperimenteret med at støbe platformene i naturlige materialer så som cellefrit extracellular matrix (ECM) og silkeprotein. ”Scaffoldens” in-vitro biokompabilitet blev testet med HepG2 celler.

For at styre cellernes vækst på de producerede ”scaffolds” blev der udført eksperimenter med absorption og desorption af medikamenter i og fra ”scaffolden”: De færdige ”scaffold” blev eksponeret til superkritisk CO_2 samt doxycyclin og en sekundær hy-

drogel. Dette resulterede i at den oprindelige ”scaffold” blev gennemtrængt af strukturer bestående af den sekundære hydrogel og doxycyclin.
Celler dyrket på disse ”scaffolds” er slutteligt blevet sammenlignet med virkelige leverprøver, og der er observeret stor lighed.

Acknowledgments

It would not have been possible to write this PhD thesis without the help and support of the kind people around me, to only some of whom it is possible to give particular mention here. First and foremost, I would like to express my deepest gratitude to my supervisor, Assoc. Prof. Anders Wolff and co-supervisor, Prof. Jenny Emnéus for giving me continuous support, encouragement and freedom to explore new ideas throughout my PhD. Your advice on both research as well as on my career has been priceless and I have been very fortunate to have you both as my mentors. I also wish to give special thanks to Assoc. Prof. Martin Dufva for his supervision and Prof. Dang Duong Bang for his continuous support.

I address a big "thank you" to Assoc. Prof. Arto Heiskanen for his technical guidance for academics and life coaching and Asst. Prof. Alireza Dolatshahi-Pirouz for providing creative inspiration and helpful feedback on my work. I would also like to thank you to Asst. Prof. Sun Yi and Esben for putting their great support for correcting the thesis.

My warmest regards goes to all the members of BioLabchip and Bioanalytics group who have enriched my stay and helped me in so many ways. I would also like to thank my colleagues at DTU Nanotech. It has been a pleasure working with all of you. A big thanks to all my Indian friends living in Copenhagen for their strong support. Many thanks to Dr. Martin Alm from Biomodics, Anders Aspegren from Clontech and Jon Trifol from DTU chemical engineering for providing cells, polymer materials, equipment use and technical guidance.

Lastly, I would like to thank my parents for giving me unconditional support and encouragements throughout my life, no matter what path I chose. I am sincerely grateful for all the things they have done for me.

Finally, I would like to thank the EU project NanoBio4trans project for providing my funding during my PhD program.

List of abbreviations

2D	Two dimensional
3D	Three dimensional
3DP	Three dimensional printing
ALF	Acute liver failure
ACLF	Acute-on-chronic liver failure
AM	Additive manufacturing
ALs	Artificial livers
ATR-FTIR	Attenuated total reflection Fourier transform infrared spectroscop
BALs	Bioartificial liver
CE	Counter electrode
CFD	Computational fluid dynamic
CAD	Computer-aided design
DPMD	Direct polymer melt deposition
dsDNA	Double stranded DNA
DOX	Doxycycline
EIS	Electrochemical impedance spectroscopy
ES	Electrospinning
eSC	Embryonic stem cells
ELISA	Enzyme-linked immunosorbent assay
ECM	Extracellular matrix
EBAL	Extracorporeal BAL
FTIR	Fourier transform infrared
FDM	Fused deposition modeling
GFP	Green fluorescent reporter
hiPSC	Human iPSC
hPCLS	Human precision-cut liver slices
iPSC	Induced pluripotent stem cells
IPNs	Interpenetrating polymer networks
LIPS	Liquid induced phase separation
LSS	Liver support system
MIP	Mercury intrusion porosimetry

HEMA	2-hydroxyethyl methacrylate
hMSCs	Mesenchymal stem cells
MCS	Mutable cloning site
nBG	Nano-bioactive glass
NPC	Non-parenchymal cells
Pt	Platinum
PSC	Pluripotent stem cell
Phema	poly(2-hydroxyethyl methacrylate)
PMMA	poly(methyl methacrylate)
PVA	poly(vinyl alcohol)
PCL	poly(ϵ-caprolactone)
PDMS	Polydimethylsiloxane
PEGMEA	polyethyleneglycol monomethacrylate
hPHs	Primary hepatocytes
RP	rapid prototyping
RFP	Red fluorescent protein
SEM	Scanning electron microscopy
SLS	Selective laser sintering
SFF	Solid Free-Form Fabrication
SLA	Stereolithography
$scCO_2$	Supercritical carbon dioxide
TIPS	Thermally induced phase separation
TPP	Two-photon polymerization

List of Publications and Submitted Manuscripts

Journal publications

1) **Mohanty, S**., Muhammad, H. B., Trifol, J., Szabo, P., Burri, H. V. R., Canali, C., Wolff, A. (2015). Fabrication of scalable and structured tissue engineering scaffolds using water dissolvable sacrificial 3D printed moulds. *Materials Science and Engineering: C, 55*, 569-78. doi:10.1016/j.msec.2015.06.002
2) **Mohanty, S**., Kuldeep, K., Heiskanen, A., Trifol, J., Szabo, P.,… Wolff, A. (2015). Fabrication of scalable tissue engineering scaffolds with dual-pore microarchitecture by combining 3D printing and particle leaching. *Materials Science and Engineering: C, 61*, 180-89. doi: 10.1016/j.msec.2015.12.032
3) **Mohanty, S**., Heiskanen, A., Hemmingsen, M., Trifol, J., Alm, M., Dufva, M., Emnéus, J., Wolff, A., "3D interpenetrating polymer networks of silicone hydrogel scaffolds for tissue engineering and drug delivery applications." **Accepted to** *ASC Biomacromolecules.*
4) Sofie Bruun Hartmann, **Soumyaranjan Mohanty**, Kerstin Skovgaard, Louise Brogaard, Frederikke Bjergvang Flagstad, Jenny Emnéus, Anders Wolff, Artur Summerfield and Gregers Jungersen. (2016) "Investigating the role of surface materials and three dimensional architecture on *in vitro* differentiation of porcine monocyte-derived dendritic cells". **Submitted to** PLOS One.
5) Canali, C., **Mohanty, S**., Heiskanen, A., Muhammad, H. B., Martinsen, Ø. G., Dufva, M., … Emnéus, J. (2015). Impedance Spectroscopic Characterisation of Porosity in 3D Cell Culture Scaffolds with Different Channel Networks. *Electroanalysis*, *27*(1), 193–199. doi:10.1002/elan.201400413
6) V., Starokozhko, M., Hemmingsen, L., Larsen, **S., Mohanty**, M., Merema, R., Pimentel, A., Wolff, J., Emnéus, A., Aspegren, G., Groothuis, and M., Dufva "In Situ Hepatic Differentiation of Human Induced Pluripotent Stem Cell Derived Definitive En-doderm Cells at Flow Conditions for Liver Tissue Engineering" **Manuscript in preparation.**
7) L.B. Larsena, C. Canalia, M. Hemmingsena, K. Kuldeepa, **S. Mohanty**, R. Pimentela, L.H. Jensenb, M. Skolimowskia, A. Wolffa, F. Okkelsa, A. Heiskanena, M. Dufvaa, J. Emnéus."Perfusion bioreactor array with integrated impedance sensors for tissue engineering applications" **Manuscript in preparation.**

Patents

1) **Mohanty, S**., Emnéus, J., Wolff, A., Dufva, M., Muhammad, H. B., Skolimowski, M., & AMATO, L. (2015). "Method Of Manufacturing A Porous Polymer Component Involving Use Of A Dissolvable, Sacrificial Material." Google Patents. Retrieved from (http://www.google.com/patents/EP2826814A1?cl=en)
2) **S. Mohanty,** J. Emnéus, A. Wolff, A. Heiskanen, "A METHOD FOR FABRICATING A THREEDIMENSIONAL CARBON STRUCTURE." Date of filing to European patent office: 28.08.2015. Application no./Patent No. 15182928.0 – 1355.

Conference

Oral

1) **S. Mohantya**, A. Heiskanena, …, A. Wolff and J. Emnéus. "Three-dimensional (3D) Scaffolds for Bioartificial Organ-on-a-Chip Systems and Bioelectroanalysis." 41st International Conference on Micro and Nano Engineering, 2015, The Netherlans
2) **Mohanty, S**; Hemmingsen, M; Wojcik, M; Alm, M; Dufva, M; Emnéus, J; Wolff, A. "Novel scalable silicone elastomer and poly(2-hydroxyethyl methacrylate) (PHEMA) composite materials for tissue engineering and drug delivery applications." 15th International Conference on Biomedical Engineering, 2013, Singapore
3) **Mohanty, S**; Amato, L;...Emnéus, J. "Conducting pyrolysed carbon scaffold for tissue engineering." 39th International Conference on Micro and Nano Engineering, 2013, London.
4) Larsen, LB; Canali, C; **Mohanty, S**; Hemmingsen, M; Skolimowski, M; Dufva, M; Wolff, A ; Emnéus, J. "Design and optimisation of a lab-on-a-chip system with integrated sensors for 3D tissue engineering." 39th International Conference on Micro and Nano Engineering, 2013, London
5) Larsen, LB; Canali, C; **Mohanty, S**; Hemmingsen, M; Skolimowski, M; Dufva, M; Wolff, A; Emnéus, J. "Development of a lab-on-a-chip system with integrated sensors for 3D tissue engineering applications." 15th International Conference on Biomedical Engineering, 2013, Singapore

Poster

1) **S Mohanty**, I Mantis, AM Chetan, LB Larsen, M Dufva, J Emnéus, A Wolff. "Fabrication of three dimensional tissue engineering polydimethylsiloxane (pdms) microporous scaffolds integrated in a bioreactor using a 3d printed water dissolvable sacrificial mould." *Proceedings MicroTAS 2015*, South Korea.(PP 1439-1441)
2) Canali, C., Heiskanen, A., Martinsen, Ø. G., **Mohanty, S**., Dufva, M., Wolff, A., & Emnéus, J. (2015). II Latin American Conference on Bioimpedance, *54*, 36–39. doi:10.1007/978-981-287-928-8
3) Hemmingsen, M; Larsen, LB; **Mohanty, S** ; … Dufva, M. "Gene Expression of Albumin is Down-regulated in hIPS-derived Hepatocyte-like Cells Cultured at Flow Conditions." Stem Cell Niche 2014, Copenhagen.
4) Hemmingsen, M; Larsen, LB; **Mohanty, S**; Wolff, A; Emnéus, J; Aspegren, A; Dufva, M. "Hepatic Differentiation of Human Induced Pluripotent Stem Cells in a Perfused 3D Porous Polymer Scaffold for Liver Tissue Engineering." 3rd International Conference on Tissue Science & Regenerative Medicine, 2014, Valencia
5) Canali, C; Larsen, LB; Heiskanen, A; **Mohanty, S**;… Emnéus, Jenny. "Electrochemical impedance spectroscopy is a versatile technique for new challenges in 3D cell culture." 15th International Conference on Electroanalysis , 2014, Malmö, Sweden.
6) Canali, C; Larsen, LB ; Heiskanen, A; **Mohanty, S**; Dufva, M; Wolff, A; Emnéus, J. "Electrochemical impedance spectroscopy is a versatile technique for new challenges in 3D cell culture." Conference on Electrochemical Science and Technology 2014, 2014, Copenhagen
7) Frey, O., **Mohanty, S**., Moritz, W., & Hierlemann, A. (2012). Towards a " Body on a Chip " Using Spherical Microtissues. *Proceedings MicroTAS 2012*, Japan 1540–1542.

1. CHAPTER 1. Introduction: Scope of the Thesis

The loss or failure of an organ or tissue is one of the most frequent, devastating, and costly problems in human health care [1]. Organ transplantation has been a major scientific and clinical breakthrough in the 20th century, in spite of many associated problems, such as lack of organ donors and/or rejection of the transplanted organs and life-long heavy medication with considerable side effects. To circumvent these problems, the innovative therapeutic approach of the 21th century is focusing on bioartificial organs using a multidisciplinary and complementary approach with the long-term goal of achieving better treatment Liver failure results from the liver's inability to perform its normal functions. In acute liver failure (ALF) [2], liver function is normal 2–8 weeks before the onset of the disease. In acute-on-chronic liver failure (ACLF), liver function decreases abruptly in a patient already suffering from chronic liver insufficiency. Extracorporeal liver support system (LSS) have been developed to either bridge patients to liver transplantation or to allow the recovery of the native liver from injury. There are two types of LSSs: artificial livers (**AL**s) and bioartificial liver (BALs). AL devices use physical/chemical gradients and adsorption with anion- or cation-exchange columns or sorbent suspensions to cleanse the blood or plasma of its toxins. Detoxification alone is, however, not sufficient to replace liver function, as there are at least 500 different functions that the healthy liver organ performs. Therefore, extracorporeal BAL (**EBAL**) would be ideal for substitution of many physiologically relevant functions such as biosynthesis, metabolism, and detoxification. An **EBAL** is a cell-based system (a bioreactor) which performs most of the hepatic functions lacking in patients with liver failure (oxidative detoxification, biotransformation, excretion and synthesis). EBALs should be designed for the individual patient's needs and long-term maintenance of hepatocyte differentiated functions *in vitro*. EBALs should be reproducible, automatable, controllable, and compliant with clinical applications.

1.1 Various extracorporeal liver support systems

One of the technical challenges is *ex vivo* culturing of large masses of cells in a suitable environment while maintain all major cellular functions. Since hepatocytes are anchorage-dependent cells, various biomaterials for *in vitro* hepatocyte culture such as

membrane, microcarriers, polymeric matrix, or scaffold have been incorporated in EBAL design for cell attachment. There are mainly four different EBAL configurations under current investigation: (1) hollow fiber cartridges, (2) packed-bed systems, (3) encapsulation systems, and (4) flat plate systems, some of which are under clinical testing[3].

Table 1. Summarizes bioreactor configurations and designs [4].

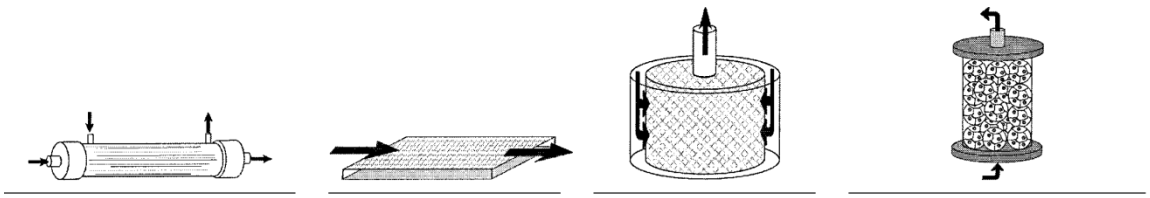

Hollow Fiber	Flat Plate and Monolayer	Perfused Packed Bed	Encapsulation and suspension
Pros: attachment surface, potential for immunoisolation, well characterized, cells protected from shear	Pros: uniform cell distribution and microenvironment	Pros: ease of scale-up, promotes 3-dimensional architecture, minimal transport barrier	Pros: ease of scale-up, uniform microenvironment
Cons: nonuniform cell distribution, transport barrier with membranes or gels	Cons: complex scale-up, potential large dead volume, cells exposed to shear, low surface area-to-volume ratio	Cons: nonuniform perfusion, clogging, cells exposed to shear forces	Cons: poor cell stability in suspension, transport barrier due to encapsulation, degradation of microcapsules over time, cells exposed to shear forces

I. Hollow fiber systems[5,6] are most commonly used: generally, they consist of a cylindrical column with hundreds of thousands of hollow fibers aligned longitudinally through the column. Cells are cultured outside the hollow fiber while culture medium or patient's blood/plasma is perfused in the fiber lumen along the hollow fiber.

II. Packed bed systems: The matrix for hepatocyte attachment is filled into the reactor, which is perfused with medium or the patient's blood/plasma. Various packing materials for hepatocyte entrapment, such as microchanneled polyurethane foam [7], polyvinyl resin cubes [8], alginate beads [9], porous hydroxyapatite beads [10], and polyester fabric cell scaffold [11] have been explored.

III. Encapsulation system: Hepatocytes are enveloped in a polymeric matrix to form a small capsule. The encapsulated hepatocytes are then packed into a chamber for perfusion. Various materials have been used for hepatocyte encapsulation, including hydrogels [12], alginate [13], and copolymers such as hydroxyethyl methacrylate-methyl methacrylate (HEMA-MMA) [14]. There is some evidence indicating that spheroids enhance cell-cell interaction [15] and facilitate the formation of bile-duct structure between cells, improving cell functions. In some of these systems, hepatocyte spheroids are thus formed before entrapment in a capsule [3].

IV. Flat-plate systems: Hepatocyte monolayer culture on a substrat such as collagen, laminin, fibronectin, or Matrigel is a common *in vitro* method. Overlay of a matrix gel layer on top of a monolayer culture, forming a sandwich configuration, stabilizes the hepatocytes' cuboidal structure. The establishment of hepatocyte polarity and maintenance of differentiated functions for several weeks can thus be achieved[16,17].

1.2 Sources of hepatocytes for large scale EBALs

Hepatocytes are highly polarized cells that have a unique position as a barrier between the blood and the bile, and the substances trafficking between sinusoids and bile canaliculi predominantly rely on this cell polarity. The generation of hepatocyte polarity involves: (1) the establishment of cell-cell and cell-matrix interactions, (2) the organisation of cytoskeleton, and (3) the sorting and localisation of membrane proteins. The maintenance of normal liver function in a patient can be satisfied with about 20% of the whole liver mass, approximately 200 g (2×10^{10} hepatocytes). The LSS to date make use of cryopreserved or freshly isolated human or porcine-derived hepatocytes and cell lines at 100-600 g.

1) Primary human hepatocytes are the ideal cells for EBAL with benefits including better biosafety and a satisfactory level of hepatic biofunctionality, particularly the ability to provide homologous biologically active substances[18]. Primary human hepatocytes, however, are scarce, do not proliferate *in vitro*, and normal functions cannot be maintained *in vitro* for longer than 1 or 2 weeks. Moreover, great variation in functional performance between different cell batches[19] has been seen, and there is also a risk for contamination with viruses, bacteria, and tumor cells[20].

2) Primary porcine hepatocytes are the preferred and the most widely used animal-derived liver cells for EBALs due to their convenient availability, low cost, and well-established isolation methods. However, there are a number of drawbacks, such as (1) they present xenogenic antigens to the human body and can thus cause immune response during treatment; and (2) the potential danger of transfection with Pig endogenous retrovirus (PERV) common in pigs.

3) Human liver cell lines, with the C3A cell line permitted for use in EBAL systems. Cell lines have the major advantage that they can be obtained in large amounts continuously and reproducibly; however, there are some serious drawbacks. For example, compared to primary porcine hepatocytes, C3A has a lower metabolic capability partic-

ularly with respect to ammonia, an important reason why some EBAL systems using C3A have not been able to obtain significant efficacy in clinical treatment.

4) Co-cultures*:* In a normal liver tissue, the cell-cell, cell-extra-cellular matrix (ECM), and cell-microenvironment interactions have been widely explored and acknowledged for their major role in the maintenance of hepatic functions. Several studies have therefore aimed to simulate the physiological organization of liver tissue by recruitment of the non-parenchymal cells (NPC) into EBALs, and shown that the hepatic functions could be preserved for longer in the co-culture systems[21–24]. Ohno *et al*.[22,25] found that in the hepatocyte-endothelial cell sheets layered co-culture system, drug metabolism related gene expression is better preserved than in hepatocyt cultures alone, and the ECM molecular composition and cell-adhesion molecules changes in the system correlate with genes expression in a time-course pattern. The study suggested that the co-culture system can generate beneficial ECM to maintain the hepatic function *in vitro*.

To ensure the availability of an EBAL at any desired time, cryopreserved hepatocytes have been suggested as first choice; however, the recovery of viability after thawing is still problematic. Hepatocytes are anchor-dependent cells and their maintenance depends on the support from ECM and cell-cell communication[26]. Cryopreservation configurations such as monolayer collagen, sandwich collagen, microcarrier, and microcapsule stock of hepatocytes have shown better post-thawing viability and function than the suspension cell cryopreservation.

However tissue engineering and stem cell biology have uncovered groundbreaking opportunities for cellular re-programming, i.e., some cell types can be changed into a pluripotent stem cell (**PSC**) by over-expressing key transcription factors. These, so called induced pluripotent stem cells (**iPSC**) [27] share the two key characteristics with embryonic stem cells (**eSC**): self-renewal and pluripotency (i.e. they can differentiate to form any cell type in the human body). Crucially they are generated from adult cells circumventing many ethical concerns associated with using human eSC. Therefore discovery of human iPSC (**hiPSC**) enables the growth of an almost unlimited supply of a patient´s own cells, potentially conferring the ability to grow and regenerate tissues and organs[28] from ‘self’, which is envisaged to resolve many organ rejection related issues[27,29]. Similarly, recent developments in material science and nanobiotechnology have produced engineered materials and devices that can be manipulated to control the physical and chemical properties, resulting in unique functional or analytical properties. The fusion of these fields with resulting synergistic effects will open up yet

unexplored scientific possibilities. The NanoBio4Trans project is fully addressing the current needs related to the future of BAL developments, as recently stated by state-of-the art scientific analysis [30].

1.3 EU project - NanoBio4Trans

The Aim of NanoBio4Trans project was to create a new paradigm to engineer cutting edge *scalable* highly vascularised BAL/EBALs on the following hypotheses:

1) The use of hiPSC as the starting material, is foreseen to enable the construction of personalized artificial organs from a patient´s own cells, which is expected to result in reduced organ rejection and increased availability of lifesaving organs for transplantation.

2) Growth and differentiation into *in vivo*-like BALs is possible if hiPSC-derived liver tissue is highly vascularized, i.e. penetrated with blood-vessel like channels lined with endothelial cells, and with immediate and nearby supply of the necessary growth factors and signaling molecules that support its growth and differentiation.

3) Creation of novel scalable two-component perfusable hybrid scaffolds (**PHS**s) is possible using: (1) a *primary* highly dense and branched blood vessel-like channel network through which a heart-mimicking pulsating flow supplies nutrients and oxygen (thus resembling natural gradients), surrounded by (2) a *secondary* porous structure enclosing hydrogel micro deposits (**HMD**s) that contains necessary growth factors and signaling molecules.

4) The use of integrated optical and electrical (bio)sensing systems for monitoring real time effects and changes during tissue growth will allow control and surveillance of BAL formation, with envisaged feed-back control.

Major steps are:

To explore different *in vitro* cellular systems for development of novel 3D cell/tissue culture systems starting from (a) existing endothelial cells and moving on to (b) hiPSCs, as they become available in the project, (c) using in a first instance miniaturized fluidic sensor array systems (**BAL-on-a-Chips**) for optimization of 3D culture and perfusion conditions, and (d) further adaption for up-scaling to a large size BAL support system to form BALs in the order of cm^3 to dm^3.

To compare and validate the developed BAL system with fluidic tissue slice sensor array systems (**Liver-on-a-chip**), containing precision-cut liver slices obtained from

surgical waste from transplant. This reference system will be used as the gold standard to which the BAL systems will be compared.

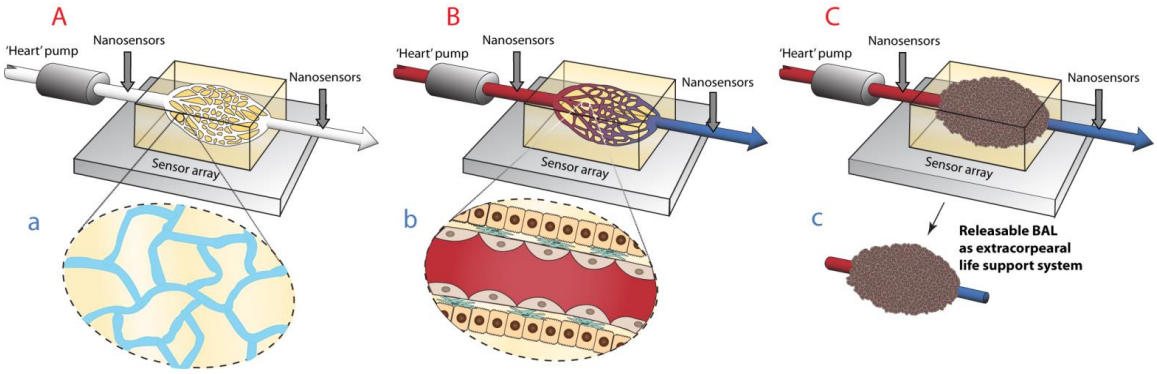

Figure 1. The NanoBio4Trans BAL support system´s development process: (A) The PHS with a primary highly branched perfusable channel network that allows flow through the material from one inlet to one outlet, and a secondary more arbitrary porous network (Fig. 1Aa), enclosing HMDs (in blue). (B) hiPSC derived endothelial and hepatocyte cells seeded and grown inside the primary capillary channel network, to closely mimic the in vivo situation of blood vessel lined with endothelial cells on top of which hepatocyte monolayers are formed (Fig. 1Bb). (C) A fully developed BAL support system, with integrated sensing and imaging tools for control of growth and viability and use as EBAL, with a final releasable BAL (Fig. 1Cc), potentially for future transplantation.

1.4 Motivation and Objective

This thesis focuses on various aspects of liver tissue engineering such as scaffold design with controlled pore geometry, its mass fabrication, characterization and final integration into the perfusion bioreactor. The main goal is to create scalable (ranging from cm^3 to dm^3) vascularized perfusable hybrid scaffolds (PHS) structures with *(i) primary* highly branched perfusable microchannel network (Fig. 1a) that allows flow through the material from one inlet to one outlet, and *(ii)* a *secondary* more arbitrary random microporous network that connects the structured channels (Fig. 2b), and *(iii)* a nanoporous *interpenetrating network (IPN)* that encloses hydrogel deposits of e.g. drugs, extracellular matrix proteins, differentiation factors, promoting hepatocyte adhesion, growth, differentiation and function (Fig. 2c). The created PHS has the following requirements and functions, where it should: (a) serve as structural and mechanical support for growth and differentiation of the BAL, (b) be perfusable with extensive channel networks that enable growth of blood vessels and transport of O_2 and nutrients to inner tissue and as a "nearby" source of important drugs and cell factors that sustains

the growth of cells into a final BAL, and (c) be biocompatible and potentially biodegradable.

Finally developed 3D scaffolds has to be integrated into a perfusion based BAL-on-a-Chip system incorporating pumps, sample reservoirs, bioreactors and different types of sensors for long-term growth and differentiation of hiPCS-derived DE cells into functional 3D BALs.

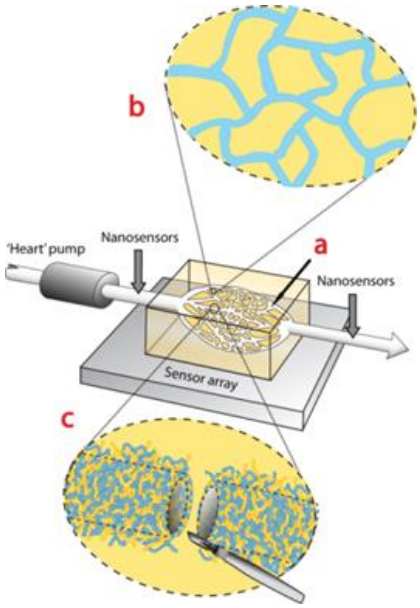

Figure 2. Illustration of PHS showing primary capillary network (a) and secondary porous HMDs, obtained in two different ways, throughout (b) and locally around the primary channels (c).

Our concept to achieve this goal is based on developing new 3D microfabrication techniques to yield a multiple layered perfusable capillary network scaffold in silicone elastomer (Fig. 3a & b). The perfusable capillary network exposed to supercritical CO_2 in the presence of a second hydrogel in order to functionalize the network prior to cell seeding (IPN technology). The supercritical CO_2 treatment leads to an expansion of the polymer structure, leaving space for inter-diffusion of hydrogel therein. When the supercritical CO_2 pressure is released the polymer-blend structure is locked/frozen, leaving it interpenetrated with networks of hydrogel (Fig. 3c). In this way, HMDs, containing the necessary biomolecule and growth factors that support endothelial and heptocyte cell growth, are formed throughout the *primary* capillary network structure in a single step. With sufficient density, these HMDs will serve as islands for cell attachment and further proliferation/spreading.

a) **b)** **c)**

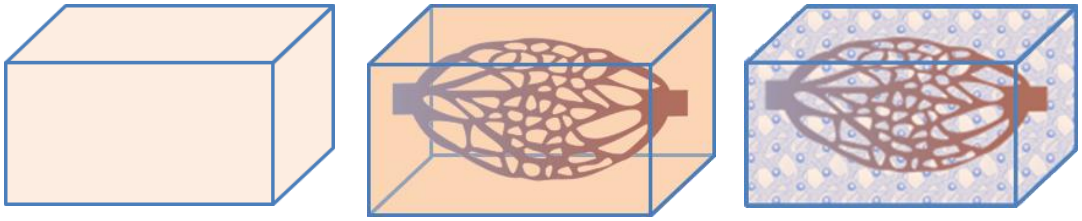

Figure 3. Illustration of the IPN scaffold concept, showing a) the base material, b) primary structured and/or random porous structure created within the base material, and c) a secondary IPN network within the PHS, enclosing hydrogel nano-deposits for in situ delivery of e.g. drugs, nutrients and growth factors.

As the short term goal of the NanoBio4Trans project was to develop an extracorporeal liver device the scaffold fabrication materials were mainly focused on biocompatible, elastic and non-degradable synthetic polymer. However in the long run to be able to transplant the artificial tissues *in vivo*, stepwise degradation of the polymer scaffold has to be investigated to produce the bioartificial liver (BALs) that ideally results in a liver piece without any synthetic scaffold material left. At the end of my PhD I have tied to fabricate scaffolds from natural protein based polymeric scaffolds with programmable degradation properties.

1.5 Thesis Outline

This thesis is organized into seven chapters. **Chapter 1** (this chapter) provides a general overview of the NanoBio4Trans project, with the aim to develop, optimize and validate a highly vascularised in-vivo-like bioartificial liver as an extracorporeal bioartificial liver. The main objective of the thesis is to develop new technologies for 3D microfabrication of scaffold structures that can be used for creating blood vessels and growing and perfusion of a bioartificial liver.

Chapter 2 presents the current detailed literature overview of aspects in scaffold design parameters and various scaffold fabrication techniques. The fabrication methods are mainly categorized into three major types such as traditional fabrication methods to generate random pore scaffolds, modern additive manufacturing fabrication methods for scaffolds with structured pore architecture and finally, the next generation dual pore scaffolds obtained by combining both traditional and modern fabrication techniques.

Different scaffolds fabrication techniques have been investigated which is rapid, inexpensive, scalable, and compatible with different polymers, making it suitable for engineering various large scale organs/tissues. In **chapter 3** I present a scaffold fabrication technique, where a sacrificial water dissolvable PVA mold was 3D printed,

polymer casted around it, cured and subsequently the sacrificial mold was dissolved, leading to a structured porous scaffold.

Similarly **chapter 4** describes the fabrication of dual-pore scaffold by combining 3D filament printing of water soluble PVA sacrificial mold for primary structured pores (as explained in **chapter 3** and **patent A**) combined with salt leaching to create random pores within the bulk scaffold. Using PDMS as the scaffold material, we have demonstrated that the fabrication process is rapid and inexpensive as well as scalable for generation of scaffolds of a size, relevant for thick tissues. This method can also be used with different biodegradable natural polymers (e.g. gelatine and silk) combined with freeze-drying, to provide scaffolds with wide range of mechanical properties.

Long term *in-vitro* studies of different types of scaffold were tested with human hepatoblastoma (HepG2) cells. The dual-pore scaffolds with highly interconnected structured pores combined with the adjacent random pores were proven to be superior to the structured and random pore scaffolds.

Along with scaffold fabrication techniques development of next generation "intelligent" instructive biomaterials that provide both physical support within a three dimensional (3D) microenvironment for controlling cell fate and direct cell differentiation through controlled drug release has attracted widespread attention in the field of tissue engineering. **Chapter 5** deals with the fabrication of 3D printed porous silicone-poly(2-hydroxyethyl methacrylate)-co-Poly(ethylene glycol) methyl ether acrylate (pHEMA-co-PEGMEA) hydrogel inter penetrating network (IPN) scaffolds using indirect 3D printing and supercritical CO_2 technology. The fabricated 3D IPN scaffolds were employed to support long-term growth of human mesenchymal stem cells (hMSC), resulting in well spread cell morphology with maintenance of high cell viability and metabolic activity. As a proof of concept, the biological activity of released doxycycline (DOX) from IPNs was confirmed using a tetracycline regulated green fluorescent reporter (GFP) gene expression assay with Hela cells.

Similarly carbon based materials have shown previously can induce the differentiation of hMSc and neuronal stem cells (NSC) into their respective lineages [31,32]. I have also developed some fabrication technique to fabricate 3D carbon scaffolds using pyrolysis presented in **patent B** and **conference abstract (A&B)**. The presented fabrication method offers new opportunities to develop 3D conductive tissue engineering scaffolds with precise control of the pore architecture and interconnectivity, facilitating scalability.

Chapter 6 summarises the contributions of developed porous scaffolds into perfusion bioreactor development, sensors integration and hiPSC derived hepatocytes differentiation during the NanoBio4Trans project. A tissue engineering bioreactor platform was developed, which integrates an array of 16 perfusable bioreactors that can be applied to culture cells in porous 3D scaffolds. The fabricated system was validated by culturing HepG2 hepatoblastoma cells in random porous 3D scaffolds. The developed bioreactor system has been integrated with impedance-based sensing technology along with perfusion for non-invasive real-time monitoring of cell proliferation in the 3D scaffolds. Next optimization study was carried out on hepatic differentiation of hiPSC-derived DE cells in the 3D perfusion bioreactor system with integrated random and dual pore scaffolds at two flow rates. Hepatic differentiation and functionality of hiPSC-derived hepatocytes are assessed using freshly obtained human liver as an *ex vivo* liver representative model.

Additionally for future work decellularized liver extracellular matrix (ECM) and natural silk protein materials have been developed and tested for enhancing the differentiation of hiPSC-derived hepatocytes and fabricating biodegradable scaffolds for *in-vivo* applications as described in **chapter 7**.

Finally the key conclusions of my PhD thesis are summarized in **chapter 8**. To be able to utilize the scaffolds for clinical use some recommendations on a number of topics have to be explored in the future to improve and optimize the 3D scaffold as proposed in this thesis.

1.6 References

[1] Langer R and Vacanti J P 1993 Tissue Engineering *Science (80-.).* **260** 920–6

[2] van de Kerkhove M P, Hoekstra R, Chamuleau R A F M and van Gulik T M 2004 Clinical Application of Bioartificial Liver Support Systems *Ann. Surg.* **240** 216–30

[3] Wang Y, Susando T, Lei X, Anene-Nzelu C, Zhou H, Liang L H and Yu H 2010 Current development of bioreactors for extracorporeal bioartificial liver (Review) *Biointerphases* **5** FA116

[4] Allen J 2001 Advances in bioartificial liver devices *Hepatology* **34** 447–55

[5] Nibourg G A A, Hoekstra R, van der Hoeven T V, Ackermans M T, Hakvoort T

B M, van Gulik T M and Chamuleau R A F M 2013 Increased hepatic functionality of the human hepatoma cell line HepaRG cultured in the AMC bioreactor *Int. J. Biochem. Cell Biol.* **45** 1860–8

[6] van de Kerkhove M P, Poyck P P C, Deurholt T, Hoekstra R, Chamuleau R A F M and van Gulik T M 2005 Liver Support Therapy: An Overview of the AMC-Bioartificial Liver Research *Dig. Surg.* **22** 254–64

[7] Gion T, Shimada M, Shirabe K, Nakazawa K, Ijima H, Matsushita T, Funatsu K and Sugimachi K 1999 Evaluation of a Hybrid Artificial Liver Using a Polyurethane Foam Packed-Bed Culture System in Dogs *J. Surg. Res.* **82** 131–6

[8] Yanagi K, Miyoshi H and Ohshima N 1998 Improvement of metabolic performance of hepatocytes cultured in vitro in a packed-bed reactor for use as a bioartificial liver. *ASAIO J.* **44** M436–40

[9] Kinasiewicz A, Gautier A, Lewinska D, Bukowski J, Legallais C and Weryński A 2007 Culture of C3A Cells in Alginate Beads for Fluidized Bed Bioartificial Liver *Transplant. Proc.* **39** 2911–3

[10] Kanai H, Marushima H, Kimura N, Iwaki T, Saito M, Maehashi H, Shimizu K, Muto M, Masaki T, Ohkawa K, Yokoyama K, Nakayama M, Harada T, Hano H, Hataba Y, Fukuda T, Nakamura M, Totsuka N, Ishikawa S, Unemura Y, Ishii Y, Yanaga K and Matsuura T 2007 Extracorporeal Bioartificial Liver Using the Radial-flow Bioreactor in Treatment of Fatal Experimental Hepatic Encephalopathy *Artif. Organs* **31** 148–51

[11] Naruse K, Sakai Y, Nagashima I, Jiang G X, Suzuki M and Muto T 1996 Comparisons of porcine hepatocyte spheroids and single hepatocytes in the non-woven fabric bioartificial liver module. *Int. J. Artif. Organs* **19** 605–9

[12] YANAGI K, OOKAWA K, MIZUNO S and OHSHIMA N 1989 Performance of a New Hybrid Artificial Liver Support System Using Hepatocytes Entrapped Within a Hydrogel. *ASAIO J.* **35**

[13] Dore E and Legallais C 1999 A New Concept of Bioartificial Liver Based on a Fluidized Bed Bioreactor *Ther. Apher. Dial.* **3** 264–7

[14] Wells G D M, Fisher M M and Sefton M V 1993 Microencapsulation of viable hepatocytes in HEMA-MMA microcapsules: a preliminary study *Biomaterials* **14**

615–20

[15] Ambrosino G, Varotto S, Strom S C, Guariso G, Franchin E, Miotto D, Caenazzo L, Basso S, Carraro P, Valente M L, D'Amico D, Zancan L and D'Antiga L 2005 Isolated Hepatocyte Transplantation for Crigler-Najjar Syndrome Type 1 *Cell Transplant.* **14** 151–7

[16] Park J, Berthiaume F, Toner M, Yarmush M L and Tilles A W 2005 Microfabricated grooved substrates as platforms for bioartificial liver reactors *Biotechnol. Bioeng.* **90** 632–44

[17] De Bartolo L, Jarosch-Von Schweder G, Haverich A and Bader A 2000 A Novel Full-Scale Flat Membrane Bioreactor Utilizing Porcine Hepatocytes: Cell Viability and Tissue-Specific Functions *Biotechnol. Prog.* **16** 102–8

[18] Poyck P P C, Hoekstra R, van Wijk A C W A, Attanasio C, Calise F, Chamuleau R A F M and van Gulik T M 2007 Functional and morphological comparison of three primary liver cell types cultured in the AMC bioartificial liver *Liver Transplant.* **13** 589–98

[19] Baccarani U, Sanna A, Cariani A, Sainz-Barriga M, Adani G L, Zambito A M, Piccolo G, Risaliti A, Nanni-Costa A, Ridolfi L, Scalamogna M, Bresadola F and Donini A 2003 Isolation of human hepatocytes from livers rejected for liver transplantation on a national basis: Results of a 2-year experience *Liver Transplant.* **9** 506–12

[20] Hughes R D, Mitry R R, Dhawan A, Lehec S C, Girlanda R, Rela M, Heaton N D and Muiesan P 2006 Isolation of hepatocytes from livers from non-heart-beating donors for cell transplantation *Liver Transplant.* **12** 713–7

[21] Nishikawa M, Kojima N, Komori K, Yamamoto T, Fujii T and Sakai Y 2008 Enhanced maintenance and functions of rat hepatocytes induced by combination of on-site oxygenation and coculture with fibroblasts *J. Biotechnol.* **133** 253–60

[22] Ohno M, Motojima K, Okano T and Taniguchi A 2008 Up-regulation of drug-metabolizing enzyme genes in layered co-culture of a human liver cell line and endothelial cells. *Tissue Eng. Part A* **14** 1861–9

[23] Thomas R J, Bhandari R, Barrett D A, Bennett A J, Fry J R, Powe D, Thomson B J and Shakesheff K M 2005 The Effect of Three-Dimensional Co-Culture of

Hepatocytes and Hepatic Stellate Cells on Key Hepatocyte Functions in vitro *Cells Tissues Organs* **181** 67–79

[24] Zinchenko Y S, Culberson C R and Coger R N 2006 Contribution of non-parenchymal cells to the performance of micropatterned hepatocytes *Tissue Eng.* **12** 2241–1251

[25] Ohno M, Motojima K, Okano T and Taniguchi A 2009 Maturation of the extracellular matrix and cell adhesion molecules in layered co-cultures of HepG2 and endothelial cells. *J. Biochem.* **145** 591–7

[26] Hoshiba T, Nagahara H, Cho C-S, Tagawa Y and Akaike T 2007 Primary hepatocyte survival on non-integrin-recognizable matrices without the activation of Akt signaling *Biomaterials* **28** 1093–104

[27] Kaji K, Norrby K, Paca A, Mileikovsky M, Mohseni P and Woltjen K 2009 Virus-free induction of pluripotency and subsequent excision of reprogramming factors *Nature* **458** 771–5

[28] Spence J R, Mayhew C N, Rankin S A, Kuhar M F, Vallance J E, Tolle K, Hoskins E E, Kalinichenko V V, Wells S I, Zorn A M, Shroyer N F and Wells J M 2011 Directed differentiation of human pluripotent stem cells into intestinal tissue in vitro *Nature* **470** 105–9

[29] Zhou H and Ding S 2010 Evolution of induced pluripotent stem cell technology *Curr. Opin. Hematol.* **17**

[30] Carpentier B, Gautier A and Legallais C 2009 Artificial and bioartificial liver devices: present and future *Gut* **58** 1690–702

[31] Stout D A and Webster T J 2012 Carbon nanotubes for stem cell control *Mater. Today* **15** 312–8

[32] Holy J, Perkins E and Xun Yu 2009 Differentiation of pluripotent stem cells on multiwalled carbon nanotubes *2009 Annual International Conference of the IEEE Engineering in Medicine and Biology Society* (IEEE) pp 6022–5

2. CHAPTER 2. State of the art: Scaffold Design Parameter and Fabrication

This work will be submitted as manuscript for a review paper to Journal of applied polymers: (2016). Fabrication of Scalable and Structured Tissue Engineering Scaffolds Using Water Dissolvable Sacrificial 3D Printed Moulds.

2.1 Introduction

Biomaterial porous scaffold plays a central role in modern regenerative medicine and tissue engineering as it offers a controlled biophysical and biochemical environment that can direct cellular behavior and function. In general, scaffold provides a tentative three-dimensional (3D) support to interact with cells to control their functionality, thereby guiding complex multicellular processes of tissue formation and regeneration [1]. Numerous scaffolds produced in various biomaterials using different fabrication techniques have been used to regenerate different tissues and organs[2]. Regardless of the tissue types, a number of parameters are important when designing or determining the suitability of a scaffold for use in tissue engineering. Fig. 1 illustrates some of the key requirements to be considered before developing smart 3D scaffolds for regenerative medicine [3]. Primarily, the construct should be biocompatible and possibly biodegradable with desired surface properties for cell adhesion, migration and normal functionality. Secondly, since tissues of the human body have selective mechanical properties ranging from soft (brain, about 0.5 kPa), to moderately stiff (skin and muscles, around 10 kPa) and stiff (precalcified bone, >30 kPa) [4], the scaffold construct must have desired mechanical strength and porosity to be able to integrate with the surrounding tissue. Moreover, the size of engineered scaffolds must be very similar to the area of the damaged tissue. In addition, it has been shown that controlled delivery of biological signals from porous scaffolds, such as small drug molecule, growth factors and cytokines in vitro or in vivo, is crucial in the support and enhancement of tissue morphogenesis, viability and functionality [5–7], therefore, the design should consider the physico-chemical properties of scaffold materials so that they can release desired biomolecule to guide and regulate biological responses of the cells into specific tissue. New biomaterials are rapidly emerging, and in future, the research will be directed towards new fabrication methods, which will not only produce materials with various

physical properties, but also offer independent control over their physical, chemical and biological properties [8].

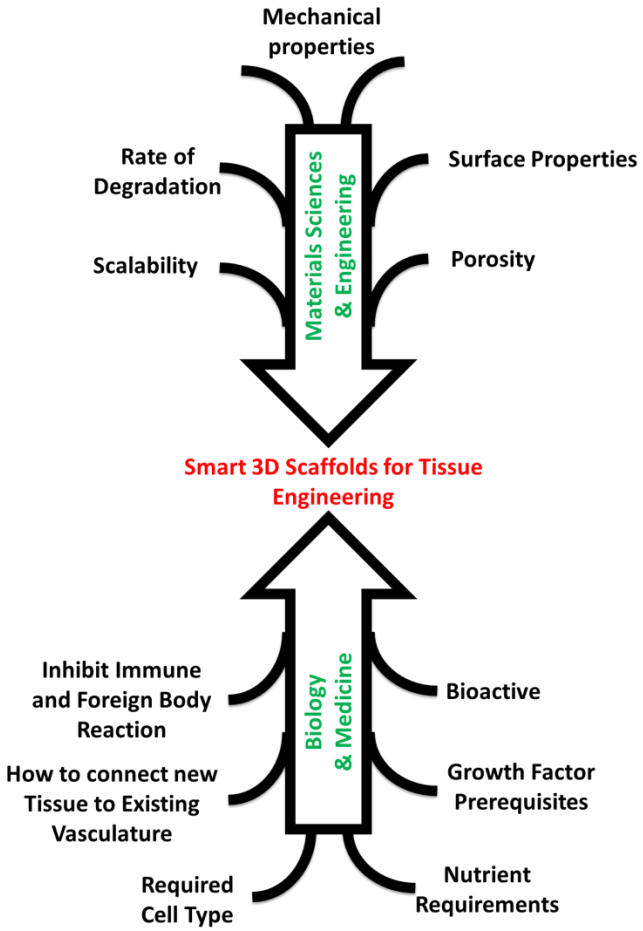

Figure. 1 Schematics of general requirements for developing 3D smart scaffolds for tissue engineering and regenerative medicine [Modified from Ref. [9]]

2.2 Scaffold fabrication methods

Polymer scaffolds need to possess many key characteristics to be useful for tissue engineering, including high porosity and surface area, structural strength, and specific 3-D shapes. These characteristics are largely determined by the scaffold fabrication technique. Until now, various successful fabrication techniques have been developed to process different natural and synthetic biomaterials into 3D polymeric scaffolds for application in tissue engineering and regenerative medicine. The scaffolds fabrication technique can be classified into two major groups as shown in the Fig. 2, I) conventional fabrication techniques also named as "Non-designed controlled scaffold manufacturing" [10], which basically generate polymeric scaffolds with stochastic,

disordered or **random** microporous structures; and II) modern fabrication techniques named as rapid prototyping (RP) or Additive manufacturing (AM) or Solid Free-Form Fabrication (SFF) or "Design controlled scaffold manufacturing"[10], which enable the formation of channels/pores with precisely defined dimensions, location and geometry to generate 3D structured microporous scaffolds. Very recently, a new type of scaffolds fabrication has been generated by combining conventional and modern fabrication methods, which could be categorized as combined fabrication techniques [11–13]. This chapter will briefly highlight a few most commonly used scaffolds fabrication method. At the end special attention will be given to the method which combines of multiple fabrication techniques to design smarter scaffolds.

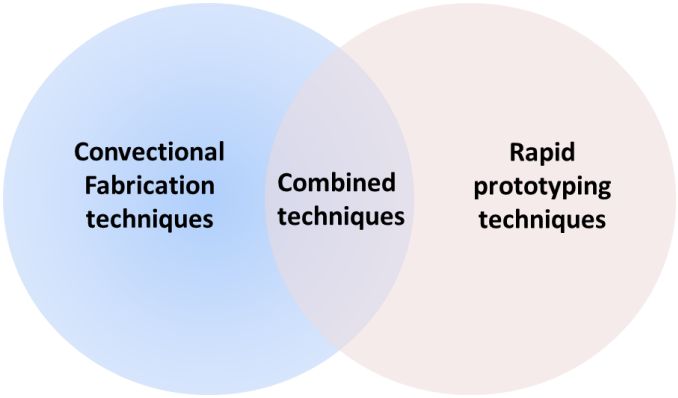

Figure 2. Classification of scaffolds fabrication techniques.

2.2.1 Random Porous Scaffold Fabrication: Using Conventional Methods

Conventional techniques such as phase separation, gas foaming, freeze-drying, solvent casting, thermal processing, electrospinning and particulate leaching as well as combination of these techniques have been used in tissue engineering to generate engineered scaffolds with random foam-like internal structure (as shown in Fig. 3A) [14].

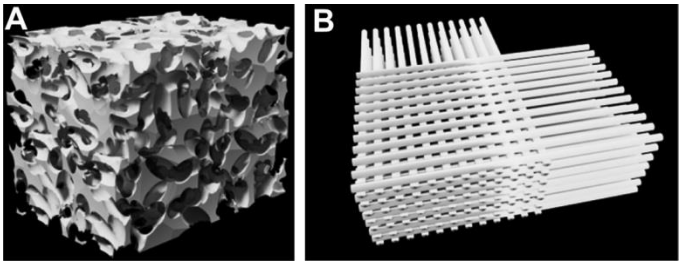

Figure 3. Illustrations of two major types of porous scaffolds with A) random pores B) structured pores.

2.2.1.1 Particulate leaching

Particulate leaching is the most commonly used scaffold fabrication method in tissue engineering and drug delivery applications [15–18]. Briefly, porogen particles (such as salt, sugar and wax, etc.) of desired dimensions were piled up into a mould and the polymer solution is casted into the mould. Subsequently the polymer solution is cross-linked or hardened and the porogen particle was removed using a solvent. The size and the shape of the porogen particles are transferred as pores in the scaffold materials. The great advantages of this process include low cost, scalability of the scaffold size and the control over pore size by varying the size of the porogen particles [16,19]. However the scaffolds fabricated using this techniques has no control on inter pore connectivity and the pore architecture [19,20].

2.2.1.2 Emulsion and phase separation

Another kind of fabrication technique to generate highly interconnected very fine random pore scaffolds is called liquid induced phase separation (LIPS) [21–23] or thermally induced phase separation (TIPS) [24,25]. In TIPS, the polymer is dissolved in a solvent (organic or aqueous) and subsequently cooled down until the polymer-solvent mixture freezes completely. Finally the solvent is removed by freeze drying process to get the 3D porous scaffold. The method can generate scaffolds with very high porosity and different pore sizes by varying freezing temperature [26,27], polymer material, polymer concentration and the type of organic solvent [28]. However, the main draw-back is the small pore size (up to 100 μm) that can be reproducibly obtained by this process [28]. Moreover, the process mainly uses organic solvents and might leach some residues after processing and therefore it is always important to monitor the complete removal of the solvents before doing the biological studies.

Similarly in emulsion freeze-drying, mixture of polymer–solvent system and water leads to formation of an emulsion [29–32]. The emulsion mixture with a continuous phase (polymer rich phase) and a dispersed phase (water) is subsequently cooled down to completely freeze the mixture. The frozen mixture is freeze-dried to create pores through the removal of frozen solvent and water. Emulsion freeze-drying can produce relatively thick scaffolds with large pores [30] compared to phase separation process. The method has been shown to generate scaffolds with porosity greater than 90%, and with medium (15 - 35 μm) and larger (greater than 200 μm) pore sizes [32,33].

2.2.1.3 Electrospinning

Electrospinning (ES) is a scaffold fabrication techniques by which small diameter fibers (ranging from nanometer to micrometer) with large surface areas can be produced. The technology relied on charging of a polymer solution and subsequent ejecting from a capillary tip or needle. The jet coming from the needle draws continuously in a steady manner towards a collector due to an applied high electric field ranging from 10 to 30 kV. Evaporation of the solvent from the jet after leaving the needle results in formation of a randomly accumulated, nonwoven mat of thin polymeric fibers on the collector [34–36].

The size of the nanofibers can be tuned by changing various parameters such as strength of the electric field, distance between the needle and collector, polymer concentration etc[37,38]. Electrospun nanofibers can also be orientated/ aligned either by using a rotating mandrel collector [39] or by inducing the electric field at the edges of the collector plates (Hall Effect) [40]. SEM image in Fig. 5C shows an example of electro-spun silk scaffolds using the method described previously [41]. Nanofiber 3D scaffolds produced from the electrospinning process might be a possible option to mimic the real ECM fibers topography and size. Moreover, high surface area and high porosity of the spun fiber scaffold enhance the cell attachment and facilitate nutrient and waste ex-change. In addition, the process is simple and inexpensive, and can provide tunable fine fiber resolution and controlled fiber alignment to induce cell and tissue alignment. However, in some solution spinning process the toxic organic solvents used during fabrication is not good for cells, but this can be partially solved by using melt spinning of some other polymers [42]. Another drawback of this method lies in limited control of pore structure. The pore size of electrospun scaffolds is dependent on the fiber diameter, and smaller diameter fibers will lead to smaller average pore sizes, which will in turn cause decreased cellular infiltration [43]. Therefore, there is great challenge to engineer 3D scaffolds with complex pore geometry when using ES techniques.

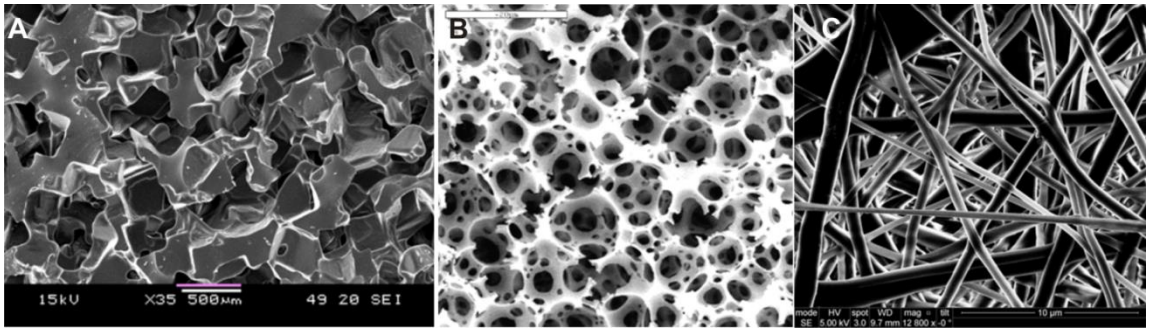

Figure 5. SEM image of a A) salt leached porous scaffold [11]. B) Typical polystyrene-based emulsion-templated (PolyHIPE) materials. [44]. C) Electrospun silk scaffold (unpublished). Scale bar: A = 500 µm, B= 20 mm and C= 10 µm.

As described above, conventional fabrication techniques are quick, scalable and economical, and advantageous in generating fine pore structures. However, they do not permit accurate control over the scaffold's micro-architecture such as the pore size, shape, interconnections and spatial distribution of pores within the scaffold [45]. The tortuous (i.e. as the ratio of the actual length of the arbitrary pathway that a molecule has to cover to pass through a pore to the shortest linear distance) pathways created by the random porous scaffolds is another major limitation for nutrient supply, waste removal and effective release of biological signals [3]. Even though the random scaffolds has very large surface area for cell attachment and proliferation, their high pore tortuosity limits the cell viability normally to 0.5–1 mm into the scaffolds [46,47]. Furthermore it has also been shown that such random pore morphology is associated with drop in the oxygen concentration from the outside to the center of the scaffold [48,49].

2.2.2 Structured porous scaffold fabrication: using solid free-form fabrication / rapid prototyping (RP)

To overcome the challenges of conventional scaffold fabrication techniques, various RP techniques recently have emerged arise where a 3D object is manufactured through layer by layer assembly process. The resulting scaffold (Fig. 3B) possesses tunable porosity, pore size and shape with complete interconnection of pores in all the directions, which improves the cell migration, proliferation and nutrient perfusion compared to scaffolds fabricated with conventional techniques.

Presently, computational techniques have allowed designing 3D anatomical porous scaffolds with balanced mass and oxygen transport properties. The philosophy of the method is to create objects by adding material layer-by-layer. It is therefore generally referred to as additive manufacture (AM) to distinguish it from conventional machining which removes material in a subtractive manner [14]. The basic principle for all current rapid prototyping techniques are mainly constructing a computer-aided design (CAD) model of a complex object, then converted into series of cross-sectional parallel layers (STL format). The RP machine manufactures the whole object by reproducing in a layer-by-layer fashion. The first layer of the physical object is created and then lowered by the thickness of the next layer. The process is repeated continuously until completion of the object. Finally the object is removed from the base platform of the machine.

There are various ways to classify the fabrication techniques either based on the type of printing principle or on type of material used in the printer. Here, some of the most common fabrication techniques used in tissue engineering scaffolds fabrication based on different printing principle is classified in Fig. 6.

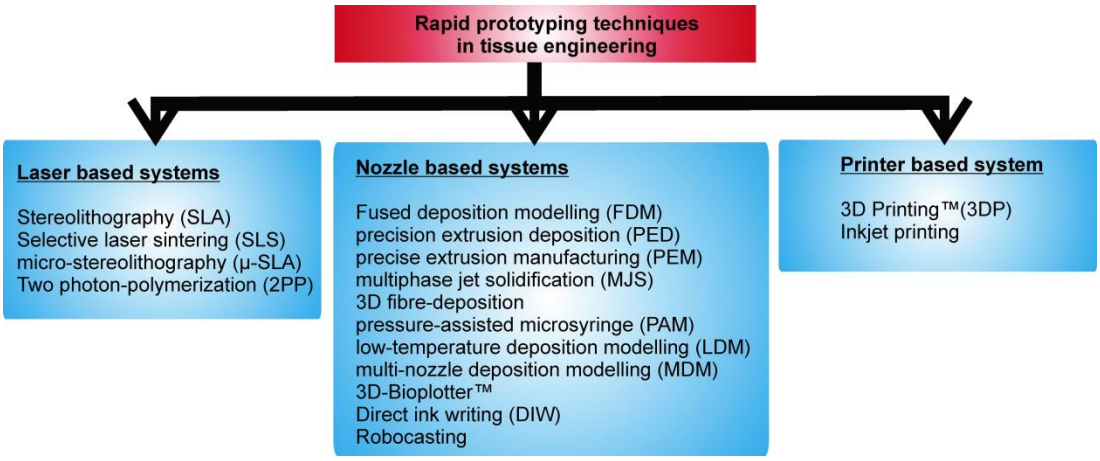

Figure 6. Classification of various RP techniques used for fabricating tissue engineering scaffolds through laser-, nozzle-, and printer-based systems. [figure modified from reference [50]]

2.2.2.1 Laser based system

Stereolithography (SLA) is laser based RP technique which uses photo-curable resin in a layer-by-layer fashion to build 3D solid objects (Fig. 7A)[51–53]. A 2D layer of the designed pattern is traced with a laser on the surface of the resin reservoir and photo-polymerizes the resin. After the first layer is cured, z-stage of the machine lowers the structure by few microns and a thin layer of uncured resin is spread on the surface of the

previously cured patterned layer. This process is repeated until the desired final solid 3D object is completed. After being built, in the post-treatment steps the printed 3D object is washed in a chemical bath in order to remove excess resin and is further cured in an ultraviolet oven. The resolution of each layer is very much dependent on the elevator layer (z-step thickness) and the spot size of the laser. In μ-SLA, a single spot laser micro features with 10 μm resolution with a 1 μm *z*-step thickness can be produced [54], but the fabrication time is significantly increased in order to achieve such high resolution. To reduce the fabrication time, the laser can be replaced with a digital photo mask [52] to cure each layer of the whole 3d object in one step. The method allows to fabricate variety of 3D shapes with much higher resolution and surface smoothness compared to other RP techniques. However, SLA techniques usually take longer time to fabricate a 3D structure and the printing materials are also more expensive. As material properties may vary over time, special care must be taken in handling printing materials.

Similar to SLA, in **selective laser sintering (SLS)** technique, the laser selectively fuses powdered material by scanning cross-sections generated from a 3D digital description of the part on the surface of a powder bed. After each cross-section is scanned, the powder bed is lowered by one layer thickness, a new layer of material is applied on top, and the process is repeated until the part is completed. Such technique has been utilized mainly for creating bone tissue engineering constructs for example temporomandibular joint (TMJ). It provides a cost effective, efficient method to construct scaffolds to match the complex anatomical geometry of craniofacial or periodontal structures. Virtually any powdered biomaterial that will fuse but not decompose under a laser beam can be used to fabricate scaffold by SLS. [55]. However, limiting factors include the requirements of post-processing steps and the instability of the materials over time.

Along with other 3D printing technologies, two-photon polymerization (TPP) microfabrication induced by a near-infrared femtosecond laser can fabricate arbitrary and ultraprecise 3D microstructures with high resolution not only on the microscopic scale but also on the nanoscale [56]. The TPP process is initiated by three-order nonlinear absorption within the focal region. 3D structures can be fabricated by moving the focused beam in photoresist according to a computer-designed 3D route with the resolution beyond the optical diffraction limit. Particularly, 3D hydrogels have been achieved by ongoing intense research activity due to their promising biomedical applications in tissue engineering and drug delivery. Many strategies have been developed to

improve the resolution of TPP to be less than 100 nm. In TPP, the spatial resolution is dominantly determined by laser power and exposure time, which largely depends on the efficiency of TPP initiators

Even though laser based technique has produced various hard and soft scaffolds, the application of process in tissue engineering is very limited due to the lack of photo-curable materials that are suitable for biomedical applications.

2.2.2.2 Nozzle-based technique

Another major group of fabrication techniques most widely used are nozzle-based system which process materials either thermally or chemically as it passes through the nozzle. **Fused deposition modeling (FDM)**[57,58] is type of nozzle-based RP technique where melted plastic filaments[59,60] or hydrogels[61,62] or biomaterial solutions [63,64] are deposited onto a build platform via a small temperature controlled extruder, layer by layer to make the 3D object (Fig. 7B). The base platform gets lowered at the end of each deposited layer so that subsequent layer can then be deposited. Each layer hardens as it is deposited and bonds to the previous layer. Elevated temperature is used in the inexpensive FDM based filament printing machines, which limits the type of biomaterials that can be employed.

2.2.2.3 Printer based system

3DP^{TM} is one of the printer based rapid prototyping techniques, where liquid binder is deposited on to sequential polymer powder layer as similar to ink-jet printing techniques. The process flow of the technique is described below in Fig. 7C. The position of the jet is controlled via a computer-assisted design and manufacture (CAD/CAM) program. 3D objects can be made layer by layer with a resolution around 50–300 μm. The polymer powder can be mixed with the salt to generate pores for porous scaffold fabrication. Various materials such as ceramics, metal, metal-ceramics composite and polymers can be processed using this technique. Even though the resolution of the printer is determined by the jet size it is difficult to fabricate scaffolds with fine micro-structures.

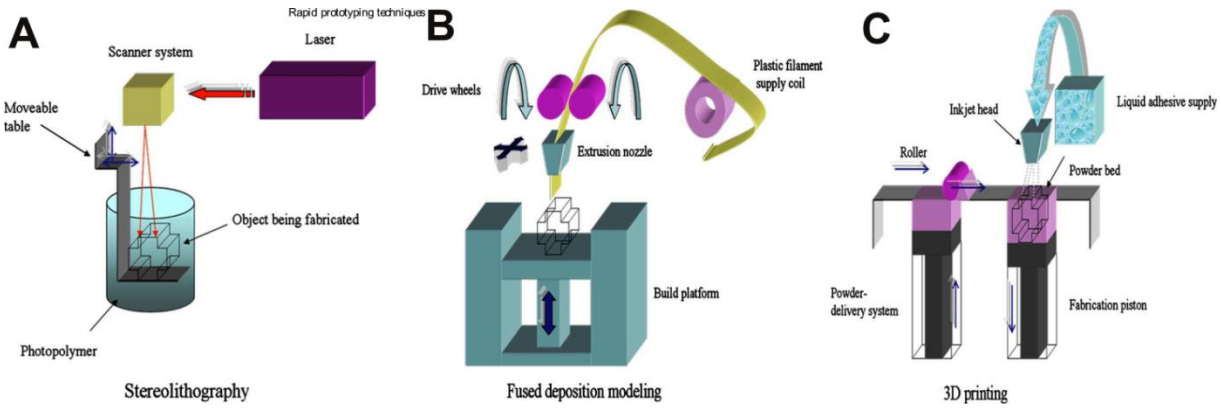

Figure 7. Schematic representations of different types of 3D printer systems. A) Stereolithography (SLA) system. An ultraviolet (UV) laser is used to solidify the model's cross-section while leaving the remaining areas in liquid form. The movable table is then lowered drops by a sufficient amount to cover the solid polymer with another layer of liquid resin. B) Fused deposition modeling (FDM) system. FDM uses a moving nozzle to extrude a fiber of melted polymeric material from which the physical model is built layer by layer. C) A typical 3DP^{TM} printer, a stream of adhesive droplets is expelled through an inkjet print head, selectively bonding a thin layer of powder particles to form a solid shape [figure modified from reference [55]].

Although RP techniques have currently gained an wide spread attention in the field of tissue engineering, each RP techniques discussed above has its own unique advantages and disadvantages in terms its capability to process different materials, printing resolutions and the processing conditions, summarized in Table. 1[55].

Table 1. Classification of AM techniques on the basis of printing materials employed for the production of tissue-engineering scaffolds with pros and cons [45,65].

Technique	**Materials**	**Resolution (μm)**	**Advantages**	**Disadvantages**
Powder-based techniques				
Stereolithography (SLS)	Polymer, ceramic or composites Ex. PEEK-HA, Polycaprolactone (PCL)	50–1000	No support material needed	Laser intensity can induce polymer degradation; scaffolds generally present low mechanical properties, limited and high-cost materials,

				trapped non-sintered material, poor control over surface topography
Three dimensional printing (3DP)	Polymer, ceramic or composites Ex. PLGA, starch based polymer	50–300	No materials heating involved in the fabrication process, no support material needed, high production rate, possibility of producing large size samples	Structure shrinking upon sintering, trapped non-bound material, low scaffold mechanical properties, high roughness of scaffold surface
Photosensitive polymer based techniques				
selective laser sintering (SLA)	Polymers: PEG-DA, hydrogels: methacrylated-Gelatin, HEMA, mixture of methacrylated-Gelatin and hyaluronic acid-methacrylate	14–150	Relatively easy to remove supports, possibility of encapsulating cells	Necessity of removing non-polymerized resin, post-curing generally required, shrinkage of the scaffolds due to post-processing steps, few suitable biocompatible and biodegradable materials
μSLA	methacrylated-Gelatin, PEG-DA,	0.5–10	High accuracy, small amount of photosensitive material necessary	Limited overall scaffold size

	and alginate + acrylated			
Two-photon μSLA	Polymers: PEG-DA	0.1–4	Possibility of producing scaffolds without layers superimposing, high accuracy	Limited overall scaffold size, distortion and shrinkage can occur
Melt–extrusion / thermoplastic based techniques				
(Fused deposition modeling (FDM), Precision extruding deposition (PED), Bioplotter, Bioextruder and Bioscaffolder)	Polymer, composites Ex. PCL, PP-TCP, PCL-HA, PCL-TCP, PLLA-TCP	100–500	Good mechanical properties, no materials trapped into the scaffold	Possible thermal degradation of polymers, relative regular structure, supports needed for structure overhangs
Solution/slurry extrusion-based techniques				
Pressure-assisted microsyringe (PAM)/PAM2	Polymers (PAM), hydrogels and cells (PAM2)	10–1000	Possibility of producing hydrogel scaffolds encapsulating cells (PAM2)	Organic solvents (PAM)
Low-temperature deposition manufacturing (LDM)	Composite slurries	300–500	High accuracy on deposition of polymeric slurries, microporosity due to freeze drying	Organic solvents
Robocasting	Ceramics or composites, Organic ink	100–1000	Highly concentrated colloidal suspensions can be used	Sinterization necessary in most cases. Precise control of ink

				properties is crucial

Abbreviations: HA, hydroxyapatite; PCL, polycaprolactone; PEEK-HA, polyether-etherketone-hydroxyapatite; PEGT-PBT, poly(ethylene glycol)-terephthalate-poly(butylenes terephthalate; PLLA, poly-L-lactide; PP-TCP, polypropylene-tricalcium phosphate.

2.2.2.4 Indirect RP fabrication method

As discussed above, various RP methods have attracted a lot of attention for directly creating micro-scale porous structure scaffolds with desired complexities [14], but all of the RP technologies are very specialized due to the fact that each technique demands a specific form of printing material such as filament, powder, solid pellet or photocurable polymers [10,45,65]. Consequently, it is challenging to fabricate scaffolds using materials which are not compatible with RP i.e, silicone elastomer, natural and synthetic hydrogels. One solution is to use indirect RP methods which first fabricate a sacrificial mould and then make a reverse structure using materials suitable for tissue engineering. Recently we have developed a multistep process (an example shown in Fig. 8) where the desired scaffolds material is casted around the sacrificial mould, crosslinked and the mould is removed by dissolving in appropriate solvent to yield the final scaffold. Such technique has the opportunity to control the scaffolds internal and external architecture with the desired materials of choice. A 3D microvascular network within polymer matrices has been fabricated by 3D printing of sacrificial wax moulds, casting of low viscosity epoxy around the moulds and subsequent removal of the moulds [66,67]. However, the use of wax (which has a melting temperature of about 60°C) limits the materials that can be cast around the mould since polymers requiring higher temperatures for cross-linking cannot be employed. Furthermore, the complete removal of the sacrificial wax components (which may not be biocompatible) can be challenging, in particular for large 3D structure with complex geometry.

Perfusable 3D scaffolds have also been demonstrated in a similar manner by casting extracellular matrix (ECM) containing cells around a 3D printed sacrificial sugar glass lattice and subsequently dissolving the lattice to form vascular networks [68]. However, it is probably difficult to print large 3D structures in the very brittle sugar glass, and the

inter-filament distance (defined by the printing process) is limited to a minimum of 1 mm. It may not be feasible to use this technique for creating dense vascular channels in large scale structures. Recently we have shown a new scalable approach involving 3D printing (using a commercially available filament based 3D printer) of a sacrificial polyvinyl alcohol (PVA) mould whose geometrical features are designed according to the required vascular channel network [69]. PVA is an ideal material because of its biocompatibility and water solubility. In addition, its high melting temperature (190°C) makes it robust for subsequent polymer casting and curing steps.

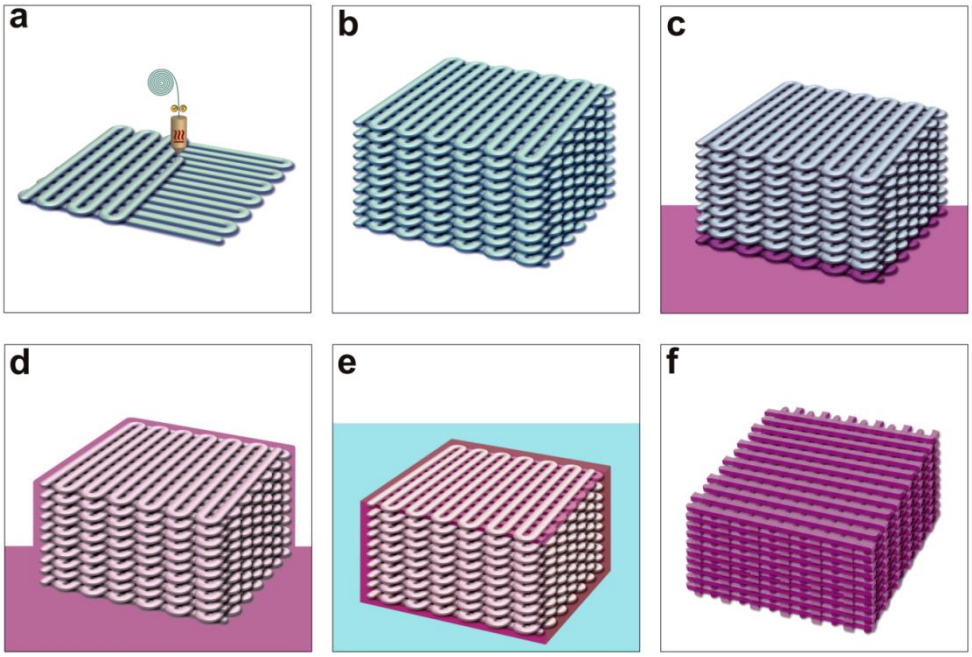

Figure 8. Schematic illustration of the steps involved in the fabrication of SFF porous elastomeric scaffolds. A sacrificial 3D mould was printed in PVA (a, b). The printed PVA mould was transferred into a container containing pre-cured PDMS (c). Vacuum was applied to ensure complete filling of pre-cured PDMS into the pores of the mould (d). Following crosslinking of the PDMS, the sacrificial PVA mould was dissolved in water (e) leaving behind the structured PDMS scaffold (f). [from our result chapter 3 [70]]

In general, RP allows easy variation of the internal architecture of a scaffold, which in turn can lead to optimized specific surface area, scaffold mechanical response to external stress, and flow resistance in a bioreactor [14]. The control of internal architecture of the scaffold can ultimately ensure the desired mechanical properties of the scaffold. Another main advantage of the technique is that the scaffolds can be tailored to match

the size of the damaged body parts. Organized pore structures of the RP scaffolds offer possibilities for regulation of efficient supply of nutrient and oxygen, which holds the promise for clinical applications.

However, these techniques also present some drawbacks, in particular low resolution (around 200-500 μm). These techniques therefore only allow fabrication of scaffolds with large pore dimensions much larger than the sizes of a cell, which ultimately leads to non-uniform cell distribution around the scaffold and low cell seeding efficiencies around 25-40% [71]. In RP scaffolds, due to the large pore size, cells generally falls through the gaps of the scaffold. The attached cells on structured pore scaffolds forms 2D monolayers on the surface of the printed layers, so the cell to cell communication is greatly reduced compared to 3D tissue organization.

2.2.3 Next generation smart scaffolds: integration of multiple fabrication methods

To overcome the disadvantages of conventional and RP methods, the third generation of scaffold fabrication techniques, so called combined fabrication methods (Fig. 4) have been proposed, which can generate scaffolds comprising structured pores (channels) in combination with local random porous regions. The structured pores help overcome the diffusion limitation, while the random pores provide a large surface area to accommodate high density of cells. By promoting rapid vascularization and improving nutrient and oxygen transport, the dual-pore scaffold can greatly enhance survival rate of the seeded cells. It is therefore a promising strategy to engineer large-scale artificial tissues or organs for regenerative medicine [13,72–77]. Recently it has been demonstrated that post-transplantation of a dual-porous scaffolds enabled more cells from the host tissue infiltrated into the scaffolds, hence, enhancing integration of blood vessels in the host tissue [78]. The dual-pore scaffold can be produced in several ways, such as combining conventional techniques with AM, microfabrication, or wire array molding process.

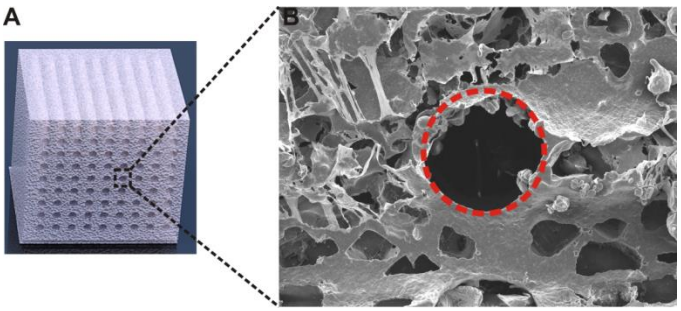

Figure 4. A) Illustrations of dual-pore scaffolds and B) SEM image of and PCL dual-pore scaffold, red circle shows the structured pore region and the random pore regions are present around it.

2.2.3.1 Combined microfabrication with conventional techniques

L. S. Wray et al. has shown a method of generating a dual pore scaffold where micro-channels fabricated using microfabrication and soft lithography were integrated into a porous TE silk scaffold [79] to mimic the scaffold supporting co-culturing of two cell types in two different pore compartments. Incorporated porous microchannels supported endothelial cells for the development of vascular tube, while the microporous scaffolds surrounding the microchannels were loaded with human mesenchymal stem cells for supporting the tissue formation. The Schematic of the micropatterned porous silk scaffold fabrication is shown in the Fig. 14.

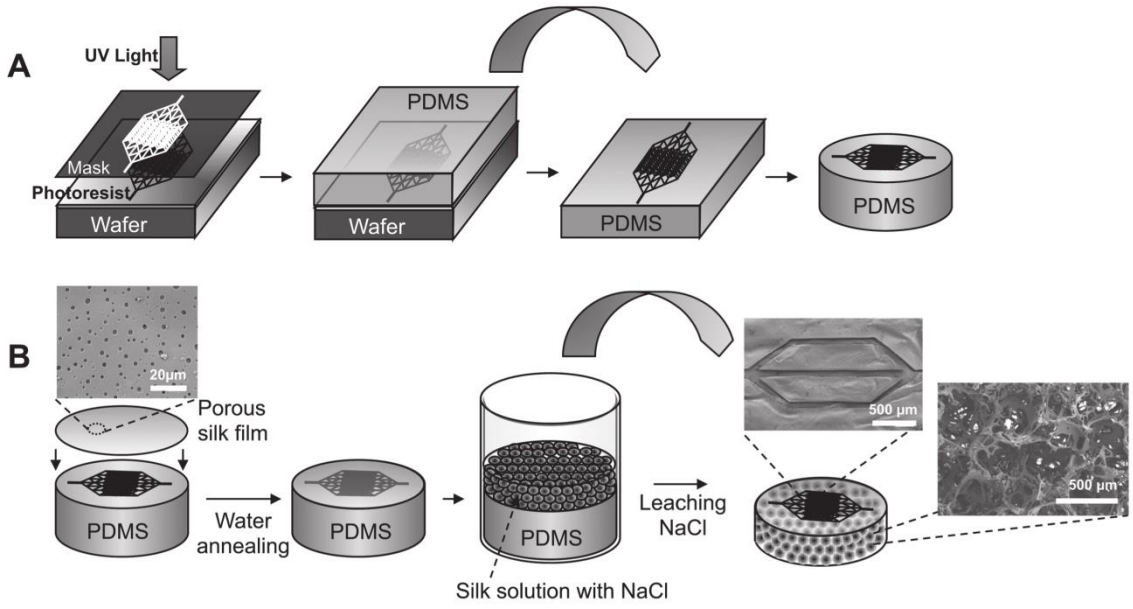

Figure 14. Schematic of micropatterned porous silk scaffold fabrication. A) Microfluidic channel patterns are transferred from a silicon wafer to polydimethyl siloxane (PDMS) using standard photolithography and soft lithography techniques. The PDMS mold is trimmed to the desired shape and size. B) A porous silk film is cast over the PDMS mold and crosslinked to induce β-sheet crystallinity. An aqueous-derived salt leached silk scaffold is assembled over the silk film. The scaffold is cured and removed from the PDMS mold. SEM images show patent microchannels on the surface of the scaffold and 100–350 μm diameter interconnected pores in the bulk of the scaffold. [Reproduced from reference [79]]

2.2.3.2 Combined wire array molding process with conventional techniques

Similar to dual-pore scaffolds fabrication techniques using AM discussed above, indirect manual assembly fabrication approaches have been developed [12,13,78,80]. In such proposed technique dual-pore scaffolds were fabricated by combining both salt leaching using powder/freeze drying and wire array network molding. The basic fabrication process flow as shown in Fig 15, a mould was fabricated with inserted various metallic wires which interns defines the structures linear pores in the final scaffold. For dual pore silk scaffold the liquid silk solution was poured into the mould and freeze dried using various temperatures depending up the required random pore size. After freeze drying the scaffold was crosslinked and the metallic wire was removed to yield the final dual-pore silk scaffold. However in case of combination of salt leaching process salt particle of desired size was mixed with the polymer materials such as PCL crystals and loaded in between the metallic wires of the mould and heated with required temperature to melt the PCL and the mould was pressed mechanically to fill the salt and polymer uniformly into the mould. Finally the mould was cooled down, both the metallic wire removed manually and salt particles were leached out in water. The salt crystals was therefore replicated as random pores into the PCL scaffold.

This simple fabrication technique offers a unique and versatile tool for engineering 'tailored' scaffolds for a range of tissue engineering application. The process offers the possibility to scale the scaffolds from millimeters to centimeters to mimic the size of anatomical organs/tissues with the hollow channel arrays supporting localized and confluent endothelialization. However the published results have shown that freeze-drying cannot yield as large a range of pore dimensions as salt leaching, which can utilise salt crystals of various dimensions depending on the requirements. Moreover metal wire based moulding process requires the choice of wire dimensions to achieve the desired pore dimension and time consuming by manual assembly of a number of wires.

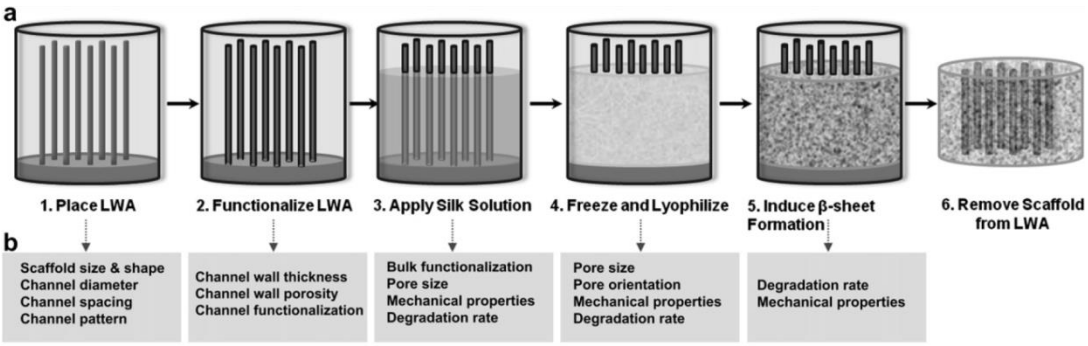

Figure 15. Silk scaffolds with hollow channels. (a) Schematic of the fabrication process for building silk-based porous scaffolds containing hollow channels using a linear wire array. (b) At each step in the process there are avenues for tuning the scaffold bulk properties (e.g. porosity, mechanical stiffness, and degradation rate) and the hollow channel properties (e.g. diameter, spacing, bioactive agent functionalization and wall morphology).

Dual-pore scaffolds comprising both global structured and local random pores, have shown tremendous potential towards engineering of complex tissues with better cell proliferation due to improved nutrient and oxygen transport [13,72–77]. This has also been demonstrated that upon transplantation of a dual-porous scaffolds into the mice, cells from the host tissue infiltrated rapidly into the scaffolds due to its smart global pore architecture compared to random porous scaffolds, hence, enhancing *in-vivo* integration of the scaffolds with host blood vessels [78]. The structured pores of the dual pore scaffold help overcome the diffusion limitation while the random pores provide a large surface area to accommodate a high density of cells. Therefore, dual-pore scaffold design with perfusable channels serves as a promising strategy for engineering of large-scale artificial tissues or organs for regenerative medicine by promoting rapid vascularization that enhances survival of the seeded cells.

2.2.3.3 Combined AM with conventional Fabrication techniques

Combination of AM with conventional scaffolding techniques such as ES, freeze-drying, salt leaching, etc., offers new opportunities to generate porous scaffolds with nanotopography.

Very recently S.M. Giannitelli et al. has summarized the advances in the combination of AM with other fabrication methods for the production of TE scaffolds and classified various fabrication techniques into three major categories based on achieved level of integration: i) assembly level; ii) fabrication level; and iii) technique level (Fig. 9) [81].

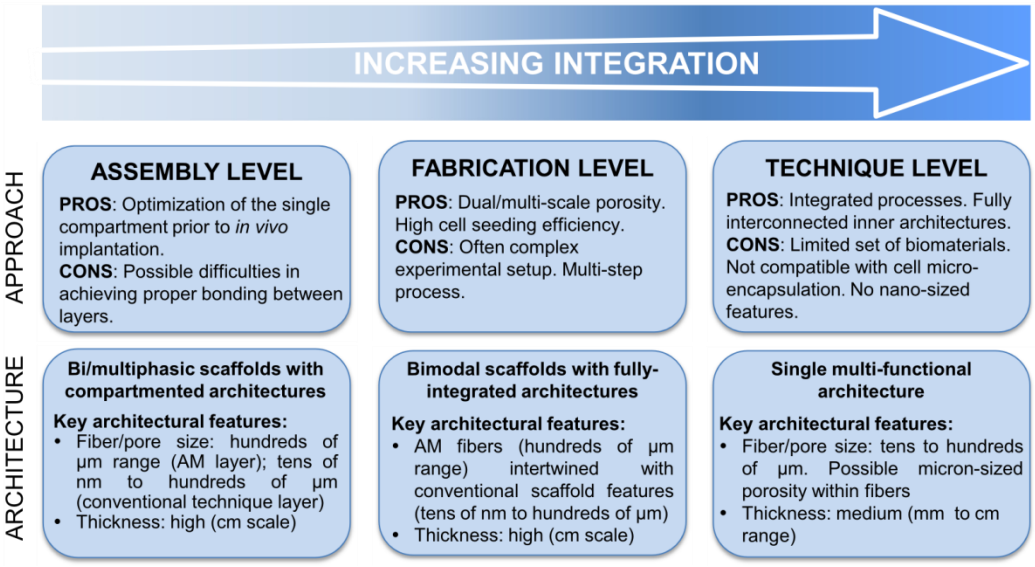

Figure 9. Classification of combined additive manufacturing approaches, with the accent on the achieved level of integration. Major pros and cons each approach, together with the key scaffold architectural characteristics are presented. Combination of AM with ES has been chosen as a representative example for the illustration of manufacturing equipment and obtained microstructures. [Reproduced with the permission from [81]]

Assembly level: At this level, ‘‘multiphasic scaffolds” that contain two or more regions with different topologies are generated [34]. In the following example, a 3D porous biphasic scaffold was fabricated with two different techniques and joined manually together (Fig. 10A&D). Firstly, PLGA/TCP skeleton wrapped in type I collagen was fabricated using the nozzle based rapid prototyping technique for the bone scaffold. The sponge-like chondral phase scaffold (Fig. 10C) was constructed using bovine cartilage extracellular matrix-derived scaffold by a modified TIPS conventional fabrication technique, as previously explained (Fig. 10B). Individual fabricated constructs were fused for each other to get the compact 3D scaffolds.

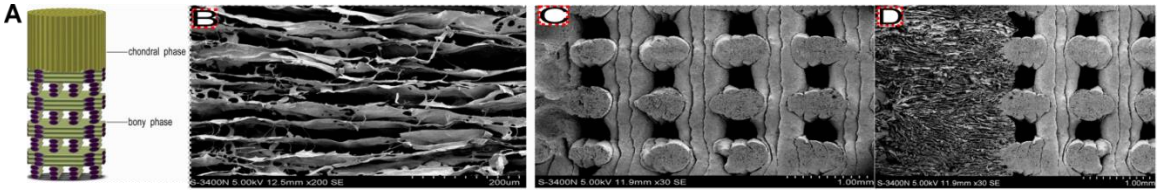

Figure 10. A) Schematic diagram of the compact layer-free biphasic scaffold. SEM images of the biphasic scaffold with B) the chondral phase C) the bony phase and D) the fused compact biphasic scaffold. [Reproduced from reference [82]]

Recently we have developed a fabrication method for dual-pore scaffold with both defined structured and random pores microarchitectures using the sacrificial 3D printed structured porous PVA filament moulds filled with salt crystals in the inter-filamentous space (**Fig. 11**). The fabrication method is simple and involves casting of the desired polymer in the mould, which specifies the microarchitecture of pores within the resulting scaffold. The scaffolds generated through such combined indirect 3D printing and salt leaching process have structured pores distributed in x, y and z directions, and random pores placed in between the structured pores of the bulk scaffold. The detail fabrication method is discussed in chapter 4.

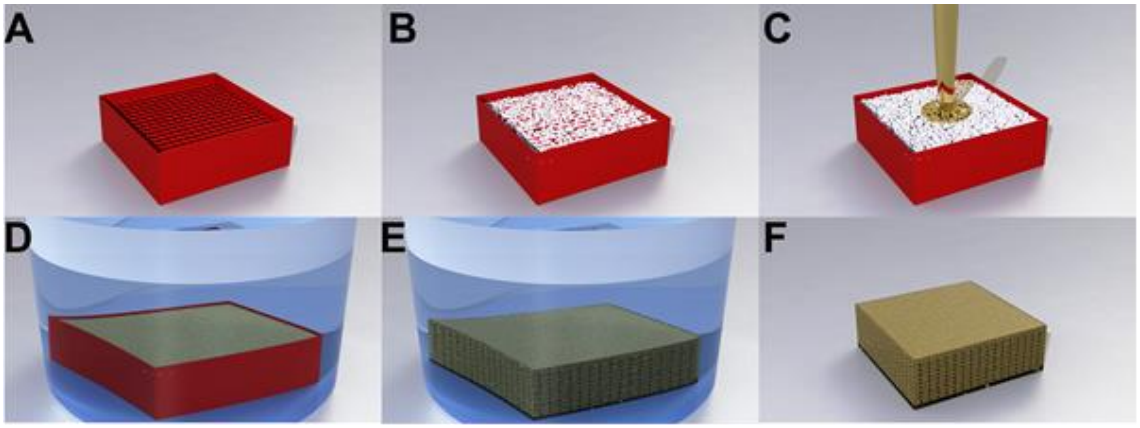

Figure 11. Fabrication of dual-pore scaffolds: A sacrificial 3D mould was 3D printed in PVA (A) and packed with salt crystals (B). The salt-filled PVA mould was transferred into a container and PDMS was cast to cover it (C). Vacuum was applied to ensure complete filling of PDMS into the pores of the mould (D). Following crosslinking of the PDMS, the sacrificial PVA-salt mould was dissolved in water (E) releasing the dual-pore PDMS scaffold (F) [11].

Fabrication level: ‘‘Bimodal scaffolds” that contain micro/nano-features inter- twined within the same architecture are generated at this level. As an example, a scaffold consisting of a microfibrous woodpile structure and nanofibrous matrices was introduced to mimic the biophysical environment (Fig. 12) [77]. The scaffold was produced by a hybrid two-step process using two different polymer solutions as shown in Fig. 12A. The woodpile-like structure was fabricated by a layer-by-layer direct polymer melt deposition (DPMD) approach. The polymeric nanofiber matrix was then spread onto the microfiber layer by ES. Subsequent microfiber layers combined with nanofiber matrices were repeatedly laminated onto the previously combined layers so that a 3D hybrid

structure was fabricated. While the DPMD process was carried out, a microfilament in a semi-molten state was extruded onto the prior unit layer. As it solidified for a few seconds, the microfilament adhered to a local region, where it came in contact with the prior unit layer. Every unit layer, therefore, was attached to the adjacent layers to form a complete 3D hybrid structure. This device was designed in such a way that the two processes could be carried out in an automated fashion. The structure fabricated (Fig. 12B) by the DPMD process provides the mechanical support and overall shape of the resulting hybrid scaffold while nanofibrous structure of the scaffold mimics the natural extracellular matrix (ECM).

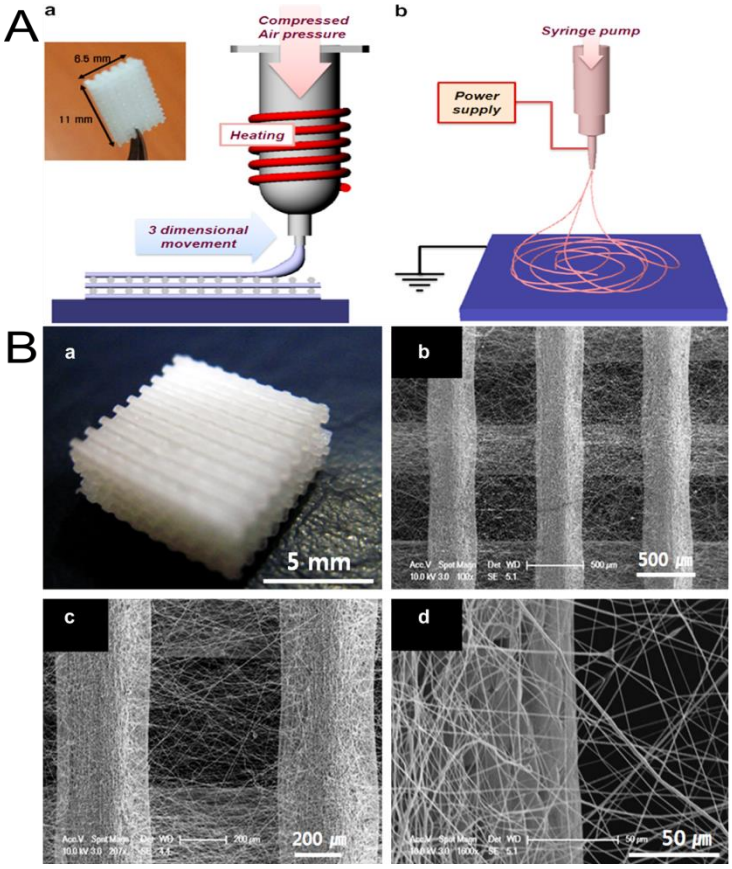

Figure 12. A) The developed hybrid process. Hybrid scaffolds containing microfibers and nanofiber matrices could be built via a combined process of continuous DPMD and ES. B) (a) Photograph of the overall 3D woodpile structure with dimensions of 9 mm x 9 mm x 3.5 mm; (b) the hybrid basic unit layer composed of microfibers and the electrospun nanofibers matrix; (c and d) magnified images of (b). [Reproduced from reference [77]]

Technique level:

Most recent works have tackled integration at the technique level by fusing the working principles of different fabrication techniques into a single, novel technology. In the following, we will refer to this last approach as ‘‘hybrid AM”.

Doej et.al has produced a novel nanocomposite scaffold for bone tissue engineering which was made of chitosan (Chit) and nano-bioactive glass (nBG) and retained dual-pore structure using a robocasting technique [83]. In this technique, composite solution was dispensed through a robot in a layer-by-layer fashion, and was rapidly solidified under a dry-ice cooled bath and freeze dried afterwards (Fig. 13A). The scaffold generated featured the pre-designed macro channeled (hundreds of micrometers) pore configuration due to the robotic dissension process and contained as well micropores (a few to 10 μm in size) throughout the framework as a result of the freeze drying process (Fig. 13B). In this fabrication technique two different scaffold fabrication processes such as AM and conventional random porous scaffolds fabrication methods were assembled together to generate a dual-pore scaffold.

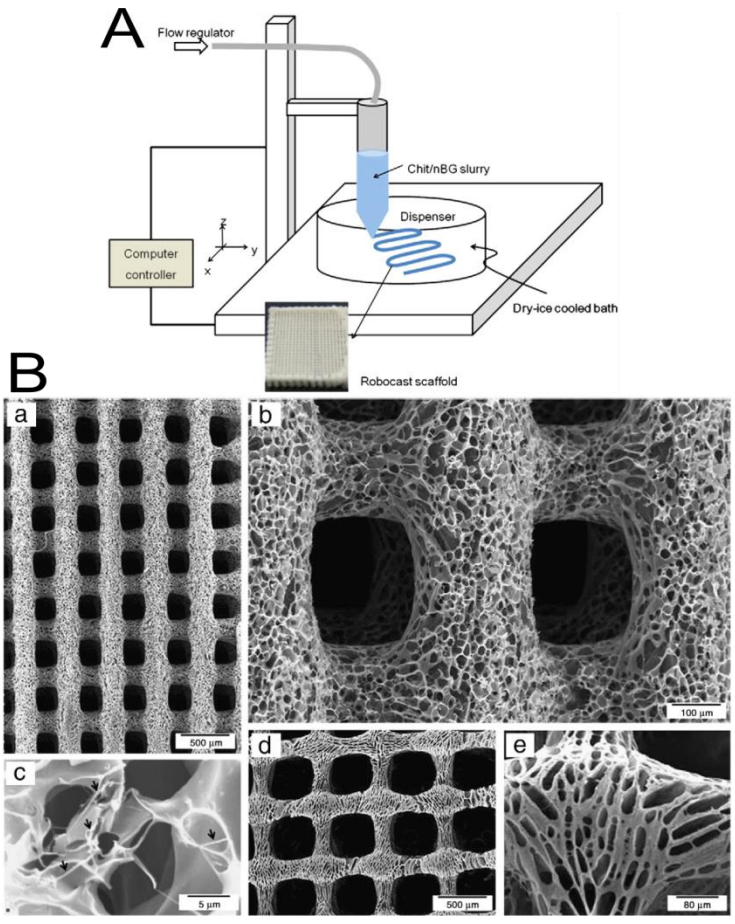

Figure 13. A) Schematic drawing of the robocasting technique to produce Chit/nBG nanocomposite scaffold. Robotic dispensing of the composite solution (10% nBG) and

layer-by-layer construction were possible by maintaining dry-ice cooled conditions. Optical image of the produced scaffold is also shown. B) SEM morphologies of the robotic-dispensed scaffolds; (a–c) Chit/nBG and (d,e) Chit, taken at different magnifications. Micropores were well in both types of scaffolds, through the rapid-solidification of ice crystals and the subsequent freeze-drying process. The existence of nBG was noticed in the nanocomposite scaffold (c). [Reproduced from reference [83]]

2.3 Conclusions

Recently in the field of tissue engineering, significant advances have been made in terms of scaffold biomaterials, smart scaffold design, and fabrication methods to control their in-vitro microenvironment, which has increased the hope for tissue engineering-based treatment in clinics. This review discussed various scaffold design parameters and fabrication technologies. The challenge still remains to find a proper combination of desired biomaterials and fabrication techniques to meet the requirements for a successful TE approach. Since past few years, a few of the dual pore fabricated scaffolds have shown tremendous potential in terms of *in vitro* and *in vivo* studies compared to random and structured porous scaffolds. In future significant efforts need to devote to the dual pore scaffold fabrication process, new types of biomaterials with desired mechanics and more tenability, as well as understanding of the cellular behaviors in different pore geometry of the scaffolds.

2.4 References

[1] Lutolf M P and Hubbell J a 2005 Synthetic biomaterials as instructive extracellular microenvironments for morphogenesis in tissue engineering. *Nat. Biotechnol.* **23** 47–55

[2] O'Brien F J 2011 Biomaterials & scaffolds for tissue engineering *Mater. Today* **14** 88–95

[3] Moroni L, de Wijn J R and van Blitterswijk C a 2008 *Integrating novel technologies to fabricate smart scaffolds.* vol 19

[4] Rehfeldt F, Engler A J, Eckhardt A, Ahmed F and Discher D E 2007 Cell responses to the mechanochemical microenvironment-Implications for regenerative medicine and drug delivery *Adv. Drug Deliv. Rev.* **59** 1329–39

[5] Dvir T, Timko B P, Kohane D S and Langer R 2011 Nanotechnological strategies for engineering complex tissues. *Nat. Nanotechnol.* **6** 13–22

[6] Richardson T P, Peters M C, Ennett a B and Mooney D J 2001 Polymeric system for dual growth factor delivery. *Nat. Biotechnol.* **19** 1029–34

[7] Quinlan E, López-Noriega A, Thompson E, Kelly H M, Cryan S A and O'Brien F J 2015 Development of collagen–hydroxyapatite scaffolds incorporating PLGA and alginate microparticles for the controlled delivery of rhBMP-2 for bone tissue engineering *J. Control. Release* **198** 71–9

[8] Mitragotri S and Lahann J 2009 Physical approaches to biomaterial design *Nat. Mater.* **8** 15–23

[9] Seal B 2001 Polymeric biomaterials for tissue and organ regeneration *Mater. Sci. Eng. R Reports* **34** 147–230

[10] Hollister S J 2009 Scaffold design and manufacturing: from concept to clinic. *Adv. Mater.* **21** 3330–42

[11] Mohanty S, Sanger K, Heiskanen A, Trifol J, Szabo P, Dufva M, Emnéus J and Wolff A 2016 Fabrication of scalable tissue engineering scaffolds with dual-pore microarchitecture by combining 3D printing and particle leaching *Mater. Sci. Eng. C* **61** 180–9

[12] Wray L S, Rnjak-Kovacina J, Mandal B B, Schmidt D F, Gil E S and Kaplan D L 2012 A silk-based scaffold platform with tunable architecture for engineering critically-sized tissue constructs *Biomaterials* **33** 9214–24

[13] Sang Y, Wha M, Kim S, Lee S, Hee J, Yul Y and Cho Y 2014 Fabrication of dual-pore scaffolds using SLUP (salt leaching using powder) and WNM (wire-network molding) techniques *Mater. Sci. Eng. C* **45** 546–55

[14] Derby B 2012 Printing and prototyping of tissues and scaffolds. *Science* **338** 921–6

[15] Cho Y S, Kim B S, You H K and Cho Y S 2014 A novel technique for scaffold fabrication: SLUP (salt leaching using powder) *Curr. Appl. Phys.* **14** 371–7

[16] Zhang Q, Luo H, Zhang Y, Zhou Y, Ye Z, Tan W and Lang M 2013 Fabrication of three-dimensional poly(ε-caprolactone) scaffolds with hierarchical pore

structures for tissue engineering. *Mater. Sci. Eng. C. Mater. Biol. Appl.* **33** 2094–103

[17] Ma P X and Langer R 1999 Fabrication of biodegradable polymer foams for cell transplantation and tissue engineering. *Methods Mol. Med.* **18** 47–56

[18] Lu L, Peter S J, Lyman M D, Lai H L, Leite S M, A. Tamada J, Vacanti J P, Langer R and Mikos A G 2000 In vitro degradation of porous poly(L-lactic acid) foams *Biomaterials* **21** 1595–605

[19] Chen G, Ushida T and Tateishi T 2002 Scaffold Design for Tissue Engineering *Macromol. Biosci.* **2** 67–77

[20] Ma P X 2004 Scaffolds for tissue fabrication *Mater. Today* **7** 30–40

[21] Kim S Y, Kanamori T, Noumi Y, Wang P and Shinbo T 2004 Preparation of Porous Poly (D , L -lactide) and Poly (D , L -lactide- co -glycolide) Membranes by a Phase Inversion Process and Investigation of Their Morphological Changes as Cell Culture Scaffolds *J. Appl. Polym. Sci.* **92** 2082–92

[22] Liu H C, Lee I C, Wang J H, Yang S H and Young T H 2004 Preparation of PLLA membranes with different morphologies for culture of MG-63 Cells *Biomaterials* **25** 4047–56

[23] Zoppi R a., Contant S, Duek E a R, Marques F R, Wada M L F and Nunes S P 1999 Porous poly(L-lactide) films obtained by immersion precipitation process: Morphology, phase separation and culture of VERO cells *Polymer (Guildf).* **40** 3275–89

[24] Nam Y S and Park T G 1999 Porous biodegradable polymeric scaffolds prepared by thermally induced phase separation *J. Biomed. Mater. Res.* **47** 8–17

[25] Guan J, Fujimoto K L, Sacks M S and Wagner W R 2005 Preparation and characterization of highly porous, biodegradable polyurethane scaffolds for soft tissue applications *Biomaterials* **26** 3961–71

[26] Moshfeghian A, Tillman J and Madihally S V 2006 Characterization of emulsified chitosan–PLGA matrices formed using controlled-rate freezing and lyophilization technique *J. Biomed. Mater. Res. Part A* **79A** 418–30

[27] Rowlands A S, Lim S A, Martin D and Cooper-White J J 2007 Polyurethane/poly(lactic-co-glycolic) acid composite scaffolds fabricated by thermally induced phase separation *Biomaterials* **28** 2109–21

[28] Hutmacher D W 2001 Scaffold design and fabrication technologies for engineering tissues--state of the art and future perspectives. *J. Biomater. Sci. Polym. Ed.* **12** 107–24

[29] Ho M-H, Kuo P-Y, Hsieh H-J, Hsien T-Y, Hou L-T, Lai J-Y and Wang D-M 2004 Preparation of porous scaffolds by using freeze-extraction and freeze-gelation methods *Biomaterials* **25** 129–38

[30] Sultana N and Wang M 2012 PHBV/PLLA-based composite scaffolds fabricated using an emulsion freezing/freeze-drying technique for bone tissue engineering: surface modification and in vitro biological evaluation. *Biofabrication* **4** 015003

[31] Sultana N and Wang M 2012 Fabrication of Tissue Engineering Scaffolds Using the Emulsion Freezing/Freeze-drying Technique and Characteristics of the Scaffolds *Integrated Biomaterials in Tissue Engineering* (Hoboken, NJ, USA: John Wiley & Sons, Inc.) pp 63–89

[32] Whang K and Healy K E 1995 A novel method scaffolds to fabricate bioabsorbable **36** 837–42

[33] Whang K, Tsai D C, Nam E K, Aitken M, Sprague S M, Patel P K and Healy K E 1998 Ectopic bone formation via rhBMP-2 delivery from porous bioabsorbable polymer scaffolds *J. Biomed. Mater. Res.* **42** 491–9

[34] Garg K and Bowlin G L 2011 Electrospinning jets and nanofibrous structures *Biomicrofluidics* **5** 013403

[35] Li D and Xia Y 2004 Electrospinning of nanofibers: Reinventing the wheel? *Adv. Mater.* **16** 1151–70

[36] Burger C, Hsiao B S and Chu B 2006 Nanofibrous Materials and Their Applications *Annu. Rev. Mater. Res.* **36** 333–68

[37] Moroni L, Licht R, de Boer J, de Wijn J R and van Blitterswijk C A 2006 Fiber diameter and texture of electrospun PEOT/PBT scaffolds influence human mesenchymal stem cell proliferation and morphology, and the release of

incorporated compounds *Biomaterials* **27** 4911–22

[38] Boudriot U, Dersch R, Greiner A and Wendorff J H 2006 Electrospinning approaches toward scaffold engineering--a brief overview. *Artif. Organs* **30** 785–92

[39] Rockwood D N, Akins R E, Parrag I C, Woodhouse K a and Rabolt J F 2008 Culture on electrospun polyurethane scaffolds decreases atrial natriuretic peptide expression by cardiomyocytes in vitro. *Biomaterials* **29** 4783–91

[40] Kakade M V., Givens S, Gardner K, Lee K H, Chase D B and Rabolt J F 2007 Electric field induced orientation of polymer chains in macroscopically aligned electrospun polymer nanofibers *J. Am. Chem. Soc.* **129** 2777–82

[41] Rockwood D N, Preda R C, Yucel T, Wang X, Lovett M L and Kaplan D L 2011 Materials fabrication from Bombyx mori silk fibroin *Nat Protoc* **6** 1612–31

[42] Loh Q L, Choong C, Oxon D, Hons M and Mimmm C 2013 Three-Dimensional Scaffolds for Tissue Engineering Applications : **19**

[43] Saw S H, Wang K, Yong T and Ramakrishna S 2006 Polymeric Nanofibers in Tissue Engineering *Nanotechnologies Life Sci.* **9** 66–134

[44] Carnachan R J, Bokhari M, Przyborski S a. and Cameron N R 2006 Tailoring the morphology of emulsion-templated porous polymers. 608–16

[45] Yeong W-Y, Chua C-K, Leong K-F and Chandrasekaran M 2004 Rapid prototyping in tissue engineering: challenges and potential. *Trends Biotechnol.* **22** 643–52

[46] Sachlos E and Czernuszka J T 2003 Making tissue engineering scaffolds work. Review: the application of solid freeform fabrication technology to the production of tissue engineering scaffolds. *Eur. Cell. Mater.* **5** 29–39; discussion 39–40

[47] Muschler G F, Nakamoto C and Griffith L G 2004 Engineering Principles of Clinical Cell-Based Tissue Engineering *J. Bone & Jt. Surg.* **86** 1541–58

[48] Malda J, Woodfield T B F, van Der Vloodt F, Kooy F K, Martens D E, Tramper J, van Blitterswijk C A and Riesle J 2004 The effect of PEGT/PBT scaffold architecture on oxygen gradients in tissue engineered cartilaginous constructs.

Biomaterials **25** 5773–80

[49] Lewis M C, Macarthur B D, Malda J, Pettet G and Please C P 2005 Heterogeneous Proliferation Within Engineered Cartilaginous Tissue: The Role of Oxygen Tension *Biotechnol. Bioengeneering* **91** 607–15

[50] Billiet T, Vandenhaute M, Schelfhout J, Van Vlierberghe S and Dubruel P 2012 A review of trends and limitations in hydrogel-rapid prototyping for tissue engineering *Biomaterials* **33** 6020–41

[51] Wicker R B, Ranade A V., Medina F and Palmer J A 2005 Embedded micro-channel fabrication using line-scan stereolithography *Assem. Autom.* **25** 316–29

[52] Sun C, Fang N, Wu D M and Zhang X 2005 Projection micro-stereolithography using digital micro-mirror dynamic mask *Sensors Actuators A Phys.* **121** 113–20

[53] Gauvin R, Chen Y-C, Lee J W, Soman P, Zorlutuna P, Nichol J W, Bae H, Chen S and Khademhosseini A 2012 Microfabrication of complex porous tissue engineering scaffolds using 3D projection stereolithography. *Biomaterials* **33** 3824–34

[54] Xia C and Fang N X 2009 3D microfabricated bioreactor with capillaries *Biomed. Microdevices* **11** 1309–15

[55] Peltola S M, Melchels F P W, Grijpma D W and Kellomäki M 2008 A review of rapid prototyping techniques for tissue engineering purposes *Ann. Med.* **40** 268–80

[56] Xing J-F, Zheng M-L and Duan X-M 2015 Two-photon polymerization microfabrication of hydrogels: an advanced 3D printing technology for tissue engineering and drug delivery *Chem. Soc. Rev.* **44** 5031–9

[57] Zein I, Hutmacher D W, Tan K C and Teoh S H 2002 Fused deposition modeling of novel scaffold architectures for tissue engineering applications *Biomaterials* **23** 1169–85

[58] Choong C, Triffitt J T and Cui Z F 2004 Polycaprolactone Scaffolds for Bone Tissue Engineering *Food Bioprod. Process.* **82** 117–25

[59] Lee H, Ahn S, Bonassar L J, Chun W and Kim G 2013 Cell-laden poly(ε-caprolactone)/alginate hybrid scaffolds fabricated by an aerosol cross-linking

process for obtaining homogeneous cell distribution: fabrication, seeding efficiency, and cell proliferation and distribution. *Tissue Eng. Part C. Methods* **19** 784–93

[60] Ahn S, Kim Y, Lee H and Kim G 2012 A new hybrid scaffold constructed of solid freeform-fabricated PCL struts and collagen struts for bone tissue regeneration: fabrication, mechanical properties, and cellular activity *J. Mater. Chem.* **22** 15901

[61] Billiet T, Gevaert E, De Schryver T, Cornelissen M and Dubruel P 2014 The 3D printing of gelatin methacrylamide cell-laden tissue-engineered constructs with high cell viability. *Biomaterials* **35** 49–62

[62] Hanson Shepherd J N, Parker S T, Shepherd R F, Gillette M U, Lewis J a and Nuzzo R G 2011 3D Microperiodic Hydrogel Scaffolds for Robust Neuronal Cultures. *Adv. Funct. Mater.* **21** 47–54

[63] Sun L, Parker S T, Syoji D, Wang X, Lewis J a and Kaplan D L 2012 Direct-write assembly of 3D silk/hydroxyapatite scaffolds for bone co-cultures. *Adv. Healthc. Mater.* **1** 729–35

[64] Das S, Pati F, Choi Y-J, Rijal G, Shim J-H, Kim S W, Ray A R, Cho D-W and Ghosh S 2015 Bioprintable, cell-laden silk fibroin–gelatin hydrogel supporting multilineage differentiation of stem cells for fabrication of three-dimensional tissue constructs *Acta Biomater.* **11** 233–46

[65] Mota C, Puppi D, Chiellini F and Chiellini E 2015 Additive manufacturing techniques for the production of tissue engineering constructs *J. Tissue Eng. Regen. Med.* **9** 174–90

[66] Therriault D, Shepherd R F, White S R and Lewis J a. 2005 Fugitive Inks for Direct-Write Assembly of Three-Dimensional Microvascular Networks *Adv. Mater.* **17** 395–9

[67] Therriault D, White S R and Lewis J a 2003 Chaotic mixing in three-dimensional microvascular networks fabricated by direct-write assembly. *Nat. Mater.* **2** 265–71

[68] Miller J S, Stevens K R, Yang M T, Baker B M, Nguyen D T, Cohen D M, Toro E, Chen A A, Galie P A, Yu X, Chaturvedi R, Bhatia S N and Chen C S 2012

Rapid casting of patterned vascular networks for perfusable engineered three-dimensional tissues. *Nat. Mater.* **11** 768–74

[69] Mohanty S, Larsen L B, Trifol J, Szabo P, Burri H V R, Canali C, Dufva M, Emnéus J and Wolff A 2015 Fabrication of scalable and structured tissue engineering scaffolds using water dissolvable sacrificial 3D printed moulds *Mater. Sci. Eng. C* **55** 569–78

[70] Mohanty S, Mantis I, Chetan A M, Larsen B, Dufva M, Emnéus J and Wolff A 2015 Fabrication of Three Dimensional Tissue Engineering Polydimethylsiloxane (Pdms) Microporous Scaffolds Integrated in a Bioreactor Using a 3D Printed Water Dissolvable Sacrificial Mould . *Proc. MicroTAS 2015* 50–2

[71] Sobral J M, Caridade S G, Sousa R a, Mano J F and Reis R L 2011 Three-dimensional plotted scaffolds with controlled pore size gradients: Effect of scaffold geometry on mechanical performance and cell seeding efficiency. *Acta Biomater.* **7** 1009–18

[72] Wray L S, Rnjak-Kovacina J, Mandal B B, Schmidt D F, Gil E S and Kaplan D L 2012 A silk-based scaffold platform with tunable architecture for engineering critically-sized tissue constructs *Biomaterials* **33** 9214–24

[73] Kang H W, Rhie J W and Cho D W 2009 Development of a bi-pore scaffold using indirect solid freeform fabrication based on microstereolithography technology *Microelectron. Eng.* **86** 941–4

[74] Cho Y S, Hong M W, Kim Y Y and Cho Y-S 2014 Assessment of cell proliferation in salt-leaching using powder (SLUP) scaffolds with penetrated macro-pores *J. Appl. Polym. Sci.* **131** 40240–8

[75] Dorj B, Park J H and Kim H W 2012 Robocasting chitosan/nanobioactive glass dual-pore structured scaffolds for bone engineering *Mater. Lett.* **73** 119–22

[76] Park K, Jung H, Son J S, Park K D, Kim J J, Ahn K D and Han D K 2007 Preparation of biodegradable polymer scaffolds with dual pore system for tissue regeneration *Macromolecular Symposia* vol 249-250 pp 145–50

[77] Park S H, Kim T G, Kim H C, Yang D Y and Park T G 2008 Development of dual scale scaffolds via direct polymer melt deposition and electrospinning for

applications in tissue regeneration *Acta Biomater.* **4** 1198–207

[78] Zhang W, Wray L S, Rnjak-Kovacina J, Xu L, Zou D, Wang S, Zhang M, Dong J, Li G, Kaplan D L and Jiang X 2015 Vascularization of hollow channel-modified porous silk scaffolds with endothelial cells for tissue regeneration *Biomaterials* **56** 68–77

[79] Wray L S, Tsioris K, Gil E S, Omenetto F G and Kaplan D L 2013 Microfabricated porous silk scaffolds for vascularizing engineered tissues *Adv. Funct. Mater.* **23** 3404–12

[80] Rnjak-Kovacina J, Wray L S, Golinski J M and Kaplan D L 2014 Arrayed Hollow Channels in Silk-Based Scaffolds Provide Functional Outcomes for Engineering Critically Sized Tissue Constructs *Adv. Funct. Mater.* **24** 2188–96

[81] Giannitelli S M, Mozetic P, Trombetta M and Rainer A 2015 Combined additive manufacturing approaches in tissue engineering *Acta Biomater.* **24** 1–11

[82] Da H, Jia S-J, Meng G-L, Cheng J-H, Zhou W, Xiong Z, Mu Y-J and Liu J 2013 The impact of compact layer in biphasic scaffold on osteochondral tissue engineering. *PLoS One* **8** e54838

[83] Dorj B, Park J-H and Kim H-W 2012 Robocasting chitosan/nanobioactive glass dual-pore structured scaffolds for bone engineering *Mater. Lett.* **73** 119–22

3. CHAPTER 3. Fabrication of Scalable and Structured Tissue Engineering Scaffolds Using Water Dissolvable Sacrificial 3D Printed Moulds

This work was previously published as: Mohanty, S., et al. (2015). Fabrication of Scalable and Structured Tissue Engineering Scaffolds Using Water Dissolvable Sacrificial 3D Printed Moulds. Materials Science Engineering C (55): 569-78.

3.1 Introduction

In recent years, there has been a great demand for the development of bioartificial organs/tissues in the field of organ transplantation and *in vitro* toxicological drug screening [1]. One of the primary challenges in translation of tissue engineering to clinical application is the difficulty in scaling up complex, biological effective tissues and organs to the size relevant for human [2]. Although small scale three-dimensional (3D) scaffold constructs has been achieved to mimic organs for e.g. *in vitro* drug testing [3], the applied fabrication approaches are not easily translated to constructs of human organ size. When engineering tissues *in vitro,* there is a requirement for structures or scaffolds that are able to support cell growth and at the same time mimicking the physiological environment including the geometrical, topographical and physical features of the targeted tissue. Specifically for the generation of thick 3D tissues, the development of highly dense vascular networks that can meet the nutrient and oxygen requirements of large masses of living cells remains a tissue engineering challenge. This often limits the size of engineered tissues to a few hundred micro meters [4]. The ideal tissue engineering scaffold supports the spatial distribution of cells in a three dimensional structure, provides mechanical stability to the cells and enables optimum nutrient transport and metabolic waste removal [5,6]. Numerous approaches exist to create 3D highly vascularized engineered tissue scaffolds to accommodate a high density of cells in high surface to volume ratio structures [6,7]. One strategy has been to use highly porous structures with interconnected pores/microchannels that provide space for penetration and growth of cells and enable favourable mass transport characteristics [8]9]. The structural, mechanical and mass transport properties of such scaffolds are determined by parameters such as pore size, pore shape, porosity, pore interconnectivi-

ty, permeability, scaffold surface area, scaffold effective stiffness and scaffold material [10].

Scaffolds consisting of stochastic, disordered or random micropores are one of the oldest and most widely used templates for tissue engineering [11,12]. Manufacturing techniques such as solvent casting-particulate leaching [13], phase separation [14], gas foaming [15], emulsion freeze drying [16] and fibre meshes [17] have been used to generate engineered scaffolds of foam-like internal structure with a random architecture and a limited control of scale [18]. Although such processing techniques are quick, scalable and economical, they do not enable accurate control of the microarchitectural details such as the pore size, geometry, their interconnections and distribution within the scaffold [19]. The possibility to control the inner architecture of scaffolds is desirable as it enables the control over its mechanical strength, the effective surface area for cell growth, and nutrient flow profiles within the scaffold [18]. To produce scaffolds with fine control over scaffold architecture in three dimensions, layer-by layer assembly techniques, where layers of polymers, patterned by moulding or embossing processes, are stacked, have been investigated by many researchers [20,21]. These techniques enable the formation of channels with precisely defined dimensions. However, the requirement for microfabricated master moulds and manual alignment of layers implies a slow and tedious process for achieving a multi-layered 3D construct [22].

Recently there has been a move towards employing 3D printing [10,23,24] as a rapid prototyping technique to fabricate micro-scale porous structures of desired complexities, allowing a true engineering of the scaffold [18]. These methods involve the creation of 3D objects using layer by layer deposition approch. Such techniques have successfully been employed in tissue engineering to develop scaffolds based on hard polymeric materials [25,26] and hydrogels [27,28]. The application of scaffolds made from soft polymers or elastomeric materials is desirable when engineering soft tissues [12,29,30]. For the fabrication of elastomeric scaffolds with microfluidic networks, micromoulding and individual layer-by layer assembly techniques have commonly been used [20,31]. However such techniques require the use of complex fabrication technologies and manual assembly for producing large scale structures. Thus the fabrication of 3D elastomeric scaffolds with defined microarchitectural details in cost-effective, scalable manner remains a challenge.

Recently, processes combining 3D printing and moulding have been used for making structured 3D scaffolds. For example, 3D microvascular networks within polymer

matrices have been fabricated by 3D printing of sacrificial wax moulds, casting of low viscosity epoxy around the moulds and subsequent removal of the moulds [23,32]. However the use of wax (which has a melting temperature of about 60°C) limits the materials that can be cast around the mould to form the scaffold since polymers requiring higher temperatures for cross-linking cannot be employed. Furthermore, the complete removal of the sacrificial wax components (which may not be biocompatible) can be challenging, in particular if you have a large 3D structure with complex geometry. Perfusable 3D scaffolds have also been demonstrated in a similar manner by casting extracellular matrix (ECM) containing cells around a 3D printed sacrificial sugar glass lattice and subsequently dissolving the lattice to form vascular networks [24]. However, it is probably difficult to print large 3D structures in the very brittle sugar glass, and the interfilament distance (defined by the printing process) is limited to a minimum of 1 mm. It may therefore not be feasible to use this technique for creating dense vascular channels in large scale structures.

This paper presents a new scalable and general approach for manufacturing structured pores/channels in 3D polymer based scaffolds. The method involves 3D printing (using a commercially available filament based 3D printer) of a sacrificial polyvinyl alcohol (PVA) mould whose geometrical features are designed according to the required vascular channel network. In addition to its biocompatibility, PVA is an ideal material because of its water solubility in combination with its high melting temperature (190°C) makes it robust for subsequent polymer casting and curing steps. A desired polymer is cast around the PVA mould, cross-linked and then the mould is dissolved, leaving behind a structured porous scaffold in the desired polymer material. The fabrication method was here demonstrated for two different polymers, the silicone elastomer polydimethylsiloxane (PDMS), and the syntetic hydrogel poly(2-hydroxyethyl methacrylate) (pHEMA). The scalability of the method was demonstrated by fabricating a 75 cm^3 large PDMS scaffold structure with 16,000 channels. Moreover, it was also shown that the PDMS scaffolds when properly pre-treated could support hepatocyte growth and proliferation for up to 12 days with high viability and proper function.

3.2 Materials and Methods

2.1 Fabrication of structured porous elastomeric scaffolds

The method used to fabricate elastomeric polymer scaffolds with structured channels is schematically presented in Figure 1. First, a commercial, low-cost 3D filament printer (MakerBot 2X) was used to print a sacrificial mould. A solid 3D cube of the specified length, width and height was designed using a computer aided design (CAD) software package (Solidworks 2013). The 3D CAD design was exported as .STL mesh file format for processing using the 3D printer software (Makerware 2.4.1, Makerbot). Commercially available water dissolvable polymer, Polyvinyl alcohol (PVA) (Makerbot, USA) filaments were used to print the sacrificial mould. In the printing process a moving nozzle (x- and y-axis control) extrudes a heated polymer filament which then solidifies as it is deposited (Fig. 1(a)). Following deposition of each layer, the mould is lowered (z-axis control) and the extrusion procedure is repeated such that successive layers are built on top of each other to form a 3D object (Fig. 1(b)). The printer settings used for printing PVA moulds are given in table 1. The extrusion temperature and feed-rates were optimised for printing PVA.

Table 1: 3D printing parameters used for fabricating sacrificial PVA mould

3D printing parameters	Settings
Layer height	0.2 mm
Infill pattern	Woodpile or hexagonal
Nozzle temperature	200 °C
Build platform temperature	40 °C
Feed-rate	20 mm/s

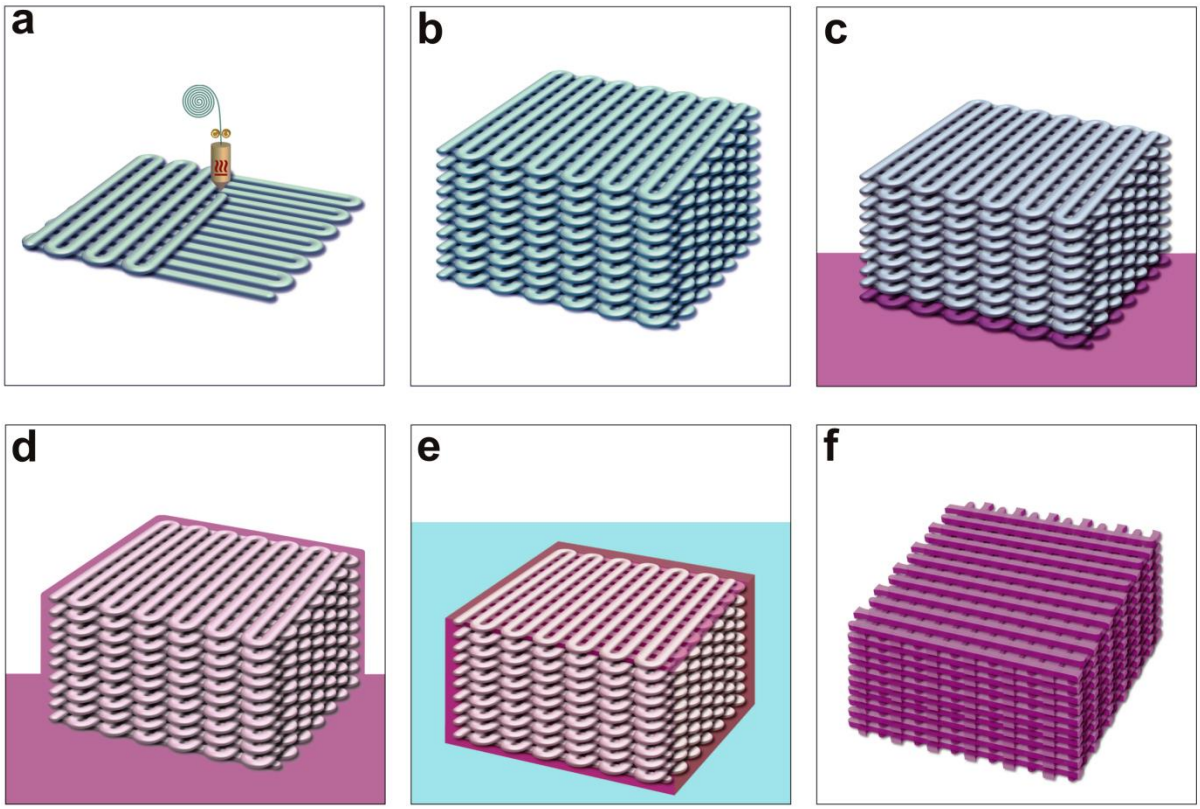

Figure 2: Schematic illustration of the steps involved in the fabrication of structured porous elastomeric scaffolds. A sacrificial 3D mould was printed in PVA (a, b). The printed PVA mould was transferred into a container containing pre-cured PDMS (c). Vacuum was applied to ensure complete filling of pre-cured PDMS into the pores of the mould (d). Following crosslinking of the PDMS, the sacrificial PVA mould was dissolved in water (e) leaving behind the structured PDMS scaffold (f).

The printing infill density was varied to generate structures with varying porosity. The infill density is the parameter that defines the amount of material filled into the object and subsequently relates to the porosity of the 3D printed structure. The infill density can range from 0% to 100%, where 0% results in a completely hollow object and 100% infill results in a completely solid object. In order to generate structures with different porosities, moulds were printed with infill densities ranging from 20% to 80%. An illustration of the infill patterns and densities that were employed are shown in supplementary Fig. 1.

The 3D printed microvascular network of the PVA mould was replicated into elastomeric structures of polydimethylsiloxane (PDMS): PDMS pre-polymer solution (Sylgard 184, Dow Corning) was mixed with the curing agent in a 10:1 ratio (as per manufacturer's guidelines). The mixture was degassed in vacuum and poured into a petri dish

containing the printed mould (Fig. 1(c)). PDMS fills the pores of the mould through capillary action and, in addition, vacuum was applied for 2-3 hours to ensure complete filling of the micro-channels of the mould with PDMS (Fig. 1(d)). PDMS was cured at a temperature of 60°C in an oven for 4 hours. Once cured, excess PDMS around the mould was removed to expose the PVA layer. This was done to assist the subsequent dissolution of PVA in water: The whole structure was immersed into a water bath (Fig. 1(e)) until the PVA mould was completely dissolved (6 hours), and the elastomeric PDMS with microvascular network architecture was obtained (Fig. 1(f)).

Cuboidal PVA moulds of 25 × 25 × 10 mm^3 and 25 × 25 × 4 mm^3 (length × width × height) were printed and used for casting PDMS scaffolds and these scaffolds were used for mechanical testing and cell culturing studies respectively.

2.2 Characterizations of scaffolds

2.2.1 Scanning electron microscopy (SEM) imaging

The structural morphology and microstructure of the printed PVA mould as well as the resulting PDMS porous scaffolds were analysed using scanning electron microscopy (JEOL, Tokyo, Japan). Prior to SEM analysis, moulds and scaffolds were dried in an oven at 50°C overnight and sputter coated with gold. Samples were then analysed using 12 kV of accelerating voltage. Pore sizes of the moulds and scaffolds were measured from SEM micrographs using Image J software. For each sample, ten measurements of pore dimensions were acquired.

For cell-seeded scaffolds, samples were washed with PBS and fixed with 2.5% glutaral-dehyde in PBS overnight. Next the samples were dehydrated in a series of ethanol solutions (50%, 70%, 90% and 100%), the samples were further air-dried and then the samples were ready for SEM observation.

2.2.2 Porosity measurement

The porosity of the PDMS scaffold was measured using equation (1) as described in the literature [33].

$$\text{Porosity}\ (\%) = \frac{V - \left(\frac{M}{\rho}\right)}{V} \times\ 100\% \qquad (1)$$

Where V is the volume of the scaffold, which is calculated using its outer dimension, M is the mass of the porous PDMS scaffold, and ρ is the density of PDMS (0.965 gm/cm^3). Four scaffolds from each type of scaffold (with dimensions 23 × 23 × 6 mm^3) were dried overnight at 80°C, and weighed to obtain the mass of the samples. The porosity was then calculated from the weight and the dimensions using equation 1.

2.2.3 Mechanical testing

The mechanical properties of dry PDMS scaffolds (with dimensions of 25 × 25 × 10 mm^3) of varying porosity (20 - 80%) were tested by conducting uniaxial compression tests. A constant compression speed of 0.5 mm/min was applied to each sample using a tensile test machine with a 5 kN load cell (INSTRON Model 4301, Instron Engineering Corporation, Canton, MA, USA). The compressive modulus was estimated from the slope of the stress – strain curve in the elastic region, which was in the range of 12% - 20% strain. The stress at 20% strain was obtained. The values reported were an average from four tested samples.

2.2.4 Surface roughness

The surface topography of the PVA mould and PDMS scaffold was visualized using SEM. PDMS scaffold surface roughness was measured using an optical measuring device (Alicona infinite focus). The parameters R_a and R_z were obtained from a standard spectrum of roughness.

2.2.5 Wettability

To assess wettability of the scaffolds, contact angle measurements were carried out on scaffolds before and after treatment with oxygen plasma. The contact angle was measured using the sessile drop method by depositing 3 µl of an ultrapure water drop on the scaffold. Three individual measurements were carried out on three independent scaffolds.

2.2.6 Surface area calculation

To estimate the surface area of the scaffolds, the dimensions of the filaments constituting the mould was acquired from SEM images of the mould. As previously described, the scaffold is formed by printing layers of filaments (with a height of 0.2 mm) organised in the xy axis. The surface area was calculated from the SEM images of a single layer and then multiplied by the number of layers.

2.3. Culturing cells in scaffolds

2.3.1 Cells

Human hepatoblastoma (HepG2) cells were obtained from the German Collection of Microorganisms and Cell cultures (DMSZ, Braunschweig, Germany). The cells were maintained in Roswell Park Memorial Institute (RPMI) 1640 growth medium supplemented with 10% fetal bovine serum (FBS, Sigma-Aldrich Chemie GmbH, Switzerland) and 100 µg/ml penicillin and 10 µg/ml streptomycin in a humidified incubator at 37°C and 5% CO_2. Cells were cultured to confluence in standard polysty-

rene cell culture flasks, and then released using 0.025% trypsin/EDTA solution. The cell suspension was centrifuged and the cell pellet was washed twice with phosphate buffered saline (PBS) and then re-suspended in fresh growth medium. The cell density was measured using a haemocytometer and adjusted as required for the seeding on the 3D scaffolds.

2.3.2 Scaffold preparation for cell culture

PDMS scaffolds (fabricated with 80% infill moulds) were frozen in liquid nitrogen and punched into cylindrical scaffolds (having a diameter of 6 mm and height 4 mm) using a tissue puncher (Harris Uni-Core, USA). To render them hydrophilic, the scaffolds were modified with oxygen plasma using a 13.56 MHz RF generator equipped Atto Plasma System (Diener Electronic GmbH, Ebhausen, Germany). Initially the plasma chamber was evacuated to a pressure below 15 Pa, after which oxygen was introduced (pressure stabilization at 30 Pa) and the plasma was ignited (power 50 W) for a duration of 2 min for each side of the scaffold.The treated scaffolds were transferred into an autoclavable glass vial containing sterile water and autoclaved at 120˚C for 20 minutes for sterilisation. To promote cell attachment to the scaffolds, the scaffolds were coated with 40 µg/ml of Collagen I (Collagen I rat protein, Life Technologies, A1048301) at 4°C overnight. The scaffolds were washed twice with phosphate buffered saline (PBS) and excess collagen was removed by centrifugation of the samples at 1000 rpm. Finally, the scaffolds were placed in a petri dish containing RPMI medium and incubated inside a humidified incubator at 37°C and 5% CO_2 for 2 hours prior to cell seeding.

2.3.3 Cultivation of hepG2 cells inside the scaffolds

HepG2 cells were cultured in the fabricated scaffolds to evaluate the ability of PDMS 3D constructs to support cell adhesion, proliferation and spreading. For cell seeding a customised cell loading platform was developed as shown schematically in supplementary figure 2. A cell seeding plate with 16 cylindrical holes (having a diameter of 6 mm) and a rectangular support frame was fabricated in 6 mm thick Poly(methyl methacrylate) (PMMA) using a CO_2 laser cutter machine (Epilog Mini 18 Laser, CO 80403, USA). The seeding plate and frame were sterilized by immersion in 0.5 M sodium hydroxide solution for 2 hours followed by rinsing in sterile water. The frame and seeding plate were placed inside a sterile petri dish such that the seeding plate was raised and had no direct contact with the petri dish. The collagen coated scaffolds from the incubator were inserted into the holes in the seeding plate. A suspension containing 250000 cells in 20 µl of media was prepared and loaded into each scaffold. After

seeding, the petri plate was incubated at 37 ˚C for 3 hours to allow the cells to attach to the scaffold. Every hour the loading plate was inverted upside down to enable better cell infiltration into the scaffold. Finally the scaffolds were removed from the seeding plate and transferred into a 24 well plate. 1 ml of cell culture medium was added to each well. The medium was refreshed every 2 days and old media was collected for cellular functionality assays. On day 4, 8 and 12 of the culture period, two scaffolds from each time point were sacrificed and used for live/dead staining.

2.3.4 Biochemical assays

Cell proliferation was estimated using the colorimetric indicator alamarBlue® assay (Life Technologies). The cell-scaffold constructs were transferred into a 24 well plate each containing 1 ml of RPMI and alamarBlue® solution (in a 10:1 ratio) and incubated for 2 hours in a humidified incubator at 37°C. The absorbance of the extracted dye, which is proportional to the number of cells attached to the scaffold, was measured spectrophotometrically using a microplate reader (PerkinElmer, USA) at wavelengths of 570 nm. Three independent scaffolds were measured in triplicates, and the background (i.e. alamarBlue® absorbance measured at day 0) was subtracted.

For the HepG2 functionality test, extracellular concentration of albumin secretion from the HepG2 cells was determined by using an enzyme-linked immunosorbent assay (ELISA) (Bethyl Laboratories, USA) according to the manufacturer`s instructions. All samples were measured in triplicates and the standard deviation (SD) of mean was determined from 3 independent scaffolds. The absorbance was measured at 450 nm using a spectrophotometer (PerkinElmer, USA).

2.3.5 Cell Imaging

To visualize cell viability in the scaffolds, a live/dead-assay was performed using a live/dead cell imaging kit (Life technologies LIVE/DEAD® Cell Imaging Kit), which is based on a cell-permeable dye for staining of live cells (excitation/emission 488 nm/515 nm) and a cell-impermeable dye for staining of dead and dying cells (excitation/emission 570nm/602 nm). Briefly, the cell-laden scaffolds were removed from the culture medium and gently washed with PBS. They were then incubated in the dye solution for 30 min at 37°C (as per manufacturer's instructions). The scaffolds were imaged using a fluorescence microscope (Zeiss Axio Observer, ZI). 3D reconstructions were compiled from 20 imaged sections (each of 30 μm thickness).

To visualize the cell proliferation and distribution through the cross section of the scaffolds, cell-laden scaffolds were stained with cell-permeable nuclear stain Hoechst 33342 (NucBlue® Live Ready Probes® Reagent, life technologies) for live cell nuclei and ethidium homodimer-1 (life technologies) for dead cell nucleus for 10 minute. The scaffolds were then dissected longitudinally using a sterile scalpel and each section was observed under a fluorescence microscope. 3D reconstructions were compiled from 20 imaged sections (each of 30 μm thickness).

An immunofluorescence study was performed to visualise the morphology of cells attached to the scaffold surface: After 12 days of cell growth, the cell-laden scaffolds were immunostained with beta-tubulin as cell cytoskeleton and nucleus. The construct was fixed (4% paraformaldehyde), permeabilized (30 min, 0.1% Triton-X in phosphate buffered saline (PBS)), and blocked (30 min, 0.1% Tween20 and 1% bovine serum albumin in PBS) for unspecific binding of the antibodies. The construct was stained with primary antibody as monoclonal Anti-α-Tubulin IgG1 (2 h, 1:200, Life Technologies) followed by TO-PRO-3 nuclear stain (1:1000, Life Technologies). The scaffold was then cut through the centre using a sterile scalpel and visualized under a Zeiss ApoTome fluorescence microscope. 3D reconstructions were compiled from 20 imaged sections (each having a thickness of 5 μm).

3.3 Results

3.1 Scaffold fabrication

Scaffolds were fabricated by casting PDMS around sacrificial moulds printed using two different infill patterns (woodpile and hexagonal) and four different infill densities. Photographs and SEM images of the printed moulds and resulting PDMS scaffolds of the two different infill patterns are shown in Fig. 2. The scaffolds possessed well-defined, porous structures. The square and hexagonal pore structure of both PVA moulds and PDMS scaffolds were observed to be uniform and consistent (Fig 2 (a, b, e, f)). The structural features of the PVA mould are faithfully replicated in the PDMS scaffold (Fig 2 (c, d, g, h)).

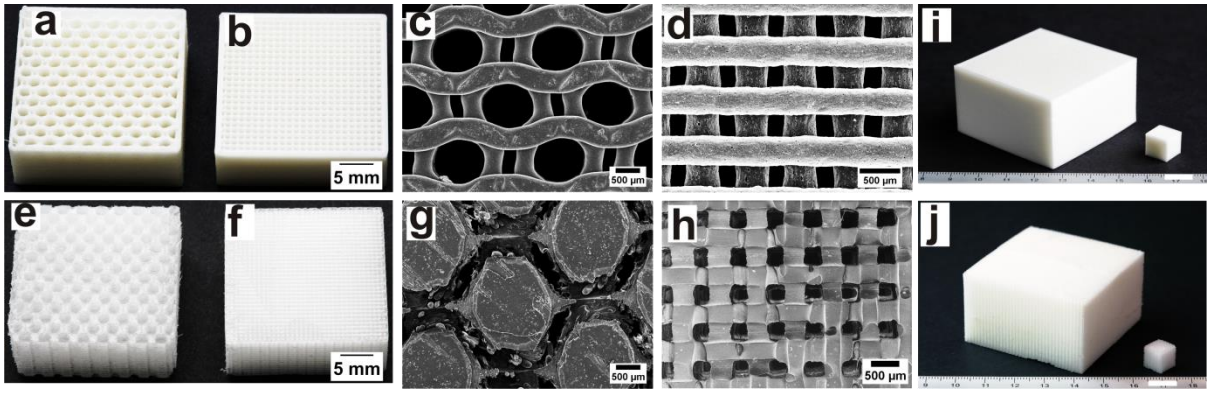

Figure 3: Photographs of moulds and scaffolds with hexagonal (a, e) and woodpile (b, f) infill patterns. SEM images of moulds and scaffolds with hexagonal (c, g) and woodpile (d, h) infill patterns. (i) optical image of a 50 layered (1 cm^3 cube) and 150 layered (75 cm^3 cube) 3D printed PVA mould (j) optical image of 50 layered (1 cm^3 cube) and 150 layered (75 cm^3 cube) PDMS scaffolds replicated from the mould (i). Scale bar in (i) and (j): 1 cm.

The woodpile infill pattern results in structures comprising orthogonal arrays of filaments with the centre-to-centre spacing between adjacent filaments differing based on the chosen infill density (Fig. 3). Infill densities of 20, 40, 60 and 80 % produces structures where filaments in a layer had a distances of 1482, 593, 253 and 78 µm respectively. As the infill density increases, the centre-to-centre spacing of the filaments in the PVA mould decreases (Fig. 3a-d). SEM images of the mould showed that the printed PVA filaments have an elliptical cross-section with a width of 400 µm and a height of 200 µm (supplementary fig). The channels in the resulting PDMS scaffold have an elliptical profile from a cross section view (width 344µm, height 190 µm) (shown in supplimentory fig 5) and a square profile (average side length 344 um) from the top view. The channels dimensions in the PDMS scaffold are slightly smaller than the dimension of the PVA filaments of the mould due to shrinkage of PDMS during the curing process. The channel to channel distance varied from 1.4 mm at 20 % infill density down to 78 µm at 80 % infill density of the printed mould. Thus the employed 3D printing technique enables the layer by layer assembly of a different number of PVA filaments forming a porous 3D mould. To demonstrate the scalability of the fabrication process, a larger cubic mould (75 cm^3) was fabricated and employed for generating a replica PDMS scaffold with the same dimensions. Fig, 2(i) shows an image of two cubic moulds of dimensions 1 cm^3 and 75 cm^3 printed using 80% infill settings and Fig. 2(j) shows the resulting PDMS scaffolds. Thus, as demonstrated in Fig. 2, the periodic

micro and macroscale structural patterns of the PVA mould were well replicated in the PDMS scaffolds.

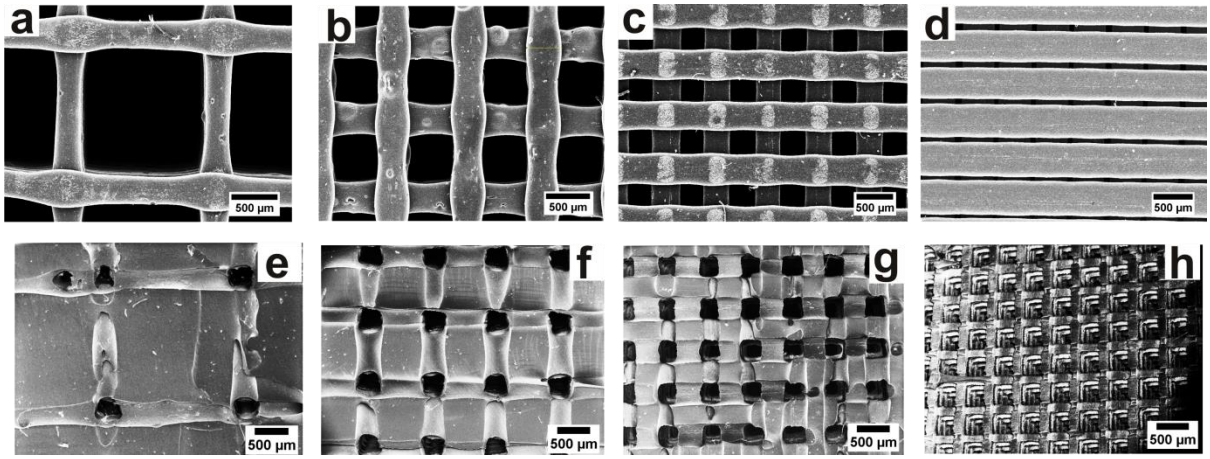

Figure 4: SEM micrographs of 3D printed PVA moulds of 20, 40, 60 and 80% infill densities (a-d) and corresponding PDMS scaffolds (e-h).

3.2 Scaffold characterisation

3.2.1 Porosity

The experimentally determined porosity of fabricated scaffolds is presented in Fig. 4. The porosity of the scaffolds varied linearly as a function of the infill density of the printed mould from 19.9% porosity at 20% infill up to 81.2% porosity at 80% infill (Fig 4(a)).

3.2.2 Surface area

The calculated surface areas of a 1 cm^3 fabricated scaffolds of varying porosities are shown in Fig. 4 (b). As the infill density of the mould increases from 20 % to 80 %, there is also a corresponding increase (from 52.5 cm^2/cm^3 to 150.9 cm^2/cm^3, respectively) in the surface area of the channels within the PDMS scaffold volume. As the infill density of the mould increases (Fig 3 (a-d) the density of channels also increases (Fig 3 (e-h)), which results in a linear increase in the total surface area of the channels (Fig 4 (b)).

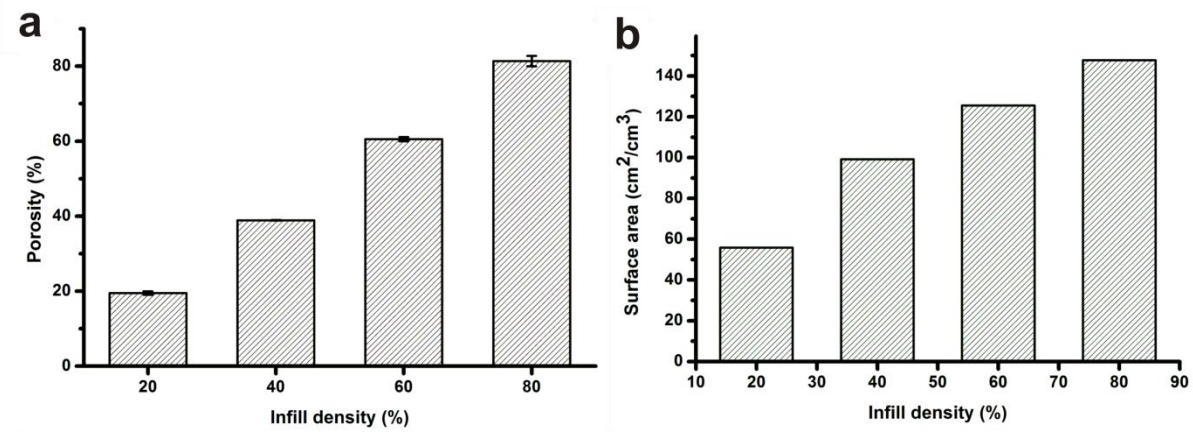

Figure 4: Measured porosity (error bars = SD, n = 4) (a) and calculated surface to volume ratio (b) of scaffolds fabricated from mould with different infill density.

3.2.3 Mechanical testing

The assessment of the compressive characteristics of scaffolds is known to play a significant role in many tissue-engineering applications [34]. Compression tests of the scaffolds varying in porosity were performed to assess the stress-strain relationship and evaluate their compressive moduli (Fig. 5). The compressive modulus was determined as the slope of the initial linear portion of the stress vs. strain curve (12 – 20%). The compressive modulus were determined to be 1.84 ± 0.023, 0.84 ± 0.044, 0.36 ± 0.046 and 0.075 ± 0.047 MPa for the 20, 40, 60, and 80 % porosity scaffolds, respectively. Results showed that the energy absorption of the scaffolds is greatly reduced with increasing porosity. There is also a dramatic decrease in the compressive modulus and in the stress at 20% strain with increasing scaffold porosity

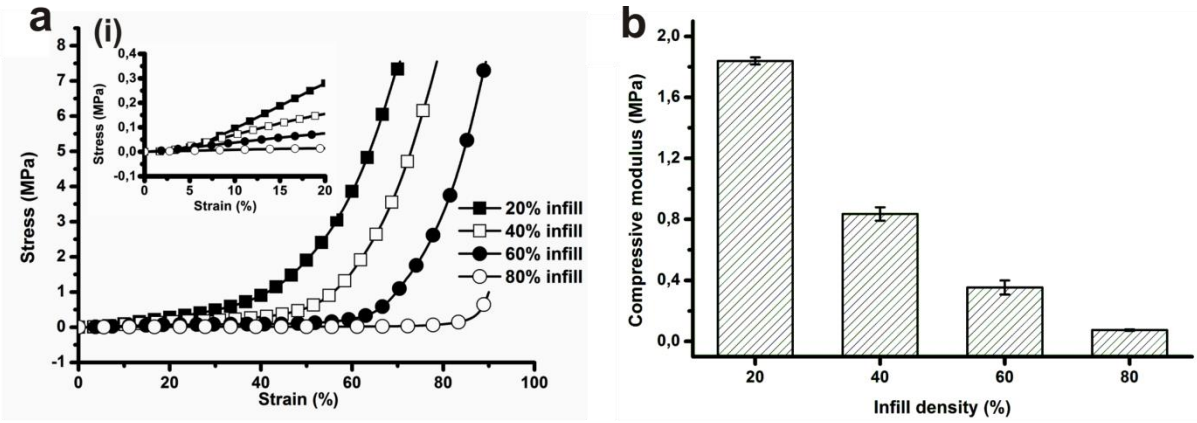

Figure 5: (a) Stress–strain curves at 4N load for different scaffolds, (b) compressive moduli of different PDMS scaffolds (Error bars = standard deviation of 4 samples (n = 4)).

3.2.4 Surface roughness

The roughness of the 3D printed PVA mould and corresponding PDMS scaffold was assessed using SEM. As shown in Fig. 6 (a-d), the presence of features such as pillars and grooves visible on the PVA mould are faithfully replicated in the PDMS scaffolds. The roughness of the PDMS scaffold was measured using an optical profilometer. The relative height and surface roughness is shown in the surface profile image (Fig. 6(e)) and the roughness parameters R_a and R_z of the PDMS scaffold surface were measured to be approximately 1.036 µm and 1.32 µm, respectively.

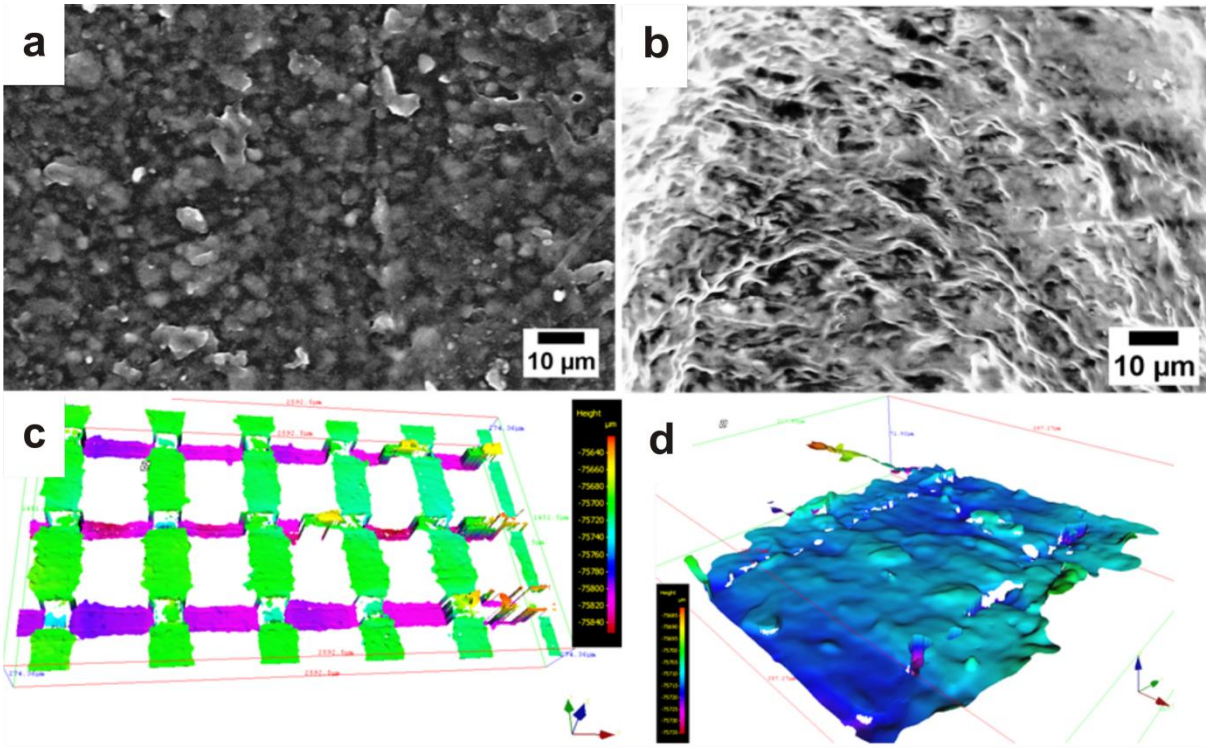

Figure 6: Surface roughness analysis: SEM images showing microfeatures in the PVA mould surface (a) and PDMS scaffold (b, c & d), Surface profile image of PDMS scaffold surface generated from optical profilometer (c) and zoom in of image c (d).

3.3 Culturing cells in scaffold

3.3.1 Preparing scaffold for cell culturing (surface treatment)

To enable cell seeding and culturing within a porous scaffolds, it is important to render the scaffold surface hydrophilic [35]. This is required to ensure that the cell suspension and culture media can be absorbed within the scaffold pores. Oxygen plasma treatment was applied to the fabricated scaffolds to achieve this. Using this treatment, the contact angle of the scaffold surface decreased from 122° ± 3.5° to 0° and media was able to infiltrate the pores of the scaffold (Supplementary Fig. 3).

3.3.2 Cell proliferation, viability and function

Following the surface treatment, the scaffolds were prepared for cell culturing, seeded with cells, and incubated as described in materials and methods. Cell viability and proliferation in the PDMS scaffolds with 80 % porosity were investigated over a 12 days culture period using biochemical assays and imaging techniques. Cell proliferation in the scaffold was quantified using the alamarBlue® assay. As shown in Fig. 7 (a), the fluorescence intensity increased linearly over the culture period, indicating increase in the number of cells in the scaffolds with time. The functionality of HepG2 cells cultured on the scaffolds was established by measuring the extracellular albumin production (Fig. 7 (b)). There was an increase in albumin production from day 1 to day 12 of the cultures which correlate with the increased cell density in the scaffolds.

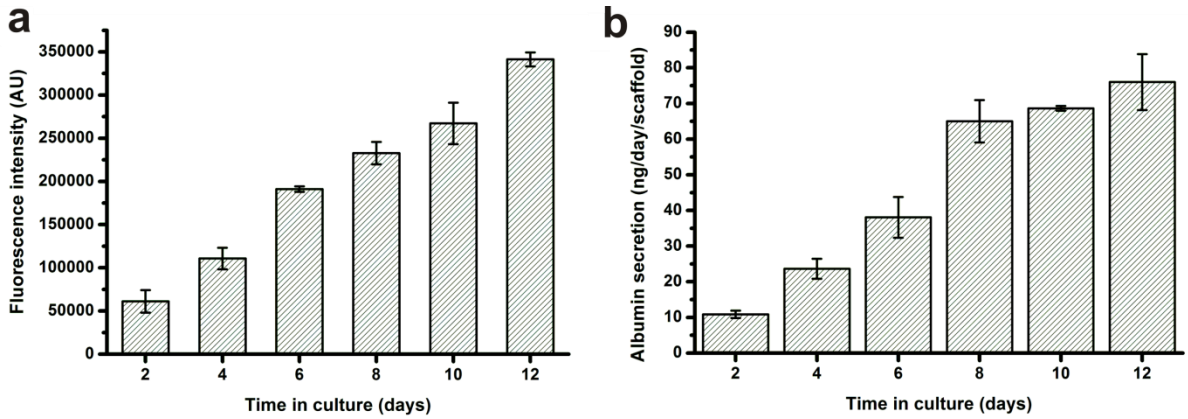

Figure 7: (a) Change in alamarBlue® florescence intensity of scaffolds over culture time. The fluorescence intensity is proportional to the amount of cells. (b) Albumin production of HepG2 cells grown in PDMS scaffolds over 12 days of culture. Error bars indicate standard deviation of 3, independent scaffolds.

Live/dead staining of the cell-scaffold construct was carried out to assess the viability of cells cultured on the scaffolds. Fig. 8 shows the confocal microscopy images of stained HepG2 cells on day 4, 8 and 12 of the culture period. Through the culture period, the density of living cells (stained green) increased. On day 12 of the culture, a confluent layer of live cells was visible on the scaffolds. In all cases, no dead cells were observed, so close to 100 % cell viability was maintained throughout the 12 days culture period.

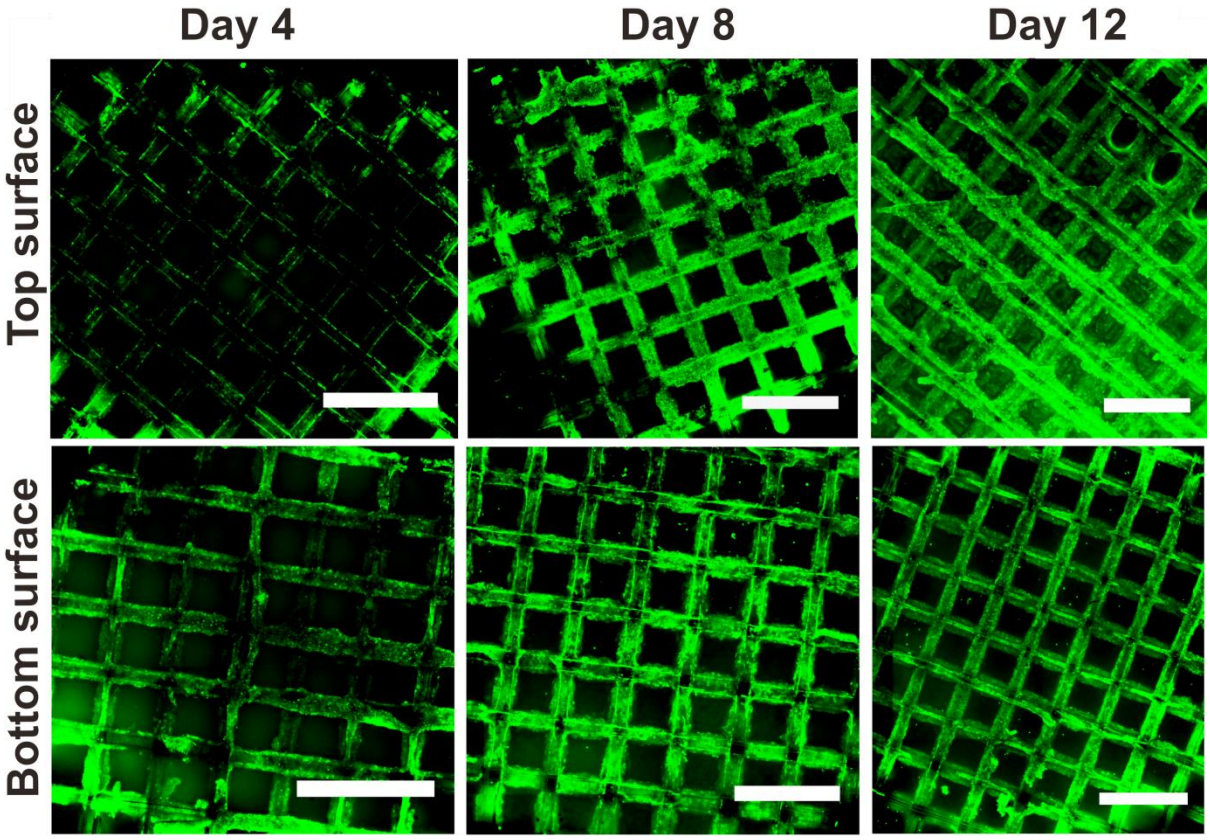

Figure 8: Live/dead staining of HepG2 cells grown on top and bottom part of the PDMS scaffold for 4, 8 and 12 days. Scale bars represent 1 mm.

3.3.3 Cell infiltration and distribution within the scaffolds

At different time points during the culture period, the infiltration and distribution of HepG2 cells within the PDMS scaffolds was investigated. This was done by staining the scaffolds with nuclear stain Hoechst 33342 (NucBlue® Live Ready Probes® Reagent, life technologies) for live cell nuclei and ethidium homodimer-1 (life technologies) for dead cell nucleus. To visualise cell distribution through the cross section of the scaffold, it was dissected along its central axis and imaged using fluorescence microscopy. Fig. 9 shows live cell nuclei (stained blue) on the scaffold on day 4, 8 and 12 of the culture. Close to 100 % cell viability was observed (no dead cells could be seen) with cells present throughout the cross section of the scaffold by the end of the culture period. Scaffolds acquired from day 4 of the culture showed a higher density of cells closer to the top and bottom face of the scaffold and a sparse density of cells in the central regions of the scaffold. But with longer culture time, cells appeared to proliferate and are seen to be homogenously distributed throughout the channels of the scaffolds at day 8 and 12.

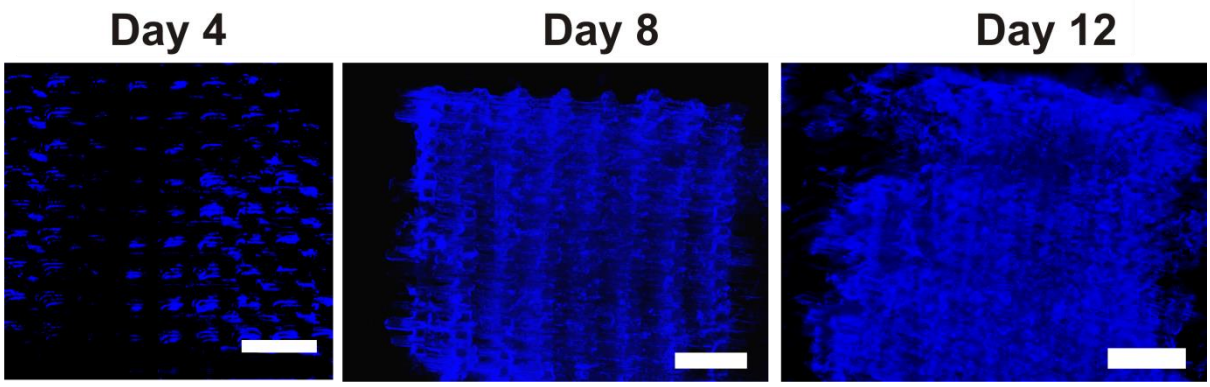

Figure 9: Visualization of cell distribution through the central section of the scaffold stained with NucBlue® (live cells: blue) and ethidium Homodimer-1 (EthD-1) (dead stain: red) on day 4, 8 12 of HepG2 cell culturing. Scale bars 1 mm.

Immunostaining of the scaffold was carried out to visualise the morphology of cells cultured on the scaffolds. Fig. 10 shows a homogeneous and confluent distribution of cells in the central region of the scaffold, highlighting the cytoskeleton beta-tubulin (green) and cell nucleus (red). After 12 days of cell culture the cells were uniformly distributed with high density of live cell in the centre of the scaffold. Immunofluorescence staining of the beta-tubulin demonstrated that the cells were well attached to the surface with a spread-out cell morphology.

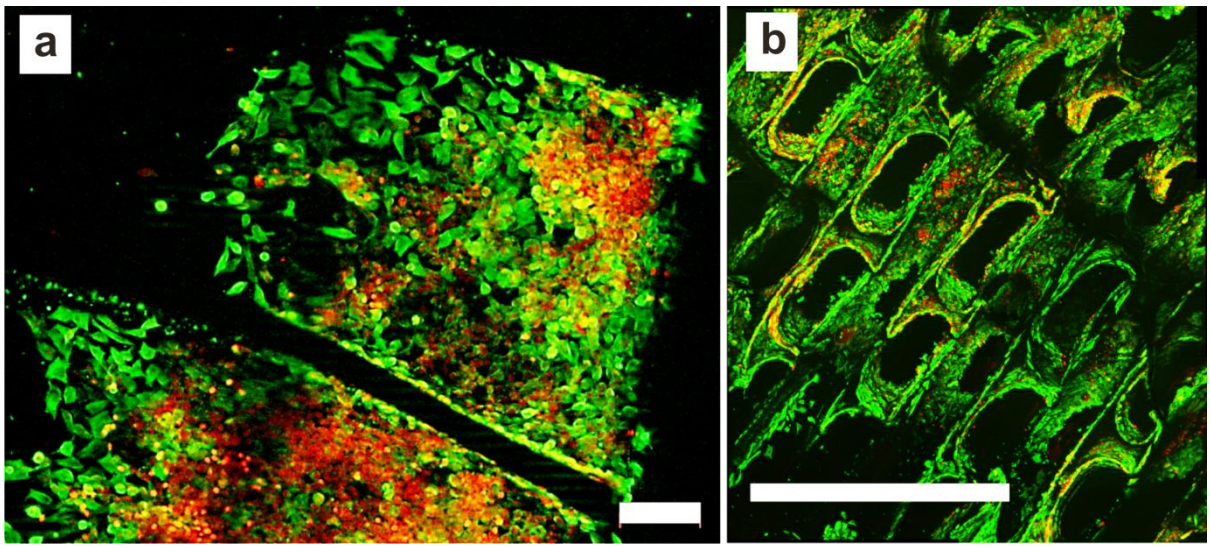

Figure 10: Hepg2 cell morphology and attachment to PDMS scaffold using immunostaining (a & b). Cell cytoskeleton beta tubulin (green) and nucleus (red). (a) Top surface of the scaffold. (b) Longitudinal cross section of the scaffold. Scale bar of image a) with 100 µm , b) with 1 mm.

HepG2 cell adhesion on scaffold was also investigated through SEM as shown in the supplementary figure 5 (a, b & c). After 4 days of culture, the interaction between cells and the scaffold surface was examined. Cells cultured on PDMS scaffold formed a well spread morphology and exhibited excellent cell adhesion.

3.4 Discussion

In this paper, a new scalable and reproducible technique for fabricating 3D polymer scaffolds with defined micro-architectures has been presented. The technique is simple and involves casting of a desired polymer material within a 3D printed water-soluble PVA mould, which defines the microarchitecture/geometry of pores or channels within the scaffold (Figs. 1-3). 3D printing parameters were optimised to enable the production of reproducible moulds with high yield. The technique was applied to fabricate 'wood-pile' like scaffolds with regularly spaced aligned polymer filaments in the x and y directions. Scaffolds of porosities ranging from 20 – 80% and channel to channel distances ranging from 78µm to 1482µm were fabricated by specifying the infill density of the moulds. Scaffolds with hexagonal micro-features were also obtained by using moulds with hexagonal infill patterns. The dimensions of the channels formed in the PDMS replica scaffolds were ellipsoidal shaped with dimensions (344µm × 190µm) that were slightly smaller than that of the filaments in the printed mould (400µm × 200µm), due to shrinkage during elastomer curing.

We used the biocompatible elastiomeric polymer PDMS to demonstrate the ease of fabrication and scaling of scaffolds structure, and furthermore showed that it has potential as a scaffold for growth of liver cells. However, the method has general applicability, meaning that other mouldable materials can be structured in a similar manner. To prove this point, poly-2-hydroxyethyl methacrylate (pHEMA) hydrogel scaffolds were produced by monomer/crosslinker casting around PVA mould, photo-crosslinking (supplementary Figure. 4, and material and method in supplementary section) and subsequent dissolution of the PVA mould.

The silicone elastomer PDMS is optically clear, and, in general, inert, non-toxic, and non-flammable. Its applications range from contact lenses and medical devices to additives in cosmetics and food products. PDMS is also widely used as a material for microfluidic cell culturing and the high number of publications using it indicates that it is a biocompatible material [36]. In general the effects of PDMS or silicones on cells need to be evaluated on a case by case situation, as PDMS in some situations have subtle effect on gene expression [37], but we clearly show here that the fabricated PDMS elastomer scaffold supports HepG2 growth and function (Figs. 7-10). This type of elastomer scaffold could be used as a part of a life support system (LSS), e.g., an extracorporeal liver [38]to temporarily relieve liver disease patients. In such application

PDMS offers several advantages: 1) It is easy to fabricate PDMS scaffold structures using the PVA sacrificial moulding method presented here 2) PDMS is a structurally strong material for building large meshes (figure 2J) 3) PDMS is easy to sterilise by autoclavation (in contrast to some hydrogels) 4) In contrast to hydrogels and many biodegradable materials PDMS does not shrink, swell or warp significantly with time meaning that rational fluidics optimisation can be done as well as robust fluidic connections for perfusions. 5) There are FDA approved medical grade silicone elastomers which should be compatible with the here described fabrication method.

It is well recognised that in order to be of clinical relevance, tissue constructs must be scaled up to the macro scale, not only in length and width, but also in thickness [20]. The presented fabrication method overcomes existing challenges in creating thicker constructs in a simple and reproducible manner by using precision assembly technology to control the micro-architectural details. The scalability of the process was demonstrated by producing a 75 cm^3 large scaffold structure with 16,000 channels with a channel to channel distance of only 78 µm (Fig. 2(j)). To our knowledge this is the largest scaffold ever to be produced with such small features sizes and with so many structured channels. Thus the process enables a more efficient scale up of scaffolds both in size and in throughput, while also allowing versatility in the implementation of 3D micro architectural designs.

It is well established that the micro-roughness of a scaffold surface plays an important role in cell attachment and proliferation [39–42]. For this reason, the topological features of the scaffold were analysed using SEM to measure the surface roughness. Geometrical and topological features of the 3D printed PVA mould (Fig. 6a and b) were well replicated in the PDMS scaffold (Fig. 6c and d), giving the scaffold micro- and nano-scale roughness. Such micro- and nano-scale roughness can be an advantage for cell attachment and proliferation [43]. Our results are in agreement with this: We observed confluent layer of well-attached cells with spread-out cell morphology (Fig. 10).

It is well known that cells respond to the material on which they grow, both in terms of cytoskeleton, cell morphology, cell differentiation and function [45,46]. The mechanical properties of the fabricated scaffolds of varying porosities were therefore characterised. The compressive modulus of the scaffolds were estimated to be 1.84, 0.84, 0.34, 0.075 MPa for 20, 40, 60 and 80% porous scaffolds, respectively. The inverse relationship between scaffold porosity and compressive modulus is expected because scaffold with a

higher porosity have less material/mass to resist applied load and therefore have a lower compressive modulus. If the stiffness of the PDMS scaffold should be a problem it can be adjusted by changing the ratio of pre-polymer to curing agent [46] or by selecting hydrogel materials such as pHEMA (supplementary Fig. 4) could be used for casting the scaffold.

A highly available surface area in a scaffold can provide high ligand density for initial cell attachment and proliferation [47]. We chose to use the scaffold with the highest porosity (80%) for culturing cells since it has the lowest compressive modulus, enables better mass transport, and has the highest specific surface area (Fig. 4b) for cell attachment.

Until now it has been a challenge to maintain viable cells within the inner cores of thick engineered tissue constructs due to insufficient oxygen and nutrient levels [33]. To regenerate artificial tissues a homogeneous cell distribution should be maintained inside the porous scaffold structure [48,49]. The scaffolds presented in this work were able to sustain cells with 100 % viability throughout the 12 day culture period. Metabolic assays and total cell DNA quantification assays do not give information on cell infiltration and distribution inside the scaffold. In order to visualise this aspect, the cell nucleus stained scaffolds were imaged at the top, bottom and cross sectional surfaces (Fig. 9). Cells were seen to be uniformly distributed throughout the channels of the scaffolds and along the cross sectional length of the scaffold. The achieved homogeneity can be attributed to the following: Firstly, the cell loading procedure employed ensures an even distribution of cells throughout the scaffolds. Secondly, the parallel and perpendicular structured channels in the scaffold allow sufficient oxygen and nutrient mass transport into the scaffold which promotes cell survival and proliferation. Thus at the end of the culture period, cells were seen to be uniformly distributed throughout the scaffolds and along the cross sectional length of the scaffold. Results from immunostaining clearly showed good HepG2 cell morphology and attachment to the scaffold surface (Fig. 10). Cell functionality was assessed by measuring albumin secretion of cells in scaffolds over time (Fig. 7b). The increase in albumin secretion through the culture period indicate that the cells were able to maintain their functionally while cultured in the presented 3D scaffold.

3.5 Conclusions

In this study, we have demonstrated a new technique for fabricating scaffolds by 3D printing a sacrificial water dissolvable PVA mould, casting polymer around it and subsequently dissolving the sacrificial mould, leading to structured scaffolds. Different designs of PDMS scaffolds were successfully prepared, and the fabrication technique allowed the tuning of physical and mechanical properties by controlling the 3D printing parameter. By observing the biological activity of the hepatocytes in the scaffold we conforms that along with maintaining very high cellular viability the scaffold could also support high level of cellular albumin secretion throughout the cultivation period. After 12 days of cell culturing we observed a very high density of cells, homogeneously distribution across the scaffold due to good mass and oxygen transport into the scaffold. The fabrication method can also be applied to other synthetic or natural polymers as demonstrated by fabricating scaffolds in the hydrogel pHEMA. Furthermore, as we have demonstrated, the fabricated scaffold can be scaled up to sizes relevant for bioartificial organs. In conclusion, the described process is scalable, compatible with cell culture, rapid, and inexpensive.

Acknowledgements

This work has been financially supported by EU project NanoBio4Trans ("A new nanotechnology-based paradigm for engineering vascularised liver tissue for transplantation", grant no: 304842). We thank K. Kuldeep and Aradhya Mallikarjunaiah Chetan for their great support in carrying out with the fabrication of 3D scaffolds and Jesper Scheel for taking photographs of the large scaffold.

3.6 References

[1] Griffith L G and Swartz M a 2006 Capturing complex 3D tissue physiology in vitro. *Nat. Rev. Mol. Cell Biol.* **7** 211–24

[2] Rustad K C, Sorkin M, Levi B, Longaker M T and Gurtner G C 2010 Strategies for organ level tissue engineering. *Organogenesis* **6** 151–7

[3] Khademhosseini A, Langer R, Borenstein J and Vacanti J P 2006 Microscale technologies for tissue engineering and biology. *Proc. Natl. Acad. Sci. U. S. A.* **103** 2480–7

[4] Khademhosseini A, Vacanti J P and Langer R 2009 Progress in tissue engineering. *Sci.*

Am.

[5] Hoganson D M, Pryor H I and Vacanti J P 2008 Tissue engineering and organ structure: a vascularized approach to liver and lung. *Pediatr. Res.* **63** 520–6

[6] Lu T, Li Y and Chen T 2013 Techniques for fabrication and construction of three-dimensional scaffolds for tissue engineering. *Int. J. Nanomedicine* **8** 337–50

[7] Almeida H a and Bártolo P J 2014 Design of tissue engineering scaffolds based on hyperbolic surfaces: Structural numerical evaluation. *Med. Eng. Phys.* **36** 1033–40

[8] Langer R 2009 Perspectives and challenges in tissue engineering and regenerative medicine. *Adv. Mater.* **21** 3235–6

[9] Guillemette M D, Park H, Hsiao J C, Jain S R, Larson B L, Langer R and Freed L E 2010 Combined Technologies for Microfabricating Elastomeric Cardiac Tissue Engineering Scaffolds *Macromol. Biosci.* **10** 1330–7

[10] Jeong C G and Hollister S J 2010 Mechanical and Biochemical Assessments of Three-Dimensional Poly(1,8-Octanediol-co-Citrate) Scaffold Pore Shape and Permeability Effects on In Vitro Chondrogenesis Using Primary Chondrocytes *Tissue Eng. Part A* **16** 3759–68

[11] Kolewe M E, Park H, Gray C, Ye X, Langer R and Freed L E 2013 3D Structural Patterns in Scalable, Elastomeric Scaffolds Guide Engineered Tissue Architecture. *Adv. Mater.* **25** 4459–65

[12] Hollister S J 2009 Scaffold design and manufacturing: from concept to clinic. *Adv. Mater.* **21** 3330–42

[13] Mikos A G, Sarakinos G, Vacanti J P, Langer R S and Cima L G 1996 Biocompatible polymer membranes and methods of preparation of three dimensional membrane structures

[14] Lo H, Ponticiello M S and Leong K W 1995 Fabrication of controlled release biodegradable foams by phase separation. *Tissue Eng.* **1** 15–28

[15] Mooney D J, Baldwin D F, Suh N P, Vacanti J P and Langer R 1996 Novel approach to fabricate porous sponges of poly(D,L-lactic-co-glycolic acid) without the use of organic solvents. *Biomaterials* **17** 1417–22

[16] Whang K and Healy K E 1995 A novel method scaffolds to fabricate bioabsorbable **36** 837–42

[17] Saraf A, Lozier G, Haesslein A, Kasper F K, Raphael R M, Baggett L S and Mikos A G

2009 Fabrication of nonwoven coaxial fiber meshes by electrospinning. *Tissue Eng. Part C. Methods* **15** 333–44

[18] Derby B 2012 Printing and prototyping of tissues and scaffolds. *Science* **338** 921–6

[19] Yeong W-Y, Chua C-K, Leong K-F and Chandrasekaran M 2004 Rapid prototyping in tissue engineering: challenges and potential. *Trends Biotechnol.* **22** 643–52

[20] Kolewe M E, Park H, Gray C, Ye X, Langer R and Freed L E 2013 3D structural patterns in scalable, elastomeric scaffolds guide engineered tissue architecture. *Adv. Mater.* **25** 4459–65

[21] Golden A P and Tien J 2007 Fabrication of microfluidic hydrogels using molded gelatin as a sacrificial element. *Lab Chip* **7** 720–5

[22] He J, Wang Y, Liu Y, Li D and Jin Z 2013 Layer-by-layer micromolding of natural biopolymer scaffolds with intrinsic microfluidic networks. *Biofabrication* **5** 025002

[23] Therriault D, White S R and Lewis J a 2003 Chaotic mixing in three-dimensional microvascular networks fabricated by direct-write assembly. *Nat. Mater.* **2** 265–71

[24] Miller J S, Stevens K R, Yang M T, Baker B M, Nguyen D T, Cohen D M, Toro E, Chen A A, Galie P A, Yu X, Chaturvedi R, Bhatia S N and Chen C S 2012 Rapid casting of patterned vascular networks for perfusable engineered three-dimensional tissues. *Nat. Mater.* **11** 768–74

[25] Sobral J M, Caridade S G, Sousa R a, Mano J F and Reis R L 2011 Three-dimensional plotted scaffolds with controlled pore size gradients: Effect of scaffold geometry on mechanical performance and cell seeding efficiency. *Acta Biomater.* **7** 1009–18

[26] Declercq H A, Desmet T, Dubruel P and Cornelissen M J 2014 The Role of Scaffold Architecture and Composition on the Bone Formation by Adipose-Derived Stem Cells **20** 434–45

[27] Bertassoni L E, Cardoso J C, Manoharan V, Cristino A L, Bhise N S, Araujo W a, Zorlutuna P, Vrana N E, Ghaemmaghami A M, Dokmeci M R and Khademhosseini A 2014 Direct-write bioprinting of cell-laden methacrylated gelatin hydrogels. *Biofabrication* **6** 024105

[28] Gauvin R, Chen Y-C, Lee J W, Soman P, Zorlutuna P, Nichol J W, Bae H, Chen S and Khademhosseini A 2012 Microfabrication of complex porous tissue engineering scaffolds using 3D projection stereolithography. *Biomaterials* **33** 3824–34

[29] Freed L E, Engelmayr G C, Borenstein J T, Moutos F T and Guilak F 2009 Advanced

material strategies for tissue engineering scaffolds. *Adv. Mater.* **21** 3410–8

[30] Gao J, Crapo P M and Wang Y 2006 Macroporous elastomeric scaffolds with extensive micropores for soft tissue engineering. *Tissue Eng.* **12** 917–25

[31] Park H, Larson B L, Guillemette M D, Jain S R, Hua C, Engelmayr G C and Freed L E 2011 The significance of pore microarchitecture in a multi-layered elastomeric scaffold for contractile cardiac muscle constructs. *Biomaterials* **32** 1856–64

[32] Therriault D, Shepherd R F, White S R and Lewis J a. 2005 Fugitive Inks for Direct-Write Assembly of Three-Dimensional Microvascular Networks *Adv. Mater.* **17** 395–9

[33] Zhang Q, Luo H, Zhang Y, Zhou Y, Ye Z, Tan W and Lang M 2013 Fabrication of three-dimensional poly(ε-caprolactone) scaffolds with hierarchical pore structures for tissue engineering. *Mater. Sci. Eng. C. Mater. Biol. Appl.* **33** 2094–103

[34] Hollister S J 2005 Porous scaffold design for tissue engineering. *Nat. Mater.* **4** 518–24

[35] Oh S 2003 Fabrication and characterization of hydrophilic poly(lactic-co-glycolic acid)/poly(vinyl alcohol) blend cell scaffolds by melt-molding particulate-leaching method *Biomaterials* **24** 4011–21

[36] Berthier E, Young E W K and Beebe D 2012 Engineers are from PDMS-land, Biologists are from Polystyrenia. *Lab Chip* **12** 1224–37

[37] Łopacińska J M, Emnéus J and Dufva M 2013 Poly(dimethylsiloxane) (PDMS) affects gene expression in PC12 cells differentiating into neuronal-like cells. *PLoS One* **8** e53107

[38] Strain A J and Neuberger J M 2002 A bioartificial liver--state of the art. *Science* **295** 1005–9

[39] Flemming R G, Murphy C J, Abrams G a, Goodman S L and Nealey P F 1999 Effects of synthetic micro- and nano-structured surfaces on cell behavior. *Biomaterials* **20** 573–88

[40] Marcotte L and Tabrizian M 2008 Sensing surfaces: Challenges in studying the cell adhesion process and the cell adhesion forces on biomaterials *Irbm* **29** 77–88

[41] Liu X, Lim J Y, Donahue H J, Dhurjati R, Mastro A M and Vogler E a 2007 Influence of substratum surface chemistry/energy and topography on the human fetal osteoblastic cell line hFOB 1.19: Phenotypic and genotypic responses observed in vitro. *Biomaterials* **28** 4535–50

[42] Sant S and Khademhosseini A 2010 Fabrication and characterization of tough

elastomeric fibrous scaffolds for tissue engineering applications. *Conf. Proc. IEEE Eng. Med. Biol. Soc.* **2010** 3546–8

[43] Dolatshahi-Pirouz A, Nikkhah M, Kolind K, Dokmeci M R and Khademhosseini A 2011 Micro- and Nanoengineering Approaches to Control Stem Cell-Biomaterial Interactions *J. Funct. Biomater.* **2** 88–106

[44] Georges P C and Janmey P a 2005 Cell type-specific response to growth on soft materials. *J. Appl. Physiol.* **98** 1547–53

[45] Yeung T, Georges P C, Flanagan L a, Marg B, Ortiz M, Funaki M, Zahir N, Ming W, Weaver V and Janmey P a 2005 Effects of substrate stiffness on cell morphology, cytoskeletal structure, and adhesion. *Cell Motil. Cytoskeleton* **60** 24–34

[46] Trappmann B, Gautrot J E, Connelly J T, Strange D G T, Li Y, Oyen M L, Cohen Stuart M a, Boehm H, Li B, Vogel V, Spatz J P, Watt F M and Huck W T S 2012 Extracellular-matrix tethering regulates stem-cell fate. *Nat. Mater.* **11** 642–9

[47] O'Brien F J, Harley B a, Yannas I V and Gibson L J 2005 The effect of pore size on cell adhesion in collagen-GAG scaffolds. *Biomaterials* **26** 433–41

[48] Thevenot P, Nair A, Dey J, Yang J and Tang L 2008 Method to analyze three-dimensional cell distribution and infiltration in degradable scaffolds. *Tissue Eng. Part C. Methods* **14** 319–31

[49] Lee H, Ahn S, Bonassar L J, Chun W and Kim G 2013 Cell-laden poly(ε-caprolactone)/alginate hybrid scaffolds fabricated by an aerosol cross-linking process for obtaining homogeneous cell distribution: fabrication, seeding efficiency, and cell proliferation and distribution. *Tissue Eng. Part C. Methods* **19** 784–93

Supplementary

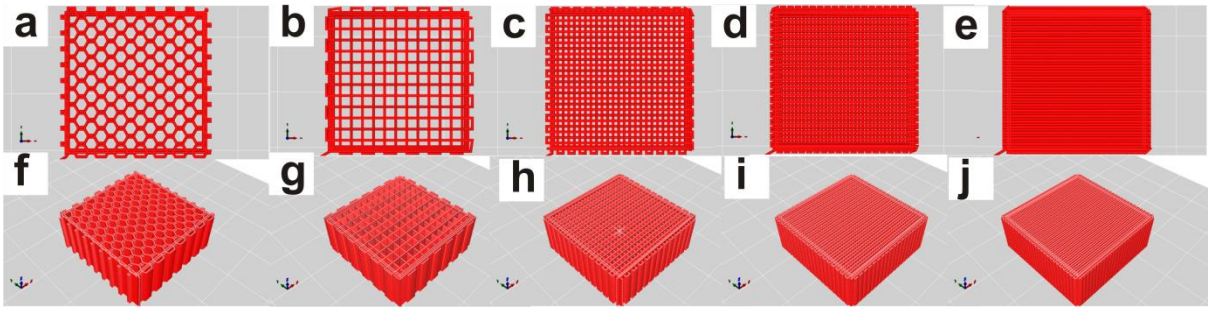

Figure 1. Top and isometric view of different pore sized and designes of mould. A-E) top single layer and F-H) combined multiple layers of the 25 × 25 × 10 mm^3 cube with woodpile and hexagonal design generated from respective g-code files using open source Repetier-Host V1 Beta1 software (http://www.repetier.com).

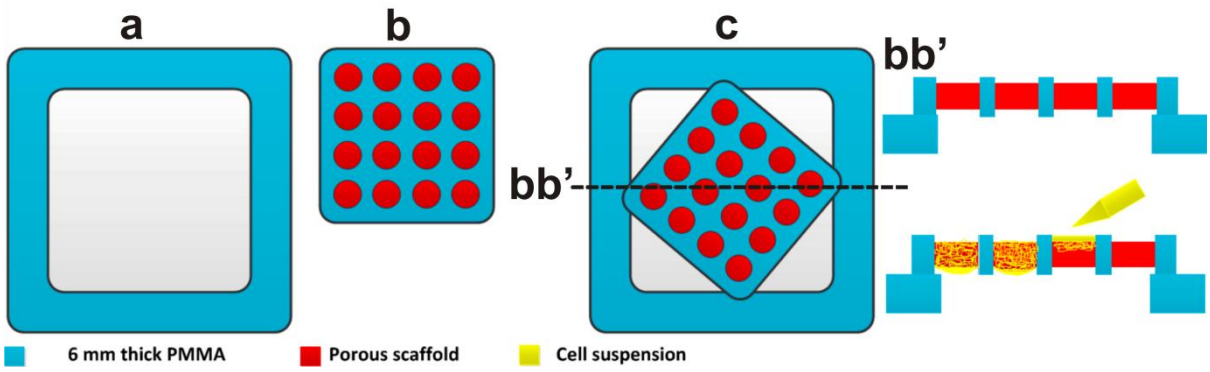

Figure 2. Schematic of cell seeding procedure. (A) Support frame, (B) Scaffolds (red) loaded in seeding plate (blue), (C) seeding plate placed on frame (D) cut through cross section of (C) BB'. Scaffolds are held raised within the holes of the tray and 20 µl of cell suspension are deposited on to each scaffold.

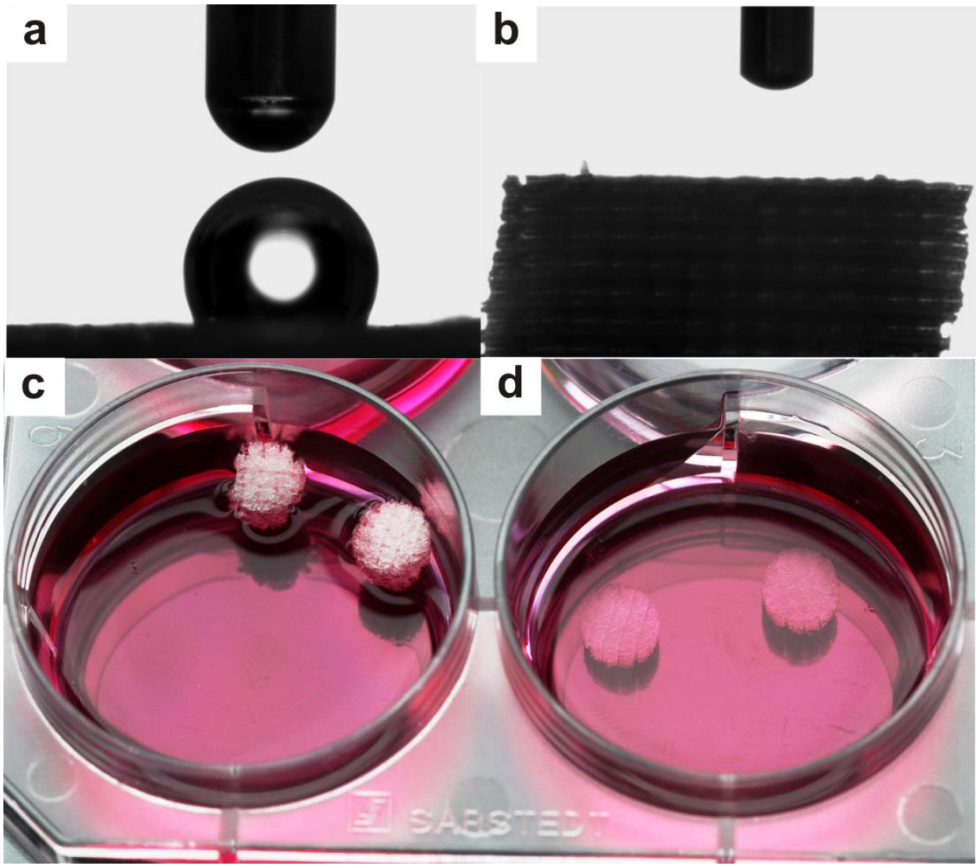

Figure 3. Contact angle measurement and wettability on the PDMS scaffold before (A&C) and after plasma (B&D) of plasma treatment.

Fabrication of structured porous pHEMA hydrogel scaffolds

Poly-2-hydroxyethyl methacrylate (pHEMA) hydrogel scaffolds were fabricated similar to the procedure for fabricating PDMS scaffolds with some modifications: 5 mL HEMA monomer (97% purity, Sigma-Aldrich Chemie Gmbh, Germany) , 0.125 mL (2.5%) of ethylene glycol dimethacrylate (EGDMA) co-monomer (98% purity, Sigma-Aldrich Chemie Gmbh, Germany), 1% (w/v) of azobisisobutyronitrile (AIBN) as photoinitiator (≥ 98 % (GC) purity, Fluka Analytical, Switzerland), and deionized water into a 50 layered PVA mould (25 × 25 × 10 mm^3) using vacuum. The mould with the polymer mixture was exposed to UV light (custom build apperatus) for ~20 min for the polymerization of HEMA and soaked in deionized water for at least 24 h to remove the sacrificial PVA mould as well as any unreacted species. SEM images of 3D pHEMA scaffolds are taken with a JEOL, Tokyo, Japan after coating samples with gold.

Results and discussion for pHEMA

The fabrication of pHEMA scaffolds was very similar to the fabrication of PDMS scaffold with minor modifications as described above. The hydrogel scaffolds contain fully interconnected porous networks with mechanically stable structure for use as scaffold materials. The average pore diameter of pHEMA scaffold was around 400 µm. The zoom in image of the pHEMA scaffold (Fig. 10c) demonstrates the rough surface, which was replicated from the PVA mould. Fabrication of pHEMA scaffold with PVA molding approach confirms that the technique is also suitable for photocrosslinkable polymer fabrication.

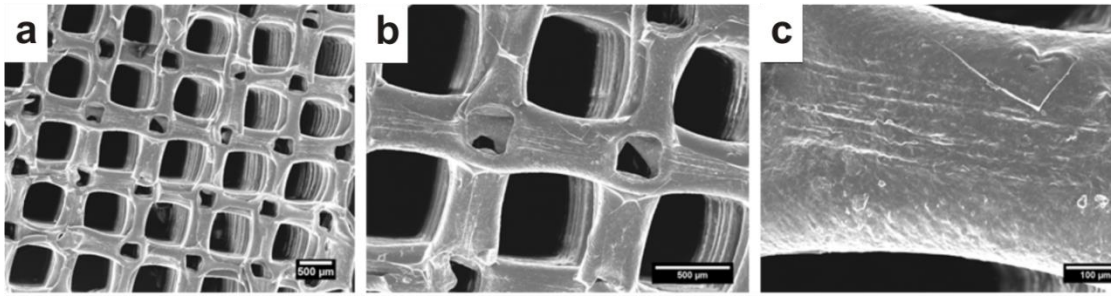

Figure 4. A, B & C) SEM micrographs of 3D pHEMA scaffolds casted from PVA molds with 40% in-fill density. The pHEMA scaffold is shown at different magnifications. The scale bare is 500 µm in A&B and 100 µm in C.

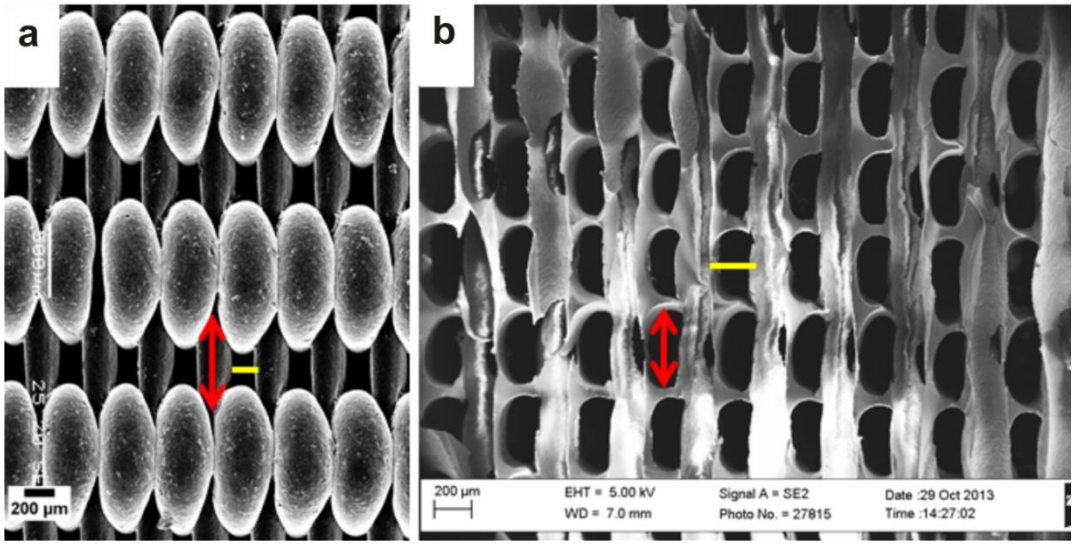

Figure 5. SEM images of cross-section views of PVA mould (A) and PDMS scaffold (B). The widths and heights were shown in red and yellow respectively. The scale bar for both A and B are 200 µm.

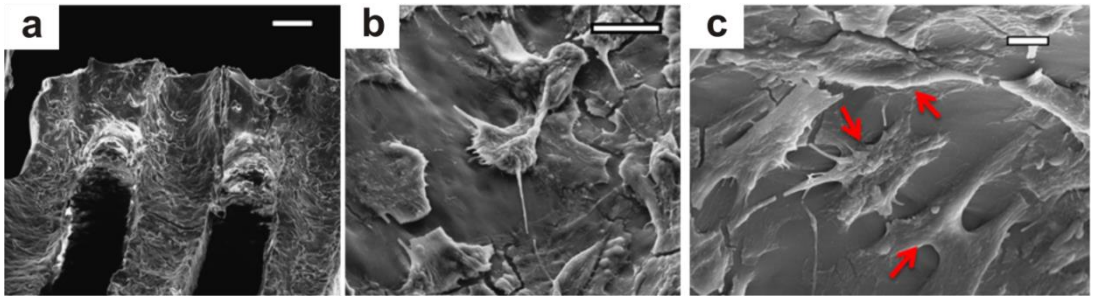

4. CHAPTER 4. Fabrication of scalable tissue engineering scaffolds with dual-pore microarchitecture by combining 3D printing and particle leaching

This work was published as: Mohanty, S., et al. (2016). Fabrication of Scalable and Structured Tissue Engineering Scaffolds Using Water Dissolvable Sacrificial 3D Printed Moulds. Materials Science Engineering C (61): 180-189.

4.1 Introduction

In recent years, there has been a significant medical demand for the development of a functional engineered tissue constructs suitable for tissue/organ replacement. One of the primary challenges in translation of tissue engineering for clinical applications is the difficulty in scaling up complex, biologically effective tissues and organs to the size adequate for human therapy [1]. Generation of a thick 3D tissue requires development of highly dense vascular networks that can meet the nutrient and oxygen requirements of a bulk tissue composed of a large quantity of living cells [2]. Blood vessel formation within the bulk tissue construct does not occur within a sufficient time frame to supply the necessary amount of nutrients and oxygen, leading to necrosis in the formed tissue [3]. Therefore, there is a great demand for a smart scaffold designs for effective and efficient nutrient and oxygen transport throughout the bulk of thick engineered tissues.

Polymeric tissue engineering scaffolds with disordered or random micropores have traditionally been fabricated using various techniques, such as particle leaching, phase separation, and gas foaming [4–6]. Even though these techniques are scalable and economical, they do not allow accurate control of the scaffold microenvironment, determined by the pore architecture, mechanical strength, surface area and mass transport within the scaffold [7]. These techniques can only generate one type of pore geometry i.e. local/random in the scaffold. It has been shown that scaffolds consisting of only random pores can significantly limit cell penetration and uniformity of the cell distribution due to limited diffusion of culture medium into the centre of the scaffolds [8–10]. Therefore, there is a need for a second type of porous structure, which can efficiently interconnects local random pores of the scaffold for better generation of large tissues under in vitro and in vivo conditions.

Recently, studies using dual-pore scaffolds, comprising structured pores (channels) in combination with local random porous regions, have shown tremendous potential towards engineering of complex tissues with better cell proliferation due to improved nutrient and oxygen transport [3,11–16]. A recent report also demonstrated that after transplantation of dual-porous scaffolds more cells from the host tissue infiltrated into the scaffolds due to its smart global pore architecture compared to random porous scaffolds, hence, enhancing integration of blood vessels in the host tissue [17]. The structured pores help overcome the diffusion limitation while the random pores provide a large surface area to accommodate a high density of cells. Therefore, dual-pore scaffold design with perfusable channels serves as a promising strategy for engineering of large-scale artificial tissues or organs for regenerative medicine by promoting rapid vascularization that enhances survival of the seeded cells.

Different approaches have been employed to fabricate dual-pore scaffolds for tissue engineering using both natural and synthetic polymers [3,11–15,18,19]. For controlling the size and degree of porosity of the random pores as well as the mechanical properties of the scaffolds, the two major fabrication techniques have been freeze-drying [3,11,13,14,20] and salt leaching [11,12,16] process. The published results have shown that freeze-drying cannot yield as large a range of pore dimensions as salt leaching, which can utilize salt crystals of various dimensions depending on the requirements. Currently various solid freeform (SFF) fabrication techniques such as stereolithography based printing have been reported to fabricate 3D porous scaffolds with well controlled pore size, porosity and mechanical properties using photo-crosslinkable materials [21]. Sacrificial moulds from SFF fabrication [11] or metallic wires [3,12,16,19] have been implemented for the generation of structured pores. Automated SFF fabricated moulds have several advantages compared to metal wire based moulds that require choice of wire dimensions and time consuming manual assembly of a number of wires. Hence, SFF based moulds are more reliable and rapid to use as well as provide easy upscaling of scaffold size. However, the SFF techniques presented by Kang et al. [11] required manual assembly of different stereolithographic printer parts and synthesis of photo curable inks for fabrication of the sacrificial mould. Moreover, fabrication of sacrificial moulds using stereolithography is a slow and expensive process requiring expensive commercial 3D printing equipment. Hence, there is an urgent need to develop SFF moulds using inexpensive 3D printing.

Recently, 3D printed poly(vinyl alcohol) (PVA) sacrificial moulds using 3D filament printer have been demonstrated to facilitate fabrication of porous polymeric scaffolds for various tissue engineering applications [22,23]. Ortega *et al*. and Jeffries *et al*. have proposed a new fabrication approach by encapsulating 3D printed single layered PVA channels using an inexpensive 3D filament printer in combination with electrospun nanofibers to create perfusable vascular networks [22,23]. However, the fabricated scaffolds only comprised a single layer of channels, hence, they didn´t generate a functional tissue/organ composed of multiple layers. Moreover, the random pores had dimensions of only a few nanometres, and were thus not able to facilitate cell penetration into the interior of the scaffolds. There is therefore a need to develop a new approach to fabricate multi-layered dual-pore scaffolds using a sacrificial mould that allows precise control over the geometry and dimensions of the structured and random pores.

In this paper, we present a new method for fabrication of dual-porous scaffolds using the combination of 3D filament printing and salt leaching process to control the geometry and dimensions of the structured and random pores, respectively. The 3D printing of a sacrificial PVA mould allows generation of structured pores with a high degree of control over the inner architecture designed according to the requirements of an application as we have described previously[24]. The parameters of the random pores, e.g., degree of porosity and pore size, are controlled by varying the size of the salt crystals used as the porogen. After casting the desired polymer in the mould and cross-linking it the PVA and salt are dissolved, leaving behind a dual-pore scaffold. The fabrication process is scalable and capable of generating scaffolds that are structurally and dimensionally relevant for tissue engineering applications. We show the fabrication using polydimethylsiloxane (PDMS) and cultured human hepatoblastoma (HepG2) cells for 16 days to demonstrate that the scaffolds could provide 3D microenvironment able to support cell growth and liver tissue functionality. The performance of the dual-pore scaffolds is compared with scaffolds having either only structured or only random pores fabricated using 3D printed PVA moulds or salt leaching, respectively.

4.2 Materials and method

4.2.1 Mould fabrication

Sacrificial moulds for both structured and dual-pore scaffolds were 3D printed using a

Replicator 2X 3D filament deposition printer (MakerBot Industries, LLC, Brooklyn, NY, USA) as described previously [24]. In brief, a 3D cube (L 25 mm x W 25 mm x H 10 mm) was designed using SolidWorks 2013 3D CAD design software (Dassault Systems, SolidWorks Corp., Waltham, MA, USA). The design was exported as STL format into the 3D printing software (Makerware 2.4.1) for G-code generation and mould printing. Water dissolvable poly(vinyl alcohol) (PVA) filaments (MakerBot, USA) were used to print the sacrificial moulds. The printing was performed at 200 ^{o}C as the nozzle temperature and 40^{o} C as the bed temperature. The PVA moulds printed with various porosities (infills) were used directly for fabrication of the structured pore scaffolds. For fabrication of the dual pore scaffolds (shown in Fig. 1 and summarised in Fig. S6), the PVA moulds were printed with 40 % infill as shown in Fig. 1A. 10 g of NaCl (Sigma-Aldrich Corporation, St. Louis, MO, USA) crystals (size 300 - 600 µm) was mixed with 1 ml of ultrapure water from a Milli-Q® water purification system (Millipore Corporation, Billerica, MA, USA) and packed manually into the PVA mould (Fig. 1B). The salt filled moulds were dried in an oven at 60 ^{o}C for 1 h. The small amount of water was used to form the interconnections between the salt crystals as well as between the salt crystals and PVA filaments. Both the PVA moulds for the structured pore scaffolds and the salt-PVA moulds for the dual-pore scaffolds were replicated into polydimethylsiloxane (PDMS) (Sylgard 184 Elastomer kit, Dow Corning Corporation, Midland, MI, USA). The PDMS base was mixed thoroughly with the curing agent in a 10:1 ratio and the mixture was degassed in a vacuum desiccator to remove air bubbles. The PDMS mixture was then cast into the mould (Fig. 1C). Then, the container with the mould covered with PDMS mixture was transferred into the vacuum desiccator for 2-3 h to ensure complete infiltration of PDMS into the mould (Fig. 1D). The PDMS was cured at 60°C in an oven for 4-6 h. After curing, the excess PDMS around the moulds was removed to expose the PVA or salt-PVA structures. This was done to allow the subsequent dissolution of PVA and salt in water. The entire mould-PDMS structures were immersed into water (Fig. 1E) until the PVA and salt had been completely re-moved (about 6-12 h), releasing the PDMS scaffolds with structured pore or dual-pore architecture (Fig. 1F).

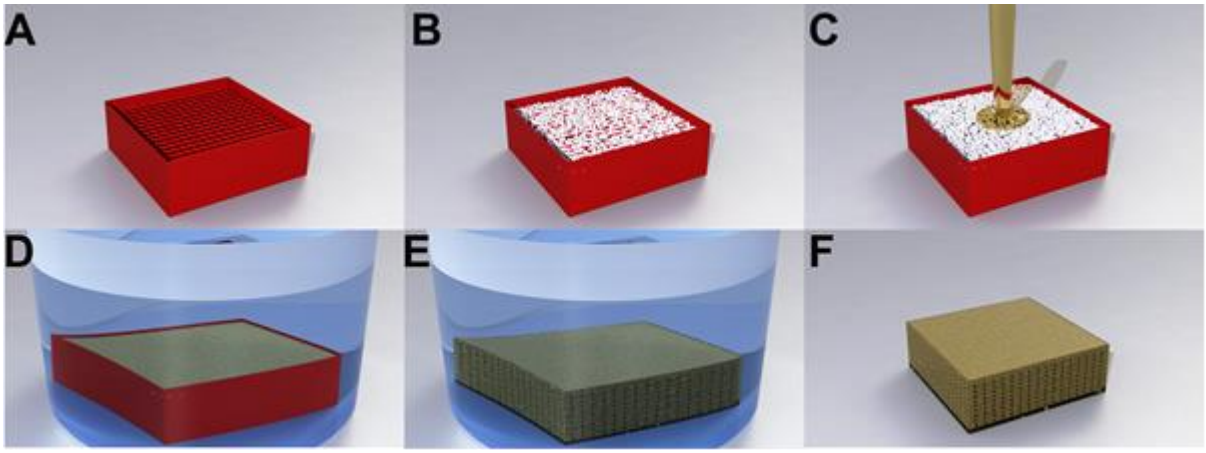

Fig. 1 Fabrication of dual-pore scaffolds: A sacrificial 3D mould was 3D printed in PVA (A) and packed with salt crystals (B). The salt-filled PVA mould was transferred into a container and PDMS was cast to cover it (C). Vacuum was applied to ensure complete filling of PDMS into the pores of the mould (D). Following crosslinking of the PDMS, the sacrificial PVA-salt mould was dissolved in water (E) releasing the dual-pore PDMS scaffold (F).

The random pore scaffolds were fabricated using salt leaching process as described previously [9,12]. 10 g of NaCl was mixed with 1ml of water on a 100 mm plastic petri plate as described above. The mixture was placed in an oven at 60 ^{0}C to generate interconnections between the salt crystals and to evaporate the excess water. The hardened salt cube was cooled at room temperature. The PDMS mixture prepared as described above and cast on the petri plate containing the salt cube. The PDMS covered salt cube was placed in a vacuum desiccator for 1 h to let the PDMS infiltrate into the pores of the salt cube. The PDMS was cured in an oven at 60 ^{0}C for 4-6 h. Finally, excess PDMS was removed and the salt was dissolved in water, as described above, to release the random porous PDMS scaffolds.

4.2.2 Characterizations of scaffolds

The structural morphology and microstructures of the porous scaffolds were imaged using scanning electron microscopy (SEM) (JEOL, JSM 5500 LV, Tokyo, Japan). Prior to SEM imaging, the dried scaffolds were sputter coated with gold. The imaging was done using 12 kV accelerating voltage. To evaluate the complete removal of sacrificial moulding materials from the scaffolds, Fourier transform infrared (FTIR) spectroscopic characterisation of the moulding materials (salt and PVA) as well as the surfaces of the structured and dual- pore PDMS scaffolds (cross-sectional surfaces after cutting the

scaffolds, as shown in the Supplementary material Fig. S1) was performed using a spectrometer (Spectrum 100, Perkin Elmer Technologies, and Waltham, MA, USA) in transmission mode. The FTIR spectra of the samples were recorded by 20 scans in the range of 400–4000 cm^{-1} at a resolution of 2 cm^{-1} using air as background.

The porosity of the PDMS scaffolds was determined using Eq 1 as described previously [12,16]. Four cylindrical scaffolds with structured, random and dual-pore architecture (Ø 6 mm, height 6 mm) were dried overnight at 60 °C, and weighed to obtain the mass of the samples. The porosity was then calculated based on the weight and the dimensions using Eq 1.

$$\text{Porosity}\ (\%) = \frac{V - \left(\frac{M}{\rho}\right)}{V} \times\ 100\% \qquad (1)$$

Where V is the volume of the scaffold, calculated based on its outer dimensions, M is the mass of the scaffold, and ρ is the density of PDMS (0.965 g/cm^3).

The compressive modulus of different scaffolds (L 25 mm × W 25 mm × H 10 mm) was determined by uniaxial compression tests using an Instron® Tensile Tester 4301 (Instron Corporation, Norwood, MA, USA). The samples were compressed at a rate of 0.5 mm min^{-1}. The compressive modulus was calculated as the slope of stress-strain curve from the linear range of the curve for each sample. The values reported were an average from testing of four independent scaffold of each type of porous scaffolds.

To assess wettability of the scaffolds, contact angle measurements were carried out on scaffolds before and after oxygen plasma treatment. The contact angle was measured optically using an OCA 20 system (Dataphysics, Germany) by the sessile drop method by depositing a 3 µl drop of ultrapure water on the scaffold surface.

4.2.3 Cell culture and assays in scaffolds

4.2.3.1 Cells

Human hepatoblastoma (HepG2) cells were obtained from the German Collection of Microorganisms and Cell cultures (DMSZ, Braunschweig, Germany). Cells were maintained in Roswell Park Memorial Institute medium (RPMI-1640) containing L-glutamine and supplemented with 10% foetal bovine serum (FBS), both from Sigma-Aldrich Corporation, St. Louis, MO, USA, and 1% penicillin/streptomycin (Life Technologies, Corporation, Paisley, UK) in a humidified incubator at 37°C and 5% CO_2. Cell culture medium was exchanged completely every 2-3 days until the cells were fully

confluent. The cells were detached from the culture flask using 0.025% trypsin/EDTA solution (Life Technologies, Corporation, UK) and the cell number was determined using a haemocytometer and adjusted to the required number before seeding into the 3D scaffolds.

4.2.3.2 Preparation of scaffolds for cell culture

The scaffolds were prepared according to the protocol published previously [24]. In brief, cylindrical PDMS scaffolds of each type (Ø 6 mm, height 6 mm) were used in the experiments. Here, for cell studies control scaffolds with only structured pores, 80% porosity were used. To render the PDMS hydrophilic, scaffolds were treated with oxygen plasma for 1 min on both sides at a power of 50 W and pressure of 35 Pa using an Atto Plasma System (Diener Electronic GmbH, Ebhausen, Germany) equipped with a 13.56 MHz RF generator. The oxygen plasma treated scaffolds were autoclaved at 120 ˚C for 20 min followed by coating with 80 µg/ml of Collagen I (Collagen I rat protein, Life Technologies) at 4°C overnight. The scaffolds were washed twice with cell culture tested phosphate buffered saline (PBS) to remove excess collagen and then incubated in culture medium at 37˚C for 2 h until cell seeding. The cells were seeded into the scaffolds using a special 6 mm thick cell seeding tray with several holes (Ø 6 mm), fabricated of poly(methyl methacrylate) (PMMA) using a CO_2 laser ablation machine (Epilog Mini 18 Laser, CO 80403, USA) as described previously [24]. The seeding tray was sterilized by washing with 0.5 M sodium hydroxide solution followed by rinsing with sterile water. Each scaffold was inserted into the hole in the seeding tray. 30 µl suspension of HepG2 cells in culture medium containing 250.000 cells were added on top of each scaffold and incubated at 37 ˚C for 3 h to achieve cell attachment. Every hour the tray was turned upside down for better cell infiltration into the scaffolds. Finally, each scaffold was transferred from the seeding tray into a well in a 24-well plate, and 1 ml of fresh culture medium was added in each well. Every 2 days the medium was collected for cellular functionality analysis and replaced with fresh medium. On day 4, 8 and 12 of the culture period, two scaffolds were sacrificed and used for live/dead staining. Similarly, for determination of the total cell number, three scaffolds of each type were sacrificed at each time point (day 2, 4, 6, 8, 12, and 16).

4.2.3.3 Biochemical assays

Cell proliferation was determined based on the DNA content of cells cultured in the

scaffolds. The cells inside the scaffolds were lysed using 1 ml of lysis buffer (10 mM Tris pH 8, 1 mM EDTA and 0.2 % (v/v) Triton X-100). To ensure that the cells inside the scaffolds were totally lysed, the samples were stored on ice for 30 min and vortexed for 10 s every 5 min. The lysate from each scaffold was homogenised 5-10 times using a 21-guage needle. The DNA concentration in the lysates was quantified using PicoGreen DNA assay (Life Technologies Corporation, UK) according to the manufacturer's protocol. A standard of DNA concentrations was prepared by isolating dsDNA from HepG2 cells (known number of cells) cultured in T25 flasks using the same protocol as for the scaffolds. The calibration curve was obtained by correlating the number of cells with the corresponding fluorescence intensity (shown in the Supplementary material Fig. S4).

The metabolic activity of the cells was measured using the alamarBlue® assay (Life Technologies Corporation, UK) as described previously [24]. In short, the scaffolds were rinsed with PBS and incubated in 1 ml of culture medium containing 10% alamarBlue® solution for 2 h in the incubator. Following incubation, 100-µl aliquots were placed into black 96 well plates and the fluorescence was quantified using a microplate reader (VICTOR3™ Multilabel Counter model 1420, PerkinElmer, USA) at the excitation wavelength of 550 nm and emission wavelength of 590 nm. The background (i.e. alamarBlue® fluorescence at day 1) was subtracted from the value.

The concentration of albumin secretion from the cells in the scaffolds was determined using human albumin enzyme-linked immunosorbent assay (ELISA) Quantitation kit (Bethyl Laboratories, Inc., Montgomery, AL, USA) according to the manufacturer's protocol. The absorbance was measured at 450 nm using a spectrophotometer (VICTOR3™ Multilabel Counter model 1420, PerkinElmer, USA). For all the biochemical assays, the tests were carried out in triplicate using 3 independent scaffolds of each type. The results are reported as average ± standard error of the mean (s.e.m). (n = 9).

4.2.3.4 Live/dead cell staining

Cell viability and distribution in the scaffolds were visualized using LIVE/DEAD® Cell Imaging Kit (Life Technologies Corporation, UK), containing a cell-permeable dye for staining live cells (excitation/emission 488 nm/515 nm) and a cell-impermeable dye for staining dead and dying cells (excitation/emission 570 nm/602 nm). The scaffolds were collected and gently washed with PBS followed by incubation in the dye solution for 30

min at 37°C according to the manufacturer's protocol. The scaffolds were imaged using an Axio Observer fluorescence microscope (Zeiss Axio Observer.Z1, Carl Zeiss, Germany). The 3D reconstructions were compiled from 20 imaged sections (each having a thickness of 30 μm).

4.3 Results and discussion

Previously engineered dual-pore scaffolds with highly interconnected global (structured) and local (random) pores fabricated of both natural and synthetic biomaterials have shown promising results with improved cell proliferation in vitro and enhanced integration into the host tissue upon transplantation [3,12,17]. However, they had significant limitations in terms of mass fabrication and scalability due to the necessary manual assembly of the sacrificial mould components, as well as control of the dimensions and number of structured pores introduced into the bulk scaffold. Thus, novel strategies can help develop mass fabrication of dual-pore scaffolds with control over physical and mechanical properties. With the goal of developing a simple, inexpensive and reproducible method for mass fabrication of dual-pore scaffolds with tuneable physical properties, we present a technique combining 3D filament printing of sacrificial moulds and salt leaching. Subsequently, to evaluate the dual- pore scaffolds in terms of physical properties and biological performance (cell loading, cell distribution and cellular functionality), two other types of scaffolds, i.e. the structured pore and random pore scaffolds were fabricated and used as controls.

4.3.1 Scaffold fabrication

3D filament printing is an inexpensive SFF technique that offers highly versatile approach to fabricate the sacrificial moulds, allowing to deposit PVA polymer layers with different geometries in the x and y directions, such as 'woodpile' or 'hexagonal' (as shown in the Supplementary material Fig. S2), that functions as vascular porous networks. As we have shown previously, PVA moulds could be fabricated with porosities in the range of 20 – 80 % depending on the infill of the mould, which were shown to correspond to channel distances ranging from 78 μm to 1482 μm [24]. Aside from effective control over channel dimensions and geometry, 3D filament printing allows to scale up the fabrication of tissue engineering scaffolds. Hence, to generate structured pores for dual-pore scaffolds, 3D printing of PVA filaments was an obvious choice for

our fabrication process presented here. In this work, 40 % infill was used to fabricate the PVA moulds for the dual-pore scaffolds, resulting in inter-filament distance of 800-850 µm. Salt leaching as the source of random pores gives the possibility to control the pore sizes range by choosing the size distribution of the salt crystals to mimic the anatomical features of the tissues or organs required to be engineered [25]. In this study the NaCl crystals were used directly as provided by the supplier, sizes ranging from 300 µm to 600 µm.

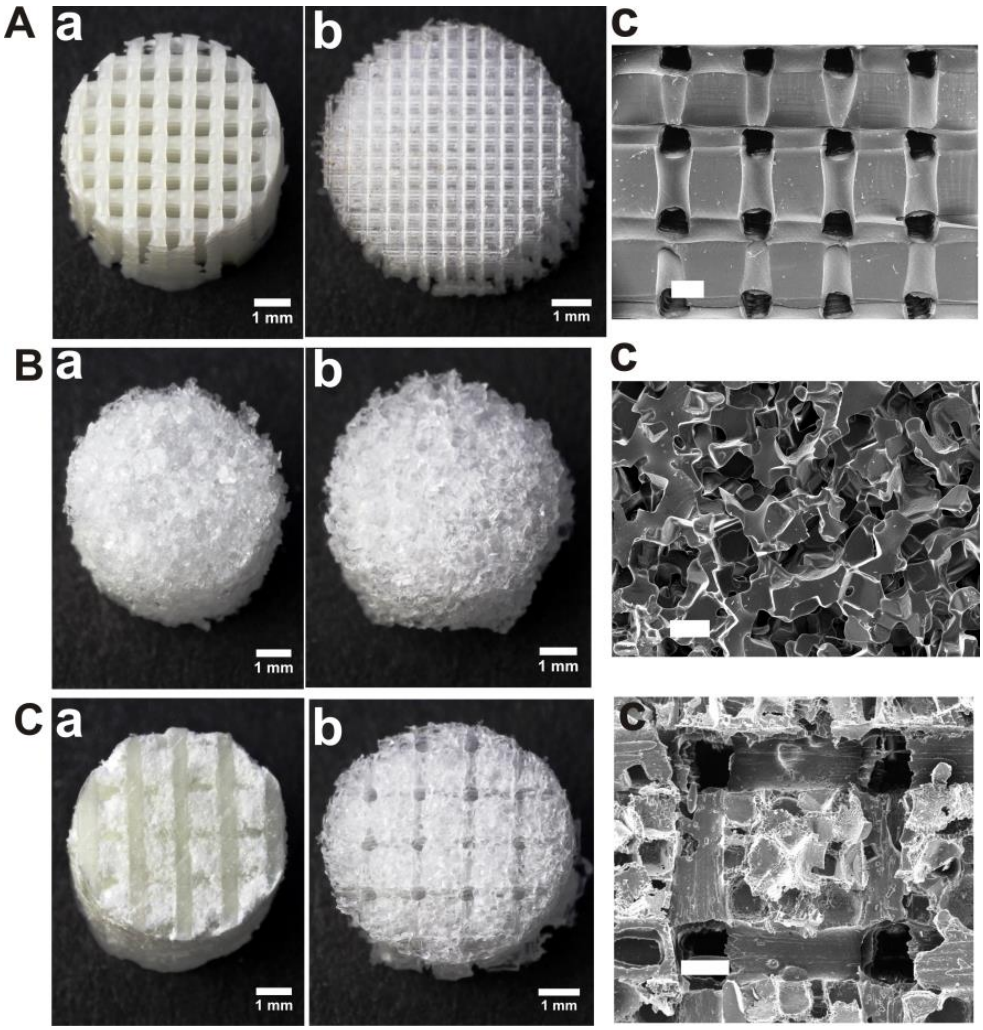

Fig. 2 Sacrificial moulds and resulting fabricated porous PDMS scaffolds: A) 3D printed PVA mould (a) and replicated structured pore scaffold with pore size of 400 µm × 400 µm (b) and SEM magnification (c); B) photo of salt mould (a) and replicated random pore scaffold with pore size of 300-600 µm (b) and SEM magnification (c); C) photo of 3D printed PVA mould filled with salt (a) and replicated dual-pore scaffolds with structured pores of 400 µm × 400 µm and random pores of 300-600 µm (b) and SEM magnification (c). Scale bars: 1 mm in A, B and C (a & b); 400 µm in A, B and C(c).

The PDMS scaffolds with structured pores (Fig. 2Ab) were fabricated using 3D printed PVA filament moulds with woodpile pattern (Fig. 2Aa), while the random pore scaffolds (Fig. 2Bb) were derived from cylindrical salt disks (Fig 2Ba) using previously described methods [24,26,27]. As shown in the SEM image of the structured pore scaffold in Fig. 2Ac, the pores are square shaped with dimension of ~ 400 µm × 400 µm and well interconnected. In the random pore scaffolds, the salt leaching process gives pores with dimensions in the range of 300-600 µm (Fig. 2Bc), as determined by the size distribution of the used salt crystals.

By combining both approaches, we fabricated dual-pore scaffolds (Fig. 2Cb) with both defined structured and random pore microarchitectures using the sacrificial 3D printed structured porous PVA filament moulds filled with salt crystals into the inter-filamentous space (fig 2Ca). The method of fabrication is simple and involves casting of the desired polymer (in this study PDMS was used) in the mould which specifies the microarchitecture of pores within the resulting scaffold. Surface top view of the dual-pore scaffold is shown in the SEM image (Fig. 2 Cc). The structured pores of dimension ~400 µm × 400 µm are distributed in x, y and z directions, whereas the random pores with dimension of 300-600 µm are shown in between the structured pores of the bulk scaffold (Fig. 2 Cc). As shown in the SEM image of the top surface of a dual-pore scaffold (Fig. 3A and its zoom-in view Fig. 3B), the scaffolds had regular, well-structured and highly interconnected structured pores in the z (yellow lines) and x-y (red lines) direction throughout the scaffold. In between the structured pores, the scaffolds had an array of square shaped random porous regions of 800 µm × 800 µm. The salt crystals of size 300-600 µm fused together and generated large interconnected pores. Fig. 3C and its zoom-in Fig. 3D, show SEM image of cross-sectional view (Supplementary material Fig. S1) of the interior of the scaffold. The channels in the scaffold have an elliptical cross-sectional profile, as the round PVA filament is flattened during printing of the mould, and the distance between two rows of structured pores is about 800 µm. The dimensions of the pores (width 344µm, height 190 µm) are slightly smaller than that of the filaments in the printed mould (400 µm × 200 µm), due to shrinkage during curing of the PDMS elastomer. A random pore region can be seen in the area between two rows of structured pores (blue dotted line). To demonstrate the possibility of controlling the size of the random pores, the previously described PVA mould was filled with smaller salt or sugar crystals, yielding scaffolds shown in the Supplementary material Fig. S4 (using 20-40 µm salt crystals) and Fig. S5 (using 100-200 µm sugar

crystals). The SEM images with different magnifications in Fig. S4 clearly show the highly interconnected small random pores (20-50 µm) along with the 400 µm × 400 µm structured pores. The inter-filament distance of a PVA mould has to be optimized according to the size of the salt or sugar crystals needed to generate the random pores. Using different size of porous mesh, it is possible to obtain salt or sugar crystals with different size distribution. If large crystals need to be used, the distance between the deposited PVA filaments has to be increased by reducing the porosity of PVA mould from 40 % infill to lower.

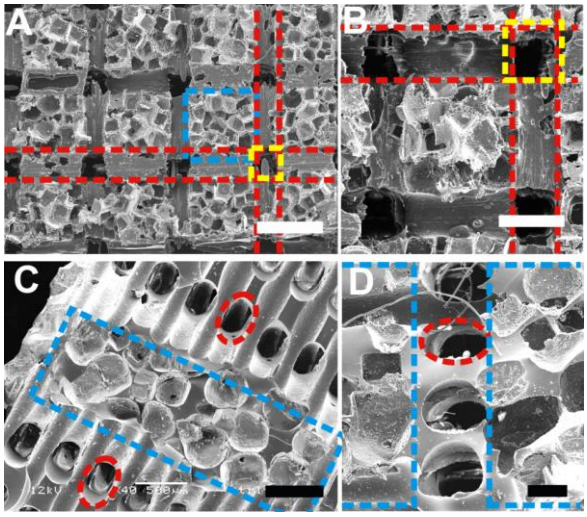

Fig. 3 SEM images of fabricated dual-pore scaffolds (structured pore size 400 µm × 400 µm, distance between structured pores 800 µm; random pore size 300-600 µm): A) top view showing structured pores and an array of random pores; B) magnification of the top view in (A); C) cross-sectional view of structured and random pores; (D) magnification of the top view in (C). (Dashed lines: yellow – structured pores in z-direction; red - structured pores in x or y-direction; blue - random pores area) Scale bars: A) 1mm; B) and C) 500 µm; D) 250 µm.

Here, we have shown the fabrication of dual pore scaffolds with dimensions of 25 mm × 25 mm × 10 mm (length × width × height). However, the scalability of the PVA mould printing and the scaffold casting process that we have demonstrated in our previous work [24], mean that the method proposed in this paper can generate dual-pore scaffolds with dimension relevant for the size required for creating artificial organs. We used the biocompatible and non-biodegradable elastomeric PDMS, which is widely used in biological and medical applications [28,29], to demonstrate the ease of fabrication to obtain different porous scaffolds for tissue engineering applications. It has already been

shown that PDMS scaffolds have the potential to support long-term growth of liver cells [24]. However, this method can also be applied to other materials, providing the possibility to fine-tune the properties of bulk scaffold by choosing a suitable biomaterial. To demonstrate this, poly(ϵ-caprolactone) (PCL), a FDA approved biodegradable polymer [30], was used to fabricate dual-pore PCL scaffolds (Supplementary material Fig. S5).
Here we have shown the biocompatibility and functionality of HepG2 cells supported by various silicone scaffolds (Fig. 5-7) however this has to be tested with the type cells required to engineer the relevant tissue. Silicone based non-degradable scaffolds could be utilized to develop life support system (LSS) such as an extracorporeal liver [31] for the short term treatment of patients with liver failure. Utilizing silicone based highly porous scaffolds for extracorporeal liver device offers several benefits such as easy fabrication of scaffold structures with dual pores, structurally strong and elastic material for building large scale porous structures, easy sterilization method by autoclavation and without any shrinking or swelling properties allows robust fluidic perfusion into the scaffolds compared to some hydrogels [24]. Furthermore, FDA approved medical grade silicone elastomers are available, which should be compatible with the described fabrication method.

4.3.2 Scaffold characterization

4.3.2.1 Removal of the sacrificial materials (salt and PVA) from the scaffolds

FTIR spectroscopy was used to monitor the complete removal of the sacrificial materials (salt and PVA) from the scaffolds. Fig. 4A shows FTIR spectra of salt crystals (black), cross-linked PDMS (blue), 3D printed PVA filament (red) and PDMS dual-pore scaffold after removal of salt and PVA (green). In the spectrum for PVA, peaks were observed at 3400 cm^{-1} (–OH) and 1740 cm^{-1} (C=O), whereas salt crystals had a peak at 3400 cm^{-1} (–OH). All of these peaks were absent in spectrum for cross-linked PDMS due to the different molecular structure [32,33]. The spectrum for the fabricated 3D scaffold (recorded from the interior regions as shown in the supplementary Fig. 1) completely resembles the one recorded for cross-linked PDMS, which clearly indicated that PVA and salts had been completely removed from the structure. Spectra were recorded from at least six different positions throughout the final scaffold to obtain a complete confirmation. Simultaneously, a basic visualization of the PVA removal was done. The PVA-salt-PDMS structures were transferred into a water beaker with a

magnetic stirrer to aid the faster dissolution of the PVA and salt. Initially, when immersing the PVA-salt-PDMS structures into water, they sank to the bottom of the container. After complete removal of PVA and salt, the hydrophobic PDMS scaffold structures were floating on the surface. During the process of dissolution the water turned cloudy due to the release of PVA into the water, and water were replaced until it remained clear.

4.3.2.2 Porosity

The degree of porosity and pore size of the scaffold material both at the macroscopic and the microscopic level play a very important role in tissue regeneration [34]. The total porosity of the scaffolds, fabricated with the three different porous geometries was determined experimentally and presented in Fig. 4B. The porosity of the dual-pore scaffold was 64.8 ± 1.05% whereas in case of structured and random pore scaffolds the porosity was 39.5 ± 0.08 % and 68.02 ± 0.95%, respectively. The porosity of the dual-pore scaffolds was higher compared to the structured pore scaffolds due to the presence of both structured and random pores. Previously, we have shown the possibilities to fabricate structured pore PDMS scaffolds with porosities ranging from 20 % to 80 % by varying the infill of the printed PVA mould from 20% to 80%. In this study, dual-pore scaffolds were fabricated using 40 % infill PVA moulds. For better comparison, the physical characterization of dual-pore scaffolds is compared with the structured pore scaffolds generated using 40 % infill PVA moulds. Previously published dual-pore fabrication methods have shown similar behaviour in terms of porosity, the total porosity of dual-pore scaffolds being always greater than the porosity of structured and random pore scaffolds [12,16]. In this study, the random pore scaffolds showed higher porosity (68.02 %) than the dual-pore scaffolds due to the larger size of the random pores in comparison with the size of the structured pores (Fig. 3). To achieve higher porosity in dual-pore scaffolds in comparison to random pore scaffolds, the size of the random pores has to be smaller than the structured pores. This concept was illustrated in the Supplementary material Fig. S4 and S5 where porosity of about 80% was achieved. The porosities of dual-pore scaffolds completely depend on the microstructure of 3D printed PVA mould and the size of the salt crystals filled in it. Hence, a desired range of pore dimensions can easily be optimized through this fabrication technique.

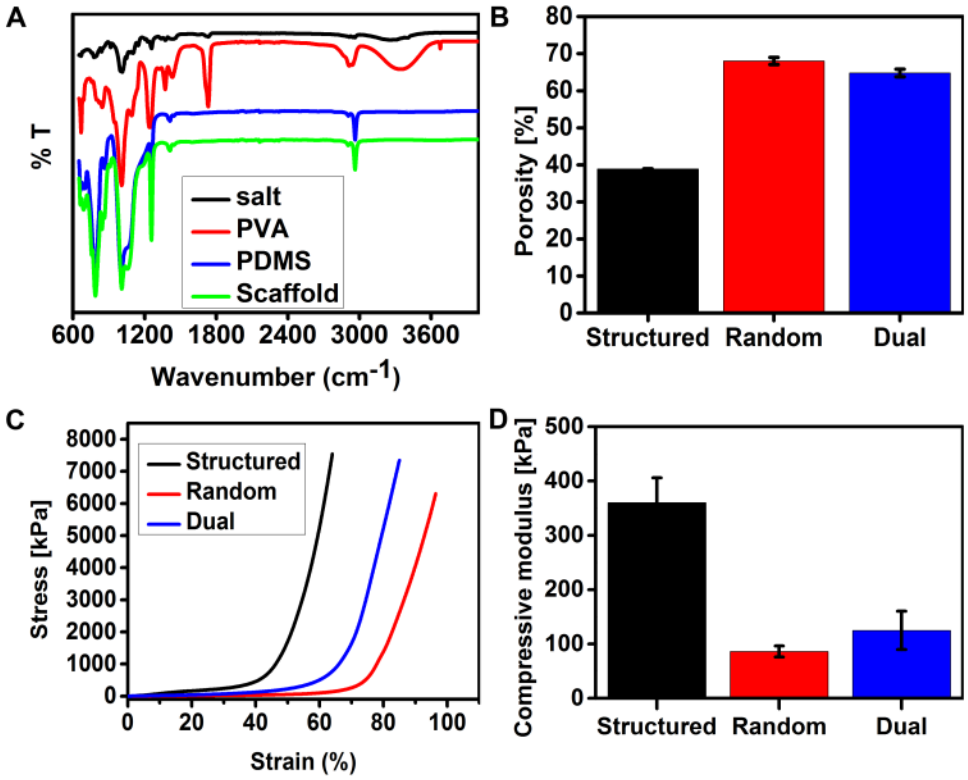

Fig. 4 A) FTIR spectra: salt crystals (black), cross-linked PDMS (blue), 3D printed PVA filament (red), and dual-pore PDMS scaffold after removal of salt and PVA (green). Mechanical characteristics of different scaffolds: B) porosity; C) stress–strain curves at 4 N load; D) compressive modulus.

4.3.2.3 Mechanical testing

The mechanical properties of tissue engineering scaffolds can modulate cell morphology, proliferation, migration and differentiation [35–37], and it is therefore important to control the mechanical properties of the bulk scaffold while engineering an artificial tissue. Mechanical compression tests were conducted with dry scaffolds with the different pore structures. Fig. 4C shows typical stress-strain curves of the different scaffolds at a constant compression rate of 0.5 mm min^{-1}. The compressive modulus of structured, random and dual-pore scaffolds was determined to be 359 ± 16, 84 ± 10 and 125 ± 35 kPa, respectively (Fig. 4D). Previously, it has been shown that the compressive modulus of porous scaffolds reduces significantly as the porosity of the scaffolds increases [24,38,39]. For the same reason, the dual-pore scaffolds showed intermediate mechanical properties compared to structured and random pore scaffolds, indicating the expected relationship between porosity and the mechanical stiffness of the scaffolds. The compressive modulus of the structured pore scaffolds was similar to our previous

study presented with similar kind of scaffolds (about 360 kPa) [24]. Moreover, our mechanical tests on the different scaffolds showed similar trend as previously reported for structured, random and dual-pore scaffolds fabricated of PCL [12,16]. The result of the mechanical test indicates that the mechanical properties of the dual-pore scaffolds can be easily modified by the combination of random and structured pores. Since the elastic moduli of human organs and tissues are very diverse, the stiffness of fabricated dual-pore PDMS scaffolds can be tuned by changing the porosity of the scaffolds or the degree of cross-linking, i.e. the ratio between the PDMS base and the curing agent [36]. As mentioned above, the fabrication technique presented in this paper can be applied to other materials than PDMS, such as the biomaterial PCL (Supplementary material Fig. S5), which provides an additional route for fine-tuning scaffold stiffness according to the requirements of in vivo tissues.

4.3.3 Cell proliferation and viability

Although the proposed dual-pore scaffold fabrication technique can be used to control the physical and mechanical properties of the scaffolds, it is important to evaluate the cell behaviour in the scaffold architecture. As PDMS is a hydrophobic material, it is important to render the scaffold surfaces hydrophilic before seeding cells into the scaffolds. To achieve this, all the scaffolds were treated with oxygen plasma. The achieved hydrophilicity was confirmed by the decrease in contact angle from 120° ± 4° to below 10°.

4.3.3.1 Biochemical assays of cell proliferation and functionality

Proliferation and functionality of HepG2 cells in the different porous scaffolds was monitored during 16 days (Fig. 5). The proliferation of HepG2 cells within the scaffolds was determined based on both the total intra cellular DNA content using the Picogreen assay and cellular metabolic activity using alamarBlue® assay. Along with cellular proliferation, the functionality of HepG2 cells was determined based on the extracellular albumin release as a liver-specific marker.

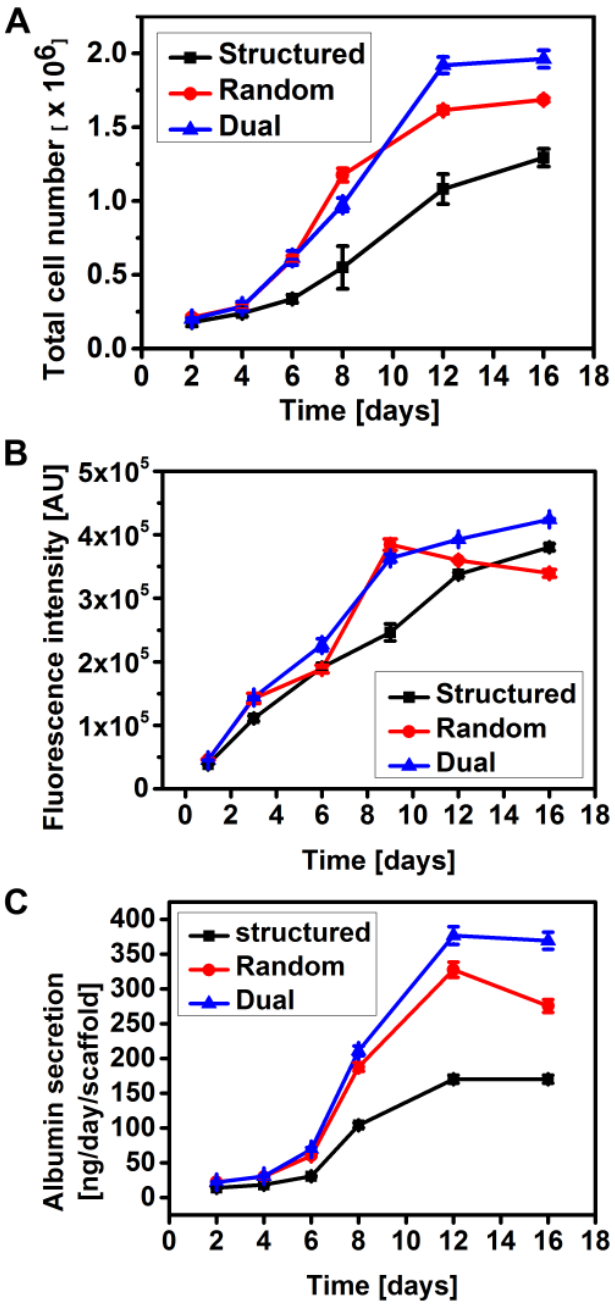

Fig. 5 HepG2 cell proliferation and functionality on different scaffolds: A) total cell number (Picogreen assay) during day 2-16 (B). B) Metabolic activity (alamarBlue® assay) over 1-16 days (D). C) Albumin secretion over 16 days (F). Data represents mean ± s.e.m. (n = 6).

As shown in Fig. 5A, from day 2 to day 4, the total cell number increased (proliferated) slowly in all three types of scaffolds, whereas after day 4 onwards the proliferation rate increased especially in the random and dual-pore scaffolds where the cell numbers increased at similar rates. However from day 9 the cellular proliferation rate in the dual-pore scaffolds were higher in comparison to the two other types of scaffolds. From day 12 the number of cells reached a steady state in both random and dual pore scaffolds

whereas the number of cells continued to increase in the structured pore scaffolds. At the same time the number of cells was lower in the structured pore scaffolds throughout the culture period in comparison with the random and the dual-pore scaffolds.

Along with cell proliferation the metabolic activity of HepG2 cells in the three different types of scaffolds was determined using the alamarBlue® assay (Fig. 5B). From day 1 to day 9, the metabolic activity increased steadily in all the different types of scaffolds (Fig. 5B) although the activity was lower in the structured pores scaffolds. Until day 9, the cells grown in the random pore and dual-pore scaffolds did not show any significant difference. However, after day 9, the metabolic activity in the random pore scaffolds started to decline whereas in dual- and structured pore scaffolds continued to increase until the end of the experiment.

Fig. 5C shows the magnitude of albumin secretion from HepG2 cells cultured in the different types of scaffolds. Similar to the cell proliferation profiles (Fig. 5A), albumin production from HepG2 cells grown in all of the three different types of scaffolds increased for the first 12 days (Fig 5C). On day 12, the cells cultured in the dual-pore scaffolds produced the highest amount of albumin (375 ng/day/scaffold) compared to the cells cultured in the random and structured pore scaffolds (325 and 145 ng/day/scaffold, respectively). However from day 12 to 16, the albumin secretion rate from cells in random scaffolds started to decline, whereas the rate remained constant for the cells grown in both the dual-pore and structured pore scaffolds.

Both the random and dual pore scaffolds contain random pores, which increase the surface area compared to structured pore scaffolds. Therefore more cells could be trapped and adhere on these scaffolds and there were also more surface for cell proliferation. In the literature it has been shown that SFF fabricated structured pore scaffolds have lower cell adherence after seeding in comparison with random and dual-pore scaffolds [12,16], which clearly agrees with our result. From day 1 until day 9, the cells grown in random pores scaffolds or in the dual-pore scaffolds did not show any significant difference in cell proliferation, metabolic activity and albumin secretion, whereas these parameters were considerable lower for the structured pores scaffolds, probably due to smaller surface area. The declining metabolic activity from day 9 or in albumin secretion from day 12 in the random pore scaffolds may be explained by insufficient nutrient and oxygen supply into the scaffold or by accumulation of cellular waste, due to limited mass transport in this type of scaffold. In summary, the results clearly indicate that the cell proliferation, metabolic activity and albumin secretion from cells

growing in the dual-pore scaffolds showed better performance compared to the cells in the structured and random pore scaffolds due to high surface area of the random pores in combination with better nutrient and oxygen supply as well as waste removal through the structured pores.

4.3.3.2 Cell distribution and viability within the scaffolds

To visualize cell distribution and viability, in the different porous scaffolds, qualitative live/dead staining was carried out on day 2, 8 and 16 after cell seeding (Fig. 6). On day 2, the number of live cells distributed on the surface of the random (Fig. 6Ba) and dual-pore scaffolds (Fig. 6Ca) was higher compared to that on the structured pore scaffolds (Fig. 6Aa), which correlates well with the biochemical assays shown in Fig. 5. From day 2 to day 16, cells grow uniformly on the surface of all the different types of scaffolds (Fig. 6 A b, c and d; B b, c and d; C b, c and d). However on day 16, more dead cells could be observed on the surface of the random pore scaffolds (Fig. 6 Bd), whereas on the surface of the structured (Fig. 6Ad) and dual-pore (Fig. 6 Cd) scaffolds only very few dead cells could be observed. In dual-pore scaffolds, cell distribution was characterized by initial (from day 2 to 8) cell growth primarily in the structured pore regions (Fig. 6Ca and b). Later, when all the structured pores regions were completely covered, the cells migrated into the random pore regions of the scaffold as shown for day 16 (Fig. 6Cc).

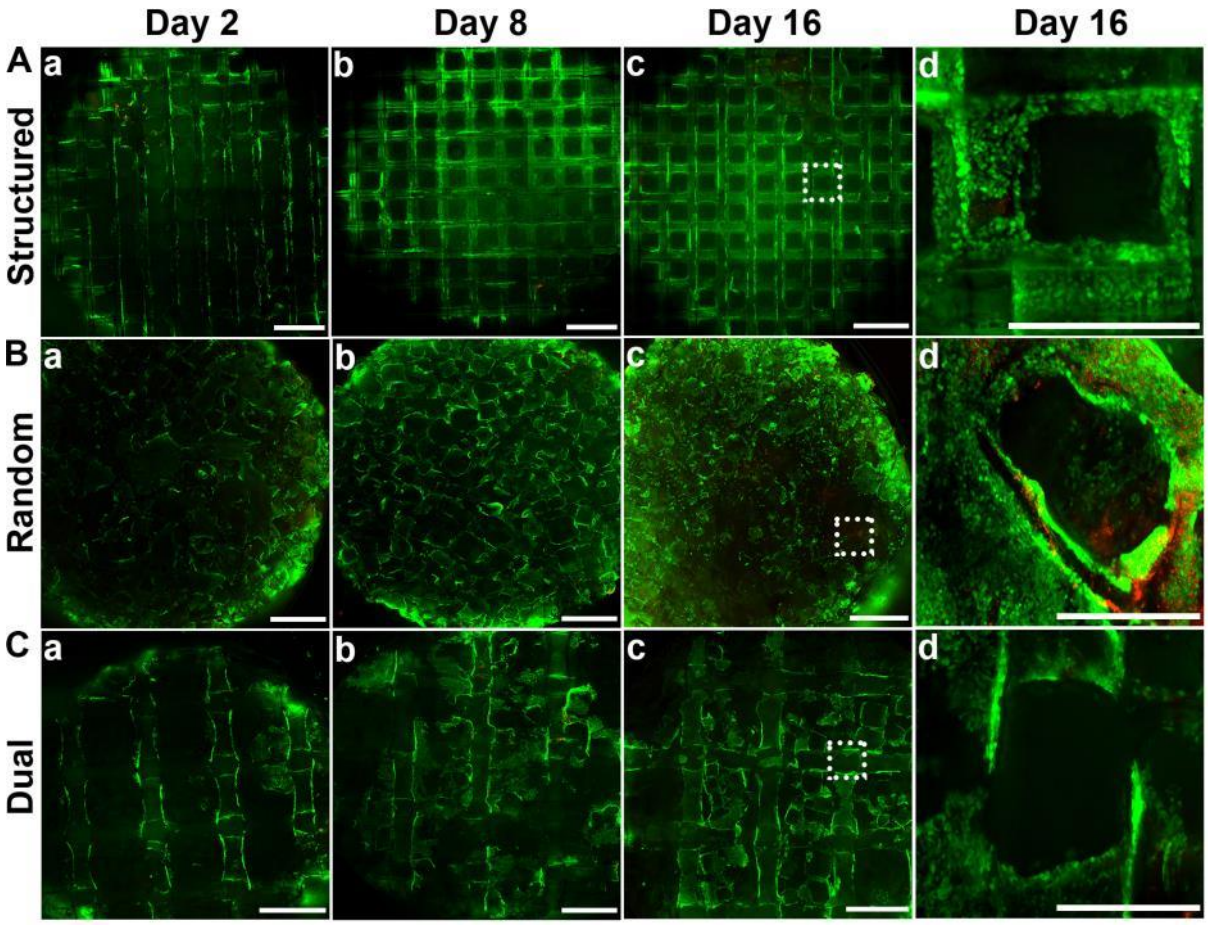

Fig. 6 Live/dead staining of HepG2 cells: Top view on A) structured, B) random, and C) dual-pore scaffolds on day a) 2, b) 8, and c) 16, as well as zoom-in of day 16. (green – live; red – dead) Scale bars: A, B & C (a,b,c) 1 mm; A,B,C (d) 350 µm.

In Fig. 6, it was not possible to see the cell distribution in the central parts of the scaffolds, which are more critical due to the limitation of nutrient and oxygen supply. Therefore, the scaffolds were cut longitudinally through the centre (Supplementary material Fig. S1) and live/dead stained to visualise the cell distribution inside the scaffolds (Fig 7). The cells were distributed more uniformly inside the structured (Fig. 7A) and dual-pore (Fig. 7C) scaffolds than inside the random pore scaffolds (Fig. 7B). On day 2, the cell distribution inside the different scaffolds was very low (Fig 7 Aa, Ba, Ca) but over time, the cell density in the structured and dual-pore scaffolds steadily increased (Fig 7 Aa-c, Ca-c). On day 16, the structured (Fig. 7Ac) and dual-pore (Fig. 7Cc) scaffolds showed uniform cell distribution throughout, whereas the random pore scaffolds (Fig. 7Bc) had very low amount of cells distributed in the central regions. For this type of scaffold the cells appeared to be mainly proliferating on the outer surface, where there is direct contact with the culture medium, instead of migrating into the

centre of the scaffold. This difference in cell distribution can be explained by the presence of the structured pores that provide interconnections in x, y and z-direction throughout the structured and dual-pore scaffolds. Previously, similar kind of results have been reported, indicating that SFF fabricated scaffolds had more uniform cell distribution and penetration of cells into the scaffolds [16,24,40]. Moreover, more dead cells appeared over time inside the random pore scaffolds (Fig. 7Ba, b and c), which completely agrees with the biochemical assay that showed first a drop in metabolic activity (Fig 5B) and later in the albumin secretion (Fig 5C) from the cells grown in random pores scaffolds. Zhang *et.el,* have reported a similar phenomenon by creating PCL random pore scaffolds with a combination of different pore dimensions [9]. They also showed that after 14 days of cell culturing, the cell distribution in the random porous scaffolds was always on the outer edges which completely agrees with our result. Homogeneous cell distribution in the bulk scaffold prolongs the proliferation period, gives uniform tissue formation and better cell differentiation characteristics as shown in previous works[40–42]. The dual-pore scaffolds are superior to the two other types of scaffold as it combines high cell number (Fig 5A), metabolic activity (Fig 5B), and albumin secretion (Fig 5C) with uniform distributing of living cells both on (Fig 6C) and into the scaffolds (Fig 7C). In future works, the effectiveness of dual-pore scaffolds will be tested for co-culturing of two different populations of cells: liver cells in the random pore region and endothelial cells as a lining of the structured pores.

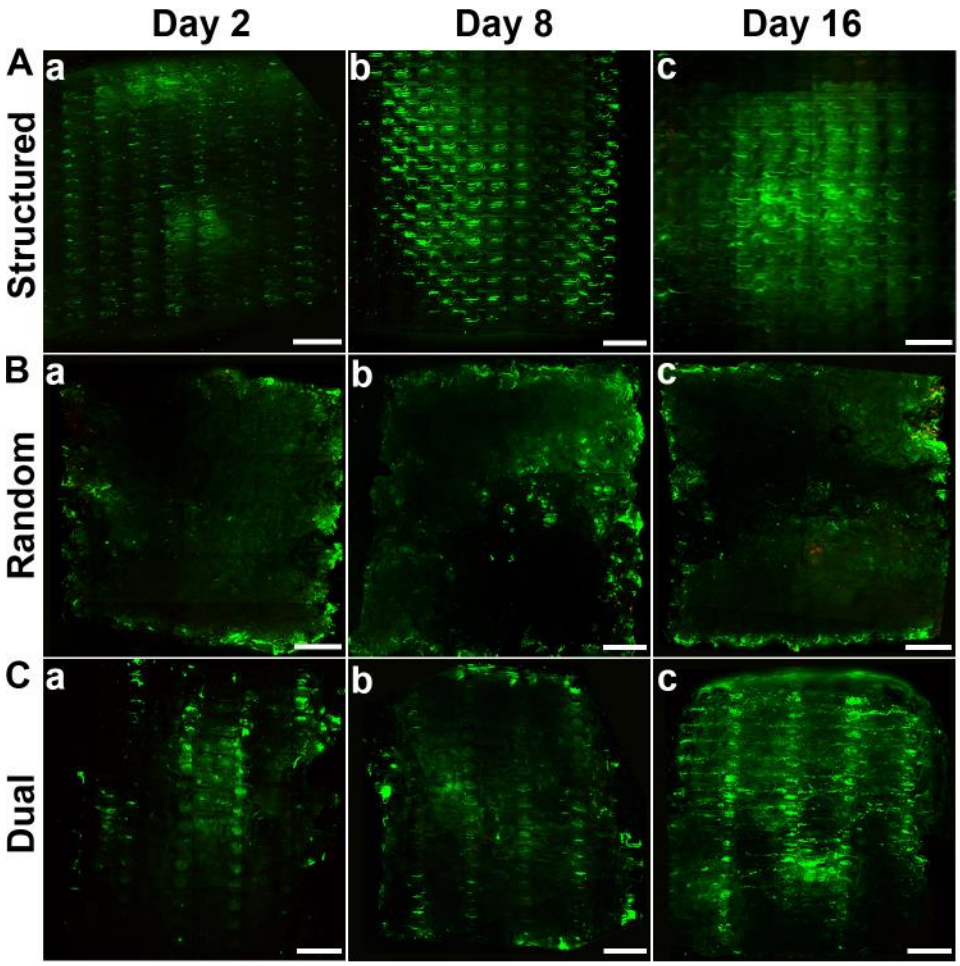

Fig. 7 Live/dead staining of HepG2 cells: Cross-sectional view in the interior of A) structured, B) random, and C) dual-pore scaffolds on day a) 2, b) 8, and c) 16. (Green – live; red – dead) Scale bar: 1 mm.

4.4 Conclusions

We present a method to fabricate dual-pore scaffold by combining 3D filament printing of water soluble PVA sacrificial mould for primary structured pores and salt leaching to create random pores within the bulk scaffold. The method provides control over pore geometry and dimensions as well as mechanical stiffness of both the structured and random pores of the dual-pore scaffold. Using PDMS as the scaffold material, we have demonstrated that the fabrication process is rapid and inexpensive as well as scalable for generation of scaffolds of a size, relevant for thick tissues. The PVA printed sacrificial moulds can also be used with different biodegradable natural polymers (e.g. gelatine and silk) combined with freeze-drying, to provide scaffolds with wide range of mechanical properties. Human hepatoblastoma (HepG2) cells were grown in different types of

scaffold for 16 days monitored with respect to attachment, distribution, proliferation, viability, metabolic activity, and albumin secretion and cells grown in dual-pore scaffolds with cells grown in only structured or only random pores scaffold. The dual-pore scaffolds with highly interconnected structured pores combined with the adjacent random pores was superior to the two other types of scaffold as it combines high cell number, metabolic activity, and albumin secretion with uniform distributing of living cells in the entire volume of the scaffold. In conclusion, the described fabrication technique is rapid, inexpensive, scalable, and compatible with different polymers, making it suitable for engineering various large scale organs/tissues.

Acknowledgements

This work has been financially supported by EU project NanoBio4Trans ("A new nanotechnology-based paradigm for engineering vascularised liver tissue for transplantation", grant no: 304842). We thank Professor Dang Duong Bang for correcting the manuscript and Jesper Scheel for taking photographs of the scaffolds.

4.5 References

[1] Rustad K C, Sorkin M, Levi B, Longaker M T and Gurtner G C 2010 Strategies for organ level tissue engineering. *Organogenesis* **6** 151–7

[2] Khademhosseini A, Vacanti J P and Langer R 2009 Progress in tissue engineering. *Sci. Am.*

[3] Wray L S, Rnjak-Kovacina J, Mandal B B, Schmidt D F, Gil E S and Kaplan D L 2012 A silk-based scaffold platform with tunable architecture for engineering critically-sized tissue constructs *Biomaterials* **33** 9214–24

[4] Chung S and King M W 2008 Design concepts and strategies for tissue engineering scaffolds. *Biotechnol. Appl. Biochem.* **58** 423–38

[5] Hollister S J 2009 Scaffold design and manufacturing: from concept to clinic. *Adv. Mater.* **21** 3330–42

[6] Kolewe M E, Park H, Gray C, Ye X, Langer R and Freed L E 2013 3D structural patterns in scalable, elastomeric scaffolds guide engineered tissue architecture. *Adv. Mater.* **25** 4459–65

[7] Derby B 2012 Printing and prototyping of tissues and scaffolds. *Science* **338** 921–6

[8] Lee M, Dunn J C Y and Wu B M 2005 Scaffold fabrication by indirect three-dimensional printing *Biomaterials* **26** 4281–9

[9] Zhang Q, Luo H, Zhang Y, Zhou Y, Ye Z, Tan W and Lang M 2013 Fabrication of three-dimensional poly(ε-caprolactone) scaffolds with hierarchical pore structures for tissue engineering. *Mater. Sci. Eng. C. Mater. Biol. Appl.* **33** 2094–103

[10] Park S, Kim G, Jeon Y C, Koh Y and Kim W 2009 3D polycaprolactone scaffolds with controlled pore structure using a rapid prototyping system *J. Mater. Sci. Mater. Med.* **20** 229–34

[11] Kang H W, Rhie J W and Cho D W 2009 Development of a bi-pore scaffold using indirect solid freeform fabrication based on microstereolithography technology *Microelectron. Eng.* **86** 941–4

[12] Cho Y S, Hong M W, Kim Y Y and Cho Y-S 2014 Assessment of cell proliferation in salt-leaching using powder (SLUP) scaffolds with penetrated macro-pores *J. Appl. Polym. Sci.* **131** 40240–8

[13] Dorj B, Park J H and Kim H W 2012 Robocasting chitosan/nanobioactive glass dual-pore structured scaffolds for bone engineering *Mater. Lett.* **73** 119–22

[14] Park K, Jung H, Son J S, Park K D, Kim J J, Ahn K D and Han D K 2007 Preparation of biodegradable polymer scaffolds with dual pore system for tissue regeneration *Macromolecular Symposia* vol 249-250 pp 145–50

[15] Park S H, Kim T G, Kim H C, Yang D Y and Park T G 2008 Development of dual scale scaffolds via direct polymer melt deposition and electrospinning for applications in tissue regeneration *Acta Biomater.* **4** 1198–207

[16] Sang Y, Wha M, Kim S, Lee S, Hee J, Yul Y and Cho Y 2014 Fabrication of dual-pore scaffolds using SLUP (salt leaching using powder) and WNM (wire-network molding) techniques *Mater. Sci. Eng. C* **45** 546–55

[17] Zhang W, Wray L S, Rnjak-Kovacina J, Xu L, Zou D, Wang S, Zhang M, Dong J, Li G, Kaplan D L and Jiang X 2015 Vascularization of hollow channel-

modified porous silk scaffolds with endothelial cells for tissue regeneration *Biomaterials* **56** 68–77

[18] Woo Jung J, Yi H-G, Kang T-Y, Yong W-J, Jin S, Yun W-S and Cho D-W 2013 Evaluation of the effective diffusivity of a freeform fabricated scaffold using computational simulation. *J. Biomech. Eng.* **135** 84501

[19] Peña J, Román J, Victoria Cabañas M and Vallet-Regí M 2010 An alternative technique to shape scaffolds with hierarchical porosity at physiological temperature *Acta Biomater.* **6** 1288–96

[20] Zhu M, Wang K, Mei J, Li C, Zhang J, Zheng W, An D, Xiao N, Zhao Q, Kong D and Wang L 2014 Fabrication of highly interconnected porous silk fibroin scaffolds for potential use as vascular grafts. *Acta Biomater.* **10** 2014–23

[21] Farkas B, Romano I, Ceseracciu L, Diaspro A, Brandi F and Beke S 2015 Four-order stiffness variation of laser-fabricated photopolymer biodegradable scaffolds by laser parameter modulation *Mater. Sci. Eng. C* **55** 14–21

[22] Jeffries E M, Nakamura S, Lee K-W, Clampffer J, Ijima H and Wang Y 2014 Micropatterning Electrospun Scaffolds to Create Intrinsic Vascular Networks *Macromol. Biosci.* **14** 1514–20

[23] Ortega I, Dew L, Kelly A G, Chong C K, MacNeil S and Claeyssens F 2015 Fabrication of biodegradable synthetic perfusable vascular networks via a combination of electrospinning and robocasting *Biomater. Sci.* 592–6

[24] Mohanty S, Larsen L B, Trifol J, Szabo P, Burri H V R, Canali C, Dufva M, Emnéus J and Wolff A 2015 Fabrication of scalable and structured tissue engineering scaffolds using water dissolvable sacrificial 3D printed moulds *Mater. Sci. Eng. C* **55** 569–78

[25] Mandal B B, Grinberg a., Seok Gil E, Panilaitis B and Kaplan D L 2012 From the Cover: High-strength silk protein scaffolds for bone repair *Proc. Natl. Acad. Sci.* **109** 7699–704

[26] Díaz Lantada A, Alarcón Iniesta H, Pareja Sánchez B and García-Ruíz J P 2014 Free-form rapid prototyped porous PDMS scaffolds incorporating growth factors promote chondrogenesis *Adv. Mater. Sci. Eng.* **2014**

[27] Choi S J, Kwon T H, Im H, Moon D Il, Baek D J, Seol M L, Duarte J P and Choi Y K 2011 A polydimethylsiloxane (PDMS) sponge for the selective absorption of oil from water *ACS Appl. Mater. Interfaces* **3** 4552–6

[28] Khademhosseini A, Langer R, Borenstein J and Vacanti J P 2006 Microscale technologies for tissue engineering and biology. *Proc. Natl. Acad. Sci. U. S. A.* **103** 2480–7

[29] Berthier E, Young E W K and Beebe D 2012 Engineers are from PDMS-land, Biologists are from Polystyrenia. *Lab Chip* **12** 1224–37

[30] Lee H, Ahn S, Bonassar L J, Chun W and Kim G 2013 Cell-laden poly(ε-caprolactone)/alginate hybrid scaffolds fabricated by an aerosol cross-linking process for obtaining homogeneous cell distribution: fabrication, seeding efficiency, and cell proliferation and distribution. *Tissue Eng. Part C. Methods* **19** 784–93

[31] Strain A J and Neuberger J M 2002 A bioartificial liver--state of the art. *Science* **295** 1005–9

[32] Xiong X, Wu Z, Pan J, Xue L, Xu Y and Chen H 2015 A facile approach to modify poly(dimethylsiloxane) surfaces via visible light-induced grafting polymerization *J. Mater. Chem. B* **3** 629–34

[33] Zhao F, Wang X, Ding B, Lin J, Hu J, Si Y, Yu J and Sun G 2011 Nanoparticle decorated fibrous silica membranes exhibiting biomimetic superhydrophobicity and highly flexible properties *RSC Adv.* **1** 1482

[34] Karageorgiou V and Kaplan D 2005 Porosity of 3D biomaterial scaffolds and osteogenesis. *Biomaterials* **26** 5474–91

[35] Chen G, Dong C, Yang L and Lv Y 2015 3D Scaffolds with Different Stiffness but the Same Microstructure for Bone Tissue Engineering *ACS Appl. Mater. Interfaces* **7** 15790–802

[36] Trappmann B, Gautrot J E, Connelly J T, Strange D G T, Li Y, Oyen M L, Cohen Stuart M a, Boehm H, Li B, Vogel V, Spatz J P, Watt F M and Huck W T S 2012 Extracellular-matrix tethering regulates stem-cell fate. *Nat. Mater.* **11** 642–9

[37] Yeung T, Georges P C, Flanagan L a, Marg B, Ortiz M, Funaki M, Zahir N, Ming W, Weaver V and Janmey P a 2005 Effects of substrate stiffness on cell morphology, cytoskeletal structure, and adhesion. *Cell Motil. Cytoskeleton* **60** 24–34

[38] Cho Y S, Kim B S, You H K and Cho Y S 2014 A novel technique for scaffold fabrication: SLUP (salt leaching using powder) *Curr. Appl. Phys.* **14** 371–7

[39] Ahn S, Kim Y, Lee H and Kim G 2012 A new hybrid scaffold constructed of solid freeform-fabricated PCL struts and collagen struts for bone tissue regeneration: fabrication, mechanical properties, and cellular activity *J. Mater. Chem.* **22** 15901

[40] Sobral J M, Caridade S G, Sousa R a, Mano J F and Reis R L 2011 Three-dimensional plotted scaffolds with controlled pore size gradients: Effect of scaffold geometry on mechanical performance and cell seeding efficiency. *Acta Biomater.* **7** 1009–18

[41] Li Y, Ma T, Kniss D a., Lasky L C and Yang S T 2001 Effects of filtration seeding on cell density, spatial distribution, and proliferation in nonwoven fibrous matrices *Biotechnol. Prog.* **17** 935–44

[42] Holy C E, Shoichet M S and Davies J E 2000 Engineering three-dimensional bone tissue in vitro using biodegradable scaffolds: Investigating initial cell-seeding density and culture period *J. Biomed. Mater. Res.* **51** 376–82

Supplementary

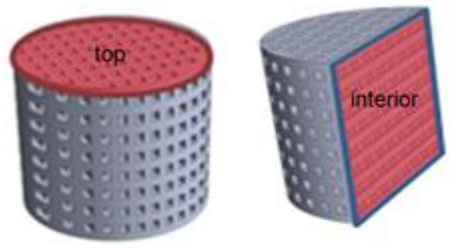

Figure S1. Schematic of top view and cross-section view of the interior regions of the scaffolds.

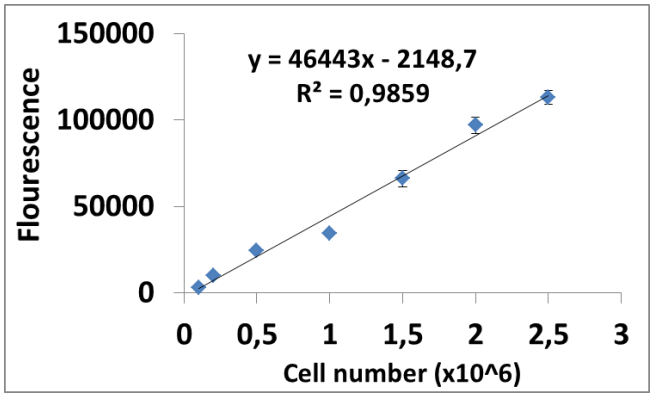

Figure S2. Standard curve for total cell number quantification using the picogreen assay

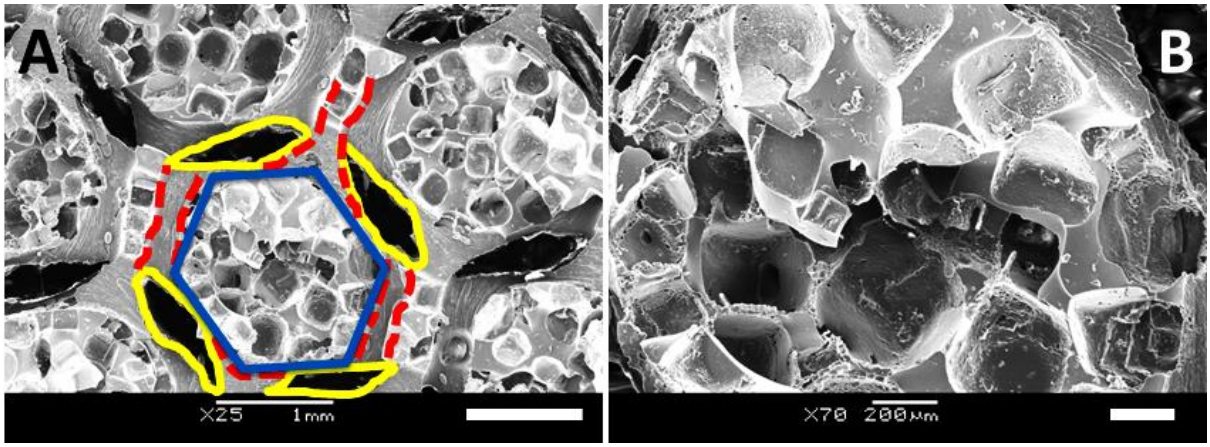

Figure S3. SEM image of hexagonal dual pore scaffolds (A) and zoom in into the random pore region of dual pore scaffold (B) (red: structured pore in x-y direction, yellow: structured pores in z direction and blue: random pore region).

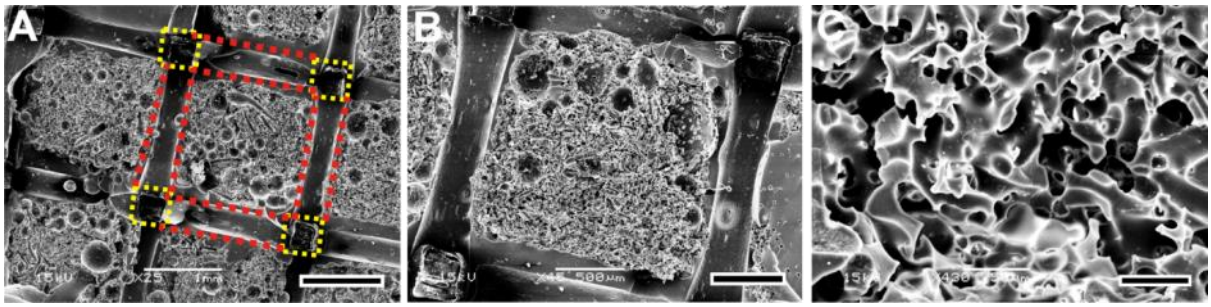

Figure S4. SEM images of dual pore scaffold with structured pore of dimension 400 µm and random pores of 20-40 µm. Scale bar: A) 1 mm, B) 500 µm and C) 50 µm.

Fabrication of dual-pore PCL scaffolds

Polycaprolactone (PCL) (average M_W ~ 80,000) crystals and chloroform (99.0-99.4% (GC) purity) were purchased from Sigma-Aldrich Corporation, St. Louis, MO, USA.

PCL dual-pore scaffolds were fabricated in a similar manner as PDMS scaffolds using 10% PCL solution in chloroform. PCL solution was prepared by dissolving PCL crystals in chloroform overnight. The sacrificial PVA mould was fabricated with 40% porosity and filled with salt crystals of size around 100-200 μm. The PVA-salt mould was covered with the PCL solution and kept in a vacuum desiccator for 1 hr to achieve proper filling of the mould. The mould with the polymer mixture was dried under fume hood overnight to completely evaporate chloroform from the mould. The dried PCL-PVA-salt mould was soaked in deionized water for at least 24 h to remove the sacrificial PVA-salt mould. Porosity and the surface morphology of the 3D dual-pore PCL scaffolds were characterized using the methods described in the materials and methods section of the paper.

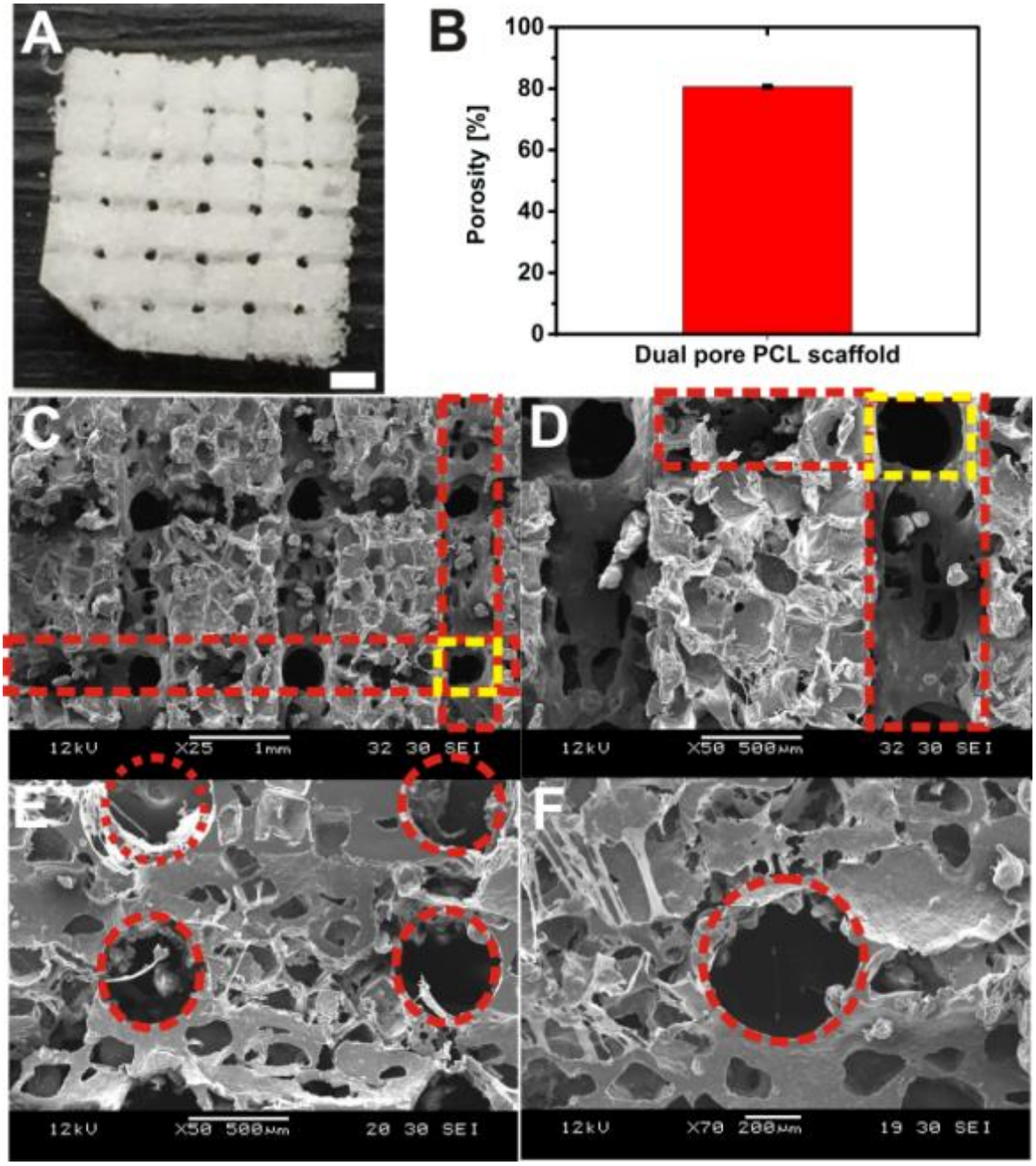

Figure. S5 A) Photographs of dual pore PCL scaffold casted from combined salt (particle size 100-200 µm) – PVA (40% porous) mould. B) Calculated porosity of the scaffold. C) SEM micrographs of 3D PCL scaffold's top view with 400 µm of structured and 100-300 µm of random pore size. D) Zoom in of C. E) Side view from the center of the PCL dual pore scaffold. F) Zoom in of E. The scale bare is 1 mm in A and C, 500 µm for D and E and 200 µm for F.

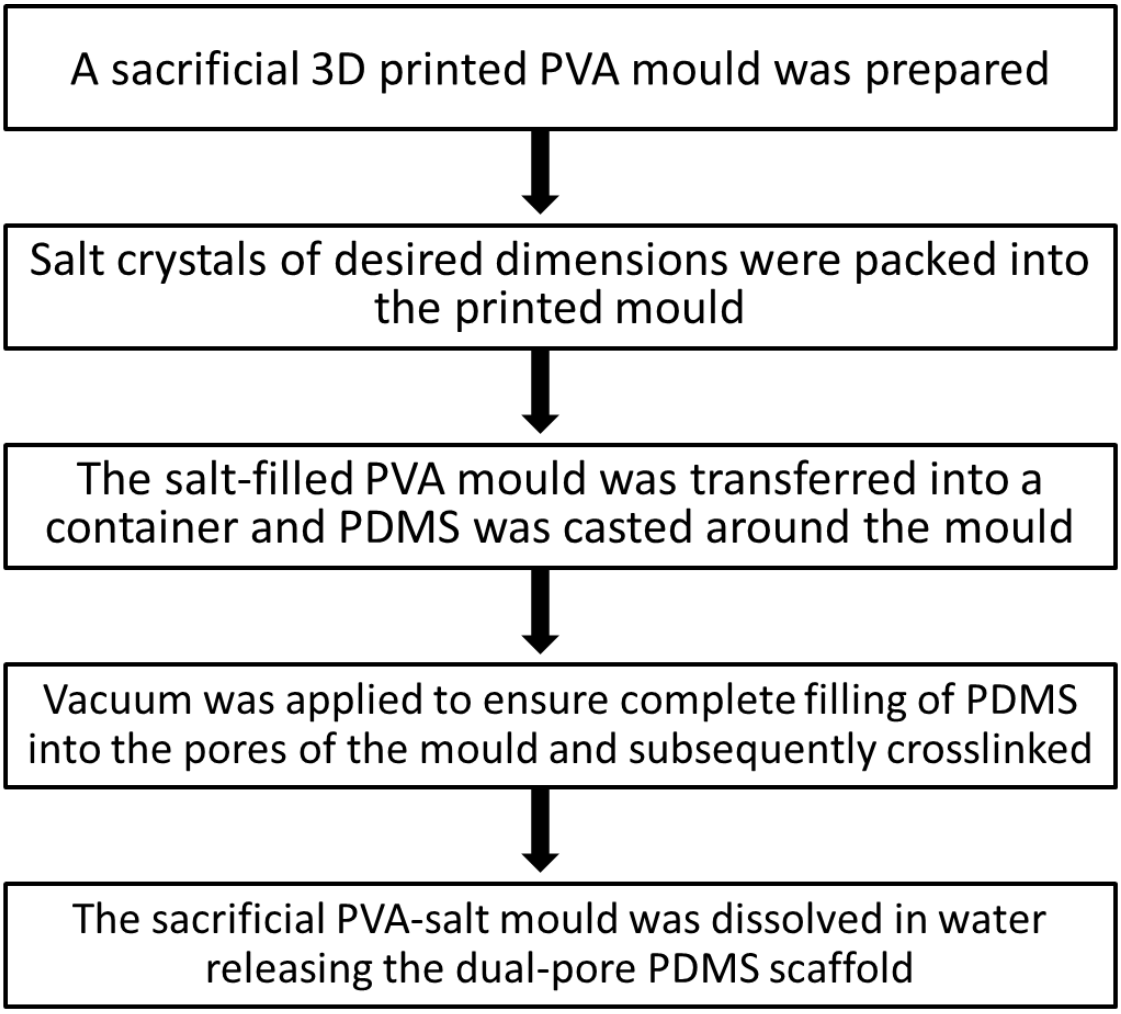

Figure. S6 Schematics flowchart for the dual pore scaffold fabrication process, shown schematic in Fig 1.

5. CHAPTER 5. A 3D printed silicone-hydrogel scaffold with enhanced physicochemical properties

This work has been accepted as manuscript to Journal of ASC Biomacromolecule: (2016). Soumyaranjan Mohanty[1], Martin Alm[3], Mette Hemmingsen[1], Alireza Dolatshahi-Pirouz[1, 2], Jon Trifol[4], Peter Thomsen[3], Marin Dufva[1], Anders Wolff[1,] Jenny Emnéus[1*]

5.1 Introduction

Over the past decades, biomaterials have received increasing attention in the field of medical devices, diagnostics, sensors, drug delivery systems and tissue engineering applications. However, the physicochemical and biological properties of some of these biomaterials either do not match with native tissues ore are not clinically approved. The ideal biomaterial for tissue engineering should enable 3D cell culturing and provide sufficient mechanical, biological and chemical support to guide cells in the desired direction. Therefore, the development of the next generation of instructive biomaterials should facilitate physical support within a three dimensional (3D) microenvironment for controlling cell fate and be able to direct cell differentiation through controlled release of cell-regulating factors[1–5]. Moreover, from a clinical perspective it is crucial to design porous scaffolds that match the morphological and anatomical structures of natural tissues[6]. Porous scaffolds with multiple functionalities have been fabricated from natural and/or synthetic polymers, metals, ceramics, and glasses that guide tissue regeneration through controlled release of tissue inductive factors[7,8]. However, several challenges still remain in fabricating dual 3D porous scaffolds from medically approved materials with high elasticity and durability to mechanical load similar to that of real tissue.

In recent years, hydrogel-based materials have received increasing attention in regenerative medicine and tissue engineering due to their biocompatibility, viscoelastic properties and ease of fabrication. They have been applied as scaffolds that provide structural integrity to tissue constructs[9,10], support tissue in growth[11,12] and that can deliver drugs and proteins to targeted cells in a well-controlled manner[13–15]. Different microfabrication techniques have been developed to fabricate 3D natural/synthetic hydrogel scaffolds with defined macroscopic and microscopic features for

various tissue engineering applications [9,16–18]. Despite all their beneficial properties, there are still challenges to overcome for their clinical use. These challenges include none native-like mechanical characteristics[19] and fabrication of scalable 3D hydrogel-based scaffolds. Additionally, hydrogels are not suitable for long-term controlled drug release due their inherent burst-release behavior, where most of the drugs are release in a short time period, lasting from a few minutes up to a few hours with almost no drug released beyond a week[20]. As an alternative to hydrogels, synthetic silicone elastomer, a FDA approved biomaterial, is used in various medical implants due its high biocompatibility, optical transparency, oxygen permeability, and tunable degrees of stiffness to mimic mechanical properties of biological tissue[21,22]. However, it is not a suitable candidate in terms of drug release or to direct cells into native-like tissue structures[23]. This is primarily due to the hydrophobic and impermeable nature of silicone elastomers.

Considerable attention has been given to generate silicone-hydrogel hybrid materials either by grafting the hydrogel materials on cross-linked silicone[24,25] or through mixing of silicone and hydrogel[26,27]. Despite the ease of fabrication of these materials, one drawback is the poor interfacial adhesion between the two phases. This can be improved by creating interpenetrating polymer networks (IPNs) consisting of silicone and hydrogel through various solvent based methods[27]. Several biocompatible silicone-hydrogel IPNs have been generated with enhanced water uptake, improved mechanical stiffness, improved hydrophilicity and ability to load and release drugs compared to the base silicone[27–30]. However the formation of hydrogel networks in the described IPNs is completely dependent on the type of solvent. Most commonly, organic solvents are used for swelling the silicone materials and it is therefore challenging to load a drug during the IPN synthesis process due to the use of often toxic solvents. Moreover, the conventional IPN synthesis methods described above are time consuming. As an alternative to organic solvents and to reduce the time required for IPN processing, Steffensen *et al* developed 2-hydroxyethyl methacrylate (HEMA) based silicone IPN materials (pHEMA-IPN), using supercritical carbon dioxide ($scCO_2$) as an auxiliary solvent for swelling the silicone[31,32]. $scCO_2$ has many potential advantages over conventional solvents in terms of being nontoxic, nonflammable, economical, widely available, eco-friendly and having unique solvating properties[31,33].

The pHEMA-IPN has been applied for controlled and sustainable drug release for various medical devices[31,32]. Due to the high glass transition temperature (Tg) of

pHEMA (90-100°C) compared to pristine silicone elastomer (-120°C), the resulting pHEMA-IPN becomes very hard and brittle[31]. However, the presence of PEG structural units with lower Tg (-67°C) has shown to dramatically lower the Tg value of a P[HEMA-co-(MeO-PEGMEA)] composite polymers[34], indicating that PEG can be used as a softener.

Here a new microporous highly elastic and durable 3D IPN scaffold is presented, which combines indirect 3D printing of a silicone scaffold (i.e. 3D printing of a sacrificial mould replicated into silicone[17,35]) with scCO2 based hydrogel impregnation to create the 3D IPN scaffold. Moreover, a polyethyleneglycol monomethacrylate (PEGMEA) HEMA random-copolymer (pHEMA-co-PEGMEA) hydrogel is employed and its physical and mechanical properties compared to the previously reported pHEMA-IPN. Drug release profiles of doxycycline (DOX) from both the pHEMA- and pHEMA-co-PEGMEA IPN systems are evaluated and the ability for human mesemchymal stem cell (hMSC) adhesion and proliferation on 2D and 3D pHEMA-co-PEGMEA IPN materials is investigated. Finally, the biological activity of DOX released from pHEMA-co-PEGMEA IPN is demonstrated using a DOX regulated green fluorescent reporter (GFP) gene expression assay in Hela cells. The proposed approach for directing cellular function through sustained release of drugs/biomolecules from IPN scaffolds may find use in engineering artificial tissue or regenerating damaged tissue.

5.2 Experimental Section

5.2.1 Materials

Two-dimensional (2D) silicone elastomer substrate PE4062 cut into appropriate disc sizes (Ø 16mm x height 2mm), were purchased from LEBO Production AB, Skogås, Sweden. 3D silicon elastomer substrates were fabricated using commercial polydimethylsiloxane (PDMS) (Sylgard 184, Dow Corning). 0.2 M diethyl peroxydicarbonate (DEPDC) was used as initiator, prepared as described previously[36]. 97% 2-hydroxyethyl methacrylate (HEMA) with 200-220 ppm monomethyl ether hydroquinone (MEHQ) used as inhibitor, and poly(ethylene glycol) methyl ether acrylate Mn 480 (PEGMEA-480) with 100 ppm MEHQ and 100 ppm BHT used as inhibitor were supplied by Sigma Aldrich (USA). To remove any residual inhibitor, HEMA and PEGMEA-480 were individually passed through an inhibitor remover column, packed with De-Hibit 200 supplied by Polysciences (USA), according to instructions given in

the technical data sheet, and stored at 5°C. HEMA was furthermore purified by distillation at reduced pressure, and the fraction at 67°C and 4 mbar was collected and stored at 5°C.

99.8% ethanol (EtOH), 98% ethylene glycol dimethacrylate (EGDMA), tetrahydrofuran (THF), NaOH pellets, 35% H_2O_2 and molecular sieves 4 Å (all from Sigma Aldrich, USA), 98% ethyl chloroformate (Fluka, Hungary), and anaerobic CO_2 4.0 (AGA, Denmark) were all used as received. Doxycycline (Clontech, USA) and Tetracycline-Free fetal bovine serum were used for cell culture (Clontech, USA).

5.2.2 Fabrication of 3D elastomer scaffolds

Porous 3D silicone elastomer scaffolds with structured channels were fabricated in PDMS, using indirect polyvinyl alcohol (PVA) filament printing, as previously described[17,35]. In brief, a water soluble PVA sacrificial 3D mould (dimension: 25 mm x 25 mm x 10 mm of length, width and height) was designed and printed using PVA filament (Makerbot, USA) and a 3D filament printer (Makerware 2.4.1, Makerbot, USA). The PVA mould was printed with 80% porosity and then replicated into elastomeric structures by casting a mixture of PDMS pre-polymer and cross-linker at a ratio of 10:1, and cross-linked at 60 °C overnight. The PVA sacrificial mould was then dissolved in water for 12 h to achieve the final desired 3D porous PDMS scaffolds.

5.2.3 Fabrication of IPNs

pHEMA-based silicone hydrogel IPN production was based on the method previously described[31,32], with a few modifications. Since the initiator DEPDC is capable of initiating the polymerisation already at 40°C, the whole process was run at 40°C and 300 bar for 16 h. The IPNs described in[31,32] had a relative limited water uptake with brittle mechanical properties due to the high T_g of PHEMA. In order to increase the water-uptake and to make the IPNs softer and more flexible, PEGMEA was added as a co-monomer in the synthesis.

Silicone hydrogel IPN samples (2D and 3D) were prepared according to the following procedure: Silicone specimens (mass ~ 40-50 g) were organized in a stainless steel grid and placed in a one-litre reactor equipped with magnetic stirring (HiP, Pennsylvania, USA). A Thar P-50 electrical driven high-pressure pump (Thar Designs Inc., USA) was applied to assure the operational pressure. Solvents (70 ml EtOH and 70 ml

THF), monomers (100 ml HEMA and optionally 100 ml PEGMEA-480), cross-linker (6 ml EDGMA) and initiator (50 ml 0.2M DEPDC) were mixed in a separate beaker for at least 10 min. The solution was added to the reactor and the reactor was closed and filled with CO_2 to a pressure of 300 bar at 40° C. After a combined impregnation and polymerization step of 16 h the pressure was released during a 30 min period. Residual monomers and non-cross-linked polymers were removed from the samples by extraction in EtOH for one week. The hydrogel content of the IPNs was calculated according to eq. (1):

$$Hydrogel\ content = \frac{m_{IPN} - m_{silicone}}{m_{IPN}} \cdot 100\% \quad \textbf{(1)}$$

Where $m_{silicone}$ *and* m_{IPN} represents the difference in mass of the silicone samples and when loaded with IPN, respectively. The structural morphology and microstructure of the 3D porous PDMS and corresponding IPN scaffolds were visualized using scanning electron microscopy (SEM) (JEOL, Tokyo, Japan). Prior to SEM analysis, the scaffolds were dried in an oven at 50°C overnight and sputter coated with gold. Samples were then analysed using 12 kV of accelerating voltage. Pore sizes of scaffolds were measured from SEM images using ImageJ software.

5.2.4 Water uptake kinetics

Five 2D IPN discs (Ø=16.2 mm), each containing 22% w/w of PHEMA or PHEMA-co-PEGMEA, were tested for their ability to swell in water. To evaluate the water uptake on dry IPN discs, they were kept in a desiccator for at least 30 minutes after which they were weighed (W_0) and placed in individual vials containing PBS (pH 7.4) (n = 5). At given time points the IPN discs were individually removed, wiped gently with tissue paper to remove excess water and weighed (W_t). The IPN discs were then transferred back into their respective vials. The water content of the IPN discs was calculated using eq. (2):

$$Water\ content(\%) = \frac{w_t - w_0}{w_t} \cdot 100\% \quad \textbf{(2)}$$

5.2.5 Surface characterization

Attenuated total reflection Fourier transform infrared spectroscopy (ATR-FTIR) was used to characterize the samples, using a FTIR spectrophotometer (Spectrum 100,

Perkin Elmer Technologies, USA). The average value after 40 scans at 4 cm^{-1} resolution was collected for each sample. ATR-FTIR spectra were taken of both dry and of fully water-swollen samples.

To assess the wettability of IPN samples and their base silicone material, contact angle measurements were carried out on the 2D disc sample surfaces before and after treatment with oxygen plasma. The contact angle was measured using the sessile drop method by depositing a 3 µl ultra-pure water drop on the discs. Two individual measurements were performed on five individual discs.

5.2.6 Mechanical properties

The mechanical properties of the silicone elastomer (PE4062) and its corresponding pHEMA-co-pEGMEA (PE4062|pHEMA-co-pEGMEA) IPNs were tested using uniaxial tensile stress tests with INSTRON Model 4301 (Instron Engineering Corporation, Canton, MA, USA). For this purpose, 5-7 dumbbell specimens (ASTM D638-5) of each sample were preconditioned in water at ambient temperature for 1 week. The tensile stress tests were carried out at 50 mm/min.

5.2.7 In-vitro cell studies

Human bone marrow derived mesenchymal stem cells (hMSCs)(PT-250, Lonza Bioscience, DK) (passage no 3–4) were cultured in mesenchymal stem cell growth media (MSCGM)(Lonza Bioscience, DK) at 37°C and 5% CO_2. The cell culture media was exchanged completely twice a week and cells were passaged at 80-90 % confluence. Before cell seeding 2D IPN discs (Ø 16mm, thickness: 2mm) and 3D porous IPN PDMS scaffolds (Ø 6 mm x height 4 mm) were treated with oxygen plasma for 1 min on both top and bottom surfaces. The samples were sterilized by autoclavation and then stored at room temperature for one week in sterile water for complete hydration of the hydrogel networks of IPNs. Before cell seeding, all IPN samples were coated with 80 µg/ml collagen I (Life Technologies, A1048301) in sterile water overnight at 4 °C. To avoid cell migration from IPN discs and 3D IPN scaffolds onto the tissue culture plastic plate during long term culture, 12-well plates containing both IPN discs and scaffolds were coated with 5% w/v Pluronic®F127 (Sigma-Aldrich, USA) for at least three hours, then washed three times with sterile PBS and allowed to dry to avoid cell attachment to the plates. Cells cultured in tissue culture polystyrene (TCP) wells without any coatings were used as controls.

For 2D in-vitro cell culture, collagen coated IPNs were transferred into the previously prepared 12-well plate and 2 ml of cell culture media was added onto the IPN discs in each well. 20 µl of cell suspension containing 30000 hMSCs were seeded slowly on to the 2D IPN disc and TCP. The well plates containing IPN discs and the controls were transferred to an incubator at 37°C and 5% CO_2 and cell culture media was exchanged every 3 days.

For 3D cell culturing a special cell loading method was followed to ensure uniform cell distribution into the IPN scaffolds, as described previously[17]. In brief, a 6 mm thick cell seeding tray with several holes (Ø 6 mm) was fabricated from poly(methyl methacrylate) (PMMA) using a CO_2 laser ablation machine (Epilog Mini 18 Laser, CO 80403, USA). The seeding tray was cleaned with 0.5 M sodium hydroxide solution followed by rinsing with sterile water for sterilization. Collagen coated 3D IPN scaffolds were inserted into the holes in the seeding tray. 100 µl of cell suspension media containing 250000 hMSCs were loaded on top of each scaffold and then transferred into an incubator (at 37 °C and 5% CO_2) for 2 h to achieve cell attachment. Every hour the tray was turned upside down for uniform cell infiltration into the scaffolds. Finally, the 3D IPN scaffolds were transferred into a Pluronic®F127 treated 12-well plate containing 3 ml of fresh culture medium. To ensure efficient diffusion of media components into the interior of the scaffolds, they were rotated in the incubator (at 37 °C/5% CO_2) and the cell culture medium was refreshed every 3 days.

Cell proliferation over the culture period was evaluated using the Alamar blue metabolic quantification assay (Life Technologies, USA) according to the manufacturer's instructions. Pristine silicone discs, 2D IPN and 3D IPN scaffolds without cells were used as negative controls to adjust for background fluorescence. Viability of cells was determined using a Live/Dead cell viability staining Kit (Life Technologies, USA), according to the manufacturer's instructions. Cells were incubated with calcein AM and ethidium homodimer-1 (EthD-1) for 30 min to stain live (green) and dead cells (red), respectively, for 30 min at 37 °C and 5% CO_2. Following incubation, samples were washed twice with PBS and imaged using a fluorescence microscope (Zeiss Axio Observer, ZI) with excitation at 488 nm and emission at 515 nm for live cells and excitation at 570 nm and emission at 602 nm for dead cells.

To investigate cell attachment and proliferation of hMSCs, actin filament and nuclei were stained and investigated by immunofluorescence, according to the following: At day 1 and 8 after cell seeding, cells were fixed with 4% paraformaldehyde (pH 7.4),

permeabilized (30 min, 0.1% Triton X-100 in PBS)), and blocked (30 min, 0.1% Tween 20 and 1% bovine serum albumin in PBS) for unspecific binding of the antibodies. The cells were then stained with Alexa Fluor 555 conjugated phalloidin (1:200, Life Technologies) for actin filament visualization and counterstained with TOPRO-3 (1:1000, Life Technologies) for visualization of the nucleus. The cells were visualized with a confocal laser-scanning microscope (Leica microsystems, Germany).

5.2.8 Doxycycline drug release studies

IPN discs (Ø=10:2mm) containing 22% wt of pHEMA or pHEMA-co-PEGMEA hydrogel were loaded by soaking the IPN discs in 5 ml of 20 mg/ml of DOX solution (mixed in PBS) for one week at 4°C. The DOX loaded IPN discs were washed twice with Milli-Q water and dried at room temperature for 48 hr. For the drug release study IPN discs were immersed in closed dark-glass vials containing 5 ml PBS (pH 7.4), which was placed on a shaker at room temperature for 1 month. At regular time intervals the concentration of drug released into the PBS supernatant was collected and the absorbance measured at 351 nm using UV-Visible spectrophotometer (UV-2600, SHIMADZU Corporation, USA). For each time interval and sample an UV-Vis spectra was recorded between 250 and 600 nm to determine the stability of DOX over time. After each measurement the whole volume of PBS and DOX mixture was replaced completely by fresh PBS. IPN discs, containing 22 % wt of pHEMA-co-PEGMEA hydrogel IPN, was used as a negative control. Three independent IPN discs were used for repeatability.

5.2.9 Induction of gene expression of Hela Tet-On cells through doxycycline release from IPNs

For biological assessment of drug-releasing IPNs, a DOX regulated green fluorescent reporter gene expression assay was used for HeLa cells as described in[37]. In summary, a pTRE-Tight-BI-DsRed-Express plasmid from Clontech, consisting of a bidirectional tetracycline sensitive promoter, which in one direction encodes the red fluorescent protein (RFP) reporter DsRed-Express, and in the other direction has a mutable cloning site (MCS) ZsGreen1-DR, encoding the green fluorescent protein (GFP) reporter, was inserted in-frame into this MCS. When this plasmid construct is transfected into HeLa Tet-On Advanced cells (631155, Clontech), which stably express the Tet-On trans-activator, gene expression of the fluorescent reporter proteins can be

induced by addition of DOX (a tetracycline analogue) to the cell culture medium in the range of 100-1000 ng/mL. Different concentrations of DOX (0, 0.00001, 0.001, 0.1, 10 and 1000 µg/ml) were prepared in PBS, sterile filtered through 0.22 µm filter and stored at 4 °C. For drug-loading, sterilized pHEMA-co-PEGMEA IPN discs were transferred into solutions with different concentrations of DOX for one week. Following drug-loading, IPN discs were removed, washed three times with sterile water and then coated with 80 µg/ml collagen I solution for 2 h at 37 °C for cell attachment. Finally, IPN discs were washed with sterile PBS and transferred into 24-well plates containing cell culture media (DMEM supplemented with 10% Tet System Approved Fetal Bovine Serum (FBS) (631106, Clontech), penicillin 100 U/mL, streptomycin 100 µg/mL (P4333, Sigma), and geneticin (G-418) 100 µg/mL (11811–023, GIBCO). HeLa Tet-On cells were trypsinized and 4 x 10^4 cells were seeded on each IPN disc and cultured at 37 °C and 5% CO_2. After culturing overnight the cell density was about 60-70% of confluence. For transfection of the reporter plasmid, a transfection solution was prepared by mixing 500 ng of plasmid DNA into 100 µL Opti-ME (31985, GIBCO) and 1.25 µL of Lipofectamine LTX (15338–100, Invitrogen). The solutions were mixed gently and incubated for 25 minutes at room temperature to form DNA-Lipofectamine complexes. The growth medium from each well was replaced with 0.5 mL of fresh medium. Cells grown on the IPN discs were transfected with the reporter plasmid by adding 100 µL of the solution containing DNA-Lipofectamine complexes. The cells were incubated at 37 °C and 5% CO_2. After 6 h of transfection, the cell culture medium containing DNA-Lipofectamine complexes was removed, and cells were rinsed with PBS and added to 0.6 mL of fresh medium. Finally, the transfected HeLa cells on the IPN discs were incubated at 37 °C and 5% CO_2 for 18-24 h before assaying for fluorescent transgene expression. As a proof of concept for 3D IPN scaffolds, the same experimental procedure was followed as described above for 2D IPN discs, but with some modifications. Only a single DOX concentration (1000 µg/ml) was tested and 2 x 10^5 cells seeded into each scaffold. HeLa Tet-On cells grown on 2D IPN discs and 3D IPN scaffolds without DOX loading were utilized as negative controls. The cells on 2D IPN discs and 3D IPN scaffolds were imaged using a fluorescence microscope (Zeiss Axio Observer, ZI).

5.2.10 Statistical analysis

All the data presented are means and standard deviations of the experiments (n = 5 or 6). Statistical analysis was carried out using OriginPro 9. The significant differences

between sample groups were determined using the nonparametric test, one-way analysis of variance (ANOVA), and Tukey's post-hoc analysis for pairwise mean comparisons. The statistical significance was defined as *$p < 0.05$, **$p < 0.01$, ***$p < 0.005$.

5.3 Results and Discussion

5.3.1 Fabrication of 3D IPN scaffolds

Different geometries and porosities of scalable perfusable microporous 3D silicone elastomer scaffolds was recently realised by indirect 3D printing[17,35]. Here we have impregnated pHEMA-co-PEGMEA hydrogel into the 3D silicone scaffolds to fabricate 3D IPN scaffold. Figure 1A shows a perfusable microporous 3D PDMS scaffolds (with 80% porosity) impregnated with 82% wt of pHEMA-co-PEGMEA hydrogel using sCO_2. SEM images of the top- (Figs. 1B a&b) and side view (Figs. 1B c&d) of the scaffolds show a highly interconnected square profile (average side length 350 um) with elliptical shaped channels (average width 400 μm, height 200 μm), respectively. The channel dimensions are slightly smaller than the dimension of the base 3D PDMS scaffold due to the swelling of the PDMS when impregnated with hydrogel. The advantage of using 3D printing to make 3D IPN scaffolds is that dimensions and geometries of the pores of the scaffolds are highly tuneable and controllable. Moreover, since the pores of the scaffolds are structured with interconnected channels they are easy to clean, removing any uncross-linked monomers or cross-linked hydrogels deposits connected around the porous scaffolds, by simple perfusion with water/buffer.

Both pHEMA and pHEMA-co-PEGMEA impregnated 2D IPN discs and pHEMA-co-PEGMEA impregnated 3D IPN scaffolds were investigated. 2D IPN discs with 22% (w/w) hydrogel were used for general comparison of physicochemical, mechanical and drug releasing properties. Finally the *in-vitro* hMSC studies and drug induced gene

expression of Hela cells were tested with 3D pHEMA-co-PEGMEA IPN scaffolds.

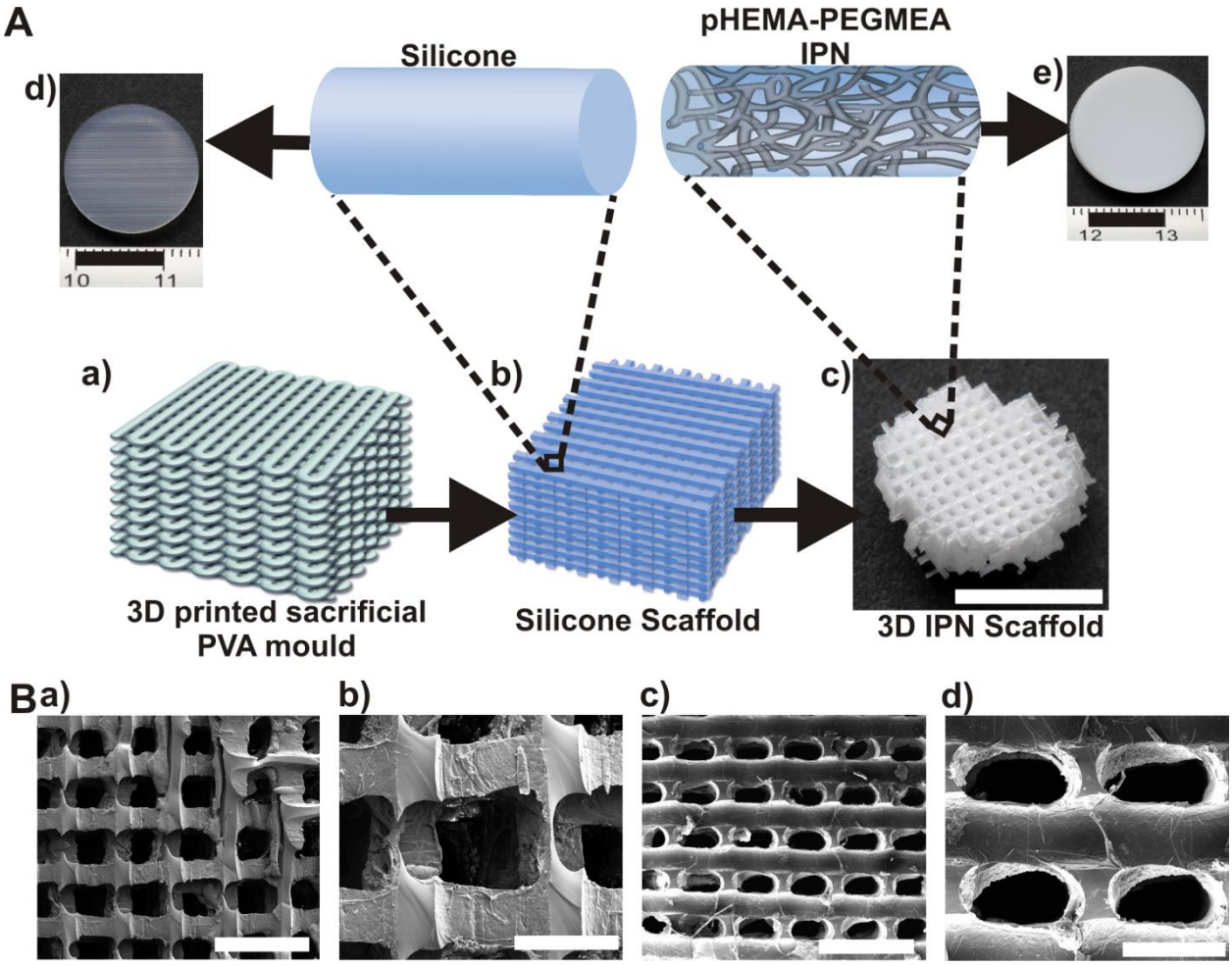

Figure 1. (**A**) Schematic illustration of the process of producing a 3D IPN scaffold, starting from a 3D printed sacrificial water soluble PVA mould (a), via silicone elastomer casting around the PVA mould and its subsequent removal to form a 3D silicone scaffold replica (b), to its subsequent hydrogel impregnation via sCO2, generating an 3D IPN scaffold (optical image) (c). Optical image of semi-transparent silicone (d) and 22% w/w pHEMA-co-PEGMEA (e) IPN discs. (**B**) SEM images of 3D IPN scaffolds with 52% w/w pHEMA-co-PEGMEA with woodpile infill pattern from top (a & b) and cross sectional (c & d) view. Scale bars: 1 cm for A (d & e), 1 mm for B (a & c) and 400 µm for B (b & d).

5.3.2 Physicochemical characteristics and mechanical properties of 2D IPNs. Figure 2 shows the physicochemical characteristics of 2D IPN discs and the base silicone elastomer. FTIR spectra of silicone (black line) and the corresponding IPNs with PHEMA (red line) and pHEMA-co-PEGMEA (blue line) are shown in Figure 2A. The characteristic absorption peaks observed at wavenumbers of 2962 cm^{-1} (C–H stretching in CH_3), 1259 cm^{-1} (CH_3 symmetric bending in Si–CH_3), 1076 cm^{-1} and 1018 cm^{-1} (Si–O–Si), identifies different functional groups present in silicone. The absorption peaks at around 1700 cm^{-1} and 3400 cm^{-1} are characteristic absorption peaks for carboxyl (C=O) and OH groups and were observed for both the IPNs, which clearly

demonstrates the presence of pHEMA and pHEMA-co-PEGMEA hydrogels in the bulk silicone elastomer of the IPNs. Water contact angle (CA) measurements (Figure 2B) revealed that pHEMA-co-PEGMEA IPN had a lower CA (of 84.5^{O}) than pHEMA IPN (92^{O}) and the base silicone material (103^{O}), indicating a decrease in CA with impregnation with a more hydrophilic hydrogel. Water uptake kinetics for the two IPNs over a period of 22 days (Figure 2C) show an increase until day 5-6 after which the equilibrium-swelling ratio is reached; pHEMA-co-PEGMEA IPN clearly having a higher water uptake (11.56 %) than pHEMA IPN (8.25 %). The water uptake kinetics and total water uptake in the pHEMA IPN is very similar to what was previously reported[31]. While it has been shown that the water uptake capacity increases linearly with the weight of hydrogel content in IPN composites[28,29,31], the pHEMA-co-PEGMEA IPN had a 1.4 fold higher water uptake compared to the pHEMA IPN in spite of containing the same amount of hydrogel (22% w/w). This is likely due to the fact, that PEG is more hydrophilic than HEMA, giving the pHEMA-PEG conjugate an improved water uptake capacity compared to the corresponding pHEMA hydrogel[34,38–40]. Another reason can be that the porosity of the bulk cross-linked polymer network increases by increments in PEG concentration[38], also leading to a higher water uptake capacity of the pHEMA-co-PEGMEA.

A hydrogel scaffold used as tissue matrix should be structurally stable to withstand *in vivo* mechanical stress while providing support to the ingrowing tissue[41,42]. Therefore, evaluation of mechanical properties of a biomaterial has an important role in design of an ideal tissue engineering scaffolds with desired stiffness equivalent to real anatomical tissues and organs[43]. The tensile properties of the base silicone and the two different hydrogel-IPNs were compared (Figure. 2D-F). Figure 2D clearly shows that the PHEMA-co-PEGMA-IPN behaves very similarly to the silicone elastomer while the pHEMA-IPN is softer and less robust with low strain at break. The tensile Young's modulus (Figure 2E) of the bare silicone was higher (4.50 ± 0.12 MPa) compared to pHEMA and pHEMA-PEGMEA IPNs (3.27 ± 0.10 and 3.38 ± 0.14 MPa, respectively), indicating that impregnation of hydrogels into the silicone significantly reduces the Young's modulus in the IPN-based scaffolds. The ultimate stress sustained by pHEMA-PEGMEA IPN (8.95 ± 0.15 MPa) was slightly higher than for silicone (8.66 ± 0.26 MPa) and significantly higher than for pHEMA IPN (4.55 ± 0.18 MPa). Similarly, the ultimate tensile stress (Figure 2F) sustained by pHEMA-PEGMEA IPN was slightly higher than for silicon (796 ± 35% and 721 ± 24%, respectively) and

significantly higher than for pHEMA IPNs (105 ± 23%). Thus, the addition of pHEMA-co-PEGMEA to silicone does not have a dramatic influence on the mechanical properties with only a slight increase in Young modulus, ultimate stress and tensile strain compared to base silicone material. Previously reported results have shown that brittleness of pHEMA IPN was due to the impregnation of HEMA molecules with high glass transition temperature (Tg)[32]. However, the introduction of PEGMEA with lower (Tg)[34] into the pHEMA IPN would have helped the base silicone to improve the mechanical properties of the IPN by enhancing the ultimate tensile stress and strain. The investigated pHEMA-co-PEGMEA IPN has a young's modulus equivalent to that of cartilage (1-10 MPa)[44] with the mechanical properties tuneable by varying the hydrogel content as well as by controlling the level of crosslinking of the silicone material.

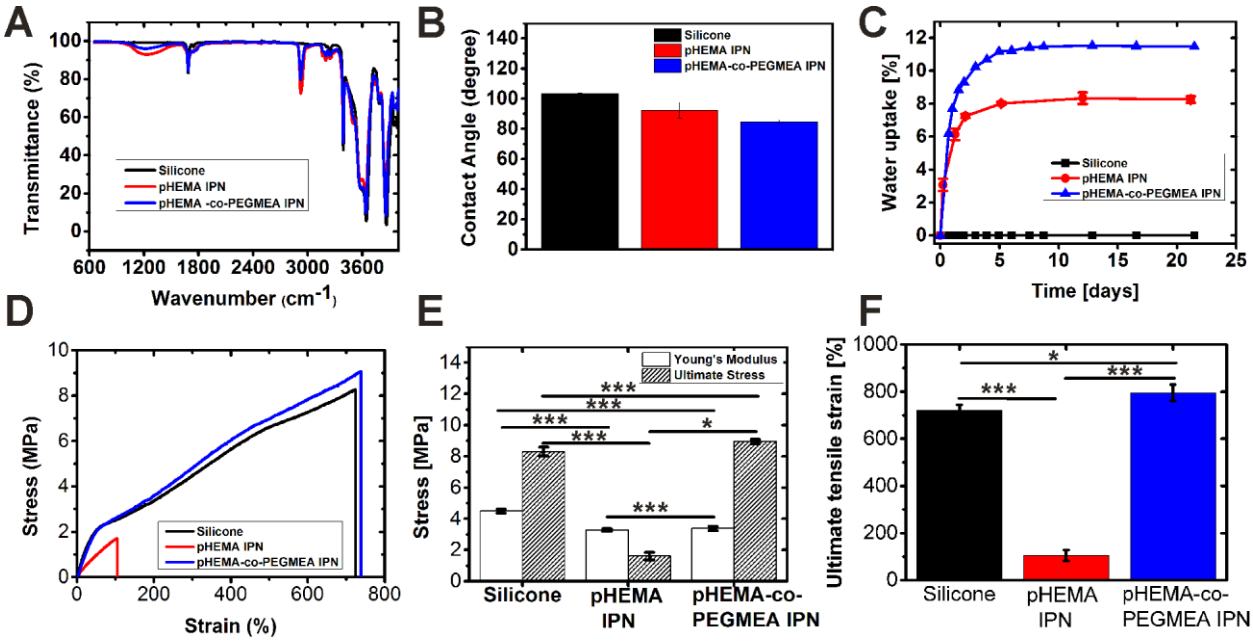

Figure 2. Physicochemical characteristics of pHEMA IPN, pHEMA-co-PEGMEA IPN, each containing 22% (w/w) of hydrogel, and the base silicone discs: (A) FTIR spectra, (B) contact angle- and (C) water uptake measurements. Effect of hydrogel impregnation on the mechanical properties of IPN materials was determined using uniaxial tensile testing: (D) Stress–strain curves. (E) Young modulus, calculated from linear (10-20% strain) regions of stress-strain curve and the ultimate stress. (F) The comparison of ultimate tensile strain. The data represents mean± standard deviation (n=5).

5.3.2 In-vitro cell studies on pHEMA-co-PEGMEA 2D and 3D IPN materials

The ability of materials to support cell adhesion and proliferation plays a key role in tissue engineering applications. In the following study, we continued the work on the pHEMA-co-PEGMEA IPN since it proved to have better mechanical and physicochem-

ical properties than pHEMA IPN. hMSCs were used to evaluate and compare cell-matrix interactions on 2D pHEMA-co-PEGMEA IPN discs and conventional TCPs as a control, using quantitative Alamar blue assay and qualitative live/dead staining. PEG hydrogels have been shown not to promote cell adhesion, resulting in a round shaped cell morphology due to poor cell–matrix interactions[45]. hMSC attachment on IPNs coated with and without collage-I extra cellular matrix (ECM) was therefore investigated (Figure 3 and supplementary information Figure S1). The IPN without ECM showed similarly as before hMSC adhesion with aggregated cell morphology, whereas with ECM (Figure 3A) good adhesion was observed, although slightly lower than that on the TCP control surface. The proliferation rate on IPN discs was lower than on TCP over 21 days of cell culture (Figure 3B), which might be due to a lower number of cells on IPN surface compared to TCP, the former having a lower surface area (2 and 1,767 cm^2, respectively). Nevertheless, the cell proliferation rate followed the same pattern and was in the same order of magnitude on both surfaces. The fluorescence images of live/dead staining of cells (Figure 3C) gives additional evidence that until 14 days cells proliferated with 100% viability on the IPN discs. The corresponding images of hMSCs grown on TPC can be found in supplementary information, Figure S2. Moreover, confocal fluorescence images (Figure 3D) show well spread hMSC morphology and high proliferation on the IPN surfaces over the 21-day culture period. Thus, cell–IPN interactions

can be promoted by providing adhesion sites through ECM coating of the IPN materials.

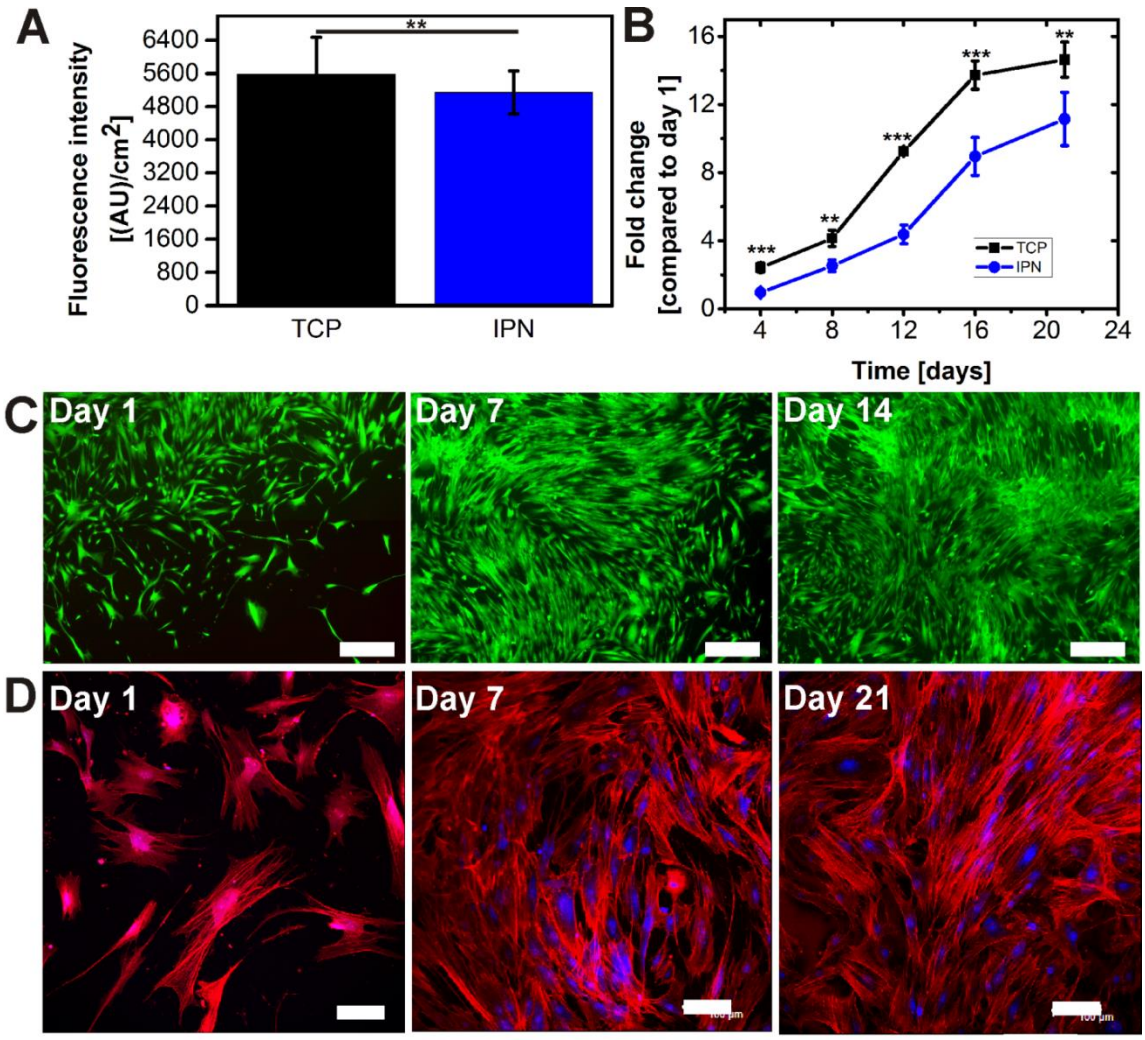

Figure 3. hMSCs growth on TCP and collagen-I coated pHEMA-co-PEGMEA IPN discs (22% (w/w)): Alamar blue assay was used to determine hMSC (**A**) attachment on IPN and TCP at day 1 post-seeding and (**B**) proliferation on IPN and TCP presented as fold change over a 21-day period compared to day 1. (**C**) Fluorescence images of live (green) and dead (red) staining of hMSC cells proliferating on IPN discs over a 14-day period (Scale bars = 200 µm). (**D**) Confocal fluorescence images of immunostained hMSCs proliferating on the IPN surface after 1, 7 and 14 days post cell seeding. The cytoskeletal F-actin fibres (red) and nuclei (blue) were stained with Alexa Fluor 555-labelled phalloidin and TO-PRO-3 iodide, respectively (Scale bars = 100 µm).

A challenge with 3D scaffolds compared to 2D surfaces is to ensure that the scaffolds are highly porous with interconnected channels for cell attachment and efficient oxygen and nutrient supply as well as waste removal[46]. Moreover, the scaffold should support formation of tissue-like 3D cellular morphology and spreading across and into the material, as well as with cellular extensions across the voids of the porous scaffold[46,47]. The 3D IPN scaffolds were fabricated with 400 µm filament-to-

filament distances with 80% porosity, subsequently loaded with 52% (w/w) pHEMA-co-PEGMEA hydrogel. hMSCs were seeded into the scaffolds and examined over a 28-day culture period and metabolic activity determined by the Alamar blue assay. Figure 4A shows that the proliferation rate steadily increase over the 28 days. To visualise that cells were proliferating inside the scaffolds, the cell viability after 4 and 8 days were investigated by cutting the scaffolds through the centre, following live/dead staining (Figure 4BC). On day 4 the hMSCs were well spread all over the IPN scaffolds with 100% viability (Figure 4B). On day 8 very similar viability was observed, however with a few dead cells (Figure 4C), which most likely was caused by insufficient diffusion of oxygen and nutrients into the interior of the scaffold. The morphology of the hMSCs on the IPN scaffolds was visualized using immunostaining of the cytoskeleton and nuclei on day 15 post cell seeding (Figs. 4D-G). hMSCs clearly proliferate nicely with well spread cell morphology within the IPN scaffolds (Figure 4E). Interestingly, the scaffolds seem to promote native-like 3D microtissue architecture with cells interconnected in between the 400 µm inter filament pore space of opposite filaments inside the IPN scaffold (highlighted with white dotted lines in Figure 4F and G). Overall our results show that the hMSCs proliferate with high viability inside the 3D IPN scaffolds, with a clear increase in metabolic rate over 28 days.

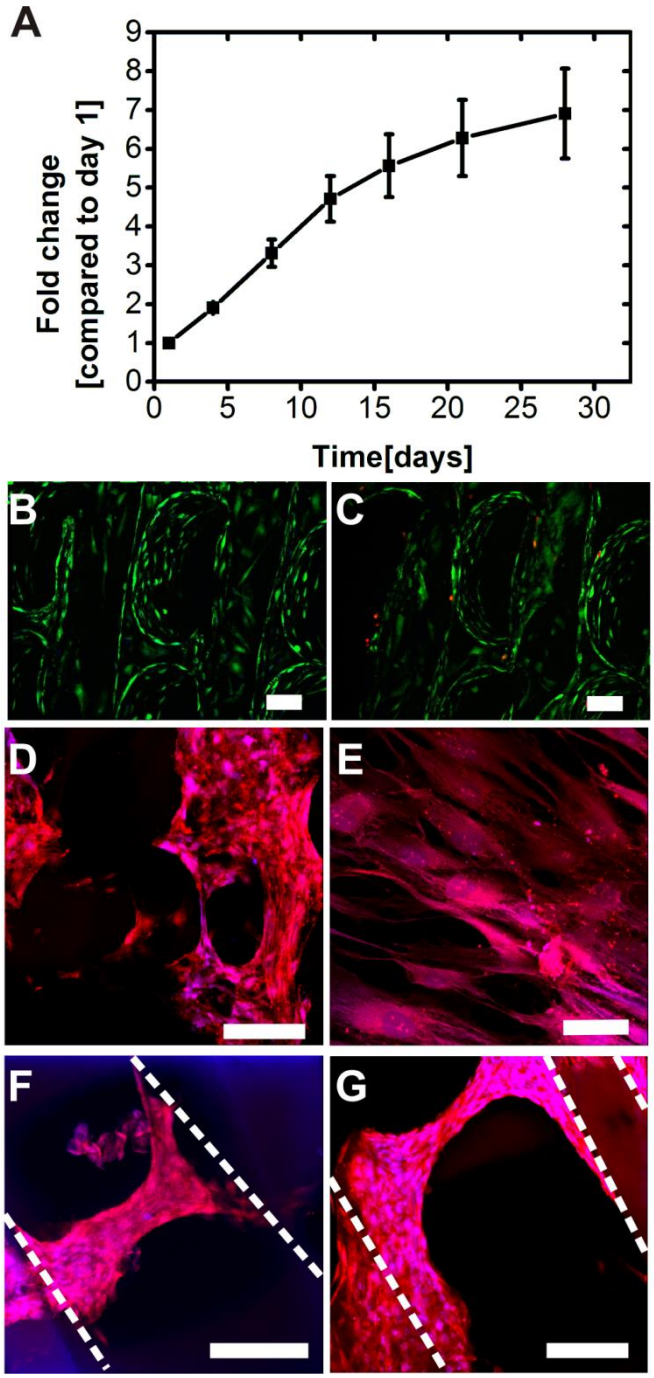

Figure 4. hMSCs cultured on pHEMA-co-PEGMEA 3D IPN scaffolds (52 % w/w): (**A**) hMSC proliferation inside 3D IPN scaffold over a 28 day period: Alamar blue metabolic assay presented as fold change in florescence compared to day 1 post seeding. (**B-C**) Fluorescent images of live (green) and dead (red) cells on day 4 (B) and 8 (C) cultured on 3D IPN scaffolds. (**D-G**) Confocal images of immunostained hMSCs cultured on 3D IPN scaffolds after 15 days post seeding: The cytoskeletal F-actin fibres (red) and nuclei (blue) were stained with Alexa Fluor 555-labeled phalloidin and TO-PRO-3 iodide, respectively. (D) Cells were visualized from the top surface of the scaffolds where (E) is a zoom in of (D). The centre of the scaffold is visualised in (F) and (G), showing that the IPN scaffold supports native-like 3D microtissue architecture. White dotted lines represent single layers of the IPN scaffold. Scale bars: 100 µm for B-C and 200 µm for D-G.

5.3.3 DOX release studies from IPNs

In a previous study it was demonstrated that it was possible to release antibiotics from pHEMA IPNs and that the release profile could be controlled by varying the hydrogel content as well as the concentration of drug loaded into the IPN[48]. Our hypothesis was that the introduction of a more hydrophilic PEGMEA network into the pHEMA IPN would improve the drug release profile compared to the previously synthesized pHEMA IPNs. Figure 5Aa compares the DOX release profile over a 7-day period from 2D pHEMA and pHEMA-co-PEGMEA IPN discs containing equal amounts of hydrogel (22% w/w). The cumulative DOX release from pHEMA-co-PEGMEA IPNs was almost 2 fold higher compared to pHEMA IPNs. This was expected due to the more hydrophilic PEG network in the copolymer structures, resulting in a faster movement from DOX loaded IPNs [38,49] and is in good agreement with the water uptake data described in Figure 2Ac. Controlled and systematic long term delivery of bioactive molecules from biomaterials is required to minimize the release of the agent to non-target sites[14,50] and to direct stem cells into a tissue-specific lineage[3]. The ability of long term release of the DOX from pHEMA-co-PEGMEA IPNs is shown in the Figure 5Ab. A consistent release profile can be seen with a continuous release for 30 days after initial 5-days of burst release. The stability of the drug released into the surrounding PBS was examined regularly at different time points, using UV-Vis spectrophotometry. Figure 5Ac shows that the freshly made DOX solution (green line) and the DOX released from IPN (blue line) after 30 days of incubation had similar UV-Vis spectra with the same absorption maximum at 351 nm, indicating stability of the drug released from the IPN discs. Current observation is consistent with previous studies, reporting the short term stable release of DOX from various ceramic biomaterials[51,52]. The difference in absorbance peak height for DOX release from IPN and DOX standard solution is simply due to the different concentrations of DOX in the measured solutions. For negative control UV-Vis spectra (in black) was measured on a degraded DOX solution by exposing the solution to light during a week, which resulted in the disappearance of the absorbance maximum at 351 nm, clearly confirming that the pHEMA-co-PEGMEA IPN is a good drug delivery system maintaining the stability of DOX during long-term release.Delivery of DOX to cells from IPNs

The biological activity of DOX released from pHEMA-co-PEGMEA IPNs was assessed using a DOX regulated GFP gene expression assay in HeLa Tet-On cells, expressing

GFP under the control of a tetracycline inducible promoter. DOX is a hydrophilic analogue of tetracycline, which upon contact with ZsGreen1-DR transfected cells activates GFP expression, which thus can be used to turn on the reporter gene [37]. We used this model system to demonstrate the release of DOX molecules from pHEMA-co-PEGMEA IPN, activating gene expression of the HeLa Tet-On cells grown on the surface of the IPN materials (as shown schematically in Figure 5B). Different concentration of DOX loaded pHEMA-co-PEGMEA IPN discs were first tested to determine the lowest concentration required for the induction of GFP expression. As shown in the Figure 5C, gene expression of ZsGreen1-DR was induced by the release of DOX at different concentration from the IPN discs into the culture medium. We found that 10 µg/ml and 1000 µg/ml DOX induced strong GFP expression and that DOX concentrations below 0.1 µg/ml did not result in any fluorescent signal. As a control, a similar experiment was performed on IPN discs loaded with 10 µg/ml DOX, but not transfected with ZsGreen1-DR plasmid, with no fluorescence observed after 24 h of cell culture (Supplementary Figure S3). Next, 3D pHEMA-co-PEGMEA IPN scaffolds, loaded with 10 µg/ml of DOX, was tested and as shown in Fig 5D, a clear florescent signal can be observed after 24 hr of incubation, indicating that drug delivery form the 3D IPN scaffold is effective. In a future perspective this type of scaffold could be used for directed induction of stem cell differentiation. For instance dexamethanose, a small molecule with similar size and molecular weight as DOX that induces differentiation of hMSC to osteoblast over 21 days[3], could potentially be released from these types of IPN scaffolds for developing various bone and cartilage based tissue implants.

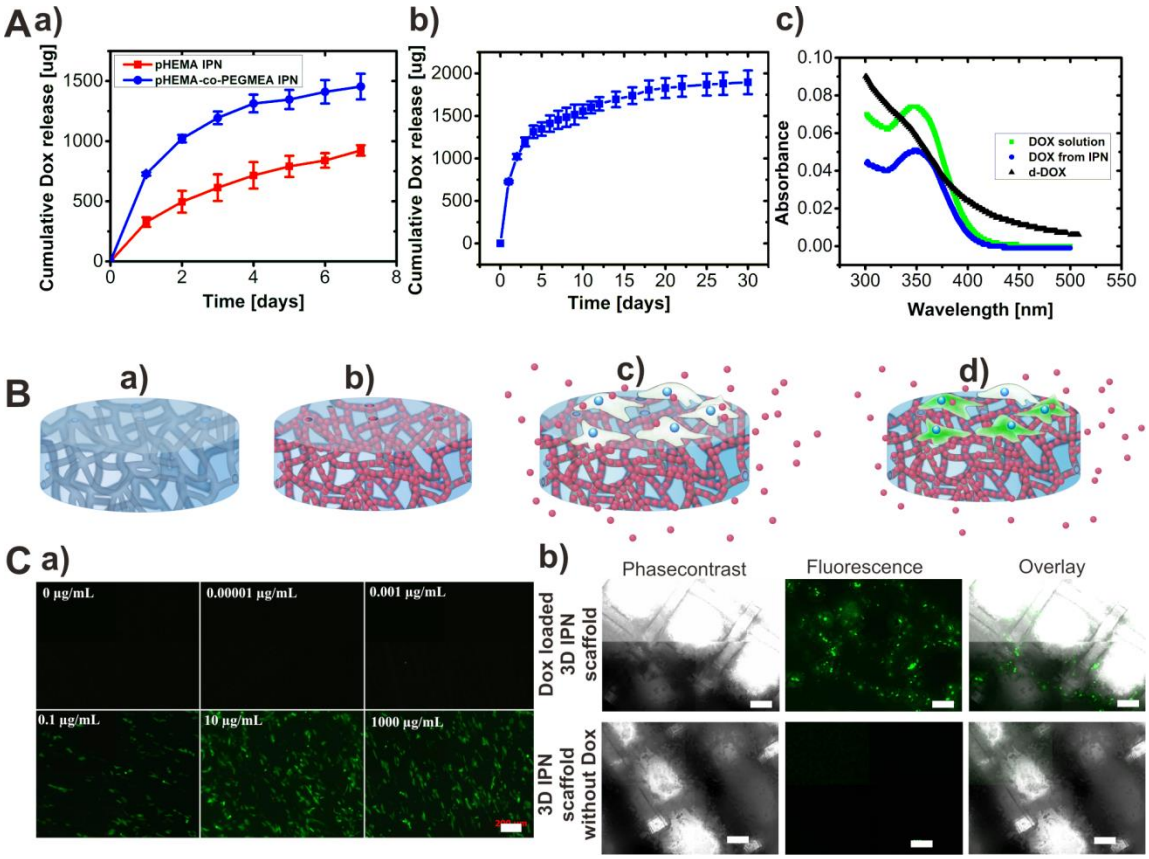

Figure 5. (**A**) *In-vitro* doxycycline release study: Amount of DOX released from: (a) pHEMA and pHEMA-co-PEGMEA IPN discs with 22% (w/w) hydrogel content over a 7-day period, (b) pHEMA-co-PEGMEA IPN hydrogel over 30 days, and c) stability of released doxycycline from IPNs confirmed using UV-Vis absorbance spectra of the DOX solution in PBS (green line as positive control), DOX released from pHEMA-co-PEGMEA IPN into supernatant after 30 days (blue line) and degraded DOX solution in PBS by exposure to light for 1 week (black line as negative control). **B)** Schematics illustration of the induction of GFP expression in Hela-Tet-On cells through DOX release from IPNs. Different concentration of DOX loaded IPN discs (a & b) were seeded with Hela-Tet-On cells and cultured overnight (c). Then cells were transfected with plasmid for GFP expression and finally the cells grown on IPN surface was observed by green fluorescence after 24 hr of transfection (d). **C)** Fluorescent images of GFP-expressing Hela-Tet-On cells at different concentrations of DOX loaded 2D pHEMA-co-PEGMEA IPN discs (a). GFP-expressing Hela-Tet-On cells seeded and cultured on 3D IPN scaffolds loaded with 10 ug/ml of DOX concentrations over night after which cells were transfected with plasmid for GFP expression and green fluorescence observed after 24 hr of transfection. Phase contrast channel (left), green fluorescence channel (middle), and an overlay of both channels (right) (b). Scale bar for all images in Fig. C (a & b) is 200 µm.

5.4 Conclusions

The present work demonstrates successful fabrication of microporous 3D silicone hydrogel IPN scaffolds using indirect 3D printing of silicone elastomer and subsequent impregnation with hydrogel IPN using supercritical carbon dioxide. Compared to the

existing p-HEMA IPN, the new p-HEMA-co-PEGMEA IPN appears to be better in both physicochemical and mechanical properties. The material is biocompatible and medical grade silicone materials can be applied with this process for *in-vivo* use. Moreover, *in vitro* cell studies demonstrated that the developed material could support long-term (21 days) hMSC growth with very high metabolic activity and viability. Doxycycline was furthermore loaded into the IPN scaffolds and it's *in vitro* release quantified over 30 days, following confirmation of biological activation GFP expression in the Hela Tet-on-cell model system. It is anticipated that the developed p-HEMA-co-PEGMEA IPN scaffolds potentially could be used as a long-term bioactive drug delivery system for various tissue-engineering applications.

5.5 Associated Content

Supporting Information

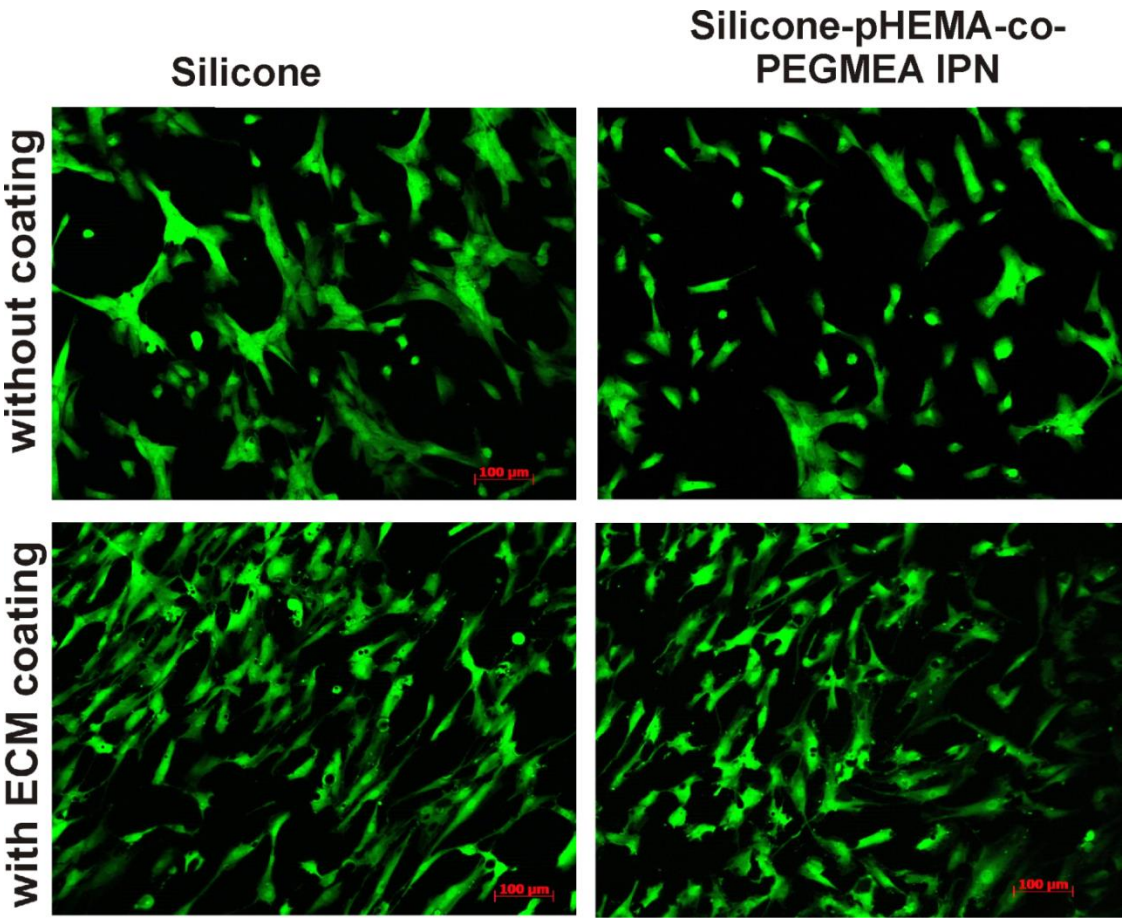

Figure S1. Cell attachment and morphology visualization using Live (green)/dead (red) staining hMSCs grown with and without collagen-I coated pHEMA-co-PEGMEA IPN surface.

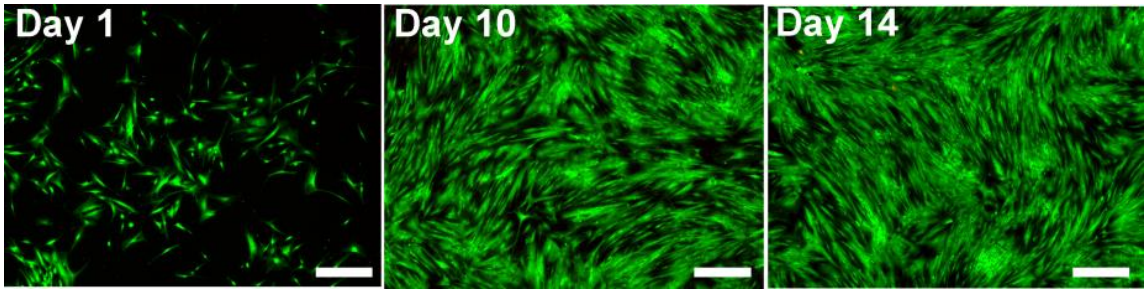

Figure S2. Live (green)/Dead (red) staining of hMSCs grown on TPC over 14 days period.

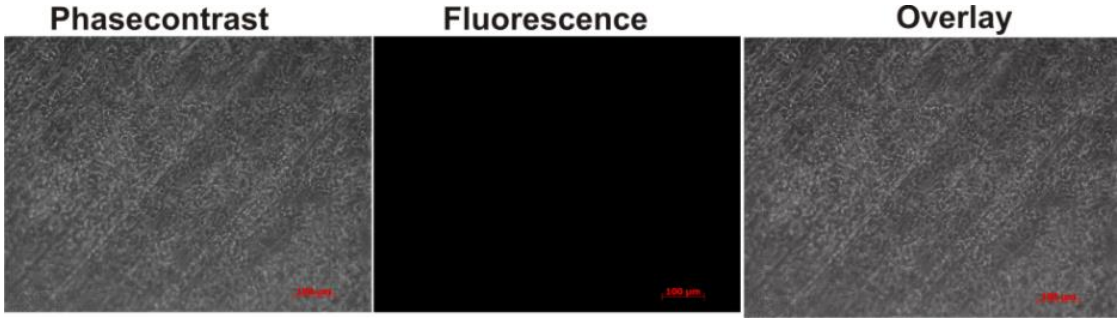

Figure S3. Negative control: pHEMA-co-PEGMEA IPN discs loaded with DOX, but not transfected with ZsGreen1-DR plasmid. No fluorescent signal was observed after 24 hour of Hela-Tet-On cells culture.

5.6 References

[1] Lau H K and Kiick K L 2015 Opportunities for Multicomponent Hybrid Hydrogels in Biomedical Applications *Biomacromolecules* **16** 28–42

[2] Liu X, Zhao K, Gong T, Song J, Bao C, Luo E, Weng J and Zhou S 2014 Delivery of Growth Factors Using a Smart Porous Nanocomposite Scaffold to Repair a Mandibular Bone Defect *Biomacromolecules* **15** 1019–30

[3] Gaharwar A K, Mihaila S M, Kulkarni A a., Patel A, Di Luca A, Reis R L, Gomes M E, Van Blitterswijk C, Moroni L and Khademhosseini A 2014 Amphiphilic beads as depots for sustained drug release integrated into fibrillar scaffolds *J. Control. Release* **187** 66–73

[4] Irmak G, Demirtas T T, Çetin Altindal D, Çalis M and Gümüsderelioglu M 2014 Sustained Release of 17β-Estradiol Stimulates Osteogenic Differentiation of Adipose Tissue-Derived Mesenchymal Stem Cells on Chitosan-Hydroxyapatite Scaffolds *Cells Tissues Organs* **199** 37–50

[5] He X, Liu Y, Yuan X and Lu L 2014 Enhanced Healing of Rat Calvarial Defects with MSCs Loaded on BMP-2 Releasing Chitosan/Alginate/Hydroxyapatite

Scaffolds ed S Agarwal *PLoS One* **9** e104061

[6] Shen H, Niu Y, Hu X, Yang F, Wang S and Wu D 2015 A biomimetic 3D microtubule-orientated poly(lactide-co-glycolide) scaffold with interconnected pores for tissue engineering *J. Mater. Chem. B* **3** 4417–25

[7] Zhao X, Kim J, Cezar C a, Huebsch N, Lee K, Bouhadir K and Mooney D J 2011 Active scaffolds for on-demand drug and cell delivery. *Proc. Natl. Acad. Sci. U. S. A.* **108** 67–72

[8] Shea L D, Smiley E, Bonadio J and Mooney D J 1999 DNA delivery from polymer matrices for tissue engineering. *Nat. Biotechnol.* **17** 551–4

[9] Das S, Pati F, Choi Y-J, Rijal G, Shim J-H, Kim S W, Ray A R, Cho D-W and Ghosh S 2015 Bioprintable, cell-laden silk fibroin–gelatin hydrogel supporting multilineage differentiation of stem cells for fabrication of three-dimensional tissue constructs *Acta Biomater.* **11** 233–46

[10] Billiet T, Gevaert E, De Schryver T, Cornelissen M and Dubruel P 2014 The 3D printing of gelatin methacrylamide cell-laden tissue-engineered constructs with high cell viability. *Biomaterials* **35** 49–62

[11] Paul A, Hasan A, Kindi H Al, Gaharwar A K, Rao V T S, Nikkhah M, Shin S R, Krafft D, Dokmeci M R, Shum-Tim D and Khademhosseini A 2014 Injectable Graphene Oxide/Hydrogel-Based Angiogenic Gene Delivery System for Vasculogenesis and Cardiac Repair *ACS Nano* **8** 8050–62

[12] Partlow B P, Hanna C W, Rnjak-Kovacina J, Moreau J E, Applegate M B, Burke K a, Marelli B, Mitropoulos A N, Omenetto F G and Kaplan D L 2014 Highly tunable elastomeric silk biomaterials. *Adv. Funct. Mater.* **24** 4615–24

[13] Alam M A, Takafuji M and Ihara H 2014 Silica nanoparticle-crosslinked thermosensitive hybrid hydrogels as potential drug-release carriers *Polym. J.* **46** 293–300

[14] Lee K Y, Peters M C, Anderson K W and Mooney D J 2000 Controlled growth factor release from synthetic extracellular matrices. *Nature* **408** 998–1000

[15] Ehrbar M, Schoenmakers R, Christen E H, Fussenegger M and Weber W 2008 Drug-sensing hydrogels for the inducible release of biopharmaceuticals *Nat.*

Mater. **7** 800–4

[16] Jhaveri S J, McMullen J D, Sijbesma R, Tan L S, Zipfel W and Ober C K 2009 Direct three-dimensional microfabrication of hydrogels via two-photon lithography in aqueous solution *Chem. Mater.* **21** 2003–6

[17] Mohanty S, Larsen L B, Trifol J, Szabo P, Burri H V R, Canali C, Dufva M, Emnéus J and Wolff A 2015 Fabrication of scalable and structured tissue engineering scaffolds using water dissolvable sacrificial 3D printed moulds *Mater. Sci. Eng. C* **55** 569–78

[18] Billiet T, Gevaert E, De Schryver T, Cornelissen M and Dubruel P 2014 The 3D printing of gelatin methacrylamide cell-laden tissue-engineered constructs with high cell viability *Biomaterials* **35** 49–62

[19] Ahearne M, Yang Y, El Haj A J, Then K Y and Liu K-K 2005 Characterizing the viscoelastic properties of thin hydrogel-based constructs for tissue engineering applications. *J. R. Soc. Interface* **2** 455–63

[20] Rambhia K J and Ma P X 2015 Controlled drug release for tissue engineering *J. Control. Release* **219** 119–28

[21] Sparks J L, Vavalle N A, Kasting K E, Long B, Tanaka M L, Sanger P A, Schnell K and Conner-Kerr T A 2015 Use of Silicone Materials to Simulate Tissue Biomechanics as Related to Deep Tissue Injury *Adv. Skin Wound Care* **28** 59–68

[22] Hron P 2003 Hydrophilisation of silicone rubber for medical applications *Polym. Int.* **52** 1531–9

[23] Park J Y, Ahn D, Choi Y Y, Hwang C M, Takayama S, Lee S H and Lee S H 2012 Surface chemistry modification of PDMS elastomers with boiling water improves cellular adhesion *Sensors Actuators, B Chem.* **173** 765–71

[24] Lin C H, Jao W C, Yeh Y H, Lin W C and Yang M C 2009 Hemocompatibility and cytocompatibility of styrenesulfonate-grafted PDMS-polyurethane-HEMA hydrogel *Colloids Surfaces B Biointerfaces* **70** 132–41

[25] Ging-Ho H, Shyh-Dar L, Chee-Chan W, Michael Hung-I S and Patricia Chuen-Tsuei C 1994 Plasma-induced graft copolymerization of HEMA onto silicone

rubber and TPX film improving rabbit corneal epithelial cell attachment and growth *Biomaterials* **15** 163–71

[26] Cífková I, Lopour P, Vondrácek P and Jelínek F 1990 Silicone rubber-hydrogel composites as polymeric biomaterials. I. Biological properties of the silicone rubber-p(HEMA) composite. *Biomaterials* **11** 393–6

[27] Abbasi F, Mirzadeh H and Katbab A A 2002 Comparison of viscoelastic properties of polydimethylsiloxane/poly(2-hydroxyethyl methacrylate) IPNs with their physical blends *J. Appl. Polym. Sci.* **86** 3480–5

[28] Wang J and Li X 2011 Interpenetrating polymer network hydrogels based on silicone and poly(2-methacryloyloxyethyl phosphorylcholine) *Polym. Adv. Technol.* **22** 2091–5

[29] Alizadeh M, Abbasi F, Farahi M and Jalili K 2012 Silicone-based hydrogels prepared by interpenetrating polymer network synthesis: Swelling properties and confinements effects on the formation kinetics *J. Appl. Polym. Sci.* **124** 985–92

[30] Tang Q, Yu J-R, Chen L, Zhu J and Hu Z-M 2011 Porous silicone hydrogel interpenetrating polymer networks prepared using a template method for biomedical use *Polym. Int.* **60** 1136–41

[31] Steffensen S L, Vestergaard M H, Møller E H, Groenning M, Alm M, Franzyk H and Nielsen H M 2015 Soft hydrogels interpenetrating silicone-A polymer network for drug-releasing medical devices *J. Biomed. Mater. Res. Part B Appl. Biomater.* **00B** 1–9

[32] Steffensen S L, Vestergaard M H, Groenning M, Alm M, Franzyk H and Nielsen H M 2015 Sustained prevention of biofilm formation on a novel silicone matrix suitable for medical devices *Eur. J. Pharm. Biopharm.* **94** 305–11

[33] Cooper A I 2000 Polymer synthesis and processing using supercritical carbon dioxide *J. Mater. Chem.* **10** 207–34

[34] Baker M V., Brown D H, Casadio Y S and Chirila T V. 2009 The preparation of poly(2-hydroxyethyl methacrylate) and poly{(2-hydroxyethyl methacrylate)-co-[poly(ethylene glycol) methyl ether methacrylate]} by photoinitiated polymerisation-induced phase separation in water *Polymer (Guildf).* **50** 5918–27

[35] Mohanty S, Sanger K, Heiskanen A, Trifol J, Szabo P, Dufva M, Emnéus J and Wolff A 2016 Fabrication of scalable tissue engineering scaffolds with dual-pore microarchitecture by combining 3D printing and particle leaching *Mater. Sci. Eng. C* **61** 180–9

[36] Xu W Z, Li X and Charpentier P a. 2007 In situ ATR-FT-IR study of the thermal decomposition of diethyl peroxydicarbonate in supercritical carbon dioxide *Polymer (Guildf).* **48** 1219–28

[37] Skafte-Pedersen P, Hemmingsen M, Sabourin D, Blaga F S, Bruus H and Dufva M 2012 A self-contained, programmable microfluidic cell culture system with real-time microscopy access *Biomed. Microdevices* **14** 385–99

[38] Jung Y P, Kim J-H, Lee D S and Kim Y H 2007 Preparation and properties of modified PHEMA hydrogel with sulfonated PEG graft *J. Appl. Polym. Sci.* **104** 2484–9

[39] Jeon Y, Son Y, Hong K H and Kim J 2008 Drug release characteristics of modified PHEMA hydrogel containing tethered PEG sulfonate *Macromol. Res.* **16** 379–83

[40] Lee W-F and Lin W-J 2002 Preparation and Gel Properties of Poly[hydroxyethylmethacrylate-co-poly(ethylene glycol) methacrylate] Copolymeric Hydrogels by Photopolymerization *J. Polym. Res.* **9** 23–9

[41] Griffith L G and Naughton G 2002 Tissue engineering--current challenges and expanding opportunities. *Science* **295** 1009–14

[42] Hutmacher D W 2000 Scaffolds in tissue engineering bone and cartilage *Biomaterials* **21** 2529–43

[43] Patel M and Fisher J P 2008 Biomaterial scaffolds in pediatric tissue engineering. *Pediatr. Res.* **63** 497–501

[44] Pal S 2014 Mechanical Properties of Biological Materials *Design of Artificial Human Joints & Organs* (Boston, MA: Springer US) pp 23–40

[45] Gaharwar A K, Rivera C, Wu C J, Chan B K and Schmidt G 2013 Photocrosslinked nanocomposite hydrogels from PEG and silica nanospheres: Structural, mechanical and cell adhesion characteristics *Mater. Sci. Eng. C* **33**

1800–7

[46] Knight E and Przyborski S 2015 Advances in 3D cell culture technologies enabling tissue-like structures to be created in vitro *J. Anat.* **227** 746–56

[47] Bokhari M, Carnachan R J, Cameron N R and Przyborski S a. 2007 Culture of HepG2 liver cells on three dimensional polystyrene scaffolds enhances cell structure and function during toxicological challenge *J. Anat.* **211** 567–76

[48] Steffensen S L, Vestergaard M H, Groenning M, Alm M, Franzyk H and Nielsen H M 2015 Sustained prevention of biofilm formation on a novel silicone matrix suitable for medical devices *Eur. J. Pharm. Biopharm.* **94** 305–11

[49] Bayramoğlu G, Batislam E and Arica M Y 2009 Preparation and drug-release behavior of minocycline-loaded poly[hydroxyethyl methacrylate- co -poly(ethylene glycol)-methacrylate] films *J. Appl. Polym. Sci.* **112** 1012–20

[50] Chen R R and Mooney D J 2003 Polymeric Growth Factor Delivery Strategies for Tissue Engineering *Pharm. Res.* **20** 1103–12

[51] Victor S P and Kumar T S S 2008 BCP ceramic microspheres as drug delivery carriers: Synthesis, characterisation and doxycycline release *J. Mater. Sci. Mater. Med.* **19** 283–90

[52] Tamimi F, Torres J, Bettini R, Ruggera F, Rueda C, López-Ponce M and Lopez-Cabarcos E 2008 Doxycycline sustained release from brushite cements for the treatment of periodontal diseases *J. Biomed. Mater. Res. Part A* **85A** 707–14

6. CHAPTER 6: Application of 3D porous scaffolds in the NanoBio4Trans project for perfusion bioreactor array with integrated sensors and differentiation of iPSC into hepatocytes.

This chapter summarises the use of the developed porous scaffolds into a perfusion bioreactor with integrated bio-impedance sensors for differentiation of hiPSC derived hepatocytes during the NanoBio4Trans project. Two types of BAL support systems have been developed: (1) 16-bioreactor array intended for improved throughput optimization experiments of cell culture and differentiation conditions. (2) 8-bioreactor array incorporating needle-electrodes for bioimpedance analysis of real time cell proliferation in 3D over time. Efficient operation of the BAL support system requires precise control of their key physical, chemical and physiological parameters. To implement this, advanced electrochemical sensors and assays have been developed and applied for monitoring hiPSC-derived liver tissue. Finally the different scaffolds designs were integrated into the perfusion bioreactor and the hiPSC derived DE cells differentiation was optimized for BAL development. Various functions, such as metabolite secretion as well as expression of hepatic genes responsible for liver development, drug metabolism, synthesis and transport, were tested.

6.1 Perfusion bioreactor array for tissue engineering applications

Two versions of a perfusion bioreactor array platform – **the BAL support system** - were developed. The first version (**Fig. 1**) is a 16-bioreactor array intended for optimimization of cell culture conditions. The second version (**Fig. 1Ab**) is an 8-biorector array with integrated vertical needle electrodes for electrical impedance spectroscopy (EIS) analysis of cell proliferation over time. The main components of the BAL support system include: (1) an exchangeable bioreactor array chip (BAL-on-a-Chip) for performing cell culture in a 3D environment, and

(2) a mother board containing all necessary components such as vials and vial trays for storage of culture medium and waste and peristaltic pumps and motors for perfusion of cell culture medium. **Fig. 1Ae** schematically illustrates the perfusion culture system and fluidic/air circuit, which is the same for both platforms. Four (**Fig. 1Aa**) or two 8-channel micropumps generate pulsatile flow and are controlled by motors and controllers from the Lego Mindstorm kit (Lego, Billund, Denmark). This allows culturing of cells at up to four different flow rates in a single experiment. The pumps allow flow rates from sub-µL·min^{-1} and up to approximately 90 µL·min^{-1}. The fluidic circuit is formed by the pumps, bioreactor array and medium storage vials that are connected using PTFE tubing with inner diameter of 0.8 mm. Inlet and outlet vials are coupled with PTFE tubing and supplied with air supplemented with 5 % CO_2 through a sterile 0.22 µm filter. All components are mounted onto a base platform for portability and easy handling. The entire system is placed in conventional cell culture incubators during the experiments.

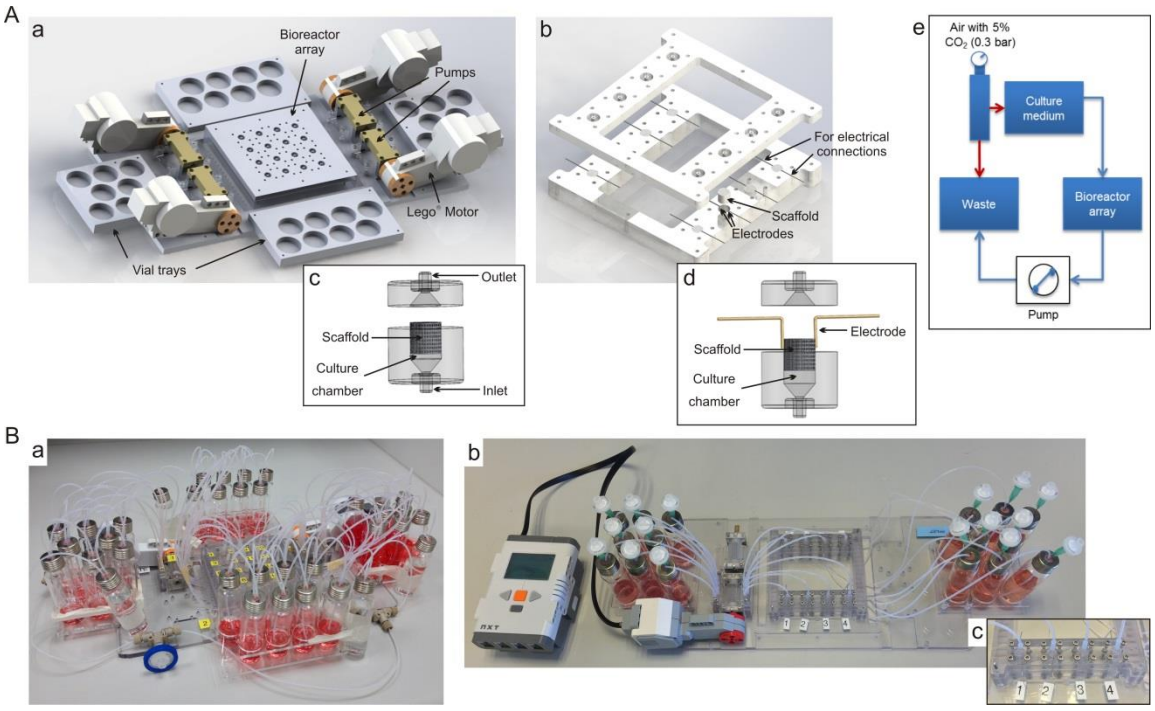

Figure 1. (A) Schematic design of a motherboard having an exchangeable bioreactor array with (a) 16 bioreactors (4 × 4 array) inserted and (b) an 8 bioreactor array (4 × 2 array) with integrated needle electrodes for electrical impedance monitoring of cell proliferation over time. Schematic of the bioreactors in the (c) 4 × 4 array and (d) 4 × 2 array. (e) Schematic of fluidic circuit (blue arrows) and pressure circuit (red arrows). – (B) Assembled perfusion array platform with (a) 16

and (b) 8 bioreactors, the latter with (c) two integrated vertical needle electrodes in each bioreactor.

The bioreactor array allows cell culture in cylindrical 3D scaffolds having diameter of 6 mm and height of 5 mm (**Fig. 1Ac** and **1Ad**). Each bioreactor consists of an inlet port (at the bottom), a cylindrical chamber for housing a 3D scaffold and an outlet port (at the top). Silicone tubes (inner diameter of 1.8 mm and height of 10 mm) are press fitted to the ports of the bioreactor (inner and outer diameter of 1 mm of 2 mm, respectively) and serve as connectors between the bioreactor and the rest of the perfusion network. The bioreactor units are implemented into the arrays to enable parallel analysis. **Fig. 1Ac** and **1Ad** show the schematic of a single bioreactor in the case of the 16- and 8-bioreactor array, respectively. For the impedance measurements, two platinum (Pt) needle electrodes (diameter of 0.4 mm and height of 5 mm) were vertically placed at the opposite sidewalls of each bioreactor (**Fig. 1Ad**). Moreover, in the 8-biorector array an opening was introduced between the two rows of bioreactors to allow electrical connections to the electrodes via crocodile clips (**Fig. 1Ab**)

6.2 Impedance based sensor integration and monitoring of cell growth in BAL support system

We present the application of electrochemical impedance spectroscopy (EIS) as a method for discriminating between different polydimethylsiloxane (PDMS) scaffolds for three-dimensional (3D) cell cultures. The validity of EIS characterisation for scaffolds having different degree of porosity (networks of structured or random channels) is discussed in relation to Archie's law. The EIS based method was used to provide porosity information in physiological buffer that agrees well with a more conventional weight-based approach. Different frequency ranges have been proposed that may serve as means of single-frequency measurements for fast scaffold characterization combined with in vitro monitoring of 3D cell cultures (Published in paper 4). Table 1 shows the values of porosity determined for random and structured scaffolds (20 - 80% infill) using both EIS- and weight-based techniques. The obtained porosity values using the two approaches are comparable. The weight-based method shows a higher standard deviation, which may be due to errors in the weighing, whereas EIS measurements provide a higher precision for the obtained porosity values reflected by the small standard

deviations. Nevertheless, the porosity values determined using the more conventional weight-based technique were considered as guidelines for validation of the EIS-based technique.

Table 1. Porosity values (%) for random and structured scaffolds (20 - 80% infill) determined using the weight-based method [13] and EIS measurements in PBS. Values are reported as mean ± standard deviation (n = 3) with suitable frequency ranges for EIS analysis.

Scaffold type	Porosity (%): weight-based method	Porosity (%): EIS[a]	Frequency range (kHz) for EIS analysis
Random	64 ± 1	67.75 ± 0.01	50 - 70
Structured 20%	19.5 ± 0.5	23.47 ± 0.01	50 - 70
40%	38.89 ± 0.07	45.80 ± 0.04	50 - 70
60%	60.5 ± 0.5	60.99 ± 0.03	50 - 70
80%	81 ± 1	89.17 ± 0.05	50 - 70

[a] In porosity calculation involving Eq. 1 and 2, the following parameters are used: m = 1 for structured scaffolds and m = 2 for random scaffolds; C = 1 for all scaffolds and σ_0 = 1.35 S/m.

Using the BAL support system in **Fig. 1Bb**, impedance monitoring of cell growth in the porous 3D scaffolds over a 19-day period was performed after loading of cells using a suspension with density of 2×10^6 Heg2 cells in 30 µL. **Fig. 2A** shows the measured impedance magnitude at 10 kHz over time. A drop in impedance was observed during the first three days of culture, which was unexpected. However, we reasoned that this most likely was due to a loss of non-adherent cells when perfusion was turned on, moreover calculations on the theoretically predicted number of cells that could be housed in the scaffolds was determined to be much lower than the number of cells that were loaded/seeded (see task 4.3 for calculations). After an initial decrease of impedance during the first three days, the impedance started to continuously increase over time. To understand these results, the cell number was determined based on the dsDNA content of cells in the scaffolds, using the PicoGreen assay. In fact the number of cells at the end of the 19 days cell culture period was found to be lower than the number of cells seeded into the scaffolds at the start of the experiment. This is also indicated by

the impedance spectra of **Fig. 2A**, showing a lower impedance magnitude at the end of the culture period compared with the magnitude at the beginning. **Fig. 2B** shows correlation between the measured impedance at day 19 (evaluated at 10 kHz) and the determined dsDNA quantity (day 19) in the different scaffolds. A parallel experiment was performed where scaffolds were loaded with 2×10^6 cells and then perfused with medium in the bioreactors. After 24 hours, we found that only 0.9 ($\pm$ 0.2) $\times 10^6$ cells (mean $\pm$ SD, n = 4) remained in the scaffolds, confirming the initial loss of cells and thus the decrease in impedance.

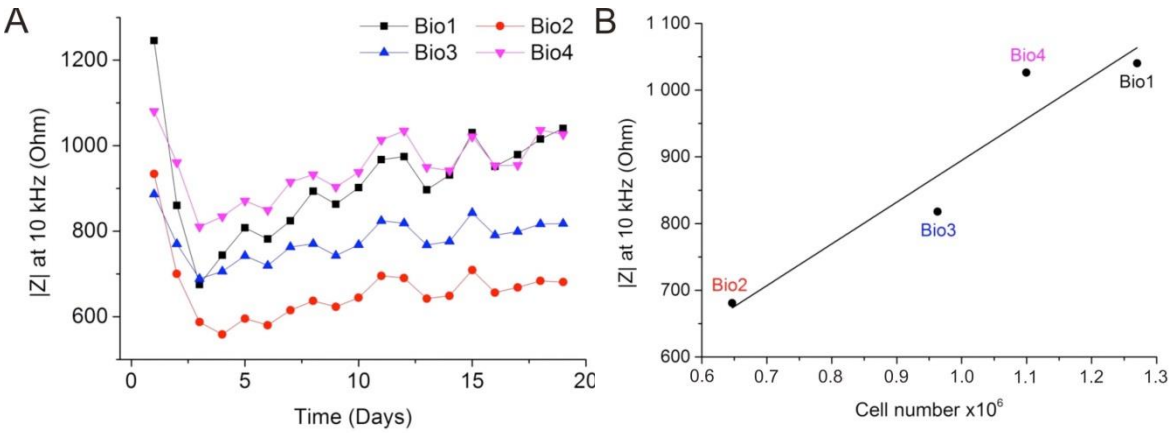

Figure 2. (A) Dynamic measurement of |Z| over 19 days of perfusion culture with HepG2 loaded bioreactors. (B) Linear correlation between the cell number found at day 19 and |Z| at 10 kHz (R^2 = 0.982).

6.3 Assessment of hiPSC derived BAL function at different conditions

6.3.1 Distribution, attachment and differentiated morphology of hiPSC-derived DE cells

The distribution, attachment and differentiated cell morphology of hiPSCs-derived DE cells were evaluated by imaging of the middle of a cross-sectioned scaffold after 22 days of culture at 1 µL/min flow rate in differentiation medium in the 16-bioreactor array system in **Fig. 1Ba**.

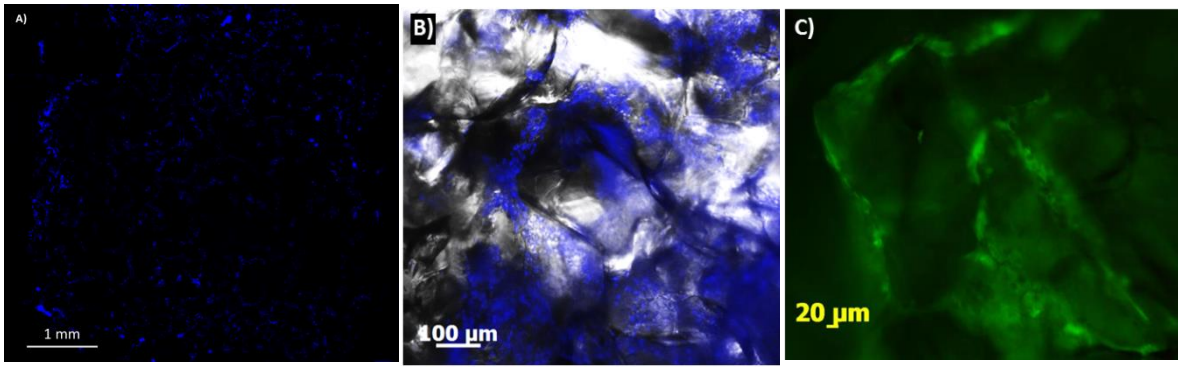

Figure 3. Microscopy imaging of hiPSC-derived DE cells cultured and hepatically differentiated inside a porous 3D scaffold at perfusion conditions: Image at day 22 after cell seeding of the middle of a cross-sectioned scaffold. A) Scan of entire cross-sectioned scaffold showing cell distribution. Höchst stained cell nuclei in blue color. B) Close-up view of cell distribution with Höchst stained cell nuclei. The fluorescence image is merged with a phase contrast image of the scaffold. C) Calcein-AM live-stained cells in green.

As shown in **Fig. 3A** and **B** of Höchst stained cell nuclei, the cells are uniformly distributed throughout the entire scaffold, but residing in populations in the cavities of the porous scaffold. A close-up image of live-stained cells in **Fig. 3C** displays proper cell attachment and morphology. Moreover, in **Fig. 4**, images of DE cells, differentiated on PDMS and on a polystyrene reference show that DE cells obtain identical morphology on PDMS.

The effect of scaffold design- and flow rate on hepatic differentiation, metabolic activity and function of the BAL was further investigated.

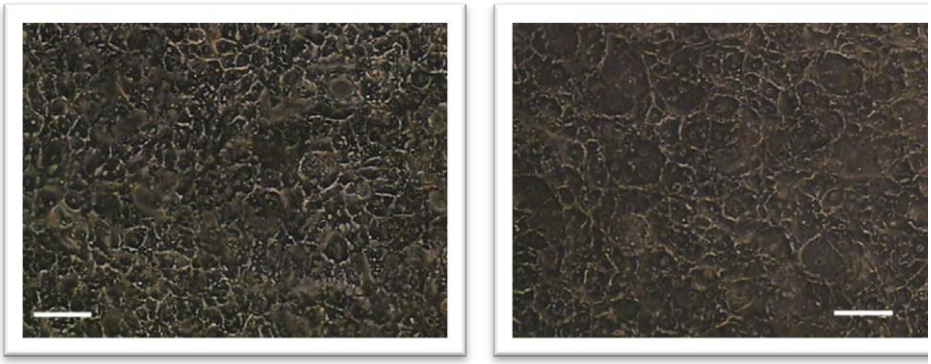

Figure 4. Optical images of the morphology of DE cells differentiated in 2D PDMS sheets (using Cellartis ECM coating), compared to a 2D static reference culture on polystyrene (using Cellartis ECM coating): Both images represent differentiated cells at day 19 of differentiation after the DE stage. **Left:** Reference culture**. Right**: PDMS sheets. Scale bars=60 µm.

6.3.2 Analysis of hiPSC-derived BAL at different conditions in comparison to PCLSs

Several BAL versions were created during the Nanaobio4Trans, using hiPSCs differentiated to the DE stage by Cellartis. The DE cells were produced from hiPSC by Cellartis and delivered to DTU. Scaffolds were prepared and loaded with hiPSC-derived DE cells and cultured for 25 days in the BAL support system with 16-bioreactor array at DTU. Two different scaffold designs (hexagonal and random**)** were tested and two flow rates (1 and 5 µL/min). The hepatic differentiation and functionality of hiPSC-derived hepatocytes were assessed at RUG using freshly obtained human PCLS as an *ex vivo* liver reference model. PCLS were incubated under static conditions in 12-well plates and in the liver-on-a-chip with a flow rate of 10 µL/min. Cells and slices were incubated in Cellartis hepatocyte maintenance culture medium.

The characteristics of these cells were determined with a palette of assays (metabolism, function, viability, and gene expression) developed by RUG. Human PCLS were cultured under static and flow conditions, using Cellartis hepatocyte maintenance medium. The same palette of assays was performed on the PCLS, static cultures and hiPSC-derived BALs. As the variation in liver function in the human population is well known to be large, the individual data of 3-9 human livers is given with the median value. The degree of hepatic differentiation in the BALs after 25 days of culture in Cellartis medium was analysed by gene expression of liver markers, albumin secretion and drug metabolism by phase I- and phase II activity.

An often used marker for hepatocyte function is albumin secreted into the medium. The medium from the respective BAL was collected and analysed using an ELISA kit. In regards to albumin, a similar or higher gene expression level (**Fig. 5**) was observed compared to the static references from Cellartis (dark blue bar) and DTU (yellow bar), which correlates with a lower expression of alpha-fetoprotein, i.e., the foetal form of albumin and should go from high to low during differentiation and maturation. The highest level of albumin expression was, however, seen for cultures in the Hex scaffold at a flow rate of 5 µL/min. The gene expression data for albumin were supported by a similar pattern in secretion level of albumin (**Fig. 6**) per scaffold for duplicate bioreactors and different conditions. Noteworthy is that the albumin secretion was increasing over time from day 21 to day 25.

The results show that albumin can be detected in the medium that passes through the BAL with the general trend that albumin secretion increases with time during the last day of differentiation, which is what should be expected.

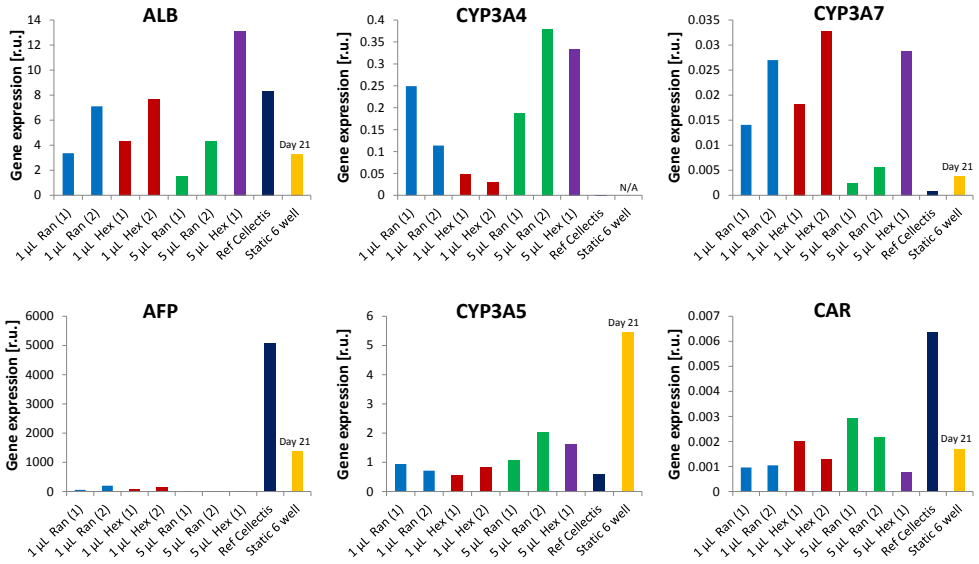

Figure 5. Effect of scaffold design and flow rate on gene expression of hepatocyte specific markers: hiPSC-derived DE cells were cultured and hepatic differentiated inside a 3D random porous scaffold (Ran) or a combined structured/random porous scaffold (Hex) at perfusion conditions at a flow rate of 1 µL/min or 5 µL/min for 25 days. Each culture condition was performed in duplicate and is shown in the diagrams as separate bars to easily visualize variation between parallel cultures at the same condition and easy comparison of gene expression of the same bioreactor culture to albumin secretion (Fig. 4.23) and phase I and phase II activity (Fig. 7), which are all shown in the same order in the diagrams. Gene expression was analyzed by qRT-PCR using Taqman® assays for the genes: Albumin (ALB), alpha-fetoprotein (AFP), CYP3A4, CYP3A5, CYP3A7, and constitutive androstane receptor (CAR). Gene expression is normalized to expression of CREB-binding protein. Two 2D static references are included: One based on cDNA from cells cultured at Cellartis (Ref Cellartis) and another based on cells cultured at DTU for 21 days in a standard 6 well plate (Static 6 well).

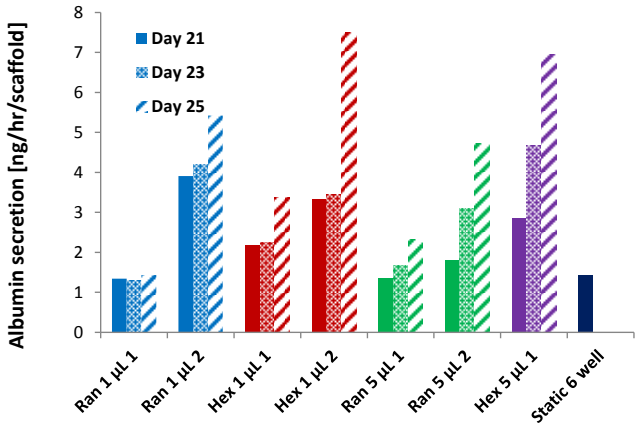

Figure 6. Effect of scaffold design and flow rate on albumin secretion: hiPSC-derived DE cells were cultured and hepatic differentiated inside a 3D random porous scaffold (Ran) or a combined structured/random porous scaffold (Hex) at perfusion conditions at a flow rate of 1 µL/min or 5 µL/min for 25 days. Each culture condition was performed in duplicate and is shown in the diagrams as separate bars to easily visualize variation between parallel cultures at the same condition and easy comparison of albumin secretion of the same bioreactor culture to gene expression and phase I and phase II activity (Fig. 4.24), which are all shown in the same order in the diagrams. Medium from the BAL outlets were collected at day 21, day 23, and day 25 and analyzed for albumin by ELISA (E80-129, Bethyl Laboratories).

A very important test for BAL function is the ability to metabolise drugs. This was done by adding test substrates to the perfusion medium and measuring the metabolite using HPLC or mass spectrometry. The BAL was first matured and then perfused with 7-ethoxycoumarin (phase I and II metabolism) or 7-hydroxycoumarin (phase II metabolism). The medium for the respective BALs was collected after the BAL was filled with medium containing the respective forms of coumarin. The medium was then frozen and shipped to P5 for HPLC analysis. The results are shown in **Fig. 7** where addition of the coumarin substrates showed the highest metabolic activity with respect to glucuronidation and sulfation at the highest flow rate, 5 µL/min, and at a level similar or higher than for liver slice cultures. Furthermore the glucuronidation activity was, as expected, higher than the sulfation activity.

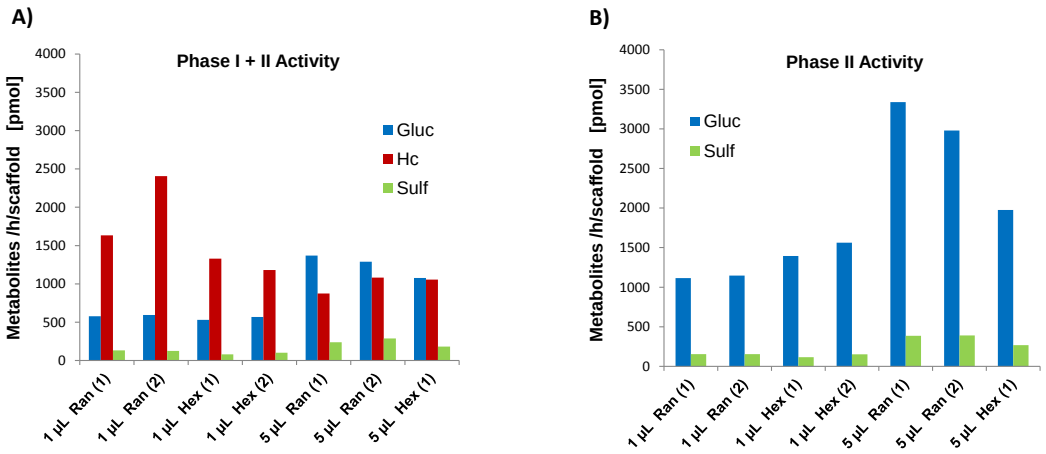

Figure 7. Effect of scaffold design and flow rate on phase I- and Phase II activity: hiPSC-derived DE cells were cultured and hepatic differentiated inside a 3D random porous scaffold (Ran) or a combined structured/random porous scaffold (Hex) at perfusion conditions at a flow rate of 1 µL/min or 5 µL/min for 25 days. Each culture condition was performed in duplicate and is shown in the diagrams as separate bars to easily visualize variation between parallel cultures at the same condition and easy comparison of phase I and phase II activity of the same bioreactor culture to gene expression (Fig. 5) and albumin secretion (Fig. 6), which are all shown in the same order in the diagrams. For the activity experiments, the scaffolds were removed from the flow bioreactor and placed in a 48 well plate in 1 mL medium with the added specific substrate(s). The scaffolds were then incubated for 2½ hours at 37°C/5% CO_2 and medium collected and stored at -20 °C for later analysis of metabolites by HPLC. A) For phase I and phase II activity measurements, the medium was added 500 µM 7-ethoxycoumarin and analyzed for the metabolites Gluc: 7-hydroxycoumarin glucuronide, Hc: 7-hydroxycoumarin, and Sulf: 7-hydroxycoumarin sulphate. B) In case no phase I activity would take place, 500 µM 7-hydroxycoumarin (product in phase I, and substrate for phase II activity) was added to the medium in another experiment, but to the same scaffolds. The medium was analyzed for the metabolites Gluc: 7-hydroxycoumarin glucuronide and Sulf: 7-hydroxycoumarin sulphate.

Expression of different hepatic genes responsible for liver development, synthesis, metabolism and membrane transport in hiPSC-derived BAL differentiated under different conditions were compared. The expression of the foetal liver marker AFP was lower in hiPSC-derived BAL cultured under flow compared to static cultures, but was higher than in PCLS, where it was nearly absent. This indicates the beneficial effect of flow on hepatocyte maturation. Expression of CYP3A7 (also mainly expressed in foetal liver) was low and similar to PCLS in all cell culture conditions. Expression of hepatic nuclear factor, HNF4α (liver differentiation marker), and nuclear receptor, CAR, which both regulate the expression of various hepatic genes, showed different expression patterns. HNF4α showed good expression levels, whereas CAR was poorly expressed

hiPSC-derived BALs cultured under all conditions compared to liver slices. Different CYP enzymes showed different expression levels. For example, CYP3A5 was expressed more in hiPSC compared to PCLS, on average 4-to 5-fold higher for hiPSC cultured at 5µL/min flow, and 9- to 12-fold higher in hiPSC cultured under static condition. On the other hand, CYP3A4 and CYP2B6 had low expression in hiPSC-derived BAL compared to hPCLS.

Overall the data indicates that hiPSC-derived BAL differentiate under flow into both hepatic and biliary directions, as epithelial biliary cell markers, such as CK7 and BGP, were well expressed in cell cultures.

6.4 Conclusions

Overall the achievements of BAL support system developed during NanoBio4Trans project demonstrates that function of hiPSC-derived hepatocytes or BALs is similar to fresh human liver tissue. Moreover, it reveals that these hiPSC-derived hepatocytes, cultured on the developed 3D scaffolds under perfusion into a BAL, show as yet unrivalled functionality, with excellent comparability of liver functions with human liver tissue. The differentiation of hiPSC-derived hepatocytes under flow conditions in the scaffolds was similar to that in normal cultures, which generates a unique possibility to differentiate and mature cells directly in a perfusion based support system.

7. CHAPTER 7. Biodegradable scaffold containing native extracellular matrix (ECM) for hiPSC derived liver tissue engineering

In previous chapters various synthetic scaffolds fabrication techniques have been explored for the differentiation and maturation of hiPSC derived hepatocytes. At the beginning the major goal of the project was to develop a platform for an extracorporeal device so synthetic polymer scaffolds coated with commercial ECM was suitable. The ECM used in standard hepatocytes cultures is mainly either collagen or fibronectin or a mixture of both which is highly expensive. However the mammalian liver tissue is composed of two major components: cells (Various liver cell types) and ECM component that provides structural support to the tissue's geometric shape. The tissue ECM is a complex mixture of proteins and polysaccharides such as collagen, elastin, hyaluronic acid, proteoglycans and glycosaminoglycans [1,2]. So to develop a better organ model much attention has to be paid to choose the right kind of ECM to specific cell types and at the same time the materials has to be economically viable. Secondly to be able to use the scaffolds for in-vivo tissue engineering applications the scaffolds has to be biodegradable [3,4] and the degradation time of the material should match the healing or regeneration process [5]. This chapter presents some preliminary findings carried out at the end of my PhD where I have tried to isolate decellularied native porcine liver ECM and tested the influence of native ECM on maturation of hiPSC derived hepatocytes. Silk fibroin, obtained from silkworms, demonstrates great biocompatibility along with outstanding mechanical properties and proteolytic degradation making it suitable for extensive use in multiple types of tissue engineering scaffolds [6]. I have therefore tried to fabricate silk protein based porous scaffolds using previously developed techniques in chapter 4 and also some bioinspired liver scaffold design.

7.1 Decellularized liver extracellular matrix (L-ECM): coating materials on to biodegradable scaffolds

In the field of liver tissue engineering, *In-vitro* culture of iPSC derived hepatocytes with better differentiation; improvement in hepatocyte-specific functions such as albumin secretion, hepatic transport activity, and ammonia metabolism; and loss of hepatocyte

polarity is a major challenge. Identification of new extracellular matrix (ECM) component that can maintain a functional hepatocyte differentiation profile would represent an advantage towards the development of an engineered liver tissue [2,7,8]. Individual extracellular matrix (ECM) components or combinations of desired ECM components have been used as substrates for hepatocyte culture systems for several decades [10]. Conventional in vitro culture models for hepatocytes include the use of sandwich configuration in which hepatocytes are either placed between two layers of type-I collagen and Matrigel (MG) or cultured on type-I collagen single layer. It has already been shown that ECM derived from the liver and type-I collagen are useful substrates for hepatocyte culture [8], [11]. However, ECM gels are not suitable for scaling up into 3D organs and cannot sustain long term cultureing: Firstly it is challenging to design porous scaffolds from those natural ECM due to their low mechanical strength and the second major problem is associated with the faster degradation of such natural ECM. So the idea of the project was to fabricate mechanically stiff (close to stiffness of liver) porous scaffolds containing liver specific ECM components and which could be programed for biodegradation over periods from months till years. The hypothesis was that silk fibroin scaffold with ECM could be a solution to the problems associated with pure ECM mentioned above. The main advantage of the natural silk fibroin was expected to be to provide the mechanical stiffness required and it can provide programed degradation of the scaffold.

In this study the first focus was to develop biomimetic ECM materials from decellularized porcine liver tissues and test this L-ECM coating material in comparison to commercially developed ECM commercially available by Cellartics (C-ECM) in terms of maintenance of hepatic phenotype, functions and hepatocyte survival of matured hepatocytes derived from hiPSC *in vitro.* Such ECM materials could subsequently be used to coat or embed into a biodegradable 3D silk scaffold. In the second part of the study the fabrication of two types of dual-pore silk scaffolds were investigated.

7.1.1 Materials and methods

Preparation of L-ECM

Adult porcine liver were obtained from the local abattoir. The liver tissue was decellularized and prepared as previously described [2]. Briefly, the chopped liver tissue was cut into small rectangular pieces, rinsed in phosphate buffered saline (PBS), and decellularized using 1% sodium dodecyl sulfate (SDS), until the tissue was white. The

resulting decellularized L-ECM was then rinsed with DI water overnight, lyophilized, and milled into a fine powder using a 40 mm mesh strainer and small tissue mill. The resulting milled powder was then solubilized by a pepsin-based enzymatic digestion in 0.1 M HCl for at least 48 h. The solubilized L-ECM was adjusted to pH 7.4 with NaOH. The final concentration of L-ECM solution was adjusted to 10 mg/mL and further diluted with PBS if necessary.

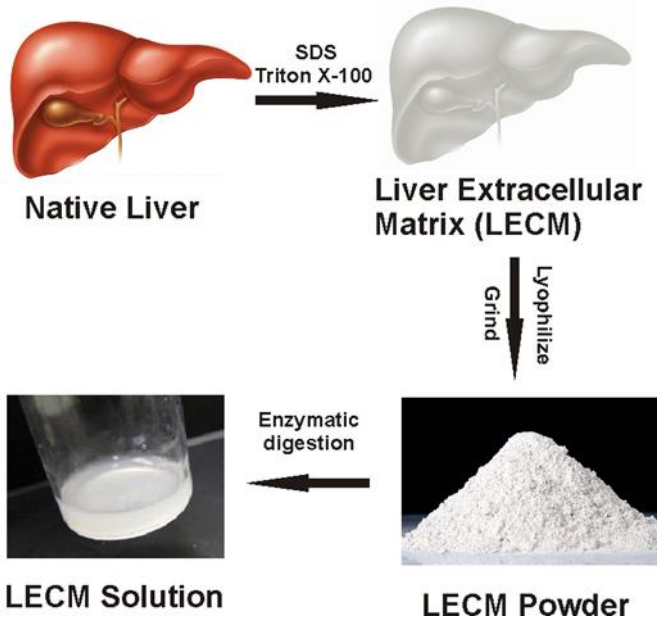

Figure 1: Schematic illustration of liver extracellular matrix (L-ECM) preparation. Native porcine liver was washed with a decellularizing solution (1% sodium dodecyl sulfate (SDS)) to remove cellular components in the liver tissue. The LEM was lyophilized and ground into powder. The powder was solubilized with 10% (w/w) pepsin in 0.1 M HCl. Ultimately LEM solution was used to prepare a 2D coating for hepatocyte culture.

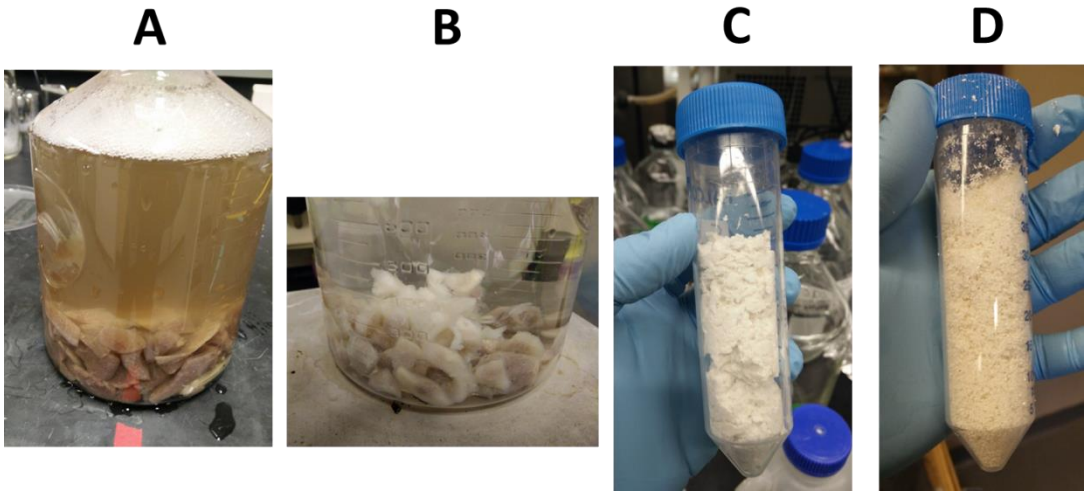

Figure 2: showing the cut liver pieces washing with 1% SDS (A&B) and lyophilized (C) and ground into powder (D).

Growing cells on ECM

Matured hepatocyte derived from human pluripotent stem cell (hiPSC) (Cellartis®, Cat. No. Y10050) (after 21 days of differentiation) were used in this work. The cell culture treated 24-well polystyrene plates 100 µg/cm^2 C-ECM or different concentrations of L-ECM overnight and air-dried in a sterile laminar air flow (LAF) cabinet. In an initial experiment maturated hepatocytes were seeded into the well plates according to the company protocol and cultured for 11 days period and the cell attachment and morphology was observed under the microscope to determine the minimum concentration required for future experiments. In a subsequent experiment 100 µg/cm^2 of L-ECM or C-ECM was coated in the wells of 24-well plates as described above and the mature hepatocytes were seeded into the wells and cultured for 16 days. On day 7, 12 and 16 the hepatocytes grown on the two different ECMs were analyzed and compared. Visual microscopy observation, liver specific biochemical assays, and quantitative reverse-transcription PCR (qRT-PCR) of liver specific gene markers were performed to evaluate the two different ECM coating materials on maturation of hepatocytes derived from hiPSC as described below.

Analyzing cells grown on ECM

The cells were lysed used lysis buffer provided by Fisher BioReagents™ SurePrep™ RNA/DNA/Protein Purification Kit (Fisher scientific, USA Cat no: BP280250). The protein content of cell lysates were measured by the Pierce® BCA Protein Assay Kit (cat. no. 23227) according to the manufacturer's microplate protocol. The absorbance was read at 570 nm and protein calculated based on a standard curve made with known concentration of bovine serum albumin.

Urea and albumin concentrations secreted from the hepatocytes into the medium were measured using albumin ELISA (Bethyl, USA) and Urea Assay Kits (Abnova, Germany) according to supplier's instruction.

Total cellular RNA was isolated using the Fisher BioReagents™ SurePrep™ RNA/DNA/Protein Purification Kit (Fisher scientific, USA Cat no: BP280250). Differentiated cells were lysed using the lysis buffer provided in the Fisher BioReagents kit. The lysate was collected in microtubes and processed according to manufacturer's instructions. The RNA was converted to cDNA using the High Capacity cDNA Reverse Transcription Kit (Applied Biosystems, 4374966). Quantitative real time PCR (qPCR)

was conducted using the TaqMan® Gene Expression Assays (Applied Biosystems 4331182, ALB (albumin) ID: Hs00910225_m1, AFP (alpha-fetoprotein) ID: Hs00173490_m1, CYP2B6 ID: Hs04183483_g1, CYP3A4 ID: Hs00604506_m1, CYP3A5 ID: Hs00241417_m1, CYP3A7 ID: Hs00426361_m1, HNF4A (hepatocyte nuclear factor-4-alpha) ID: Hs00230853_m1, NR1I3 (CAR, constitutive androstane receptor) ID: Hs00231959_m1, ABCB11 (BSEP, Bile Salt Export Pump) ID: Hs00184824_m1, ABCB1 (Pgp, permeability glycoprotein) ID: Hs00184500_m1, and KRT7 (cytokeratin-7) ID: Hs00559840_m1), TaqMan® Gene Expression Master mix (Applied Biosystems, 4370048) and RNase-free water according to the manufacturer's instructions (Applied Biosystems 11/2010). The C_t values obtained after analysis in the real time PCR thermocycling machine (MJ Research, the thermocycling program was 50ºC for 2 minutes, 95 ºC for 10 minutes and 40 cycles of 15 sec at 95 ºC and 1 minute at 60 ºC) were normalized to the C_t value of housekeeping gene CREBBP (CREB-binding protein) ID: Hs00231733_m1 (e.g. ΔC_t(ALB) = C_t(ALB)-C_t(CREBBP). The gene expression is presented as individual data points using the formula: $2^{-\Delta Ct}$.

7.1.2 Results

Figure 3 show the adhesion and morphology of hiPSC derived hepatocytes cells grown for 11 days on polystyrene (PS) well plates coated with either ?? μg/cm^2 C-ECM or different concentrations of L-ECM. In wells coated with only 50 μg/cm^2 L-ECM the cells started to delaminate from the edges of the well plate. However, at higher concentration of L-ECM as well as for the C-ECM coating no significant cell delamination were observed. So 100 μg/cm^2 was chosen as the optimal concentration for further studies.

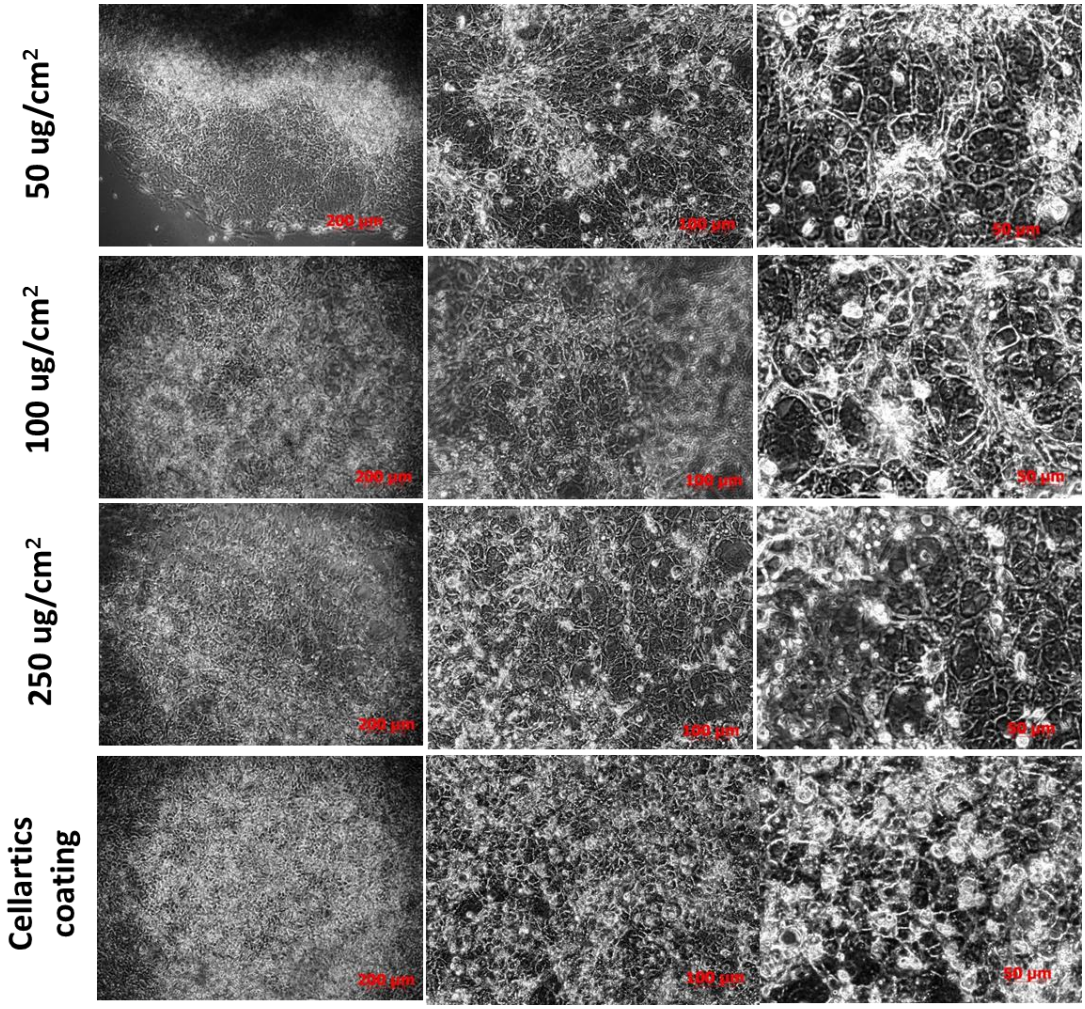

Figure. 3 Comparison of cell adhesion and morphology of hiPSC derived hepatocytes cell grown on polystyrene surfaces coated with either ?? µg/cm2 C-ECM or different concentrations of L-ECM. Phase-contrast images taken after 11 days of culture period.

In the next phase we compared mature hepatocytes derived from hiPSC, grown on either L-ECM or C-ECM coated surfaces (figure 4). On day 7 no significant difference in morphology regarding "bile-canaliculi like" structures and poly-nucleated cells were observed. However on day 12 cells grown on C-ECM coated surface started to detach and by day 18 some area without any cells can clearly be seen. The company instruction was to grow cells only until day 11 or 12 and they have also confirmed that cells lose their liver-like function after 12 days of growth. In contrast, for the cells grown on L-ECM coated surfaces cells were very strongly adhered to the surface even till the end of the experiment after18 days.

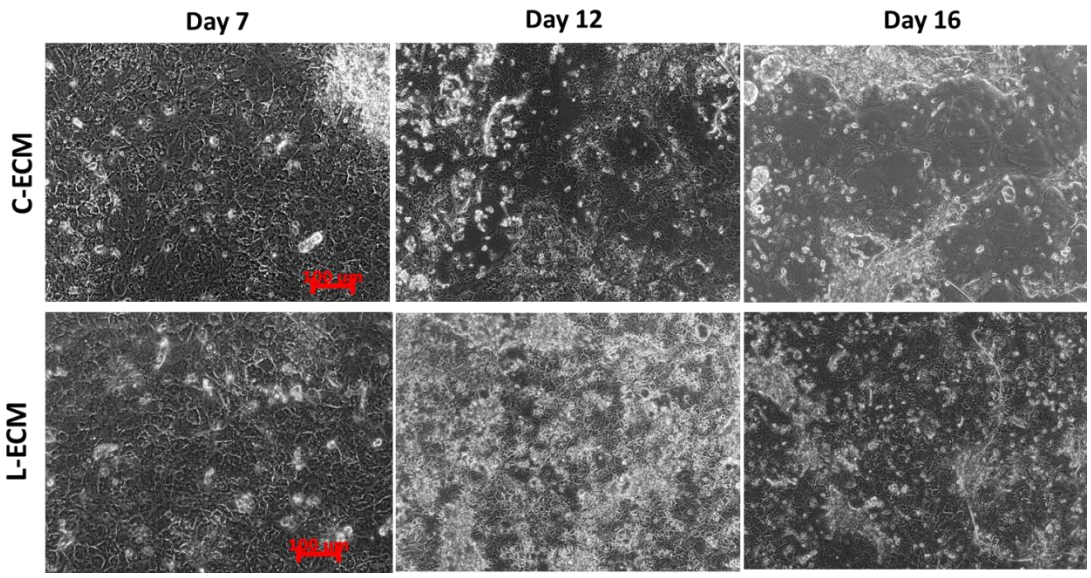

Figure. 4 Microscope imiges of hiPSCderived hepatocytes morphology, cultured on PS surface coated with either 100 µg/cm2 L-ECM coating or C-ECM (commercial cellartics ECM) over 16 days period.

Albumin and Urea production:

The changes in albumin and urea production rate from hepatocytes grown on both the surfaces were compared after 6, 12 and 18 days of growth, respectively, as shown in figure 5. The albumin secretion from hepatocytes grown on L-ECM surfaces was always higher compared to cells grown on C-ECM coated surfaces. On day 18 the hepatocyte cells grown on L-ECM surface produced just as high amount of albumin as on day 12 indicating the maintenance of maturation period. In contrast for the cells grown on C-ECM coating the amount of albumin produced was below the detection limit. This might be due to the loss of maturation (and herby loss of liver specific metabolic activity) as well as a higher number of cell detachment form the C-ECM coated compared to L-ECM as shown in the figure 4. In case of urea synthesis on day 6 and 12, from hepatocytes grown on both surfaces showed similar level, although it was a little higher from cells grown on C-ECM coated surface compared to cells grown on L-ECM coating. Similar to albumin secretion on day 18 cells grown on L-ECM surface produced significantly higher amount of urea compared to cells on C-ECM coatings. Throughout the culture period hepatocyts grown on L-ECM coated surface maintained almost constant level of urea production.

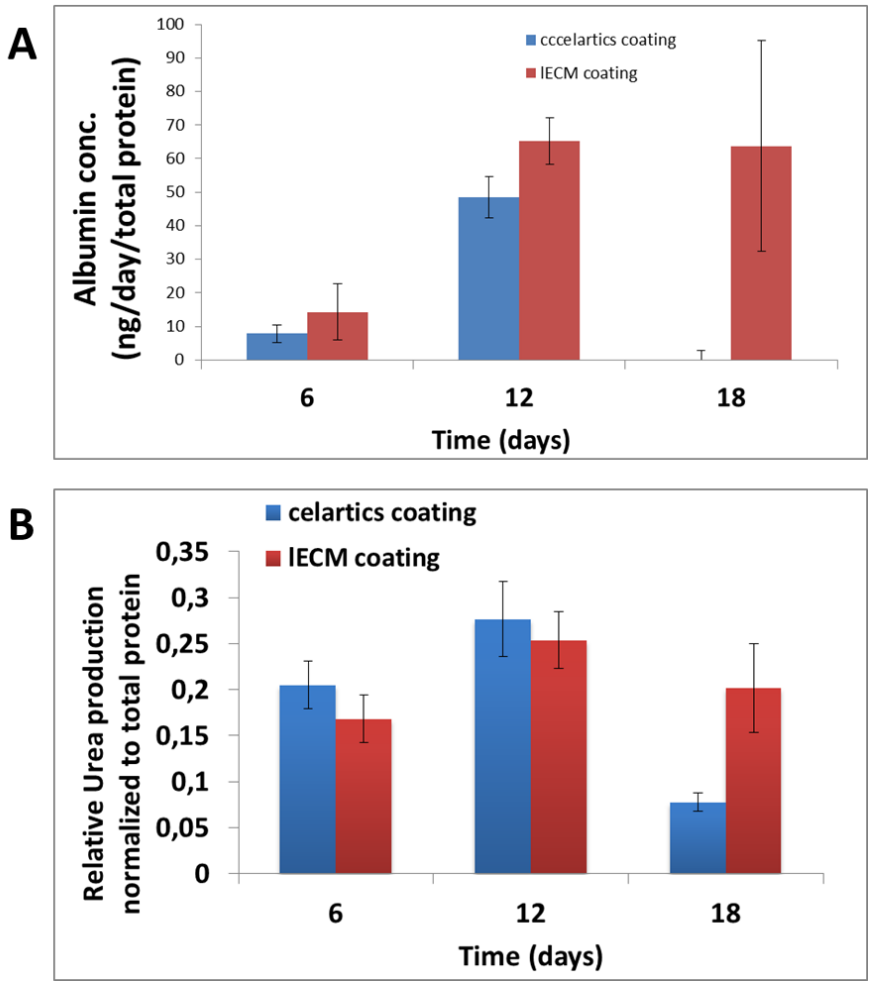

Figure 5. Measurement of (A) Albumin and (B) Urea secretion over 18 days period by matured hepatocytes derived from hiPSC.

Gene expression studies:

We have also compared various up and down regulating liver specific gene from hiPSC derived matured hepatocytes cultured on both C-ECM and L-ECM coating conditions on day 6, 12 and 18 (figure 6). From the figure 6 this was clear that in case of upregulating genes hepatocytes grown on L-ECM coated surface has shown better performance compared to C-ECM coated surface, except for HNF4A. For HNF4A both the surfaces have shown almost similar level of expression. The expression of albumin specific gene are in agreement with the albumin protein release assay shown in figure 5A. However for downregulating genes a mix level of expression was observed. For example in case of AFP expression on day 6 the level of expression was almost similar but on day 12 the expression lever was higher for cells grown on L-ECM compared to C-ECM coated surface. Again on day 18 the effect was quit opposite to day 12. For

KRT cells on L-ECM performed better compared to cells grown on C-ECM coated surface.

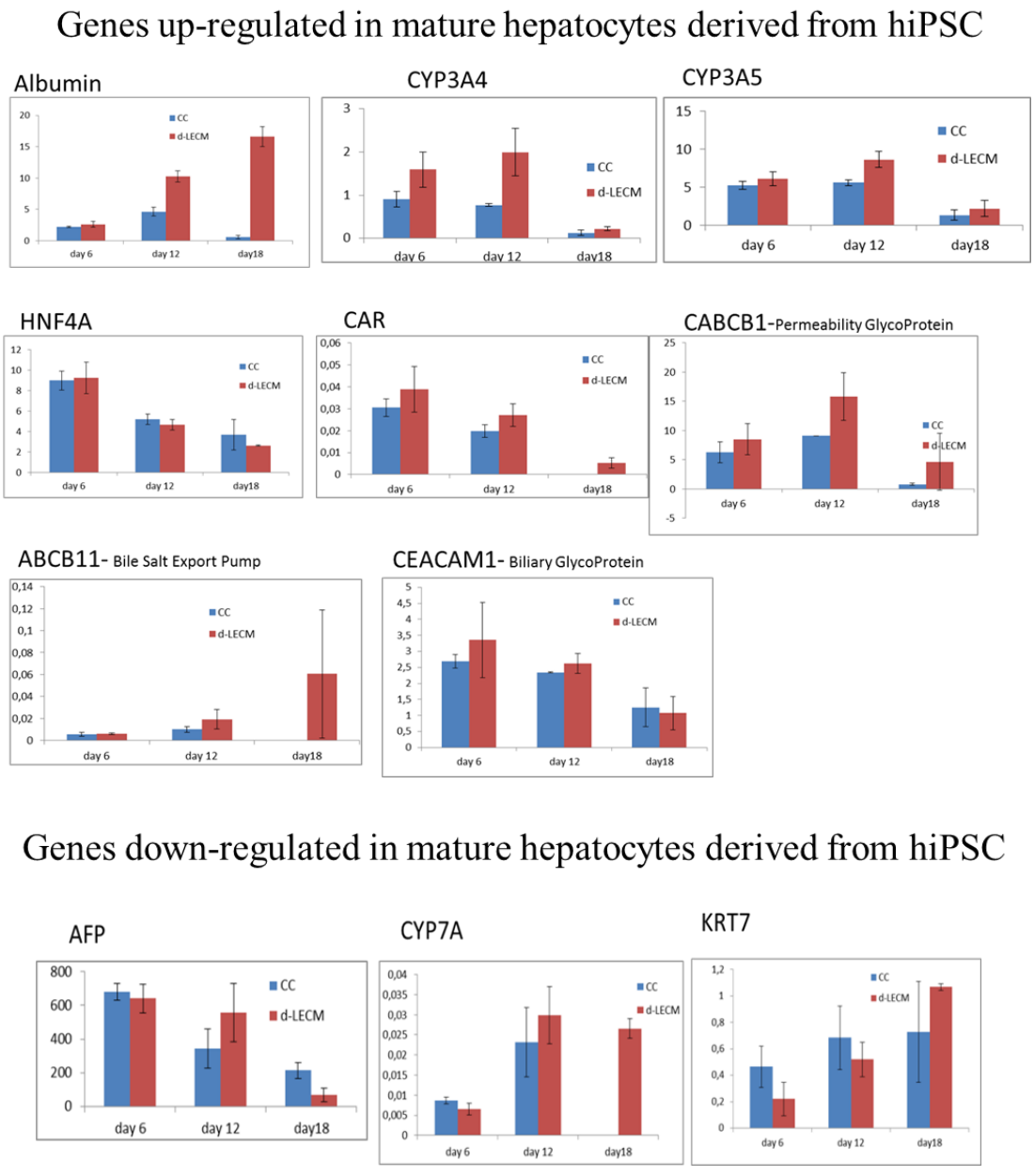

Figure 6. Time resolved gene expression of hepatocyte specific markers during differentiation: Gene expression at cc and L-ECM 2D coating conditions is shown at 6, 12, and 18 days of growth. The error bars are based on results from 6 independent chambers from 3 independent experiments.

This comparison clearly shows that the hepatocytes grown on L-ECM coated surface performed better than on C-ECM coated surface. So in future L-ECM can be utilized as better ECM material for maintaining hiPSC derived functional human hepatocytes in 3D porous scaffolds.

7.2 Fabrication of silk scaffold material for tissue engineering

The first use of silk in medicine began in ancient times for suturing. Silk makes an exceptional suture material due to its robust mechanical properties, biocompatibility, and programmable degradation profile with time[11]. Centuries later this unique protein is still being explored for its application in the biomedical field. However, its application range has broadened from its use as raw fiber sutures to aqueous and organic solvent-based silk solutions, sponges, foams, films, powders, particles, hydrogels, nanospheres, electrospun regenerated fibers, and aerogels. Currently, these formats are being applied to a wide variety of tissue engineering applications including regeneration of bone, cartilage, kidney, muscle, ligament, lung, skin, cornea, heart, nervous tissue, and intestine[12]. Our goal was to explore the fabrication of 3D silk scaffolds with various pore architectures for liver tissue engineering.

7.2.1 Materials and methods

Preparation of silk fibrion fiber from B. mori (Bombyx mori) cocoon

Figure 7 illustrates all the steps in silk extraction. For silk fibroin extraction, silkeworm cocoons were opened, the silkworms were discarded, and the cocoons were cut into small pieces. Only cocoons that looked undamaged were used. Then 3 liters of ultrapure water was boiled in a glass beaker and 6.36g of sodium carbonate (Na_2CO_3) (Sigma Aldrich, USA) was added to the boiling water and dissolved in order to prepare a 0.02M solution of Na_2CO_3. Then 7.5g of cocoon pieces were added to the boiling Na_2CO_3 solution and cooked for 30 minutes. In order to disperse the cocoons, they were stirred with a spatula every 10 minutes. The silk fibers were removed with a spatula, squeezed and cooled in 2L of cold ultrapure water in a beaker. Then the silk fibroin was rinsed in ultrapure water for 30 min . After rinsing, the fibers were removed from the water and squeezed and spread on a piece of aluminum foil and left to dry in a fume hood overnight.

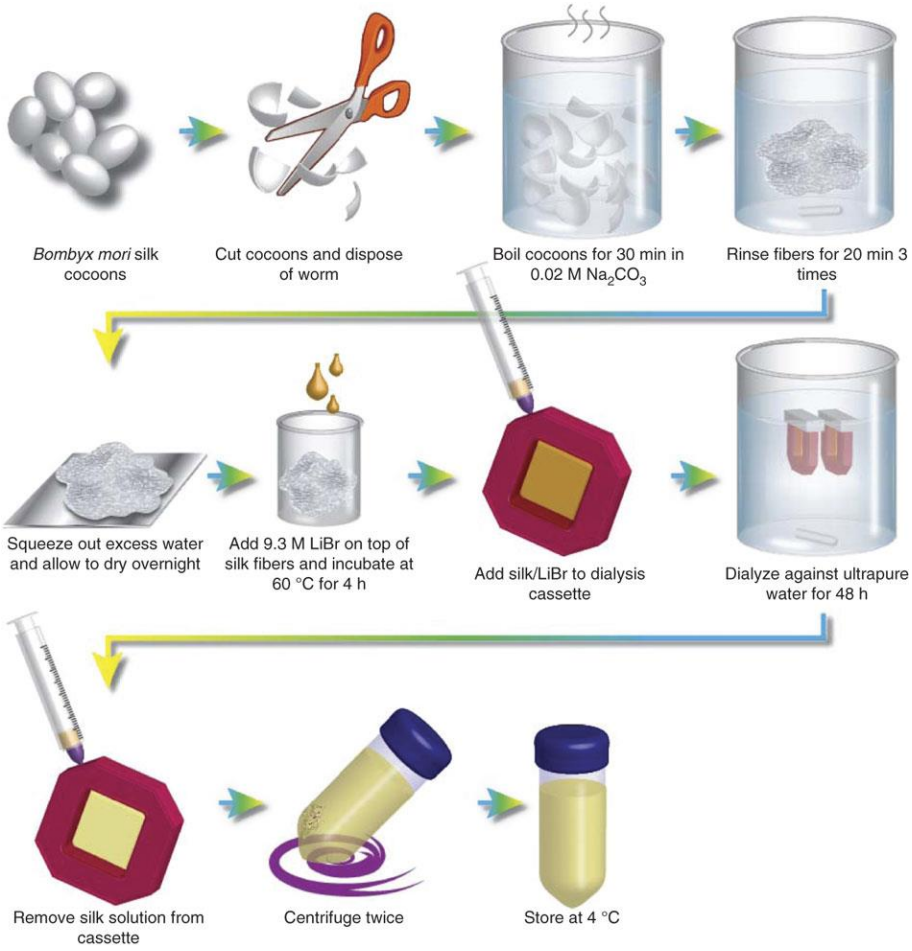

Figure 7. Aqueous-based processing of silk fibroin. Silk protein from B. mori silkworm cocoons was extracted by first boiling the cut cocoons in 0.02 M sodium carbonate, rinsing the boiled silk fibers in deionized water, and drying the fibers. The fibers were then dissolved in a 9.3M lithium bromide solution and the lithium bromide salt was subsequently dialyzed out of solution leaving behind the aqueous silk protein [From reference [12]].

Preparation of B. mori silk fibroin solution

The dry silk fibers were dissolved in a 9.3 M lithium bromide (LiBr) (Sigma Aldrich, USA) solution (25% wt/v) at 60°C for 4 to 6 hours, and the resulting solution was dialyzed with deionized water using 3500 Dalton molecular weight cut off dialysis tubing (Thermoscientific, USA) to remove the lithium bromide. The solubilized silk protein solution was then centrifuged twice (9700 RPM, 20 min, 4 °C) to remove insoluble particulates. The concentration of the silk solution was determined by drying a known volume of the solution and weighing the remaining solids. This protocol resulted in a 6–8% wtv−1 silk solution. Silk solutions were stored at 4 °C for a maximum of 3weeks.

Fabrication of dual-pore silk 3D scaffolds

Sacrificial moulds for dual-pore silk scaffolds were 3D printed using a Replicator 2X

3D filament deposition printer (MakerBot Industries, LLC, Brooklyn, NY, USA) as described previously[13]. In brief, a 3D cylindrical cube (W 20 mm x H 6 mm) was designed using SolidWorks 2013 3D CAD design software (Dassault Systèmes Solid-Works Corp., Waltham, MA, USA). The design was exported as STL format into the 3D printing software (Makerware 2.4.1) for G-code generation and mould printing. Water dissolvable poly(vinyl alcohol) (PVA) filaments (MakerBot, USA) were used to print the sacrificial moulds. The printing was performed at 200°C as the nozzle temperature and 40°C as the bed temperature. The PVA moulds were loaded into a 20 ml plastic syringe and the 6% silk solution was injected into the mould and transferred into a -20 or a -70 ^{0}C freezer and kept there overnight. The freezing temperature mainly controls the size of the random pore of the scaffold through the crystal formation of different sizes. At lower temperature the random pore size also decreases. Accordingly -20 ^{0}C was used for hexagonal PVA mould (generated microporous lamellar structure) and -70 ^{0}C for woodpile PVA mould different type of random pore generation. After freezing overnight the silk-PVA mould was freeze dried for one day. The silk was made insoluble by water annealing (this the process of crosslinking the silk) at room temperature for 24 hr to induce β-sheet formation. Scaffolds were cut into desired size and rehydrated in miliQ water for 24 hr to remove the PVA completely from the silk. Fresh miliQ water was exchanged very 2-3 hr.

7.2.2 Results of silk scaffold fabrication

Figure 8 shows a photograph of the dual-pore silk fibroin scaffold.. The woodpile silk scaffolds with dual pores were fabricated using 3D printed PVA filament moulds. As shown in the SEM image of the scaffold in figure 9, the pores have a round geometry with diameter of about 400 µm. In the random pore regions of the scaffolds, the number of random pores generated was very high with small dimension ranging from ~50-100 µm due to the low temperature used for freezing (-70 ^{0}C), but the pore size can easily be controlled by changing the freezing temperature.

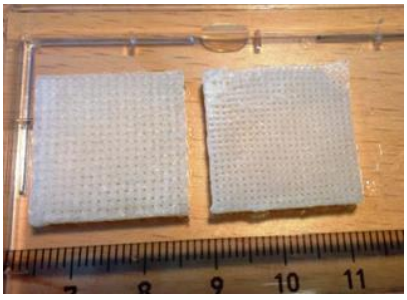

Figure 8. Photograph of porous silk fibroin scaffold.

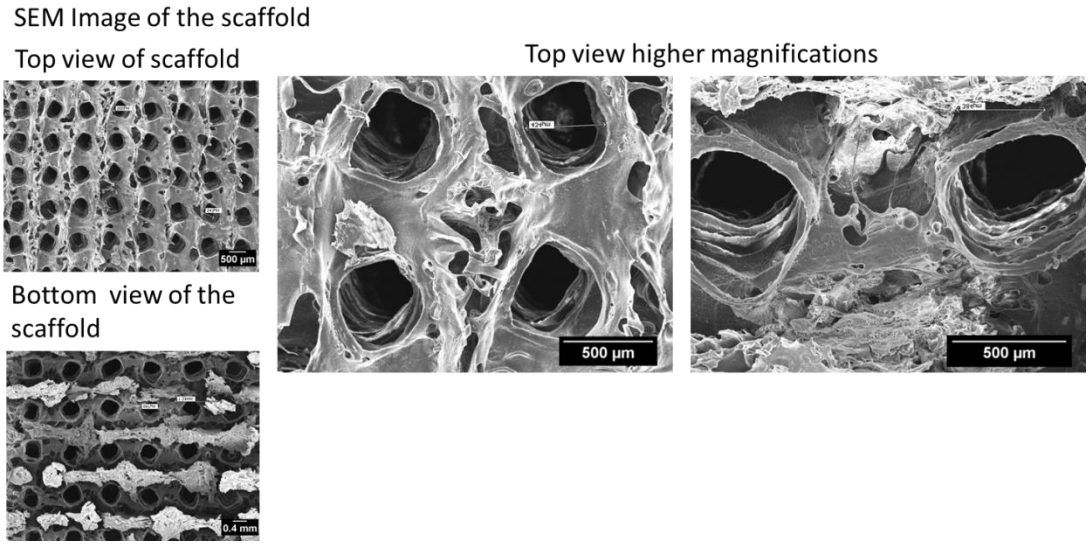

Figure 9. SEM images of woodpile designed dual-pore silk fibroin scaffold with top and bottom view.

However we have also tried to fabricate dual pore scaffolds with lamellar random pores using a similar approach by using a hexagonal PVA mould as shown in the figure 10. From the SEM figure it this is clear that the structural integrity of lamellar pores were well maintained and intact into the bulk scaffold.

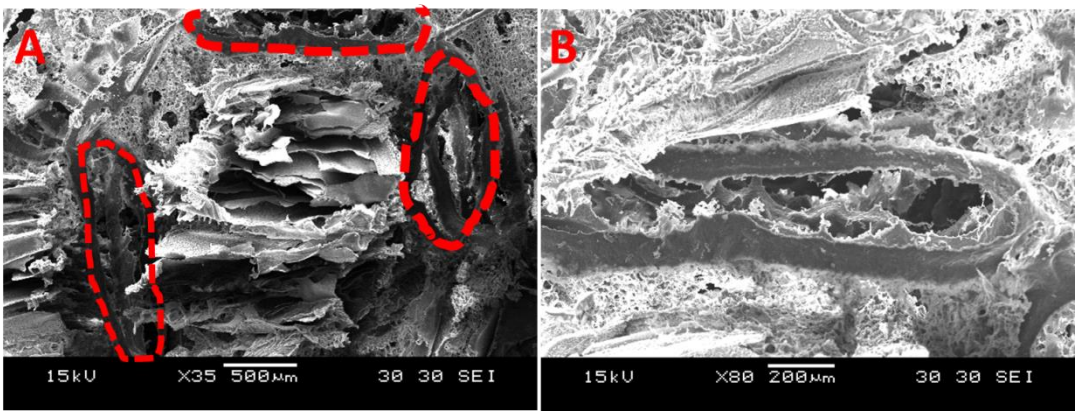

Figure 10. A) SEM images of Hexagonal dual-pore silk scaffolds for liver tissue engineering. B) is the zoom in into the structured pore region of A. round red lines:structured pores and in between red lines are the lamellar porous random pore region.

7.3 Future work: Next generation biomimetic scaffold design for liver tissue engineering

In future work to design silk scaffolds with microvascular network similar to real liver it is important to understand the internal ECM microarchitecture of it. As shown in figure 11, the ECM of liver hexagonal lobule resembles some plate like arrangement. The blood flows through small blood vessel such as hepatic artery (12-35 µm diameter) to

the central vain of diameter of 70 µm. In liver lobule, hepatocytes are always attached on a 1-2 µm 2D planer ECM structure arranged in 3D.

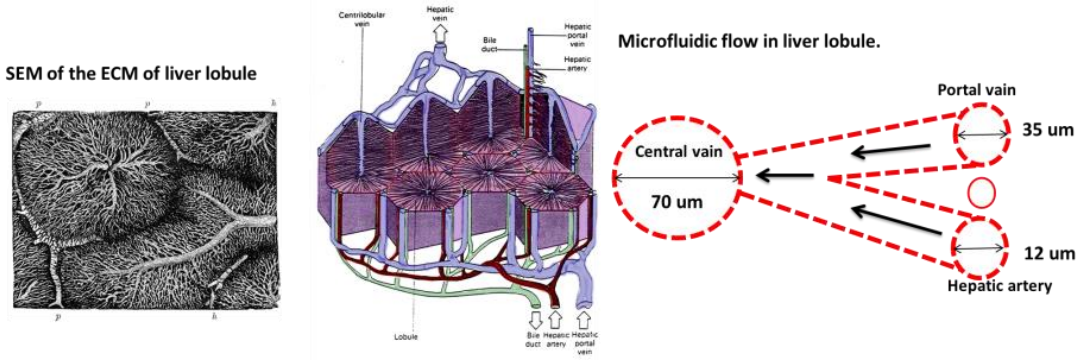

Figure 11. Liver Histology left: SEM of liver lobule of liver ECM (Baker, W. Morrant & Harris, Vincent Dormer Kirkes' Hand-book of Physiology, 13th ed. (P. Blakiston's Son & Co., 1892) 370), middle: schematics of arranged liver lobule and the blood flow into it (courses.stu.qmul.ac.uk), right: illustration of microfluidic blood flow into the cross-section of liver lobule.

To design this kind of channel morphology directional freezing silk scaffold technique has been used to fabricate the scaffold as shown in figure 12. Lower concentrations of silk and higher freezing temperature (-20°C) were used to make soft scaffolds with large pores (of diameter = 200 µm).

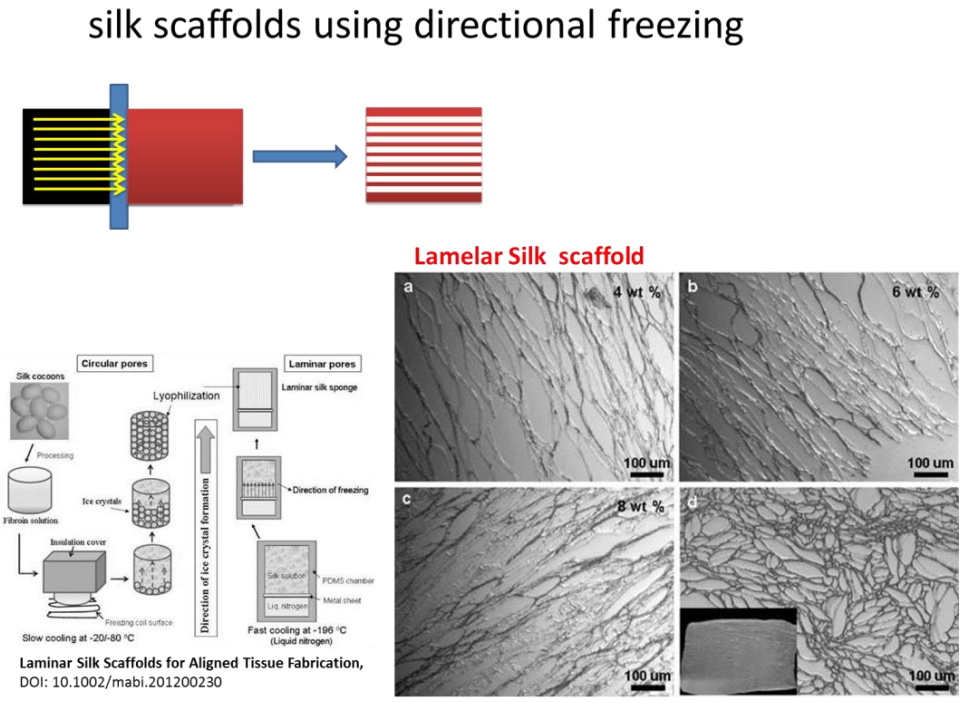

Figure 12. Fabrication of lamellar scaffolds. top and bottom left: Methods of fabricated which is adapted from the literature. Bottom right: SEM image of generated lamelar scaffolds with different concentration of silk protein (a,b,c) and scaffolds without directional freezing (d). [From reference [14]]

Figure 13 illustrates the possibility to design scaffolds with complex pore networks, which could simulate the suitable nutrient flow conditions closely similar to microenvironment of liver micro-lobule. The central large pore (2-3mm in diameter) will act as central vain and the directional pores of diameter bellow 200 µm will act as portal vain or hepatic artery.

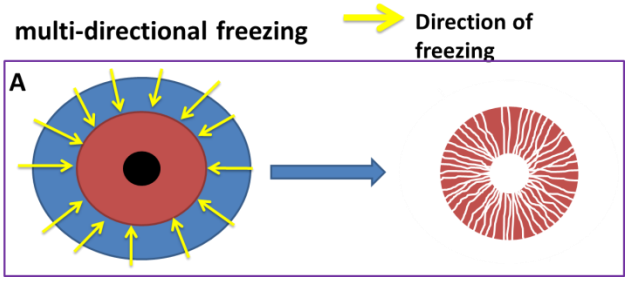

Figure 13. Multidirectional freezing scaffold. In the current design of the scaffold 200 µm cappilaris are connected into the center where it was punched to be able to use as inlet or outlet of the flow.

We have also tried to fabricate dual pore scaffolds with lamellar random pores using a similar approach (illustratd in fig 13) by using a hexagonal PVA mould as shown in the figure

7.4 Conclusion

In this chapter we have shown that L-ECM derived from decellularized native liver can serve as functional ECM surface for hepatocytes derived from hiPSC as compared to C-ECM supplied by the hiPSC company. Similarly we have also shown that biodegradable silk materials can be utilized to generate 3D dual-pore scaffolds by combining 3D PVA printing with freeze drying. More novel biomimetic approach can be adapted into the current fabrication techniques to generate more smart scaffolds materials. Finally such 3D dual-pore scaffolds can be coated or embedded with L-ECM as functional surface to induce better maturation of hiPSCs for BAL generation.

7.5 References

[1] Nakamura S and Ijima H 2013 Solubilized matrix derived from decellularized liver as a growth factor-immobilizable scaffold for hepatocyte culture. *J. Biosci. Bioeng.* **116** 746–53

[2] Lee J S, Shin J, Park H M, Kim Y G, Kim B G, Oh J W and Cho S W 2014 Liver extracellular matrix providing dual functions of two-dimensional substrate

coating and three-dimensional injectable hydrogel platform for liver tissue engineering *Biomacromolecules* **15** 206–18

[3] Holy C E, Shoichet M S and Davies J E 2000 Engineering three-dimensional bone tissue in vitro using biodegradable scaffolds: Investigating initial cell-seeding density and culture period *J. Biomed. Mater. Res.* **51** 376–82

[4] Guan J, Fujimoto K L, Sacks M S and Wagner W R 2005 Preparation and characterization of highly porous, biodegradable polyurethane scaffolds for soft tissue applications *Biomaterials* **26** 3961–71

[5] Cao Y and Wang B 2009 Biodegradation of Silk Biomaterials *Int. J. Mol. Sci.* **10** 1514–24

[6] Correia C, Bhumiratana S, Yan L-P, Oliveira A L, Gimble J M, Rockwood D, Kaplan D L, Sousa R A, Reis R L and Vunjak-Novakovic G 2012 Development of silk-based scaffolds for tissue engineering of bone from human adipose-derived stem cells *Acta Biomater.* **8** 2483–92

[7] Uygun B E, Soto-Gutierrez A, Yagi H, Izamis M-L, Guzzardi M a, Shulman C, Milwid J, Kobayashi N, Tilles A, Berthiaume F, Hertl M, Nahmias Y, Yarmush M L and Uygun K 2010 Organ reengineering through development of a transplantable recellularized liver graft using decellularized liver matrix. *Nat. Med.* **16** 814–20

[8] Struecker B, Butter A, Hillebrandt K, Polenz D, Reutzel-Selke A, Tang P, Lippert S, Leder A, Rohn S, Geisel D, Denecke T, Aliyev K, Jöhrens K, Raschzok N, Neuhaus P, Pratschke J and Sauer I M 2014 Improved rat liver decellularization by arterial perfusion under oscillating pressure conditions. *J. Tissue Eng. Regen. Med.*

[9] Martinez-Hernandez A and Amenta P S 1993 The hepatic extracellular matrix *Virchows Arch. A Pathol. Anat. Histopathol.* **423** 1–11

[10] Sellaro T L, Ranade A, Faulk D M, McCabe G P, Dorko K, Badylak S F and Strom S C 2010 Maintenance of human hepatocyte function in vitro by liver-derived extracellular matrix gels. *Tissue Eng. Part A* **16** 1075–82

[11] Li G, Li Y, Chen G, He J, Han Y, Wang X and Kaplan D L 2015 Silk-Based Biomaterials in Biomedical Textiles and Fiber-Based Implants *Adv. Healthc.*

Mater. n/a – n/a

[12] Rockwood D N, Preda R C, Yucel T, Wang X, Lovett M L and Kaplan D L 2011 Materials fabrication from Bombyx mori silk fibroin *Nat Protoc* **6** 1612–31

[13] Mohanty S, Muhammad H B, Trifol J, Szabo P, Burri H V R, Canali C, Dufva M, Emnéus J and Wolff A 2015 Fabrication of scalable and structured tissue engineering scaffolds using water dissolvable sacrificial 3D printed moulds *Mater. Sci. Eng. C* **55** 569–78

[14] Mandal B B, Gil E S, Panilaitis B and Kaplan D L 2013 Laminar Silk Scaffolds for Aligned Tissue Fabrication *Macromol. Biosci.* **13** 48–58

8. CHAPTER 8. Conclusion and Outlook

In my PhD research work, I established the scientific and engineering foundation for the development of extracorporeal bio-artificial livers. New 3D scaffold fabrication techniques were developed and shown to be highly scalable, reproducible and economical. A wide range of materials were screened for their applicability to make scaffolds or to form interpenetrating networks (IPNs) inside the 3D scaffolds. . The potential of using the fabricated 3D scaffolds for tissue engineering was demonstrated by culturing hepatocytes in integrated BAL support systems. The principle findings are summarized below:

1) Novel fabrication strategies that combine 3D filament printing of sacrificial moulds, polymer casting and sugar/salt leaching procedures were developed to realize woodpile and hexagonal scaffold 3D scaffold architecture. Microporous structures, random, and combined structures/random channel network architecture have been achieved.

For structured scaffolds fabrication, we explored 3D printed polyvinyl alcohol (PVA) as a sacrificial mould in a polymer casting process. The PVA mould network defines the channels and is dissolved after curing the polymer casted around it. It was possible to achieve 80% porosity corresponding to about 150 cm^2/cm^3 surface to volume ratio. The process is easily scalable as demonstrated by fabricating a 75 cm^3 scaffold with about 16,000 interconnected channels (about 1 m^2 surface area) and with a channel-to-channel distance of only 78 μm. To our knowledge, this is the largest scaffold ever to be produced with such small feature sizes and with so many structured channels.

For dual-pore scaffolds architecture, we innovatively combined 3D printing of PVA mould with salt leaching process. In this technique, the sacrificial PVA mould, which determines the structured pore architecture, was filled with salt crystals to define the random pore regions of the scaffold. The technique has a number of advantages over the methods reported in literature, such as automated assembly of the sacrificial mould, and precise control over pore architecture/dimensions by 3D printing parameters. The fabricated dual-pore scaffolds could support high cell density , and at the same time, provide uniform cell distribution throughout the scaffold. Higher cell proliferation and viability have been achieved attributed to efficient nutrient/oxygen transport through the structured pores.

2) New materials were explored, either as fabrication material to construct 3D scaffold or as coating material to form network inside the 3D scaffold.

Silk was investigated as an alternative to conventional materials for scaffold fabrication. Natural silks possess excellent tunable mechanical and elastic properties, and moreover, they exhibit characteristics that are interesting for medical applications such as the induction of no or very low immune response, low bacterial adherence and inherent biodegradability. We have demonstrated the fabrication of dual-pore silk scaffolds by modifying the previously developed 3D printing techniques with freeze-drying process. Similarly we have also shown that decellularized liver ECM (L-ECM) can serve as better ECM surface for hiPSC derived functional human hepatocytes compared to commercial ECM.In addition to scaffold fabrication, different combinations of materials have been produced and tested to form hydrogel-based nanostructured IPNs inside the 3D scaffolds. The hydrogels would make it possible to deliver drugs that can specifically activate gene expression from cells in the interior of the 3D scaffolds. The combination of silicone and a PEGylated acrylate, poly(ethylene glycol) methacrylate (pHEMA-PEGMEA)) has shown tunable physicochemical and drug releasing properties. We have proved that the IPN materials were able to release small molecule which could potentially induce biological response in the cells.

3) The fabricated 3D scaffolds were integrated in the BAL support systems and hepatocytes were successfully cultured in the porous scaffold.

BAL support systems under perfusion control were developed by incorporating pumps, sample reservoirs, bioreactors, 3D scaffolds and different types of sensors. Using the BAL support system, impedance monitoring of cell growth in the porous 3D scaffolds over a 19-day period was performed. The systems were successfully tested for their ability for long-term growth and differentiation of hiPCS-derived DE cells into functional 3D BALs. Moreover, it reveals that these hiPSC-derived hepatocytes, cultured on the developed 3D scaffolds under perfusion into a BAL, show as yet unrivalled functionality, with excellent comparability of liver functions with fresh liver tissue.

Perspectives

1) Fabrication techniques.

Even though the described fabrication techniques are rapid, inexpensive, compatible with different polymers and allow scaling up, the major challenges we currently face

include: (1) developing scaffolds with biomimetic microvascular networks and desired mechanical stiffness similar to biological organs/tissues, (2) using biodegradable and bioactive functional materials for long-term maintenance of mature hepatocyte's morphology and functionality, (3) advanced approaches for forming three-dimensional fully functional tissues and/or organs by controlling vascularization process. The ability to create biomimetic microvascular networks in three-dimensional designs should be the ultimate goal which would undoubtedly have in tissue engineering applications. To date, few fabrication methods exist that are capable of emulating hierarchical and branching channel designs, especially in 3D. Fabrication techniques of potential interest including direct-ink writing, soft lithography, direct-laser ablation, stereo-lithography, 2-photon polymerization, bioprinting, and electrostatic discharge have to be integrated together to achieve the scaffolds with biomimetic microvascular networks. One of the recombination as described in chapter 7 is to resemble the structural morphology liver hexagonal lobule ECM using plate like arrangement. The blood flows through small blood vessel such as hepatic artery to the central vain with diameter of 70 μm. In liver lobule, hepatocytes are always attached on a 2D planer ECM structure arranged in 3D. To design such kind of channel morphology, directional freezing silk scaffold technique can be used to achieve the anatomical morphology and dimension close to liver lobule. Such lamellar structure may be created inside a 3D printed hexagonal PVA mould with lamellar local pores for hepatocyte attachment and structured global pores generated from PVA for nutrient/oxygen transport in the bulk scaffold. Next goal would be to fabricate biodegradable composite polymer scaffolds from the mixture of L-ECM and silk protein for generating bioartifical liver tissue by growing stem cell derived functional human hepatocytes. In future combination of biomimetic/bio-inspired scaffold design and materials derived from nature can create the functional tissue for in-vivo application.

2) IPN for drug release

Even though we have shown that the IPN materials can release small molecule, the loading and release of large biological molecules such as proteins and growth factors has to be tested to determine the real potential of developed IPN scaffolds.

3) Cell culture in the BAL system

As the ultimate goal of the BAL technology is to bring the technology to the clinics to save patient's lives, there are various factors that have to be considered and evaluated in future as described below.

i. Scaffold design, which will influence the flow profile through the tissue and thereby the applied shear stress and optimized nutrient supply with the differentiation signalling factors.

ii. The optimal flow rate, which is a balance between shear forces on the cells and to ensure sufficient supply of oxygen and nutrients as well as removal of cellular waste products.

iii. Long term non-invasive online monitoring of viability and metabolic activity of the BAL system.

9. Patent Application A. METHOD OF MANUFACTURING A POROUS POLYMER COMPONENT INVOLVING USE OF A DISSOLVABLE, SACRIFICIAL MATERIAL

Authors: **Soumyaranjan Mohanty**, Jenny Emnéus, Anders Wolff, Martin Dufva, Haseena Bashir Muhammad, Maciej Skolimowski, Letizia Amato.

Filed on: 19 Jul 2013.

Published on: 21 Jan 2015.

Publication number: EP2826814 A1

9.1 ABSTRACT

The present invention relates to a method of manufacturing a porous polymer component 1 with structured and/or random pores 4 and/or channels 5. The method comprises arranging a dissolvable, sacrificial material 2 in a geometrical arrangement corresponding to an inner structure to be obtained in the polymer component 1. A component material 3, which is to form the final component 1, is arranged so that it surrounds at least a majority of the sacrificial material 2, and subsequently the sacrificial material 2 is dissolved and removed from the component material 3. The sacrificial material 2 and thereby the resulting inner structure of the component 1 is arranged in a controlled and reproducible manner. The sacrificial material 2 and possibly also the component material 3 may e.g. be arranged by use of a 3D-printer or manually. The method may e.g. be used to manufacture a three-dimensional scaffold for tissue engineering.

9.2 FIELD OF THE INVENTION

The present invention relates to the manufacturing of a porous polymer component, and in particular to methods involving arrangement of a sacrificial material which is subsequently dissolved and removed from a component material in order to form the cavities in the inner structure of the component.

9.3 BACKGROUND OF THE INVENTION

Porous polymers are used for a very large number of applications for years including as different ones as: core materials in lightweight engineering structures, thermal insulation, packaging and various products for personal care. The microstructure of the porous polymers is typically random, and the main purpose of the material typically relates to the "build-in" air bubbles being formed as part of the manufacturing process. However, for some applications it would be desirable to be able to control the microstructure of the polymer, e.g. to ensure that a fluid can pass through the material in a controllable manner.

In the field of tissue engineering, there is a requirement for porous material scaffolds that can be used to integrate biological cells or molecules to regenerate tissues. Such scaffolds support the spatial distribution of cells in a three dimensional structure, provide mechanical stability to the cells and should enable optimum nutrient transport. The desired scaffold would be highly porous and have interconnected pores. Thus, there is a need for reproducible and fabricatable scaffolds with controlled porosity.

Attempts have been made to make a porous polymer material by use of a sacrificial material constituting what are to become cavities in the final product when the sacrificial material is removed after moulding a polymer around it. US 6,900,055 discloses a method of manufacturing a porous silicone rubber for growing cells or living tissue. A silicone rubber precursor is contacted with biologically acceptable sacrificial filler; this filler is described as a ground inorganic salt. The inner structure of the porous polymer thus reproduces the structure of the filler and can only be selected by choosing the best available sacrificial filler material for a given application.

Hence, an improved method of manufacturing a porous polymer component would be advantageous.

9.4 OBJECT OF THE INVENTION

It is an object of the present invention to provide a method of manufacturing a porous polymer component with which it is possible to obtain a controlled and reproducible inner structure of the component. This may include a manufacturing which results in an inner structure that varies through the thickness of the component in a controlled manner.

It is another object of the present invention to provide a method of manufacturing a porous polymer component which removes the need for cleanroom facilities necessary for many known methods.

It is another object of the present invention to provide a method of manufacturing a porous polymer component with which it is easy to scale the dimensions of both the outer geometry of the component and the inner pores or channels to a desired size for a given application.

It is an object of at least some embodiments of the present invention to provide a method of manufacturing a porous polymer component having a structured inner structure through the thickness of the component.

It is another object at least some embodiments of the present invention to provide a method of manufacturing a porous polymer component which are more simple and efficient than known methods and which may therefore be advantageous especially for components to be produced fast or in low numbers.

It is a further object of the present invention to provide an alternative to the prior art.

9.5 SUMMARY OF THE INVENTION

The above described object and several other objects are intended to be obtained in a first aspect of the invention by providing a method of manufacturing a porous polymer component with structured and/or random pores and/or channels, the method comprising the steps of:
arranging a dissolvable, sacrificial material in a geometrical arrangement corresponding to an inner structure to be obtained in the polymer component,
arranging a component material so that it surrounds at least a majority of the sacrificial material, and
dissolving and removing the sacrificial material from the component material,
wherein the step of arranging the sacrificial material and thereby the resulting inner structure of the component is done in a controlled and reproducible manner.

By “porous component” is preferably meant that the component has a lot of very small holes in it so that a fluid, such as air or water, can pass through it.

By “pores” is preferably meant small openings or holes in a solid substance.

By “channel” is preferably meant a passageway along which something, in the present application typically a fluid, may pass or interconnected pores making such passage possible.

By “structured” is preferably meant that the pores or channels are arranged in an orderly and definable manner with respect to physical characteristics, such as dimensions or orientations.

By “random” is preferably meant that some characterising parameters relating to the geometrical arrangement in the inner structure, typically including the spatial orientation of the cavities, is not controllable. The inner structure of the component is still controlled in the sense that at least one parameter has been controlled to an extent so that it can be reproduced in a controlled manner. Such a parameter may e.g. be an average diameter of the pores or channels.
By “controlled” is preferably meant that at least some of the parameters which can be used to describe the porous structure are controllable and thereby also reproducible.

Such parameters can e.g. be the volume fraction of solid material, an average size of the pores, or an average orientation of channels.

In some embodiments of the invention, the above-mentioned steps take place one at a time and in the order in which they are mentioned. In other embodiments some of the steps happen concurrently as will be explained below.

The method may further comprise the step of curing the component material before the sacrificial material is removed. This will be the case for materials which need curing before being in their final form and ready for handling. This will be explained in further details below. The sacrificial material may also be cured.

In some embodiments of the invention, the inner structure of the component is controlled to be random substantially throughout the component. Careful design of a random structure can be used to increase the surface-to-volume-ratio which will be advantageous for some applications of the invention. It is e.g. considered to be advantageous for applications within environmental engineering, such as for spongy material used to soak-up oil spill, or other applications exploiting the effect of surface tension.

The inner structure of the component may alternatively or in combination therewith be controlled to have a predefined geometrical configuration with orderly arranged pores and/or channels.

An example of an advantage of having both random and structured regions in a component is that in order to maximise mass transport in e.g. tissue engineering scaffolds, bigger channels enable rapid transport of fluid or nutrients while the smaller pores provide a larger functional surface area e.g. for cell growth, catalytic reactions, and adsorption or absorption or release of components over time. To summarise, having pores in combination with larger channels would enable access to a larger volume of the component.

An advantage of the possibility of controlling the sacrificial material so that structured channels are obtained is that it is possible to make the channels continue towards the centre of the component. This can e.g. be used in tissue engineering to make sure that

also cells located at the centre are supplied with oxygen. The channels do not necessarily have the same size throughout the thickness of the component, but may resemble the decrease in size down to capillary in natural organs.

The inner structure of the component may be so that it comprises pores and/or channels of predefined dimensions through the thickness of the component.

The pores and/or channels may be of varying dimensions through the thickness of the component. The dimensions may e.g. vary from an outer surface of the component towards an inner region. Such a structure may e.g. find use within tissue engineering for the manufacturing of artificial organs. A graded structure in the form of a decreasing diameter of the channels towards the middle of the component can resemble the veins, arteries and/or blood vessels in a natural organ and be used to ensure that oxygen can be transported to and from a central region. It will also be possible to have one substantially constant value of a characteristic parameter, such as the average diameter, at some regions, such as near the surface, and another substantially constant value of the characteristic parameter at other regions, such as at the middle of the component.

In some embodiments of the invention the sacrificial material may be arranged by use of 3D-printing. 3D-printing is at present a quickly developing technology which can be used to precisely manufacture highly specialized structures. The obtainable dimensions and precision will depend on the 3D-printing technology used. At present it is in the order of micrometres and upwards. Hereby complex geometries of what are to become the network of porous and channels can be made in an easily controllable manner. In principle any printable and dissolvable material can be used; some examples will be mentioned below. The choice will depend both on the application of the final component and on the manufacturing method used.

By use of 3D-printing it is possible to make components in a wide range of dimensions. This technology is highly advantageous over the presently used methods as it is rapid and flexible with respect to both sizes and materials used. A further advantage is that the process can easily be automated.

In some embodiments of the invention, the sacrificial material and the component material are arranged concurrently by a use of 3D-printing. Hereby complex geometries can be built including some where part of the material for the final component needs to be supported by the sacrificial material during manufacturing until it is in a stable and self-supporting form.

In the embodiments of the invention including the use of 3D-printing, fused deposition technology may be used.

In the method as described above, two or more sacrificial materials may be arranged at different regions of the component being manufactured, the two or more sacrificial materials being dissolvable by use of different solvents, the method further comprising the step of sequentially dissolving and removing the two or more sacrificial materials from the component material. Hereby it will be possible to form more complex inner structures or outer geometries of the component.

The method may further comprise a subsequent step of pyrolyzing the component provided that a material which can be pyrolyzed is used. Examples of materials with which this step is possible are polymers such as polydimethyl siloxane (PDMS), polystyrene, block copolymers and different photo-curable carbon containing polymers. The pyrolyzed scaffold is a hard material which is suitable as a scaffold material for tissue engineering tissues, such as bone.

The component may be pyrolyzed so that an electrically conductive component is obtained. Such a component may e.g. be used for scaffolds for tissue engineering so that the conductivity allows the monitoring of cell growth and the potential for stimulating cells by electrical methods. Parameters that are relevant to control during the pyrolysis process are the temperature ramping speed, maximum temperature, time and combination of gases.

For some applications of the invention, an alternative to using 3D-printing for the manufacturing will be a method in which the sacrificial material is arranged manually with respect to a template adapted to assist in holding the filaments in a desired arrangement during manufacturing of the component. Such a manual arrangement of the sacrificial material may e.g. be winding of one or more filaments around the template.

The filaments may e.g. be made by 3D-printing or by extrusion. This method can e.g. be used for the manufacturing of microfluidic lab-on–a-chip as will be shown in relation to the figures. With this method it is possible to make any type of geometrical features, such as channels with a circular cross section, which are difficult to make with other methods, including 3D-printing. The cross sectional dimensions of such filaments are typically in the micrometre range and upwards.

The sacrificial material may be made from any polymer which is dissolvable in water or another suitable solvent which does not damage the component material. It may e.g. be made from poly(vinyl alcohol), PVA, which is soluble in water or from wax. Other examples are acrylonitrile butadiene styrene (ABS) which is soluble in acetone and polylactic acid or polylactide (PLA). In the embodiments involving 3D-printing, the material chosen should be printable with the actual printer being used.

The component material may be selected from the following group: collagen, gelatine, polyhema, SU8, polystyrene, or silicone elastomers, such as polydimethylsiloxane (PDMS). SU8 is a commonly used epoxy-based negative photoresist which is found suitable for the present invention. It is in principle possible to use any artificial or natural polymers provided that they are applicable for the precise manufacturing method used. Some of the embodiments of the invention relate to polymers which can be cured, e.g. under the influence of light, to form a cross-linked material. Other embodiments relate to thermoplastic polymers which are heated to become liquid before being moulded around the sacrificial material and then cooled to solidify, preferably before the sacrificial material is removed. Gelatine is an example of a polymer which can be used both with and without the crosslink-forming curing step. The choice of component is highly dependent on the application of the component being manufactured. E.g. it is important for some applications that the component material is biocompatible, whereas for other applications it is necessary to use a material which can be pyrolyzed.

In a second aspect the invention relates to a polymer component obtained by a method as described above. Such a component may find use in a number of applications as will be described in further details below.

In a third aspect the invention relates to the use of a component manufactured as described above as a three-dimensional scaffold for tissue engineering. An example of such a use relates to the ability to fabricate a 3D tissue engineering scaffold including domains (the porous regions) for culturing effector cells such as hepatocytes and providing artificial veins, arteries and/or blood vessels (structured part) feeding these domains.

In a fourth aspect the invention relates to the use of a component manufactured as described above as a medical device. Such medical devics could e.g. be artificial organs and tissues as well as lab-on-a-chip systems. This fourth aspect of the invention also relates to a medical device comprising a polymer component as described above or to a component manufactured as described above for use as a medical device.

A fifth aspect of the invention is the application of these structures for cultivating a high cell density. This can be used for expanding different cell types or production of e.g. recombinant proteins.

The first, second, third, fourth and fifth aspect of the present invention may each be combined with any of the other aspects. These and other aspects of the invention will be apparent from and elucidated with reference to the embodiments described hereinafter.

BRIEF DESCRIPTION OF THE FIGURES

The method according to the invention will now be described in more detail with regard to the accompanying figures. The figures show one way of implementing the present invention and is not to be construed as being limiting to other possible embodiments falling within the scope of the attached claim set.

Figure 1 shows schematically the overall steps in an embodiment of the invention used to manufacture a component with a substantially uniform inner structure throughout the component.

Figure 2 shows schematically examples of structures with pores and channels, respectively.

Figure 3 shows schematically the differences between structured and random inner structures in a component.

Figure 4 shows schematically the steps in a manufacturing method including a step of pyrolyzing the polymer component.

Figure 5 shows SEM images of a pyrolyzed component.

Figure 6 shows schematically an embodiment of the invention in which the sacrificial material is arranged manually.

DETAILED DESCRIPTION OF AN EMBODIMENT

Figure 1 shows schematically the overall steps in an embodiment of the invention used to manufacture a porous polymer component 1 with a substantially uniform inner structure throughout the component 1. In this embodiment, the inner structure of the component 1 is controlled to have a predefined geometrical configuration with orderly arranged channels. Figure 1.a shows the dissolvable, sacrificial material 2 arranged in a geometrical arrangement corresponding to an inner structure to be obtained in the polymer component 1. The upper part of figure 1.a is a three-dimensional view, and the lower part if figure 1.a is a cross sectional view. Figure 1.b shows the component material 3 which has been arranged so that it surrounds a majority of the sacrificial material 2. Figure 1.c shows the final polymer component 1 after the sacrificial material 2 has been dissolved and removed from the component material 3. An important part of the process is that the arrangement of the sacrificial material 2 and thereby the resulting inner structure of the cavities, including the pores and/or channels, in the component 1 is done in a controlled and reproducible manner. How this can be done will be explained in further details below. Depending on the actual polymer material used, the method may further comprise the step of curing the component material 3 before the sacrificial material 2 is removed. This will e.g. be necessary in the case of polydimethyl siloxane (PDMS) as a component material 3. In the case of 3D-printing two or more different polymers such as PLA and ABS, the curing occurs in the same moment as the polymers are printed.

Figure 2 shows schematically examples of structures with pores 4 and channels 5, respectively. The geometries and relative sizes of the pores 4 and channels 5 in figure 2 are examples and given for illustrative purposes only. In a real component 1, e.g. the walls of the channels 5 may be rough, and the overall path of the channels 5 need not be along a straight line. The structure of the component 1 may be so that it comprises pores 4 and/or channels 5 of predefined dimensions through the thickness of the component 1. The channels 5 may also be of varying dimensions through the thickness of a component 1, such as from an outer surface of the component 1 towards an inner region of the component 1.

Figure 3 shows schematically the differences between structured (shown to the left) and random (shown to the right) inner structures in a component 1. It will also be possible to

have regions with different structures in the component, such as structured regions with different cross sectional dimensions of the channels 5 or with different volume fractions of solid material. It will also be possible to have both random and structured regions in one component.

At least for some geometries and/or combinations of materials it will be advantageous to 3D-print both the sacrificial material 2 and the component material 3 concurrently. Hereby the pores 4 or channels 5 in the geometrical arrangement of the sacrificial material 2 are filled with the component material 3 while the component 1 is being formed. A typically used 3D-printing method is fused deposition technology.

A method as described above may further comprise a subsequent step of pyrolyzing the component 1. This method step can e.g. be used to obtain an electrically conductive component which may e.g. find use in tissue engineering and sensing applications. Figure 4 shows schematically the steps in a process as described above including the step of pyrolyzing the component. 1: A sacrificial material 2 is provided e.g. by 3D-printing. 2: The sacrificial material 2 is placed in a container 6 with component material 3. 3: Vacuum is applied, e.g. in a vacuum chamber 7, to ensure that the component material 3 infiltrates the sacrificial material 2. 4: The component material 3 is then cured in an oven 8 at raised temperature for a predetermined time period. 5: The sacrificial material 2 is dissolved by placing the cured intermediate component in a solvent 9 for a predetermined time period or until the sacrificial material 2 has been dissolved and can be removed e.g. by washing (not shown). 6: The component 1 now being constituted by component material 3 can further be pyrolized to obtain the pyrolized final component 1 shown as number 7. Figure 5 shows SEM images of an example of such a pyrolized component at two different magnifications.

An alternative to 3D-printing which will be possible for some application is to arrange the sacrificial material 2 manually. Such a method can e.g. be used to manufacture a microfluidic device without the need for cleanroom fabrication technologies. Another advantage over some known methods is the possibility to form completely cylindrical channels 5, e.g. from arrangement of filaments having a circular cross section. An example of a method wherein the sacrificial material 2 is arranged manually is shown schematically in figure 6. Figure 6.a shows a frame 10, also referred to as a template, which can e.g. be made by laser ablation of a 1 mm thick PC sheet. As shown in figure 6.b, filaments of sacrificial material 2 are arranged around the template 10, and the grooves 11 along the edges of the template 10 assist in holding the filaments 2 in a

desired arrangement during manufacturing of the component 1. Such filaments 2 can e.g. be 400 µm thick PVA filaments pre-made e.g. by extrusion or by 3D-printing. A cast and partially cured layer 12 of e.g. PDMA is arranged in a mould 13 as shown in figure 6.c, and the frame 10 with the filaments 2 are placed on top thereof as shown in figure 6.d. An upper layer of PDMS (not visible in the figure) in then is cast on top thereof as shown in figure 6.e, and the whole arrangement is cured, typically by application of heat or light depending of the type of material used. In this embodiment the component material 3 is constituted by the two layers 12 of PDMS and the template 10 which becomes cast into the component 1. After curing of the component material 3, it is removed from the mould 13, and the sacrificial filament material 2 is dissolved e.g. by placing the component 1 in hot water (not shown). The component may also be cut to a final shape as shown in figure 6.f.

Although the present invention has been described in connection with the specified embodiments, it should not be construed as being in any way limited to the presented examples. The scope of the present invention is set out by the accompanying claim set. In the context of the claims, the terms "comprising" or "comprises" do not exclude other possible elements or steps. Also, the mentioning of references such as "a" or "an" etc. should not be construed as excluding a plurality. The use of reference signs in the claims with respect to elements indicated in the figures shall also not be construed as limiting the scope of the invention. Furthermore, individual features mentioned in different claims, may possibly be advantageously combined, and the mentioning of these features in different claims does not exclude that a combination of features is not possible and advantageous.

9.6 OUR CLAIMS

1. Method of manufacturing a porous polymer component (1) with structured and/or random pores (4) and/or channels (5), the method comprising the steps of:

arranging a dissolvable, sacrificial material (2) in a geometrical arrangement corresponding to an inner structure to be obtained in the polymer component (1),

arranging a component material (3) so that it surrounds at least a majority of the sacrificial material (2), and

dissolving and removing the sacrificial material (2) from the component material (3),

wherein the step of arranging the sacrificial material (2) and thereby the resulting inner structure of the component (1) is done in a controlled and reproducible manner.

2. Method according to claim 1, further comprising the step of curing the component material (3) before the sacrificial material (2) is removed.

3. Method according to claim 1 or 2, wherein the inner structure of the component (1) is controlled to be random.

4. Method according to claim 1 or 2, wherein the inner structure of the component (1) is controlled to have a predefined geometrical configuration with orderly arranged pores (4) and/or channels (5).

5. Method according to claim 4, wherein the inner structure of the component (1) is so that it comprises pores (4) and/or channels (5) of predefined dimensions through the thickness of the component (1).

6. Method according to claim 5, wherein the pores (4) and/or channels (5) are of varying dimensions through the thickness of the component (1).

7. Method according to any of the preceding claims, wherein the sacrificial material (2) is arranged by use of 3D-printing.

8. Method according to claim 7, wherein both the sacrificial material (2) and the component material (3) are arranged concurrently by a use of 3D-printing.

9. Method according to claim 7 or 8, wherein fused deposition technology is used.

10. Method according to any of the preceding claims, wherein two or more sacrificial materials (2) arranged at different regions of the component (1) being manufactured, the two or more sacrificial materials (2) being dissolvable by use of different solvents (9), the method further comprising the step of sequentially dissolving and removing the two or more sacrificial materials (2) from the component material (3).

11. Method according to any of the preceding claims, further comprising a subsequent step of pyrolyzing the component (1).

12. Method according to claim 11, wherein the component (1) is pyrolyzed so that an electrically conductive component is obtained.

13. Method according to claim 1, wherein the sacrificial material (2) is arranged manually with respect to a template (10) adapted to assist in holding the sacrificial material (2) in the form of filaments in a desired arrangement during manufacturing of the component (1).

14. Use of a component (1) manufactured according to any of the preceding claims as a three-dimensional scaffold for tissue engineering.

15. Use of a component (1) manufactured according to any of claims 1 to 13 as a medical device.

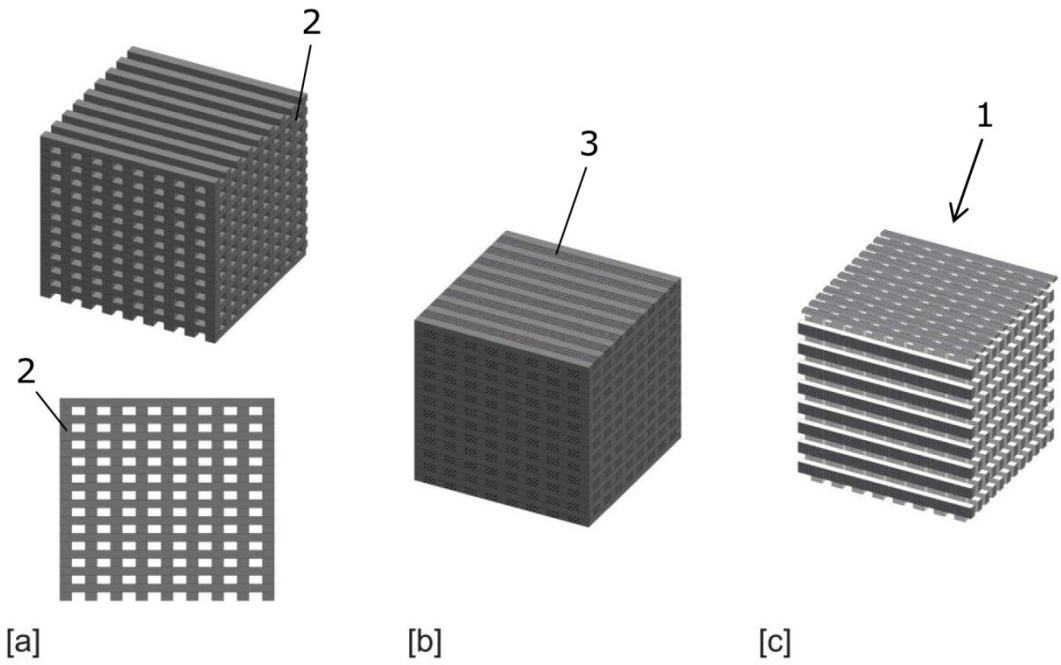

Fig 1

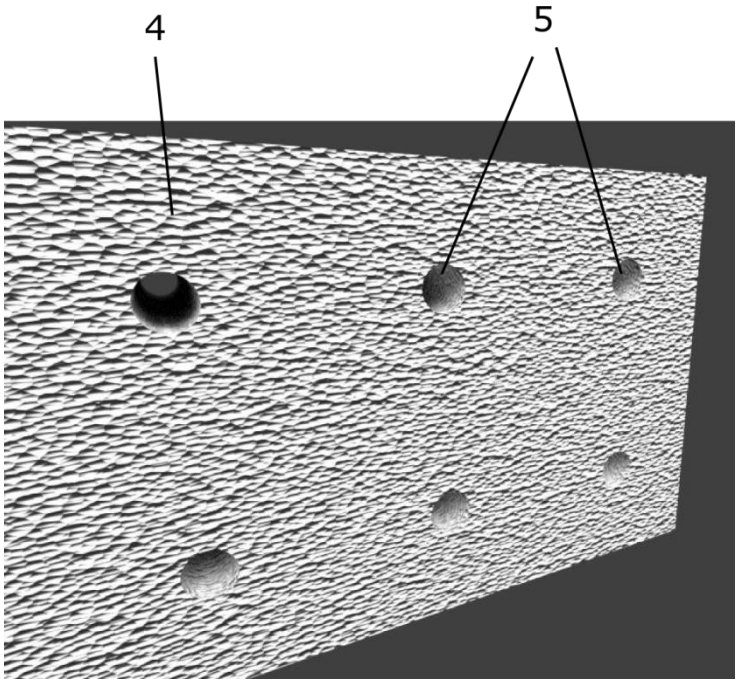

Fig 2

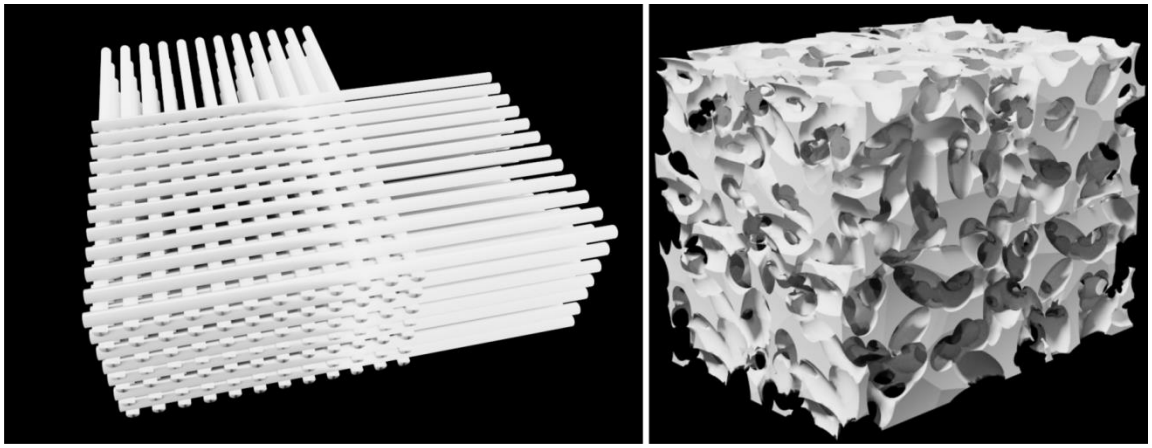

Fig. 3

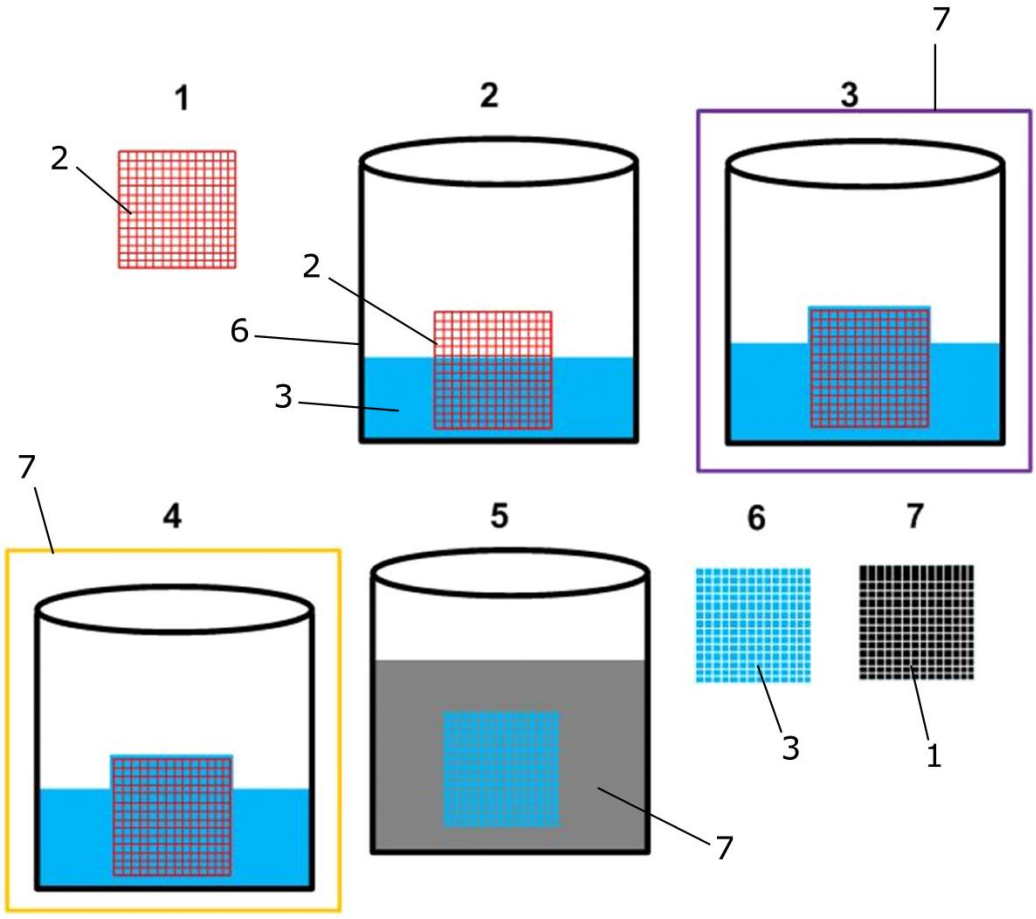

Fig 4

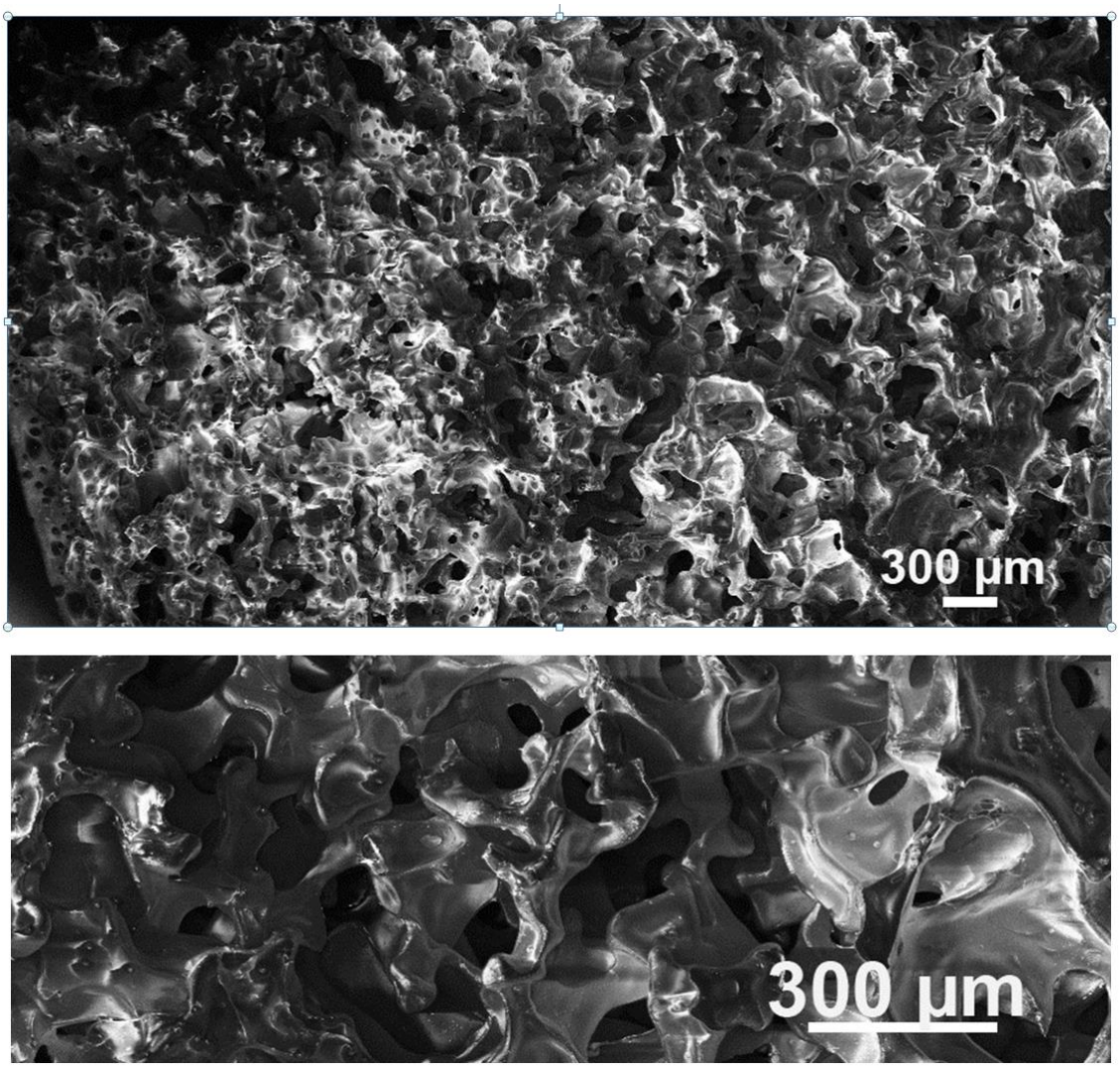

Fig 5

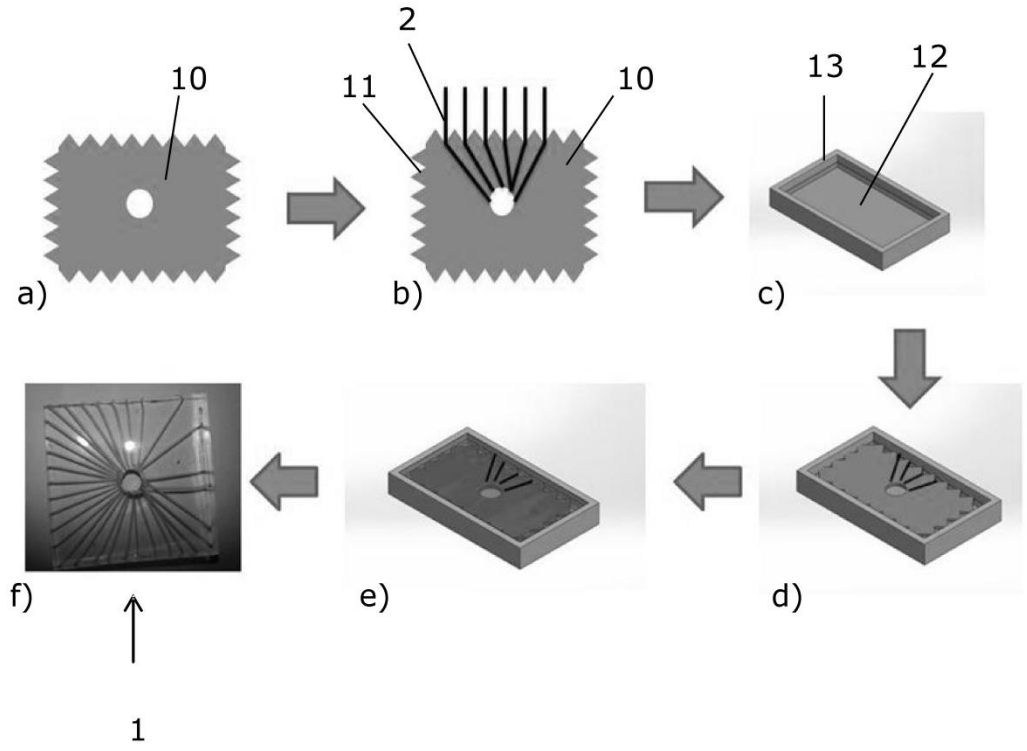

Fig 6

10. Patent Application B: A METHOD FOR FABRICATING A THREE-DIMENSIONAL CARBON STRUCTURE.

Authors: **Soumyaranjan Mohanty**, Jenny Emnéus, Anders Wolff, Arto Heiskanen.

Filed on: 28 August 2015.
Application number/Patent number: 15182928.0 - 1355

10.1 Abstract

A method for fabricating a three-dimensional carbon structure (4) is disclosed. A mould (1) defining a three-dimensional shape is provided, and natural protein containing fibres are packed in the mould (1) at a predetermined density. The packed natural protein containing fibre structure (3) is removed from the mould (1), and undergoes pyrolysis. Thereby a three-dimensional porous and electrically conducting carbon structure (4) having a three-dimensional shape defined by the three-dimensional shape of the mould (1) and a porosity defined by the density of the packed natural protein containing fibre structure (3) is obtained. The carbon structure (4) is well suited for use as a scaffold for tissue engineering, or for material for batteries, fuel cells, supercapacitors, sorbents for separation processes, gas storage, supports for many important catalysts, etc.

10.2 Field of the invention

The present invention relates to a method for fabricating a three-dimensional carbon structure, e.g. for use as a scaffold for tissue engineering, as electrode materials for batteries, fuel cells and supercapacitors, as sorbents for separation processes and gas storage, as supporters for many important catalysts, etc. When applying the method of the invention the micro-porosity of the resulting three-dimensional carbon structure can be controlled, and any desired three-dimensional shape of the structure can be obtained. Furthermore, the carbon fibres of the three-dimensional carbon structure fabricated by means of the method of the invention contain nitrogen, thereby making the structure suitable for a wide range of applications.

10.3 Background of the invention

For some purposes, such as tissue engineering, electrode materials for batteries, fuel cells and supercapacitors, sorbents for separation processes and gas storage, supports for many important catalysts, etc., there is a need for conductive porous scaffolds, made from a biocompatible material. It is, furthermore, desirable to be able to provide such scaffolds in various sizes and shapes, and with a scalable porosity. Finally, it is desirable to be able to provide such scaffolds in an easy and cost effective manner.

US 2008/0085648 A1 discloses a method of producing an electric conductive material by spirally winding a yarn composed of organic fibres on a core member. The core member is removed, and the yarn is carbonized.

US 2012/0125071 A1 discloses carbon moulds for use in the fabrication of bulk metallic glass parts and moulds. A master shape is patterned into a pyrolyzable material, and the master shape is pyrolyzed into a carbon mould.

10.4 Description of the invention

It is an object of embodiments of the invention to provide a method for fabricating a three-dimensional carbon structure in an easy and cost effective manner.

It is a further object of embodiments of the invention to provide a method for fabricating a three-dimensional carbon structure in which the porosity of the structure can be controlled.

The invention provides a method for fabricating a three-dimensional carbon structure, the method comprising the steps of: providing a mould defining a three-dimensional

shape, packing natural protein containing fibres in the mould at a predetermined density, thereby obtaining a packed natural protein containing fibre structure, removing the packed natural protein containing fibre structure from the mould, performing pyrolysis on the packed natural protein containing fibre structure, thereby obtaining a three-dimensional porous and electrically conducting carbon structure having a three-dimensional shape defined by the three-dimensional shape of the mould and a porosity defined by the density of the packed natural protein containing fibre structure.

In the present context the term 'three-dimensional carbon structure' should be interpreted to mean a structure which has a three-dimensional shape, and which contains carbon material.

According to the method of the invention, a mould defining a three-dimensional shape is initially provided. The three-dimensional shape of the mould corresponds to a desired three-dimensional shape of the carbon structure, which is fabricated by means of the method. Thus, any desired shape or size of the resulting three-dimensional carbon structure can be obtained, simply by providing an appropriate mould, defining a corresponding three-dimensional shape.

Next, natural protein containing fibres are packed into the mould at a predetermined density. Thereby a structure is obtained, which comprises or consist of packed natural protein containing fibres, i.e. a packed natural protein containing fibre structure. Since the packed natural protein containing fibre structure has been obtained by packing protein containing fibres into the mould, the packed natural protein containing fibre structure has a size and a shape which corresponds to the size and shape of the mould. Furthermore, the density of the packed natural fibre containing structure can be controlled by controlling the packing process to obtain a predetermined density.

Then the packed natural protein containing fibre structure is removed from the mould. The removed structure maintains its size, shape and density, but is no longer contained in the mould, and is therefore ready for further processing.

Finally, pyrolysis is performed on the packed natural protein containing fibre structure. Since the structure comprises protein containing fibres, the structure also comprises carbon. Accordingly, as a result of the pyrolysis, a porous and electrically conducting carbon structure is obtained. Furthermore, since the carbon structure is formed by performing pyrolysis on the packed natural protein containing fibre structure, the carbon structure has a three-dimensional shape which corresponds to the three-dimensional

shape of the packed natural protein containing fibre structure, and thereby to the three-dimensional shape defined by the mould. Furthermore, the pyrolysis process results in nitrogen containing carbon fibres being generated, since the pyrolysis process produces nitrogen doped carbon. This is an advantage, because this has turned out to be important for catalysing hydrogen evolution and for cell adhesion for, e.g., tissue engineering and microbial biofilm formation.

Furthermore, the porosity of the carbon structure is defined by the density of the packed natural protein containing fibre structure. Since the density of the packed natural protein containing fibre structure is controlled during the packing process, as described above, a desired porosity of the resulting porous and electrically conducting carbon structure can be obtained by carefully selecting a predetermined density of the packed natural protein containing fibres, and controlling the packing process to obtain the predetermined density. Furthermore, the surface area of the resulting carbon structure depends on the porosity of the structure. Accordingly, the surface area of the resulting carbon structure is controllable and scalable, and, for instance, a structure with a very high surface area can be obtained.

Thus, the method according to the invention results in the fabrication of a three-dimensional porous and electrically conducting carbon structure, having a desired and appropriate three-dimensional shape, and having a desired and appropriate porosity. The three-dimensional shape and the porosity of the carbon structure can be designed to meet any specific requirement, simply by designing the mould in an appropriate manner, and by controlling the packing process in an appropriate manner. Accordingly, the method of the invention provides an easy and cost effective manner of fabricating a three-dimensional carbon structure having a desired three-dimensional shape and porosity. This makes the resulting carbon structure suitable for use as a porous carbon scaffold for tissue engineering, or as a porous carbon material for batteries, fuel cells, supercapacitors, sorbents for separation processes or gas storage, supports for many important catalysts, etc.

The natural protein containing fibres may be silk fibres, and the method may further comprise the step of extracting the silk fibres from raw silk cocoons. Raw silk cocoons are readily available at reasonable costs. Therefore this embodiment provides suitable natural protein containing fibres in an easy and cost effective manner. Furthermore, pyrolysed single silk fibres have nanoporous structure, which increases the surfaced area of the bulk material. Thus, the method according to this embodiment of the inven-

tion makes it possible to control the macroporosity of structures composed of multiple pyrolysed silk fibres.

As an alternative, the natural protein containing fibres may be of any other suitable kind, including, but not limited to, spider silk, fibrin and sicrine.

The step of packing natural protein containing fibres may further comprise packing the natural protein containing fibres in the mould in a predetermined pattern, and the porosity of the three-dimensional porous, electrically conducting carbon structure may further be defined by the pattern of the packed natural protein containing fibre structure.

According to this embodiment, porosity of the resulting three-dimensional porous, electrically conducting carbon structure depends on the density as well as on the pattern, with which the natural protein containing fibres are packed.

According to this embodiment, a three-dimensional, conductive structure, with a high surface area and with macro-, micro- and nanoporosity is provided. Furthermore, clean room facilities are not required in order to perform the method, thereby providing a very cost effective process. Finally, the use of protein containing fibres inherently provides the possibility of tuning the nitrogen content of the resulting carbon structure.

The method may further comprise the step of using the three-dimensional porous, electrically conducting carbon structure as a scaffold for tissue engineering. As an alternative, the three-dimensional porous, electrically conducting carbon structure may be used for other purposes, such as for electrode materials for batteries, fuel cells and supercapacitors, sorbents for separation processes and gas storage, supports for many important catalysts, etc.

Since the three-dimensional carbon structure resulting from the method of the invention is produced on the basis of natural protein containing fibres, it is biocompatible. This makes the three-dimensional carbon structure suitable for use for tissue engineering purposes. Furthermore, since the three-dimensional structure is a carbon structure, the structure is electrically conducting, making it further suitable for tissue engineering purposes, such as neuronal and cardiac tissue engineering purposes. Finally, the controllable size, shape and porosity of the three-dimensional structure allows the three-dimensional structure to be designed to exactly match a required application, such as to exactly match a part which it is desired to provide by means of tissue engineering, thereby making the three-dimensional structure even further suitable for tissue engineering purposes. In summary, according to this embodiment of the invention, a suitable scaffold for tissue engineering is provided in an easy and cost effective manner.

Using the structure for other purposes than tissue engineering, the method of the invention provides suitable porous carbon structures which can be produced in an easy and cost effective manner, e.g. for applications such as batteries, fuel cells, supercapacitors, sorbents for separation processes and gas storage, supports for catalysts, etc.

The method may further comprise the step of using the three-dimensional porous, electrically conducting carbon structure as an actuator and/or as a sensor during the tissue engineering. This is possible due to the electrical conductivity of the three-dimensional carbon structure. This is further relevant for applications within the field of microbial electrosynthesis or bioremediation.

According to this embodiment, the structure facilitates direct monitoring of cellular behaviour in the tissue engineering scaffold, using electrical sensing. Furthermore, the structure facilitates electrical stimulation of cells that can differentiate into different tissue specific lineages, e.g. neurons, cardiac cells and osteoblasts. Furthermore, the structure provides electrical stimulation of microbes to intensify biofilm formation in the porous carbon structure and production of chemicals. The conductive porous carbon can be directly used as electrode material in biofuel cells. Finally, the inherent nitrogen content additionally improves cell adhesion in microbial biofilm formation and tissue engineering.

The step of performing pyrolysis on the packed natural protein containing fibre structure may comprise positioning the packed natural carbon containing fibres in a furnace and reducing an oxygen level inside the furnace. This may, e.g., be obtained by supplying an inert gas, such as nitrogen, into the furnace.

The step of performing pyrolysis may comprise increasing the temperature inside the furnace to approximately 1000°C or above.

The step of packing natural protein containing fibres may comprise the steps of:

determining a desired weight of natural protein containing fibres to be contained in the resulting packed natural protein containing fibre structure,

providing an amount of natural protein containing fibres corresponding to said desired weight, and

packing the provided amount of natural protein containing fibres into the mould in such a manner that a volume defined by the mould is filled.

According to this embodiment, the density of the packed natural protein containing fibre structure, and thereby the porosity of the resulting three-dimensional porous and electri-

cally conducting carbon structure, is controlled by determining a desired weight of natural protein containing fibres to be arranged in the mould during the step of packing the natural protein containing fibres. Since the size and shape of the mould are known, the volume defined by the mould is also known, and thereby the total weight of the natural protein containing fibres being packed into the mould defines the density of the packed fibres. Accordingly, the desired weight of natural protein containing fibres is selected in such a way that the predetermined density is obtained.

Next, an amount of natural protein containing fibres is provided, which corresponds to the determined desired weight, and the provided amount of natural protein containing fibres is packed into the mould, in such a manner that the volume defined by the mould is exactly filled by the fibres. Thereby it is ensured that the natural protein containing fibres are packed with exactly the predetermined density.

Thus, according to this embodiment, the density of the packed natural protein containing fibres is controlled by controlling the total weight of the fibres being packed. This is very simple, and thereby it is easy to perform the method and obtain a desirable porosity of the resulting three-dimensional porous and electrically conducting carbon structure.

The step of packing the natural protein containing fibres may further comprise the step of wetting the natural protein containing fibres prior to packing the natural protein containing fibres into the mould. Wetting the natural protein containing fibres will squeeze the fibres together, thereby allowing the fibres to fit more easily into the mould. The step of wetting the fibres may, e.g., be performed using water. The amount of liquid used for wetting the fibres depends on the amount of fibres to be packed. According to this embodiment, the method may further comprise the step of drying the packed fibres before performing pyrolysis on the packed natural protein containing fibre structure, e.g. by means of air drying or freeze drying.

Alternatively or additionally, the method may further comprise the step of cutting the natural protein containing fibres before packing the fibres into the mould. The cutting may be performed using mechanical or chemical methods. According to this embodiment, the size of the natural protein containing fibres is controlled, and the smaller, cut fibres fit more easily into the mould.

The method may further comprise the step of suspending the natural protein containing fibres into solution, after cutting the fibres and before packing the fibres into the mould. The fibres solution may further be dried, e.g. by means of air drying or freeze drying, before performing the pyrolysis step.

10.5 Brief description of the drawings

The invention will now be described in further detail with reference to the accompanying drawings in which

Figs. 1-4 illustrate a method according to a first embodiment of the invention, and

Figs. 5-7 illustrate a method according to a second embodiment of the invention.

detailed description of the drawings

Figs. 1-4 illustrate a method according to a first embodiment of the invention. Fig. 1 is a perspective view of a mould 1 defining a volume 2 having a substantially cylindrical shape.

In Fig. 2 natural protein containing fibres, e.g. in the form of silk fibres, have been packed into the volume 2 of the mould 1. The fibres form a packed natural protein containing fibre structure 3. The fibres have been packed in such a manner that the packed natural protein containing fibre structure 3 has a predetermined and desired density. This may, e.g., be obtained by providing a weight amount of fibres which will result in the desired density when the weight amount of fibres exactly fills the volume 2 defined by the mould 1, and then packing these fibres into the volume 2 defined by the mould 1.

In Fig. 3 the packed natural protein containing fibre structure 3 has been removed from the mould 1. It can be seen that the packed natural protein containing fibre structure 3 maintains the size and shape defined by the mould 1, i.e. the structure 3 is cylindrical. Accordingly, the density of the packed natural protein containing fibre structure 3 is also maintained, even though the structure 3 is removed from the mould 1.

In Fig. 4 pyrolysis has been performed on the packed natural protein containing fibre structure 3, and thereby a three-dimensional porous and electrically conducting carbon structure 4 has been obtained. The carbon structure 4 has the same shape and size as the packed natural protein containing fibre structure 3, i.e. the size and shape of the carbon structure 4 is determined by the size and shape of the volume 2 defined by the mould 1. Furthermore, the porosity of the carbon structure 4 is defined by the density of the packed natural protein containing fibre structure 3.

Accordingly, performing the method illustrated in Figs. 1-4 results in a porous and electrically conducting carbon structure 4 with a porosity which can be adjusted by adjusting the density of the packed fibres. Furthermore, the carbon structure 4 can be given any desired size or shape, simply by providing a suitable mould 1 which defines a

volume 2 having the desired size and shape. Thus, an electrically conducting carbon structure 4 with a desired size, shape and porosity can be provided in a simple and cost effective manner. Such a carbon structure 4 is well suited for use as a carbon scaffold for tissue engineering, or for material for batteries, fuel cells, supercapacitors, sorbents for separation processes, gas storage, or supports for many important catalysts.

It should be noted that, even though the mould 1 used when performing the method illustrated in Figs. 1-4 has a simple cylindrical shape, the method described above could be performed using a mould 1 defining a volume 2 having any desired size or shape.

Figs. 5-7 illustrate a method according to a second embodiment of the invention. Fig. 5 shows a mould 1 having eight through-going rods 5 arranged therein. The mould 1 further defines a substantially box-shaped volume 2, which is traversed by the through-going rods 5.

In Fig. 6 natural protein containing fibres have been packed in the mould, thereby obtaining a packed natural protein containing fibre structure 3, essentially in the manner described above with reference to Figs. 1-4. Since the through-going rods 5 are arranged inside and extend through the volume 2 defined by the mould 1, the fibres are packed around the through-going rods 5. As a consequence, the through-going rods 5 are embedded in the resulting packed natural protein containing fibre structure 3.

Furthermore, in Fig. 6, the packed natural protein containing fibre structure 3 and the through-going rods 5 have been removed from the mould 1.

In Fig. 7 the through-going rods 5 have been removed from the packed natural protein containing fibre structure 3, thereby leaving eight through-going channels 6 in the packed natural protein containing fibre structure 3. This may, e.g., be obtained by removing the through-going rods 6 in a mechanical manner, or by dissolving the through-going rods 5.

Furthermore, in Fig. 7, pyrolysis has been performed on the packed natural protein containing fibre structure 3, and thereby a three-dimensional porous and electrically conducting carbon structure 4 has been obtained. As described above with reference to Figs. 1-4, the carbon structure 4 has a size and shape which is determined by the size and shape of the volume 2 defined by the mould 1, including the sizes, shapes and positions of the through-going rods 5, and a porosity which is defined by the density of the packed fibres.

10.6 Our Claims

1. A method for fabricating a three-dimensional carbon structure, the method comprising the steps of:

providing a mould defining a three-dimensional shape,

packing natural protein containing fibres in the mould at a predetermined density, thereby obtaining a packed natural protein containing fibre structure,

removing the packed natural protein containing fibre structure from the mould,

performing pyrolysis on the packed natural protein containing fibre structure, thereby obtaining a three-dimensional porous and electrically conducting carbon structure having a three-dimensional shape defined by the three-dimensional shape of the mould and a porosity defined by the density of the packed natural protein containing fibre structure.

2. A method according to claim 1, wherein the natural protein containing fibres are silk fibres, and wherein the method further comprises the step of extracting the silk fibres from raw silk cocoons.

3. A method according to claim 1 or 2, wherein the step of packing natural protein containing fibres further comprises packing the natural protein containing fibres in the mould in a predetermined pattern, and wherein the porosity of the three-dimensional porous, electrically conducting carbon structure is further defined by the pattern of the packed natural protein containing fibre structure.

4. A method according to any of the preceding claims, further comprising the step of using the three-dimensional porous, electrically conducting carbon structure as a scaffold for tissue engineering.

5. A method according to claim 4, further comprising the step of using the three-dimensional porous, electrically conducting carbon structure as an actuator and/or as a sensor for tissue engineering applications and microbial electrosynthesis or bioremediation.

6. A method according to any of the preceding claims, wherein the step of performing pyrolysis on the packed natural protein containing fibre structure comprises positioning the packed natural carbon containing fibres in a furnace and reducing an oxygen level inside the furnace.

7. A method according to any of the preceding claims, wherein the step of packing natural protein containing fibres comprises the steps of:

determining a desired weight of natural protein containing fibres to be contained in the resulting packed natural protein containing fibre structure,

providing an amount of natural protein containing fibres corresponding to said desired weight, and

packing the provided amount of natural protein containing fibres into the mould in such a manner that a volume defined by the mould is filled.

8. A method according to claim 7, wherein the step of packing the natural protein containing fibres further comprises the step of wetting the natural protein containing fibres prior to packing the natural protein containing fibres into the mould.

9. A method according to any of the preceding claims, further comprising the step of cutting the natural protein containing fibres before packing the fibres into the mould.

10. A method according to claim 9, further comprising the step of suspending the natural protein containing fibres into solution, after cutting the fibres and before packing the fibres into the mould.

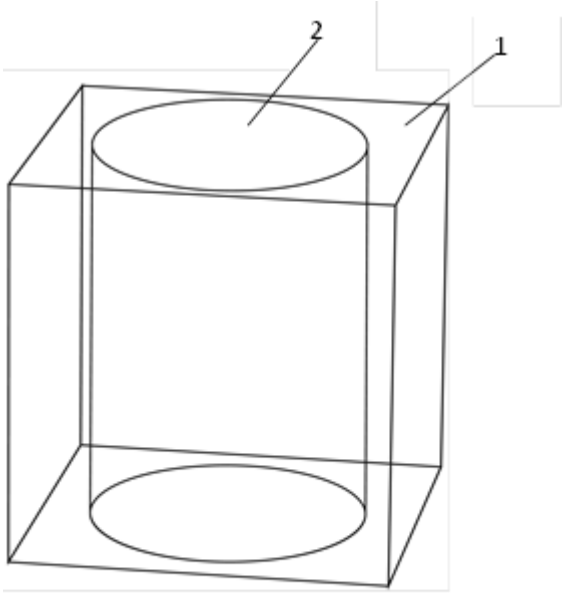

Fig. 1

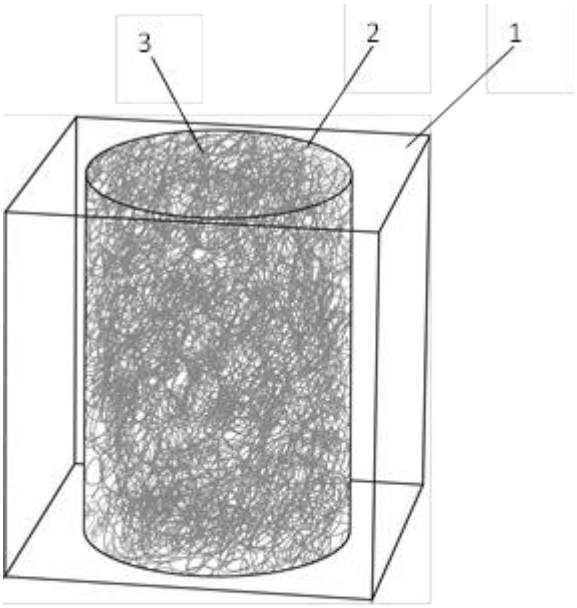

Fig. 2

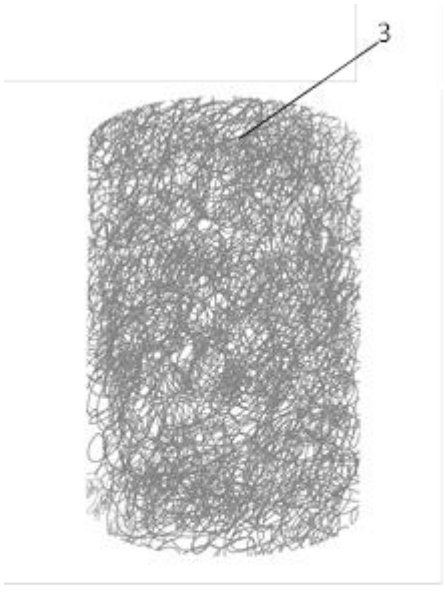

Fig. 3

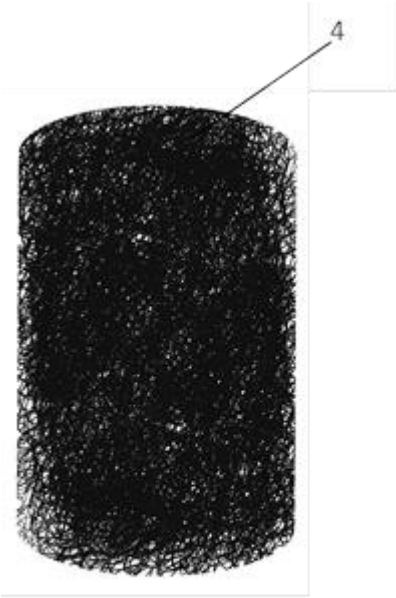

Fig. 4

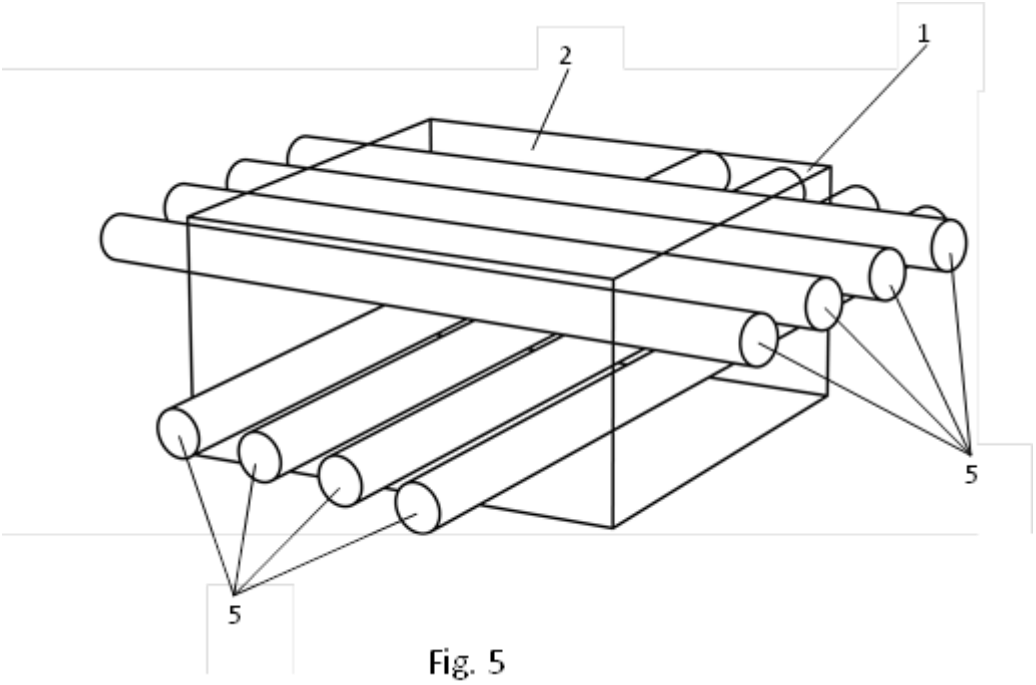

Fig. 5

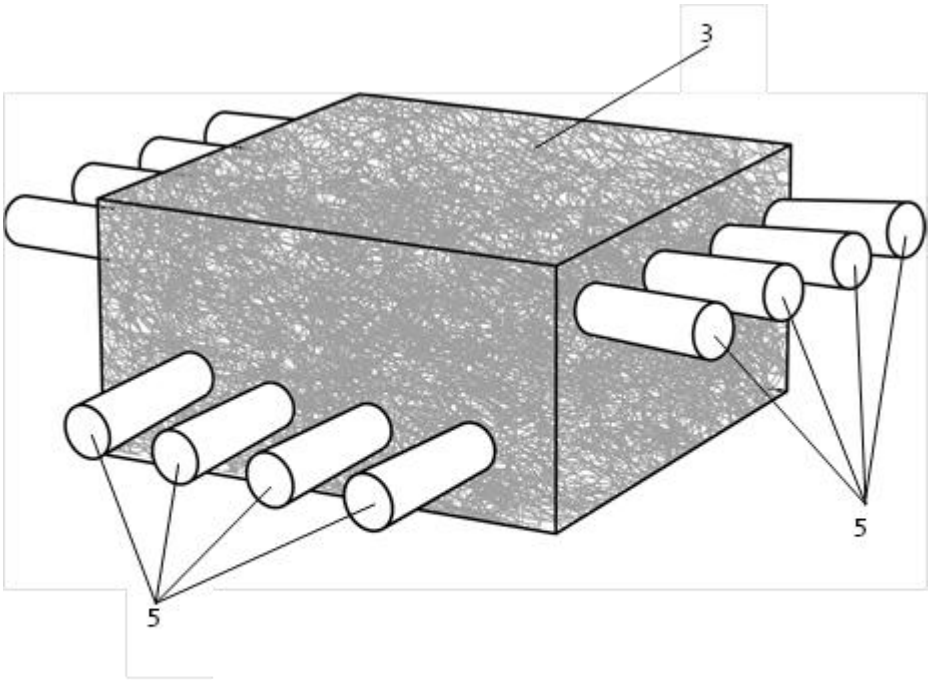

Fig. 6

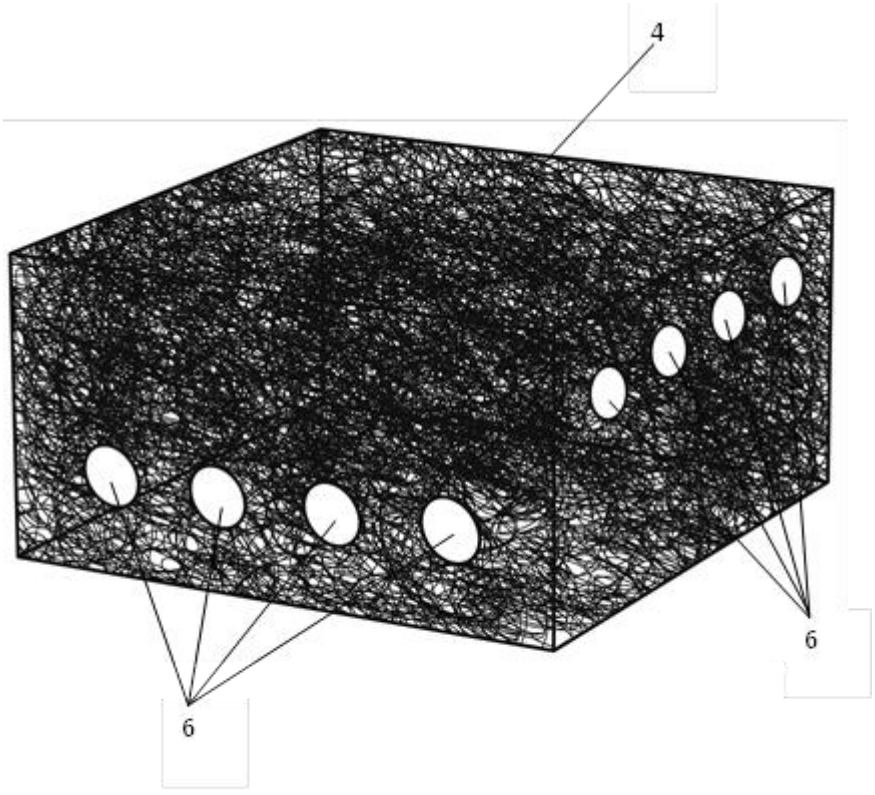

Fig. 7

Conference Abstract A. Fabrication of three dimensional tissue engineering polydimethylsiloxane (PDMS) microporous scaffolds with an integrated bioreactor using a 3D printed water dissolvable sacrificial mould.

Soumyaranjan Mohanty[1], Ioannis Mantis[1], Aradhya Mallikarjunaiah Chetan[1], Haseena Bashir Muhammad[1], Marin Dufva[1], Jenny Emnéus[1], Anders Wolff[1]*

[1]DTU Nanotech, Department of Micro- and Nanotechnology, Technical University of Denmark, Ørsteds Plads, DK-2800 Kgs. Lyngby, Denmark.

ABSTRACT

We present a new scalable and general approach for manufacturing structured pores/channels in 3D polymer based scaffolds. The method involves 3D printing of a sacrificial polyvinyl alcohol (PVA) mould whose geometrical features are designed according to the required vascular channel network. Polydimethylsiloxane (PDMS) polymer is cast around the PVA mould, cross-linked and then the mould is dissolved, leaving behind a structured porous PDMS scaffold. The fabrication method described here is demonstrated with silicone elastomer but various other natural and synthetic polymers can also be compatible with this fabrication technique

KEYWORDS: Scaffold, 3D printing, Bioreactor, Elastomeric

INTRODUCTION

In tissue engineering scaffolds play a major role to provide structural support for cell attachment and subsequent tissue development. For long-term culture, the scaffold material with attached cells has to be continuous perfused for supplying nutrient and oxygen as well as waste removal. It is therefore really crucial to design a proper porous scaffold with desired mechanical properties and with mass transport function to facilitate tissue regeneration[1].

Recently there has been a move towards employing 3D printing as a rapid prototyping technique to fabricate micro-scale porous structures of desired complexities, allowing a true engineering of the scaffold[2,3]. Processes combining 3D printing and moulding have already been used for making structured 3D scaffolds[3,4]. Different sacrificial printing materials such as wax[4] and sugar glass lattice[3] have been utilized to form vascular networks. However the use of wax limits the materials that can be cast around the mould to form the scaffold since polymers requiring higher temperatures for cross-linking cannot be employed and in case of sugar glass it is probably difficult to print large 3D structures as the sugar glass is very brittle, and the inter filament distance (defined by the printing process) is limited to a minimum distance of 1mm. It may therefore not be feasible to use this technique for creating dense vascular channels in large-scale structures for engineering large organs.

In this contribution, we focus on developing a method of fabrication with the opportunity to control the physical, chemical and morphological characteristics of the porous scaffold material by indirect 3D printing of sacrificial polyvinyl alcohol (PVA)[5].

EXPERIMENTAL

The method involves 3D printing of a PVA mould using a commercial 3D filament printer (Makerbot, USA)[5]. Geometrical features of the mould are designed according to the required vascular channel network. PDMS pre-polymer is cast around the PVA mould, cross-linked and then the mould is dissolved, leaving behind a structured porous PDMS scaffold. The fabrication method is shown schematically in Figure 1. (I). To render them hydrophilic, the scaffolds were modified with oxygen plasma using a 13.56 MHz RF generator equipped Atto Plasma System (Diener Electronic GmbH, Ebhausen, Germany). The plasma chamber was evacuated to a pressure below 15 Pa, after which oxygen was introduced (pressure stabilization at 30 Pa) and the plasma was ignited (power 50 W) for 2 min on each side of the scaffold.

Human hepatoblastoma (HepG2) cells were obtained from the German Collection of Micro-

organisms and Cell Cultures (DSMZ, Braunschweig, Germany). The cells were maintained in Roswell Park Memorial Institute (RPMI) 1640 growth medium supplemented with 10% foetal bovine serum (FBS, Sigma-Aldrich Chemie GmbH, Switzerland) and 100 µg/ml penicillin and 10 µg/ml streptomycin in a humidified incubator at 37 °C and 5% CO_2. Scaffolds were loaded with a suspension containing 250,000 cells in 20 µl of media according to the procedure described previously[5] and incubated in a 24 well plate with 1 ml culture media in each well. Medium was refreshed every 2 days.

RESULTS AND DISCUSSION

Scaffolds were fabricated by casting PDMS around sacrificial moulds printed using two different infill patterns (fig.1.II) and four different infill densities to achieve different porosity (not shown here). Photographs and SEM images of the printed moulds and resulting PDMS scaffolds of the two different infill patterns are shown in Fig. 1.II. The high scalability of the method is demonstrated in Fig. 1.II (i & j)

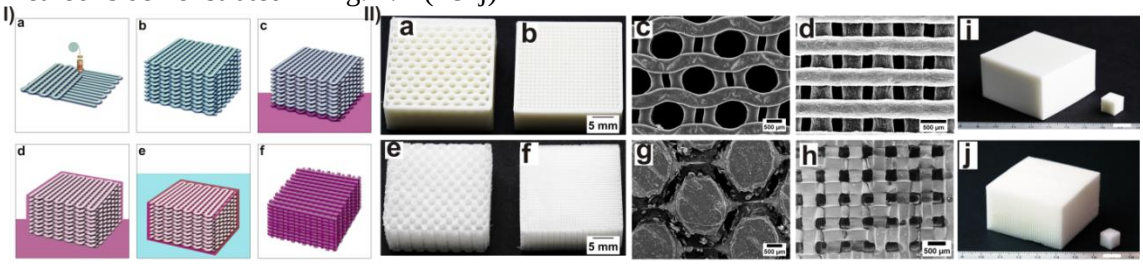

*Figure 1: **I**) Schematic illustration of the steps involved in the fabrication of structured porous elastomeric scaffolds. A sacrificial 3D mould was printed in PVA (a, b). The printed PVA mould was transferred into a container containing pre-cured PDMS (c). Vacuum was applied to ensure complete filling of pre-cured PDMS into the pores of the mould (d). Following crosslinking of the PDMS, the sacrificial PVA mould was dissolved in water (e) leaving behind the structured PDMS scaffold (f). **II**) Photographs of moulds and scaffolds with hexagonal (a, e) and woodpile (b, f) infill patterns. SEM images of moulds and scaffolds with hexagonal (c, g) and woodpile (d, h) infill patterns. (i) optical image of a 50 layered (1 cm^3 cube) and 150 layered (75 cm^3 cube) 3D printed PVA mould (j) optical image of 50 layered (1 cm^3 cube) and 150 layered (75 cm^3 cube) PDMS scaffolds replicated from the mould (i). Scale bar in (i) and (j): 1 cm* [5].

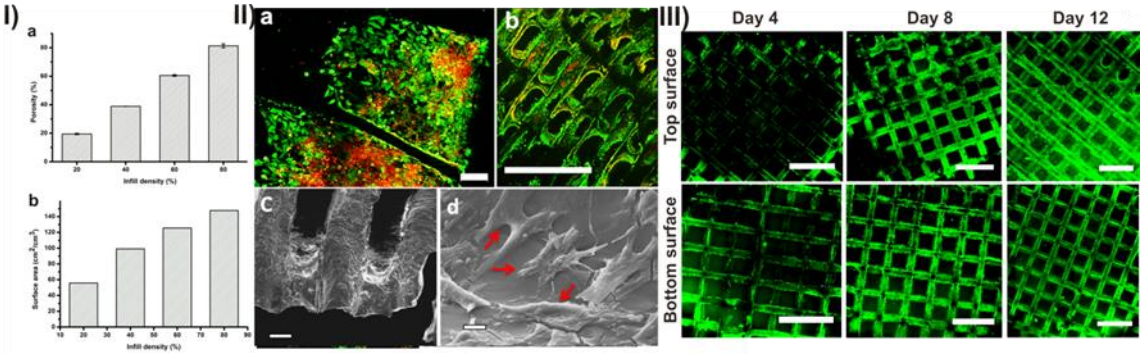

Figure 2: I) Measured porosity (a) and calculated surface to volume ratio (b) of scaffolds fabricated from mould with different infill density (standard deviation (n = 4)). II) Hepg2 cell morphology and attachment to PDMS scaffold using immunostaining (a & b) and SEM (c & e). Cell cytoskeleton beta tubulin (green) and nucleus (red). (a) Top surface of the scaffold. (b) Longitudinal cross section of the scaffold. Low- (c) and high- (d) magnified SEM images of HepG2 cells cultured on PDMS scaffolds for 4 days. Scale bar of image a) with 100 µm b) with 1 mm, C) with 50 µm and d) 5 µm. III) Live/dead (green = live, red =dead) staining of HepG2 cells grown on top and bottom part of the PDMS scaffold for 4, 8 and 12 days. Scale bars represent 1 mm.

Figure 2. I(a & b) shows physical characterization of the PDMS scaffolds. The experimentally determined porosity of the scaffolds varied linearly as a function of the infill density of the printed mould and the calculated surface areas of a 1 cm^3 fabricated scaffolds of varying infill densities increases from 52.5 cm^2/cm^3 to 150.9 cm^2/cm^3. Live/dead staining of the HepG2 cell-scaffold construct on day 12 of culture, showed a confluent layer of live cells on the scaffolds

and no dead cells were observed, throughout the culture period (Fig 2. III)). Immunostaining (fig 2. II a & b) and the SEM images (fig 2. II c & e) of the scaffold showing well-attached cell morphology with spread-out cell attachment onto the top as well in the centre of the scaffold surface.

As a proof of concept a single scaffold integrated bioreactor was fabricated using a 40% porous/infilled PVA mould as shown in the figure 3. In short, after printing the mould was placed into a Petri dish and PDMS solution was poured into it, degassed and cured. The sacrificial PVA mould was dissolved from the cross-linked PDMS and a porous scaffold with an integrated reactor part was formed. The reactor was dried at 60° C overnight. The inlet and outlet of the reactor was punched vertically. For better visualization, the PDMS device has been subsequently bonded to a glass slide using O_2-plasma activation. Before using the device was degassed and cleaned using 100% ethanol and finally cleaning with water.

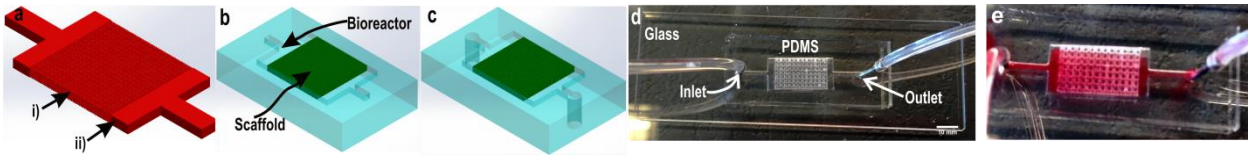

Figure 3. Schematics of fabrication of PDMS bioreactor with integrated scaffolds. A) 3D printed PVA mould using 3D filament printer. i) indicates the part designed for porous scaffolds and ii) indicated the design for bioreactor. The PVA mould was casted around uncured PDMS and cross-linked. The sacrificial PVA mould was dissolved and leaving behind the PDMS chamber with integrated porous scaffold (B). C) The integrated device was punched from its inlet and outlet and ready for bonding to a glass surface. D) Photograph of the 3D PDMS bioreactor with integrated scaffold boned to a glass slide (D) and for visualization red food dye loaded into it (E).

CONCLUSION

In this study, we have demonstrated a way for fabricating scaffolds and microfluidics chambers by indirect 3D printing of water dissolvable PVA, and the high scalability of the process is shown. Different designs of PDMS scaffolds with various porosities and surface areas were successfully fabricated and tested for in-vitro cell studies. High cellular viability and homogeneous cellular distribution across the scaffold was archived for such PDMS scaffolds. Furthermore, as we have demonstrated, the fabrication method can generate bioreactors with integrated porous scaffold materials from PDMS for perfusion. The fabrication method described here is demonstrated with silicone elastomer but various other natural and synthetic polymers can also be compatible with this fabrication technique. In conclusion, the presented process is scalable, biocompatible, rapid, and inexpensive.

ACKNOWLEDGEMENTS

This work has been financially supported by EU project NanoBio4Trans (grant no: 304842).

REFERENCES

1 S. J. Hollister, *Nat. Mater.*, 2005, **4**, 518–24.
2 B. Derby, *Science*, 2012, **338**, 921–6.
3 J. S. Miller, K. R. Stevens, M. T. Yang, B. M. Baker, D. T. Nguyen, D. M. Cohen, E. Toro, A. A. Chen, P. A. Galie, X. Yu, R. Chaturvedi, S. N. Bhatia and C. S. Chen, *Nat. Mater.*, 2012, **11**, 768–74.
4 D. Therriault, R. F. Shepherd, S. R. White and J. a. Lewis, *Adv. Mater.*, 2005, **17**, 395–399.
5 S. Mohanty, H. B. Muhammad, J. Trifol, P. Szabo, H. V. R. Burri, C. Canali, M. Dufva, J. Emnéus and A. Wolff, *Mater. Sci. Eng. C*, 2015, **55**, 569-578.

CONTACT: * **Anders Wolff**; phone: + 45-256305; anders.wolff@nanotech.dtu.dk

Conference Abstract B. CONDUCTING PYROLYSED CARBON SCAFFOLD FOR TISSUE ENGINEERING

Soumyaranjan Mohanty, Letizia Amato, Arto Heiskanen, Stephan Sylvest Keller, Anja Boisen, Martin Dufva, Anders Wolff, and Jenny Emnéus
jenny.emneus@nanotech@dtu.dk
Department of Micro- and Nanotechnology, Technical University of Denmark, 2800 Lyngby, Denmark
Keywords: Electrical conducting scaffold, pyrolysed carbon, tissue scaffold.

This work presents the fabrication, characterization and testing of pyrolysed three-dimensional (3D) porous carbon materials as potential novel 3D conducting scaffolds (3D-CS) for tissue engineering applications.

Due to the multifunctional nature, carbon nanomaterials are becoming increasingly attractive, offering numerous opportunities to design novel sensors, drug delivery systems and scaffolds for tissue engineering[1]. For tissue engineering, carbon nanotubes (CNT) have been used to mechanically stabilize commonly used "soft" scaffold materials such as hydrogels and fibrous scaffolds[2]. Moreover, electrically conductive hydrogel based scaffolds have been demonstrated using CNT composites of these otherwise nonconductive polymers, enabling electrical stimulation of e.g. neural stem cells, resulting in improved action potentials and differentiation into functional neural networks[3]. Very recently, graphene foam (GF) - a 3D porous carbon structure - has been suggested as a new promising conductive scaffold that may incorporate, in the same structure, topographical, chemical and electrical cues[4]. We have recently shown that it is possible to precisely pattern SU-8 photoresist into high aspect ratio sub-micron 3D pillar scaffold structures[5] that can be pyrolysed into their corresponding electrochemically active 3D carbon pillar scaffold structures[6] In this study, we will demonstrate how scalable both randomly and structurally controlled porous conducting 3D carbon scaffolds can be generated through the pyrolysis of correspondingly porous polymer scaffolds of various polymers and copolymers. The idea is here demonstrated for a randomly structured PDMS sponge generated from a sacrificial carbohydrate template[7] (in this case a simple sugar cube). The biocompatibility of the 3D-CS was investigated and confirmed using live/dead cell imaging of cells grown on the scaffold for 3 days, and its potential suitability as an electrochemically active scaffold was demonstrated using electrochemical impedance spectroscopy (EIS).

The procedure for fabricating the 3D-CS from a sugar cube is shown in Fig. 1: (1) A randomly porous sugar cube was placed in a container, (2) pre-cured PDMS was poured into the container, which was (3) absorbed into the sugar cube by capillary forces in a vacuum desiccator for 1 hour. (4) The pre-cured PDMS was then cured in an oven at 80 ^{0}C for 2 hour. (5) The sacrificial sugar in the sugar cube was then dissolved in water overnight, whereby (6) a randomly porous PDMS sponge was obtained. (7) The porous PDMS sponge was thereafter pyrolyzed in a furnace at 900 ^{0}C for 60 min in N_2 atmosphere, resulting in a highly porous 3D-CS, as shown in Fig. 2.

Without any further modification, the 3D-CS was sterilized and used for culturing of endothelial cells (HUVEC), which were allowed to attach and grow for 3 days on and inside the 3D-CS. Fig. 3 depicts live/dead immunostaining (Dapi) after 3 days of cell culturing, showing cytoskeleton (circle) and the nucleus (square), with no indication of dead cells, demonstrating that the support is biocompatible even without the normally necessary modification with extra cellular matrix protein coating. The EIS spectra in Fig. 4, clearly indicates that the 3D-SC has inherent electrical conductivity, indicating its potential use for electrical stimulation of cells and/or as a electrochemical sensing scaffold.

The European Union, via EU FP7 NanoBio4Trans project, is kindly acknowledged for financial support.

[1] Chaenyung Cha, Su Ryon Shin, Nasim Annabi, Mehmet R. Dokmeci, and Ali Khademhosseini, ASCNano 7 (2013) 2891–2897.
[2] Sahithi, K.; Swetha, M.; Ramasamy, K.; Srinivasan, N.; Selvamurugan, N. Int. J. Biol. Macromol. 46 (2010) 281–283.
[3] Kam, N. W. S.; Jan, E.; Kotov, N. A.Nano Lett. 9 (2009) 273–278.
[4] Ning Li, Qi Zhang, Song Gao, Qin Song, Rong Huang1, Long Wang, Liwei Liu, Jianwu Dai, Mingliang Tang, Guosheng Cheng. Scientific Reports 2013. DOI: 10.1038/srep01604.
[5] Amato L., Keller S.S., Heiskanen A., Dimaki M., Emnéus J., Boisen A., Tenje M. Microelectron. Eng. 98, (2012), 483–487
[6] Amato L., Hansen R. J., Heiskanen A., Gammelgard L., Rindzevicius T., Martinez-Duarte R., Bisht G. S., Downard A., Baronian K., Tenje M., Madou M., Boisen A., Emnéus J., Keller S. S. 38th International Conference on Micro and Nano Engineering, Toulouse (France).
[7] Jordan S. Miller, Kelly R. Stevens, Michael T. Yang, Brendon M. Baker, Duc-Huy T. Nguyen, Daniel M. Cohen, Esteban Toro, Alice A. Chen, Peter A. Galie, Xiang Yu, Ritika Chaturvedi, Sangeeta N. Bhatia and Christopher S. Chen.Nature Materials 11 (2012) 768-774.

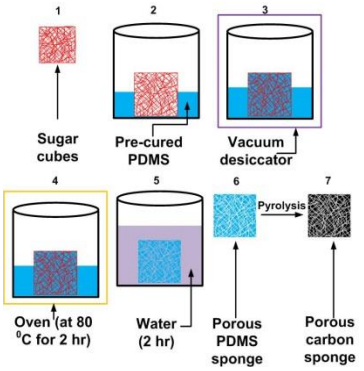

Figure 1. Fabrication of a conducting randomly porous carbon scaffold from a sugar cube.

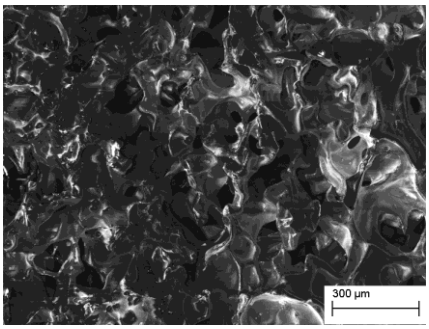

Figure 2. SEM images of the fabricated porous carbon scaffold.

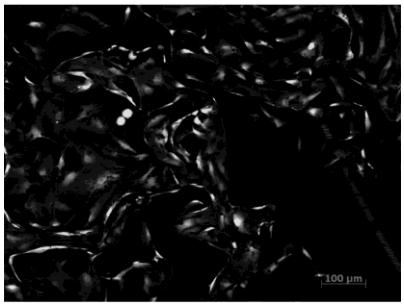

Figure 3. Live/dead cell imaging after 3 days of HUVEC cell culturing on 3D-CS. Circles - staining of cell cytoplasm. Squares staining the nucleus.

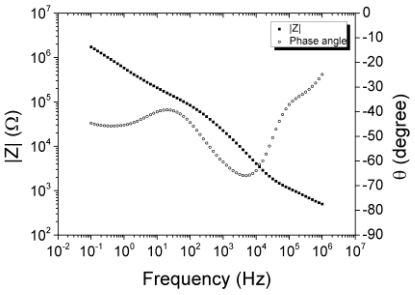

Figure 4. Electrochemical impedance spectrum (Bode plot) obtained with the carbon scaffold material.

Conference Abstract C. THREE-DIMENSIONAL (3D) SCAFFOLDS FOR BIOARTIFICIAL ORGAN-ON-A-CHIP SYSTEMS AND BIOELECTROANALYSIS

S. Mohanty[a], A. Heiskanen[a], L. Amato[a], S. Keller[a], C. Canali[a], M. Hemmingsen[a], L. Larsen[a], M. Alm[b], P. Thomsen[b], Ø. G. Martinsen[c], A. Aspegren[d], A. Martinez-Serrano[e], M. Dufva[a], A. Wolff[a] and J. Emnéus[a]

[a] Department of Micro and Nanotechnology, Technical University of Denmark, K. Lyngby, 2800, Denmark
[b] Biomodics ApS, Høje Tåstrup, 2630, Denmark
[c] Department of Physics, Oslo, University, Oslo, 0371, Norway
[d] Cellartis® by Takara Bio Europe AB, Göteborg, 413 46, Sweden
[e] Departmento de Biología Molecular and Centro de Biología Molecular, Universidad Autónoma de Madrid, Madrid 28049, Spain

Keywords: Perfusable scaffolds, liver-on-a-chip, stem cells, bioimpedance,

Background. The clinical need for functional replacement tissues and physiologically relevant drug screening models has fuelled research into engineering in-vitro tissues. In conventional 2D cell cultures, cells tend to lose key specific functions that they normally exhibit due to the absence of complex cell-cell, cell–matrix and cell factor interactions that are usually present *in vivo* [1]. There is therefore a move towards culturing cells in 3D scaffolds that act as a substrate for cells to attach, proliferate and differentiate [2]. While cells *in vivo* are typically no further than 100 – 200 µm away from a blood capillary, enabling their nutrient requirements to be met through diffusion of the necessary chemical species, the absence of functional vasculature in tissue engineered constructs poses a significant challenge when attempting to grow tissues of clinically relevant sizes [3]. Therefore, in order to cultivate tissues of clinically relevant sizes *in vitro*, an enhanced mechanism for transport of oxygen and nutrients is required with a growing trend of using porous scaffolds to guide cell assembly into 3D constructs for engineering different types of tissues such as liver [4]. Mass transport in such scaffolds can be enhanced by integrating them into perfusion bioreactors that enable continuous perfusion of media through the pores of the scaffold.

Work to be presented. In this work, polymer scaffolds are fabricated using either photo- and colloidal lithographic nano/micro patterning or by a combination of 3D printing and polymer casting techniques (Figure 1) [5], in some cases followed by pyrolysis to generated conductive carbon scaffolds [6] (Figure 2). The scaffolds are optionally designed with: (a) Primary structured perfusable channel network that allows flow through the material enabling delivery of necessary nutrients and oxygen to the interior of the scaffolds. (b) Secondary more arbitrary random porous network that optionally can enclose a hydrogel phase with a "nearby" source of important cell factors, supporting the growth and differentiation of cells. (c) Ability to conduct or sense electrical currents. The application of these scaffolds for the development of a bioartificial liver support system based on differentiation of induced pluripotent stem cells into functioning hepatocytes will be presented (Fig. 3), or for the differentiation of neural stem cells into dopaminergic neurons (Figure 2). Moreover, our work toward incorporating different electrode systems for monitoring biolectrochemical (by bioimpedance [7] (Fig. 3) and voltammetry [5]) signals generated by cells residing on 3D scaffolds will also be presented.

[1] L. G. Griffith and M. A. Swartz, Nat. Rev. Mol. Cell Biol. **7**, 211 (2006).

[2] P. Zorlutuna, N. Annabi, G. Camci-Unal, M. Nikkhah, J. M. Cha, J. W. Nichol, A. Manbachi, H. Bae, S. Chen, and A. Khademhosseini, Adv. Mater. **24**, 1782 (2012).
[3] R. K. Jain, P. Au, J. Tam, D. G. Duda, and D. Fukumura, Nat. Biotechnol. **23**, 821 (2005).
[4] J. Fan, Y. Shang, Y. Yuan, and J. Yang, J. Mater. Sci. Mater. Med. **21**, 319 (2010)
[5] S. Mohanty, L. B. Larsen, J. Trifol, P. Szabo, H. V. R. Burri, C. Canali, M. Dufva, J. Emnéus, A. Wolff. Materials Science and Engineering C 55 (2015) 569–578.
[6] L. Amato, A. Heiskanen, C. Caviglia, F. Shah, K. Zór, M. Skolimowski, M. Madou, L. Gammelgaard, R. Hansen, E. G. Seiz, M. Ramos, T. Ramos Moreno, A. Martínez-Serrano ,
S. S. Keller. J. Emnéus. Adv. Funct. Mat DOI: 10.1002/adfm.201400812.
[7] C. Canali, A. Heiskanen, H. B. Muhammad, P. Høyum, F-J. Pettersen, M. Hemmingsen, A. Wolff, M. Dufva, Ø. G. Martinsen, J. Emnéus. Biosensors and Biolelectronics 63 (2015) 72–79.

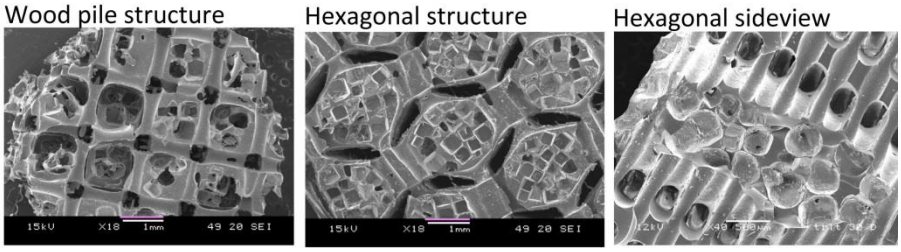

Figure 1. Examples of different types of polymer elastomer scaffolds incorporating both primary structured and secondary random porous channels.

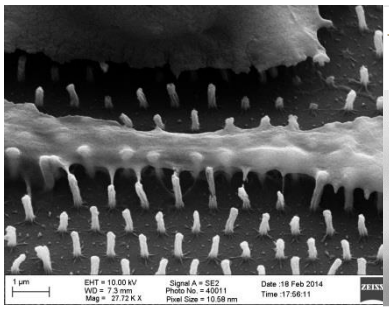

Figure 2. SEM image of differentiated neural stem cell on pyrolysed SU8 derived carbon nanopillars patterned by colloidal lithography.

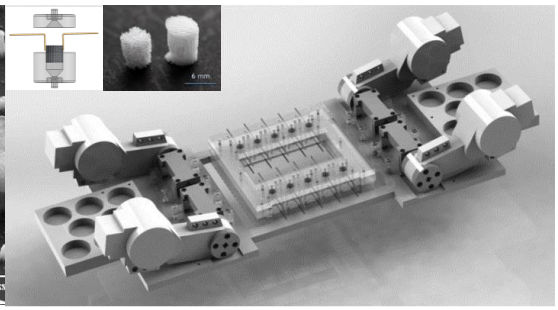

Figure 3. 8-channel perfusion based bioartificial liver support system for bioimpedance monitoring of stem cell growth and differentiation. *Inserts:* Enlargement of a single bioreactor in the array with two needle electrodes incorporated and a photo of polymer scaffolds that can be introduced into the bioreactor.

Published by:
DTU Nanotech
Department of Micro- and Nanotechnology
Technical University of Denmark
Ørsteds Plads, building 345C
DK-2800 Kgs. Lyngby